Elucidating the molecular mechanisms underlying androgen-regulated lipid metabolism in prostate cancer

RAJ KUMAR SHRESTHA

MSc Clinical Biochemistry, BSc Medical Laboratory Technology

A THESIS SUBMITTED TO THE UNIVERSITY OF ADELAIDE IN

THE FULFILMENT OF THE REQUIREMENTS

FOR THE DEGREE OF

DOCTOR OF PHILISOPHY

DAME ROMA MITCHELL CANCER RESEARCH LABORATORIES

FACULTY OF HEALTH AND MEDICAL SCIENCES

SCHOOL OF MEDICINE

THE UNIVERSITY of ADELAIDE

*

[NOVEMBER 2020]

DECLARATION

This work contains no material which has been accepted for the award of any other degree or diploma in my name in any university or other tertiary institution and, to the best of my knowledge and belief, contains no material previously published or written by another person, except where due reference has been made in the text. In addition, I certify that no part of this work will, in the future, be used in a submission in my name for any other degree or diploma in any university or other tertiary institution without the prior approval of the University of Adelaide and where applicable, any partner institution responsible for the joint award of this degree.

I give consent to this copy of my thesis when deposited in the University Library, being made available for loan and photocopying, subject to the provisions of the Copyright Act 1968.

I acknowledge that the copyright of published works contained within this thesis resides with the copyright holder(s) of those works.

I also give permission for the digital version of my thesis to be made available on the web, via the University's digital research repository, the Library Search and also through web search engines, unless permission has been granted by the University to restrict access for a period of time.

Signature: Date: 13/11/2020

Raj K. Shrestha ADELAIDE, AUSTRALIA

DEDICATION

To Dad and Mum

…who never went to school in their lives but encouraged me to go on every adventure, especially this one

SUMMARY

Prostate cancer (PCa) is the most frequently diagnosed male cancer in Australia and a leading cause of cancer-related death. Androgen receptor (AR), a ligand-activated transcription factor, regulates growth and progression of PCa. Increased AR activity is associated with PCa development and progression to lethal castration resistant PCa (CRPC). Prostate tumours are highly reliant on lipids for growth, and one of the proposed mechanisms by which AR drives PCa progression is by regulating lipid uptake and metabolism. However, the molecular mechanisms underlying AR-regulated lipid metabolism are unclear. A better understanding of this interplay between AR signalling and lipids could identify new biomarkers and therapeutic targets, which could improve outcomes associated with this common disease. Therefore, this study aimed to elucidate mechanisms by which AR regulates lipid metabolic processes, particularly those associated with tumour growth and disease progression.

By integrating cistromic and transcriptomic data, we identified Acyl-CoA Synthetase Medium Chain Family Members 1 and 3 (ACSM1 and ACSM3) as putative new AR-regulated genes in PCa. These factors are purported to activate fatty acids for their utilisation in energy production via mitochondrial beta-oxidation. Regulation of ACSM1 and ACSM3 by AR was validated using androgen and anti-androgen treatments and confirming direct binding of AR to proximal cis-regulatory elements of the genes by chromatin immunoprecipitation (ChIP). ACSM1 and ACSM3 were found to be upregulated in prostate tumours compared to non-malignant prostate tissues and expressed more highly in PCa than other cancer types. We subsequently applied metabolomics, lipidomics and functional assays to

decipher the roles of ACSM1 and ACSM3 in PCa cells. Knockdown of ACSM1 and ACSM3 in PCa cells resulted in growth arrest and ATP depletion, supporting a key role for both factors in energy production from fatty acids. Furthermore, lipidomic analysis of cells showed that poly-unsaturated fatty acids accumulate in response to loss of ACSM1 and ACSM3. Metabolomics revealed that cells adapt to loss of ACSM1 and ACSM3 by switching to a glycolytic phenotype. The metabolic dysregulation induced by knockdown of ACSM1 and ACSM3 caused mitochondrial oxidative stress and subsequent lipid peroxidation, eventually resulting in cell death. Accumulation of mitochondrial reactive oxygen species was abrogated by ferrostatin-1 (an iron chelator), suggesting that cell death was due to an iron-dependent form of apoptosis termed ferroptosis. Supporting this concept, over-expression of ACSM1 and ACSM3 elicited resistance to the ferroptosis inducers Erastin and ML210.

Our study has revealed a novel mechanism by which AR regulates lipid metabolism in PCa cells. Importantly, the critical role of ACSM1 and ACSM3 as key regulators of growth and protectors against ferroptosis emphasises their potential as novel therapeutic targets.

Key words: Prostate cancer, Androgen receptor, Lipid metabolism

ACKNOWLEDGEMENT

The work in this thesis could not have been completed without the support of a numbers of people and I would like to take this opportunity to formally acknowledge their assistance. These people have been generous enough to provide their time, help, expertise, understanding and patience throughout my PhD.

First and foremost, I am indebted to my supervisor, Associate Prof. Luke Selth for his insight, continuous support during my PhD studies, patience, motivation, and immense knowledge. His guidance helped me during my research and writing of this thesis. I could not have imagined having a better supervisor for my PhD study. It has been a privilege to work with you during these years. Besides Dr Selth, my sincere appreciation also goes to Prof. Lisa Butler and Wayne Tilley, my co-supervisors, for their insightful comments, encouragement and endless support.

My sincere appreciation goes to Prof. Wayne Tilley and Prof.. Theresa E. Hickey, who provided me with access to the Dame Roma Mitchell Cancer Research Laboratories (DRMCRL) and other research facilities. Without your support it would not be possible to conduct this research. To the wonderful people at DRMCRL, especially Scott Townley, Adrienne Hanson, Marie Pickering, Zoya Kikhtyak, Geraldine Laven-Law, Dr. Elizabeth S A Kuczek, Dr. Jean Winter and Dr. Amy Dwyer: I couldn't have asked for a better group of people to work with and I'm forever grateful for your endless support and encouragement throughout my study. A big thank you to my friends Rayzel, Leila, Mohammadreza, Ebtihal, and Danielle: I have greatly enjoyed your company working both inside and outside the lab for

the past few years. I would also like to acknowledge Dr. Steve Paltoglou and Dr. Iza Denis for sharing their expertise and ideas on ChIP, IP and PLA techniques.

Special thanks to the members of prostate cancer research group at SAHMRI, Dr. Zeyad D. Nassar, Chui Yan Mah (Shanice), Dr. Nicole Moore, Joanna Gillis, Natalie Ryan and Madi Helm for their technical and intellectual support. I have had many scientific discussions with Dr. Lake-Ee Quek, Dr. Andrew J. Hoy, Prof. Johan Swinnen and Prof. Richard Iggo, which significantly strengthened my project and this thesis. I would like to thank all of you for always making time to discuss my project and for your wise words over the years. Furthermore, I would like to acknowledge Dr. Ge Liu (Research Officer, Child Nutrition Research Centre, SAHMRI) for his time and expertise in lipidomic analysis.

I gratefully acknowledge Adelaide Scholarship International (ASI) for funding my PhD scholarship and the Freemasons Foundation Centre for Men's Health (FFCMH) for the Supplementary Scholarship. I would especially thank Prof. Gary A. Wittert (Director of FFCMH) for his endless support, love, encouragement, and guidance and Ms Margaret Mc Gee (executive officer, FFCMH), who kept me organised and for her optimistic attitude and good-natured support.

I am extremely grateful to my respected teacher Dr. Prabin Gyawali for his efforts, support, love, encouragement and guidance throughout my career in science. His dynamism, vision, sincerity and motivation have deeply inspired me. Without his encouragement and guidance, I would have never thought about my PhD. Thank you for your wonderful love, patience, empathy, and fabulous support

during my tough times. I am really touched with homely family environment provided by Mrs Nirja Adhikari, Paritosh Gyawali, Neelisha Gyawali and Sujan Niroula during my time in Adelaide for my PhD. Thank you always for being there.

Finally, my family who deserve more thanks than I can give them. Thank you to my dad and mum, Mr. Ram Lal Shrestha and Ms Tika maya Shrestha, for your unwavering love and support in absolutely everything I do and giving me strength to chase my dreams. Thank you to my brother Mr Ram Kumar Shrestha, and sister-in-law, Sunita Shrestha, for supporting me spiritually throughout the PhD and my life in general. Your unwavering support and confidence in me has helped me through the rough spots and made me realise that it has all been worthwhile. A huge bundle of love to my nephew, Mr. Riyan Shrestha.

On a personal note, to my wife, Ruja Tuladhar for her patience and tolerance over last few years. She has stood by me through all my travails, my absences, my fits of pique and impatience. I could not be able to finish this work without your support.

Finally, my thanks go to all the people who have supported me to complete the research work directly or indirectly.

Raj Kumar Shrestha

November 2020

TABLE OF CONTENTS

CHAPTER 1: INTRODUCTION AND LITERATURE REVIEW

Chapter 1: General Introduction

1.1 Anatomy and Physiology of Prostate Gland

The prostate gland is a male sex organ which surrounds the urethra of males at the base of the bladder and is responsible for the production and secretion of seminal fluid, which enhances the motility and fertility of sperm (Kumar & Majumder, 1995a). The muscular portion of the gland is involved in control and release of the urine as well as forceful expulsion of semen through the urethra during ejaculation. The prostate gland is located posterior to the lower portion of the symphysis pubis, anterior to the rectum, and inferior to the neck of the urinary bladder and superior to the external urethral sphincter. Classically described as “walnut-shaped,” the prostate gland is conical in shape and surrounds the proximal urethra as it exits from the bladder (Bhavsar & Verma, 2014).

1.1.1 Morphology of prostate gland

The prostate is the largest accessory gland in the male reproductive system and can be divided into 4 zones and 4 lobes (Figure 1.1) (McNeal, 1988). The anatomy of the prostate gland is described by lobe classification whereas the zonal classification is more commonly used to locate the pathological condition. The central zone, composed of the tall columnar cells surrounding the ejaculatory duct, comprises of 25% of total prostate volume and is the densest stromal area of the total prostate (McNeal, 1988; Muhammad, Khalid, Nadia, & Muhammad, 1970; Srodon & Epstein, 2002). The Transitional zone (TZ) surrounds the proximal part of urethra and is the origin for almost 20% of prostatic cancer. Benign prostatic

enlargement originates in this area. The peripheral zone (PZ) makes up to 70% of the prostate and is composed of loose stromal regions, moderate gland complexity and broadly spaced smooth muscle bundles. The central zone, makes up to 25% of total prostate glandular tissues and is histologically distinct from the peripheral zone (McNeal, 1988; Muhammad et al., 1970; Srodon & Epstein, 2002). The ejaculatory ducts are located in the central zone and fuses with the urethra in the same region (McNeal, 1988). The lobe system divides the prostate into anterior, posterior, lateral and median lobes (Figure 1.2, Figure 1.3).

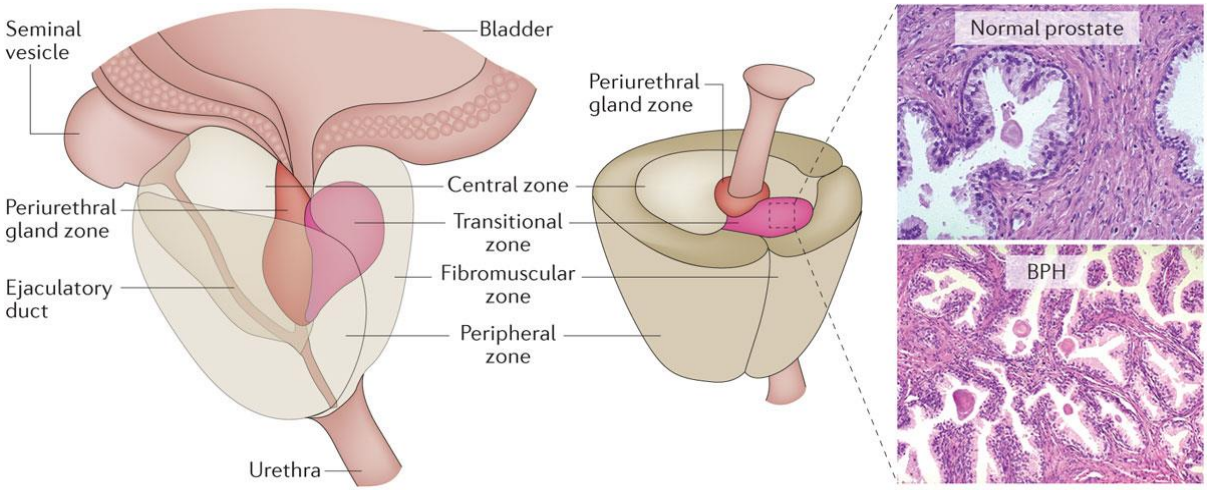

Figure 1.1: Schematic of prostate zones

Reproduced, with permission, from Chughtai, B. *et al.* (2016)(Chughtai et al., 2016)

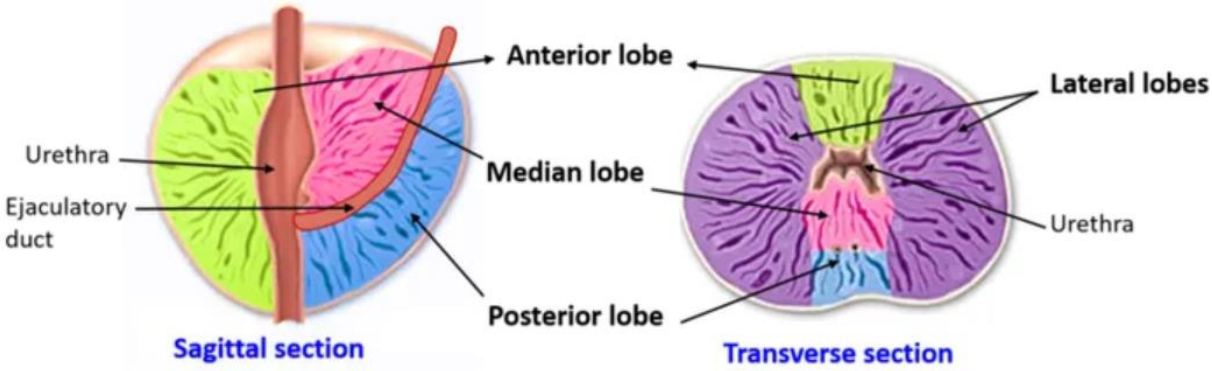

Figure 1.2: Schematic of prostate lobes

Source: (https://anatomyqa.com/prostate-gland-anatomy/)

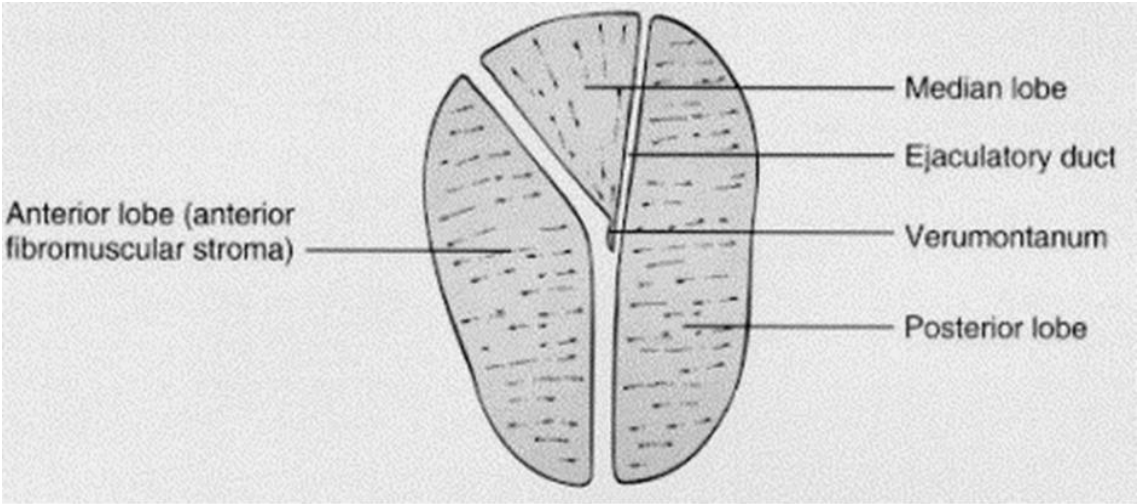

Figure 1.3: Schematic of prostate lobes [Adopted from (Coakley. et al. 2016 (Coakley & Hricak, 2000))

Table 1.1: Table summarizing the histologic composition and embryologic origins of the various zones of the prostate gland. Reproduced, with permission from Bhavsar. et al (2014) (Bhavsar & Verma, 2014).

	Central zone (CZ)	Transition zone (TZ)	Peripheral zone (PZ)
Volume of normal prostate (%)	25	5	70
Embryologic origin	Wolffian duct	Urogenital sinus	Urogenital sinus
Epithelium	Complex, large polygonal glands	Simple, small rounded glands	Simple, small rounded glands
Stroma	Compact	Compact	Loose
Origin of prostatic adenocarcinoma (%)	5	25	70
Benign prostatic hyperplasia (%)	—	100	—

1.1.2 Function of prostate gland

The main function of the prostate gland is to produce an alkaline seminal fluid that constitutes approximately one-third of the total volume of semen. Sperm are produced in testicles and stored in a jelly like matrix in the seminal vesicles. During ejaculation process the coordinate contraction of smooth muscles of the prostate gland, the seminal vesicles, the bulbourethral gland and the vas deferens help to expel semen and mix their respective contents (Kumar & Majumder, 1995b). The female vaginal tract is acidic therefore the alkalinity of the prostatic fluid neutralizes the pH and prolongs the survival of sperm. Additionally, the prostatic fluid is rich in prostate specific antigen (PSA), citrate, zinc, fructose and cholesterol, which both liquefies the gelatinous ejaculate and also and nourishes the sperm, allowing them to stay viable and move freely to fertilize an ovum (Kumar & Majumder, 1995b).

1.1.3 Regulation of prostate gland

The growth and development of normal prostate and PCa is highly dependent of androgen, the production of which is regulated by hypothalamic-pituitary axis. Gonadotropin- releasing hormone (GnRH) released from hypothalamus acts on pituitary gland and releases luteinizing hormone (LH), which thereafter induces the secretion of testosterone from the Leydig cells of the testis (Verze, Cai, & Lorenzetti, 2016). In addition, corticotropin-releasing hormone (CRH) released from hypothalamus induces secretion of adrenocorticotropic hormone

(ACTH) from the pituitary gland. ACTH act on adrenal glands and produces testosterone and other forms of androgens e.g. adrenostenediol.

The majority (~95%) of circulating testosterone is produced by Leydig cells in the testis and remaining 5% originates from adrenal glands (Green, Mostaghel, & Nelson, 2012; Krieg, Weisser, & Tunn, 1995). Only 3% of circulating testosterone is unbound and physiologically active; most of it is inactive, bound to sex-hormone binding globulin (SHBG) and albumin in the blood circulation which is required for the systemic transportation. In the prostate microenvironment, testosterone is converted to dihydroxytestosterone (DHT) by the enzyme 5α-reductase (Chandrasekar, Yang, Gao, & Evans, 2015; Green et al., 2012). Under physiological conditions, both testosterone and DHT can bind to and activate its cognate steroid receptor, the androgen receptor (AR) and DHT has a significantly greater affinity for AR (Lonergan & Tindall, 2011; Wright, Thomas, Douglas, Lazier, & Rittmaster, 1996; Z. X. Zhou, Lane, Kemppainen, French, & Wilson, 1995). Thus androgen can exert their actions via the AR in a DNA binding-dependent manner to regulate target gene transcriptions to regulate diverse range of biological actions including important roles in the development, maintenance and function of the prostate gland (Roy et al., 1999) (Figure 1.4). Thus, it is often prescribed to exogenous administered testosterone, known as testosterone replacement therapy to reverse symptoms of low testosterone (Bassil, Alkaade, & Morley, 2009).

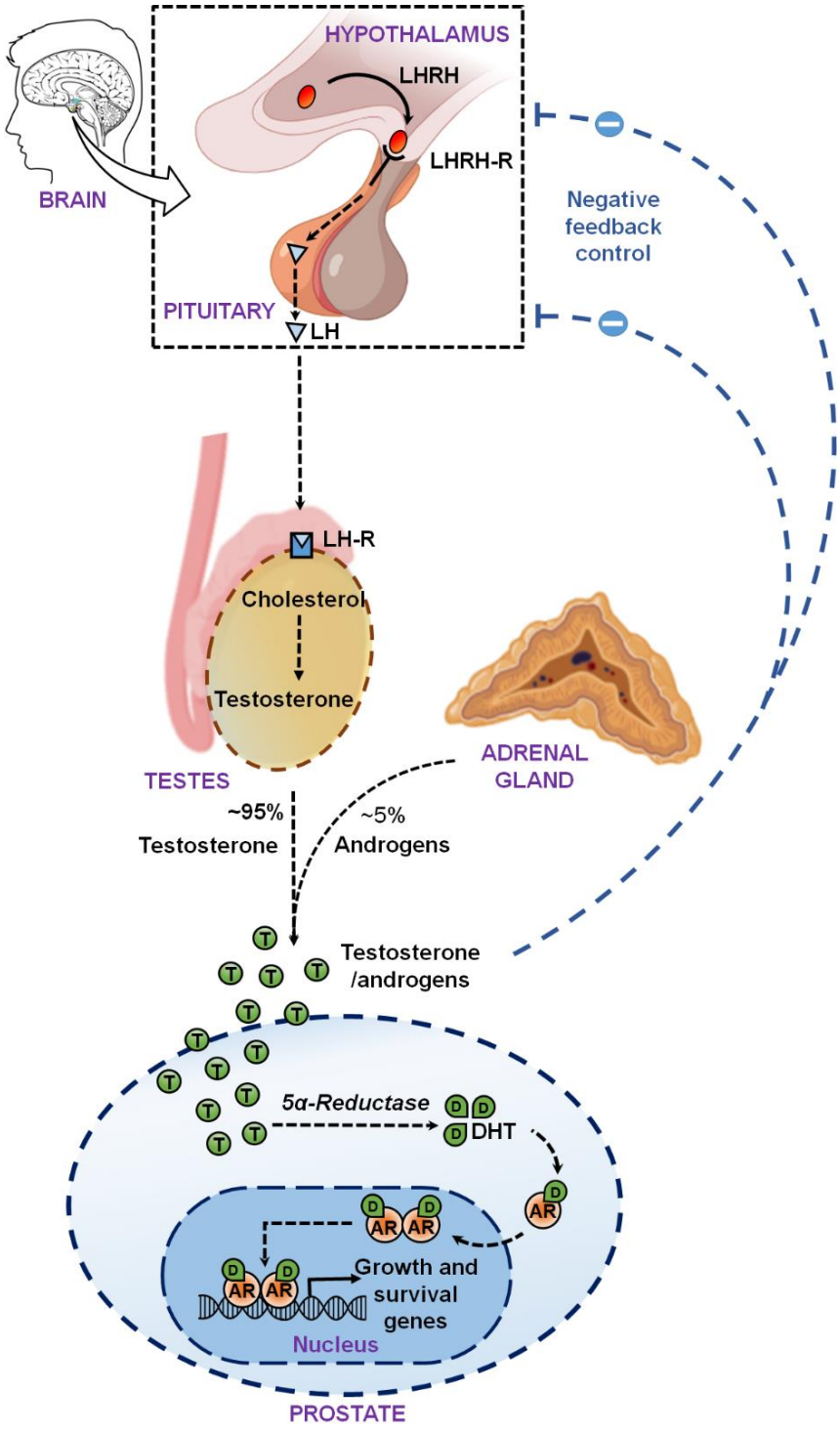

Figure 1.4: Regulation of androgen production by testes and adrenal glands.

Abbreviations: LHRH, luteinising hormone releasing hormone; LHRH-R, luteinising hormone releasing hormone receptor; LH, luteinising hormone; LH-R, luteinising hormone receptor; T, Testosterone; D, DHT (Dihydrotestosterone); AR, Androgen Receptor

1.1.4 Androgen and the androgen receptor

AR, encoded by the AR gene located on chromosome X (Xq11-12), is a ligand-activated transcription factor and member of steroid hormone nuclear receptor family. The AR is 110kDa protein, made up of approximately 919 amino acids encoded by 2757 nucleotides on eight exons (Gottlieb, Beitel, Nadarajah, Paliouras, & Trifiro, 2012; Lubahn et al., 1988; Tilley, Marcelli, Wilson, & McPhaul, 1989; van Laar, Bolt-de Vries, Voorhorst-Ogink, & Brinkmann, 1989). Wild-type full-length AR has 4 regions consisting of N-terminal ligand binding domain (NTD) encoded by exon 1, a DNA binding domain (DBD) encoded by exons 2–3, a hinge region encoded by exon 4 and a C-terminal ligand binding domain (CTD) encoded by exons 5–6 (Brinkmann et al., 1992; Jenster et al., 1991).

The function of AR is modulated after binding of agonists or antagonists to the CTD. When not bound to a ligand, AR forms a cytoplasmic complex with heat-shock proteins (HSPs) and other proteins in a conformation that prevents AR from binding to DNA (Brinkmann et al., 1999), rendering it inactive. Binding of testosterone/DHT to AR is followed by dissociation of HSPs in the cytoplasm, simultaneously accompanied by a conformational change of AR resulting in its dimerization and translocation to the nucleus. Androgen bound AR complex binds to the specific DNA sequence called AR response elements (AREs) in the regulatory (promoter / enhancer) regions of AR target genes(Brinkmann et al., 1999) (Figure 1.5) In addition, co-activators (e.g. ARA70) and corepressors proteins also bind with the chromatin bound AR complex, facilitating or preventing, its interaction with the general transcription machinery respectively. Consequently, AR binding to DNA can either stimulate or, less commonly, inhibit target gene expression (Bonora et al., 2015; Heinlein & Chang, 2002). Some of the canonical

AR target genes include PSA (also known as *KLK3* (kallikrein-related peptidase 3)), *KLK2* (kallikrein-related peptidase 3), *NKX3.1* (NK3 homebox), *FKBP5, ELL2* (Elongation factor, RNA polymerase II, 2), *SOCS2* (Suppressor of cytokine signaling 2), *PTPRM* (Protein Tyrosine Phosphatase μ) (Amler et al., 2000; S. E. DePrimo et al., 2002; H. Heemers et al., 2004; Nelson et al., 2002; Segawa et al., 2002; Waghray et al., 2001; Xu et al., 2001). Thus, androgen regulates prostate physiology, and exerts their effects through the AR.

Androgen/AR mediate key physiological processes in the prostate tissue compartments such as differentiation, secretory function, metabolism, morphology, proliferation, and survival. Androgen regulated genes are involved in cell-cycle regulation and androgen ablation therapy in PCa resulted in induction of cell-cycle arrest (Heinlein & Chang, 2004). After Hodges and Huggins first demonstrated that PCa was dependent on androgen hormones in 1941 (Huggins & Hodges, 1941), numbers of studies have revealed the elegant intercommunication between AR and the cell cycle machinery to govern receptor-dependent cellular proliferation, and that perturbations in this process occur frequently in human disease (Schiewer, Augello, & Knudsen, 2012). The role of AR and AR target genes in the regulation cell-cycle progression is further validated when androgen deprivation therapy (ADT) and/or AR silencing slows down the growth of androgen dependent cells primarily due to a block of the G1/S cell-cycle transition through AR-dependent regulation of cyclin D1, p21 and p27. Thus, AR promotes cell proliferation through regulation of the cell cycle G1/S transition only in the presence of androgen in both normal and tumour condition (Comstock & Knudsen, 2007).

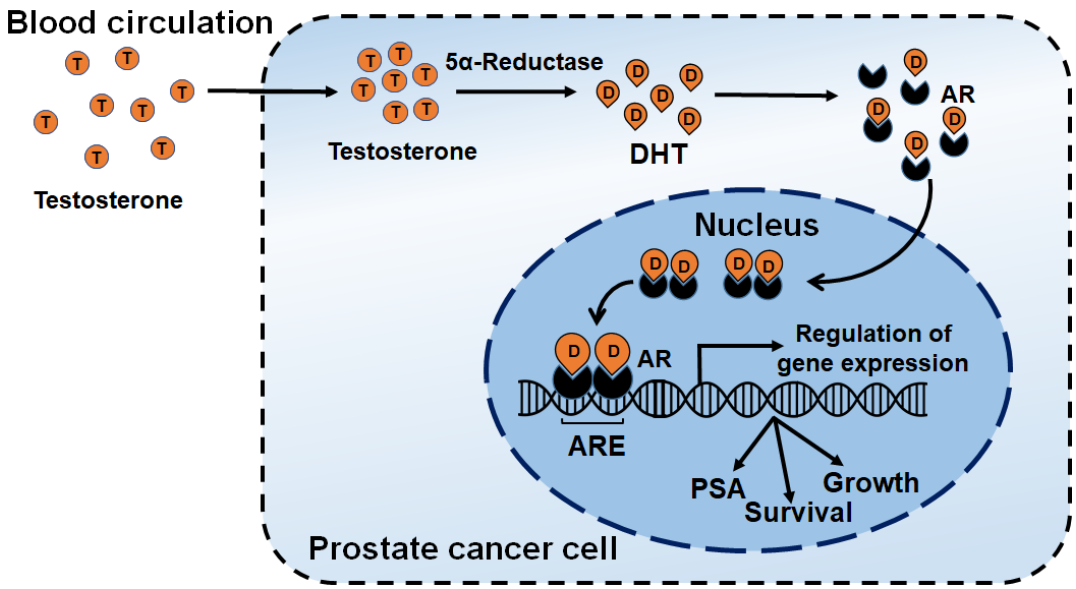

Figure 1.5 : Mechanisms of androgen receptor signalling in prostate cells.

Abbreviations: T, testosterone; D, Dihydrotestosterone; AR, Androgen receptor; ARE, androgen-responsive element; PSA, prostate-specific antigen.

AR expression and its signalling promotes growth and maturation of the prostate and the prostate normally doubles in size during puberty. After puberty AR signalling maintains homeostasis of the prostatic epithelium, promoting differentiation and maintaining a balance between proliferation and apoptosis, thereby preventing overgrowth of the prostate (Banerjee, Banerjee, Brown, & Zirkin, 2018; Mirosevich et al., 1999). AR is expressed in both stromal and epithelial cells in the prostate and this expression tends to change during PCa progression (M. Singh et al., 2014). The stromal cells start to lose AR expression as soon as it progress to early stage of PCa (M. Singh et al., 2014). The stromal cells do not appear to require AR for survival but the release of paracrine factors mediated by AR activity in stromal cells is necessary for the differentiation, growth, survival and

function of epithelial cells (Donjacour & Cunha, 1993; Prins & Birch, 1993). Androgens also act directly via epithelial AR, targeting genes that include those promoting survival of the secretory epithelia, seminal fluid proteins, factors involved in epithelial differentiation and metabolic pathway components (Balk, 2014). AR being the primary driver of primary and metastatic PCa. The AR-regulated transcriptional program switches from regulating cell differentiation and homeostatsis in the normal prostate to promoting cell proliferation and survival in PCa, resulting in continuous growth (Y. Zhou, Bolton, & Jones, 2015).

1.1.5 Effect of androgen deprivation

Androgen, acting through the AR, are required for prostate development and function (Roy et al., 1998, 1999). Therefore, androgen withdrawal largely impacts on the function of prostate gland. The loss of secretory function and decrease in cell proliferation leading to the rapid reduction in glandular size which is caused by widespread apoptosis among the epithelial cells (Medh & Thompson, 2000). For a long time, it was anticipated that the castration-induced cells death was mediated by reduced AR signalling in the epithelial cells. However, recent studies suggested that it is due to the AR in stroma that regulates the major effect observed in epithelial cells (Kurita et al., 2001; Leach et al., 2015). Further, androgen withdrawn also affects new blood vessels that the cancer cells develop to support their growth leading to the major reduction in blood flow and by apoptosis of the endothelial cells (Lissbrant, Lissbrant, Damber, & Bergh, 2001; Wikstrom, Lissbrant, Stattin, Egevad, & Bergh, 2002). Thus, castration–induced prostate involution is a cumulative effect. Thus, ADT is the primary treatment option in primary and metastatic PCa as it

supresses prostate tumour growth by reducing levels of circulating androgens and/or directly blocking the action of the AR with antagonists. ADT is also used as an adjunct to radiotherapy in some cases of high-risk and locally advanced disease, where it improves disease-free and overall survival (Kauffmann & Liauw 2017). Refer to sections 1.2.5 for more information about ADT.

1.2 Prostate cancer:

1.2.1 Incidence

PCa is the second most common cancer amongst males in Western populations and predominantly affects older men, with a median age at diagnosis of 66 years (Flaig et al., 2017). Tumours that are localised to the prostate are often slow growing and non-progressive; many such tumours do not require treatment, or can be effectively treated with surgery or radiation therapy (Dahabreh et al., 2012). However, approximately 20% of PCa patients develop advanced metastatic disease, which kills more than 3,300 men each year in Australia. Currently, more than 120,000 males are living with PCa in Australia.

1.2.2 Diagnosis of PCa

Early PCa is often asymptomatic; consequently, early PCa diagnosis is based on abnormal blood prostate specific antigen (PSA) levels followed by a trans-rectal ultrasound guided biopsy, digital rectal examination (DRE), or both. Blood PSA is one of the most widely used tumour markers for PCa screening, which correlates strongly with the risk of harbouring disease (Stephan, Rittenhouse, Hu, Cammann, & Jung, 2014) (Figure 1.6). DRE is another important physical examination method to screen abnormalities in the prostate gland, which examines the presence of nodules, or hard tissue consistency (Ojewola, Jeje, Tijani, Ogunjimi, & Anunobi, 2013). DRE or PSA results that are indicative of PCa are confirmed by histopathological examination of tissue by biopsy, the definitive diagnostic tool for PCa (Heidenreich, 2011; N. Mottet et al., 2011). Occasionally, PCa is diagnosed

during screening for other symptomatic genito-urinary conditions like epididymitis, orchitis, prostatitis or benign prostatic hyperplasia (BPH) (L. Cheng, Montironi, Bostwick, Lopez-Beltran, & Berney, 2012; Chou et al., 2011; Heidenreich et al., 2011).

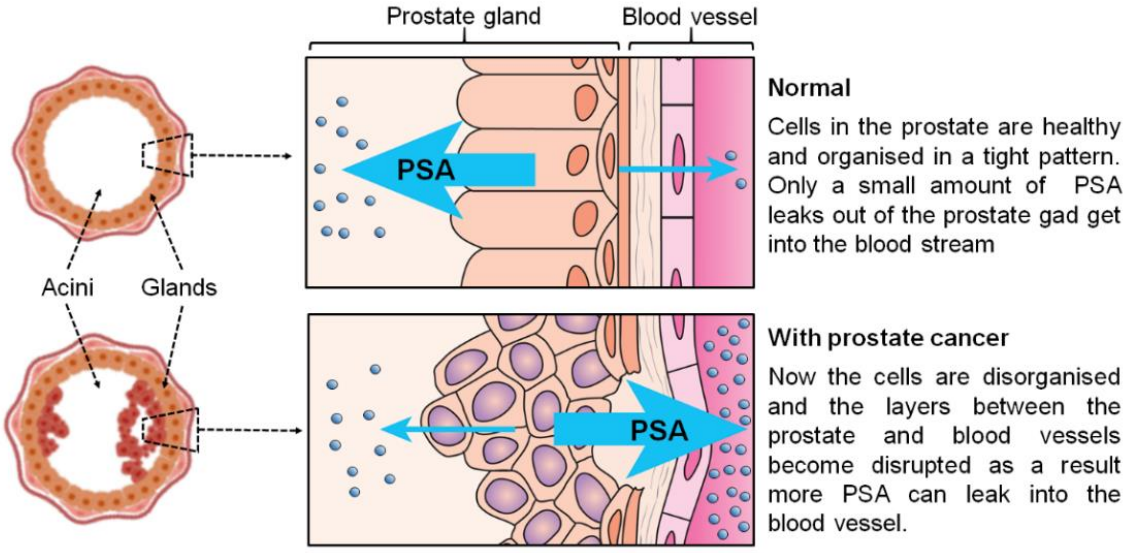

Figure 1.6 : Schematic of PSA secretion into the blood vessel. PSA as diagnostic/prognostic marker of prostate cancer. Development of PCa disrupts the prostate tissue structure and organization leading to leakage of secreted PSA into the nearby blood vessels. PSA as diagnostic/prognostic marker of prostate cancer. Development of PCa disrupts the prostate tissue structure and organization leading to leakage of secreted PSA into the nearby blood vessels. As a result, serum PSA level increases, which is why serum PSA level is used as diagnostic/prognostic marker for PCa.

Source https://www.theprostatecentre.com/prostate-information/the-psa-test/

1.2.3 Gleason grading system

The Gleason grading system (Gleason score) is used to diagnose disease and determine prognostic outcomes using samples collected at prostate biopsy (Pierorazio, Walsh, Partin, & Epstein, 2013). The Gleason scoring system involves assessment of histological properties of PCa cells under a light microscope where scores are assigned based on 5 distinct patterns/grades. The scoring system (ranging from 2-10) is used to grade the prostate tissue and is currently the best measure of a particular tumour's probability of metastasising (R. B. Shah, 2009). An overall scoring comprising the most prevalent pattern and the second most prevalent pattern (primary + secondary Gleason grade) are added to generate a Gleason score (R. B. Shah, 2009; Shore, 2014). A schematic of the Gleason grades is shown in Figure 1.7. Low-grade (Gleason score 6 and 7 (3+4)), or low-risk, PCa usually grows slowly and is less likely to spread. Higher grade PCa (Gleason score 7 (4+3) and above) are more likely to grow quickly and spread to other body parts including bone, lymph node and visceral organs and are associated with higher rates of cancer specific mortality. This scoring system is useful for assessment of overall tumour behaviour (aggressiveness), which helps in staging of PCa and appropriate treatment selection (Gleason & Mellinger, 2017).

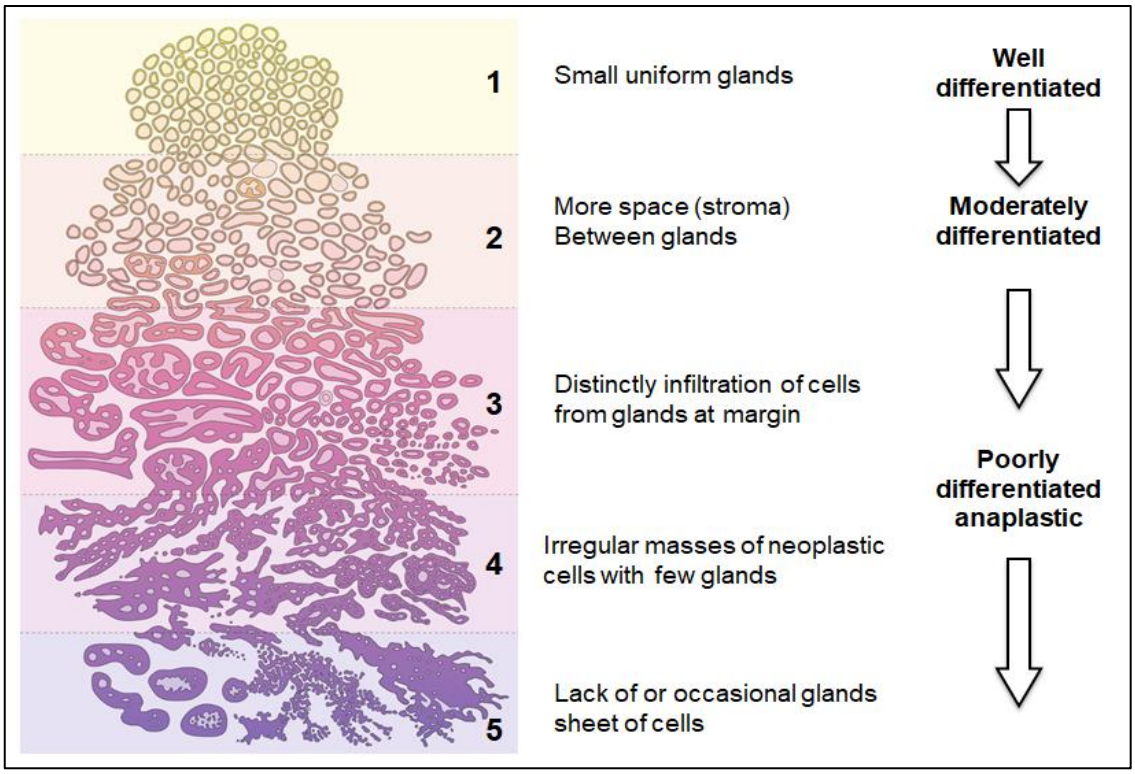

Figure 1.7: Histological patterns of PCa cells representing Gleason grades from 1 – 5 (Gleason 1966).

Prostate tumour grading and scoring system developed by Donald Gleason and is a surrogate for tumour aggressiveness (modified figure) (Sathianathen, Konety, Crook, Saad, & Lawrentschuk, 2018).

In addition to the Gleason scoring system, PCa can be classified according to the spread of the disease by the Tumour, Node and Metastases (TNM) classification system, which was first adopted in 1975 by the Joint Committee for Cancer (AJCC). Multiple revisions to this system have occurred over time, with the most recent in 2010. The TNM classification is associated with survival and prognosis of the patient (Shore, 2014) and is the most widely used method for cancer reporting and staging, thereby facilitating treatment decision making.

Table 1.2: TNM classification of PCa (Mottet et al. 2017)(Nicolas Mottet et al., 2017); G indicated grade; M, metastasis; N, Node; PSA, Prostate–specific antigen; T, tumour.

T - Primary Tumour	
TX	Primary tumour cannot be assessed
T0	No evidence of primary tumour
T1	Clinically inapparent tumour that is not palpable
T1a	Tumour incidental histological finding in 5% or less of tissue resected
T1b	Tumour incidental histological finding in more than 5% of tissue resected
T1c	Tumour identified by needle biopsy (e.g. because of elevated prostate-specific antigen (PSA) level)
T2	Tumour that is palpable and confined within the prostate
T2a	Tumour involves one half of one lobe or less
T2b	Tumour involves more than half of one lobe, but not both lobes
T2c	Tumour involves both lobes
T3	Tumour extends through the prostatic capsule[1]
T3a	Extracapsular extension (unilateral or bilateral) including microscopic bladder neck involvement
T3b	Tumour invades seminal vesicle(s)
T4	Tumour is fixed or invades adjacent structures other than seminal vesicles: external sphincter, rectum, levator muscles, and/or pelvic wall
N - Regional Lymph Nodes	
NX	Regional lymph nodes cannot be assessed
N0	No regional lymph node metastasis
N1	Regional lymph node metastasis
M - Distant Metastasis	
M0	No distant metastasis
M1	Distant metastasis
M1a	Non-regional lymph node(s)
M1b	Bone(s)
M1c	Other site(s)

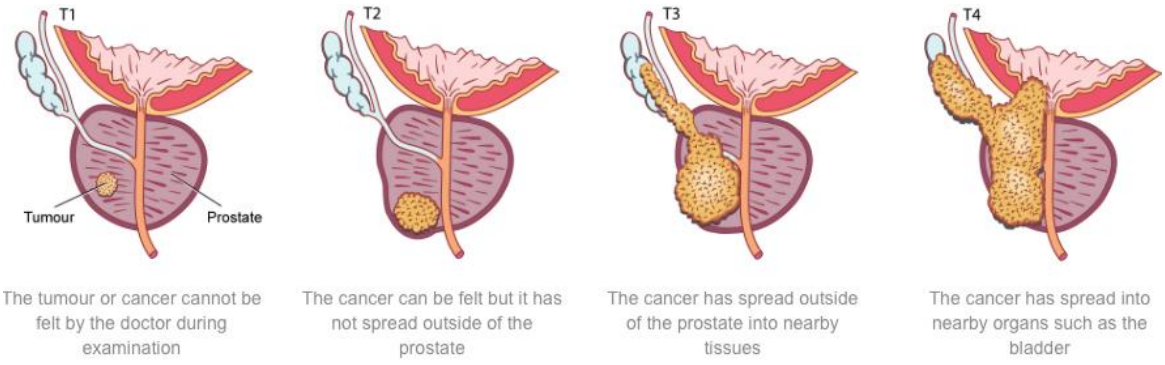

Figure 1.8: The tumor–nodes–metastasis (TNM) system recognizes four stages of local tumour growth: T1 (incidental); T2 (confined within the prostate); T3 (extending through the prostatic capsule); and T4 (invading neighbouring organs). Source: https://www.prostate.org.au/awareness/for-recently-diagnosed-men-and-their-families/partners-and-carers/diagnosis/grading-and-staging-of-prostate-cancer/

Table 1.3: Anatomical staging/prognostic groups of PCa (Shore et al 2014).

Group	T	N	M	PSA	Gleason
I	T1a–c	N0	M0	PSA <10	Gleason ≤6
	T2a	N0	M0	PSA <10	Gleason ≤6
	T1–2a	N0	M0	PSA X	Gleason X
IIA	T1a–c	N0	M0	PSA <20	Gleason 7
	T1a–c	N0	M0	PSA ≥10<20	Gleason ≤6
	T2a	N0	M0	PSA ≥10<20	Gleason ≤6
	T2a	N0	M0	PSA <20	Gleason 7
	T2b	N0	M0	PSA <20	Gleason ≤7
	T2b	N0	M0	PSA X	Gleason X
IIB	T2c	N0	M0	Any PSA	Any Gleason
	T1–2	N0	M0	PSA ≥20	Any Gleason
	T1–2	N0	M0	Any PSA	Gleason ≥8
III	T3a–b	N0	M0	Any PSA	Any Gleason
IV	T4	N0	M0	Any PSA	Any Gleason
	Any T	N1	M0	Any PSA	Any Gleason
	Any T	Any N	M1	Any PSA	Any Gleason

M indicated metastasis; N, Node; PSA, Prostate –specific antigen; T, tumor. The staging of the PCa when either PSA or Gleason is not available, grouping should be determined by T stage and/or either PSA or Gleason as available.

1.2.4 Risk stratification

The confirmed cases of PCa are stratified at diagnosis into groups based on their risk of disease progression. The D'amico risk stratification system is commonly used to access risk of biochemical recurrence over a 5 year period following treatment in PCa (Rodrigues et al., 2012). The classifier used pre-treatment serum PSA, Gleason score/grade and number and extent of cancer involvement in the biopsy cores /TMA stage to assign the patients into either low, intermediate or high risk groups. In some cases, genomic profile of tumour, imaging studies are used to assess for the extra-prostatic extension or distant metastasis of the cancer depending upon the initial clinical staging.

Importantly, the initial management of newly diagnosed PCa needs to incorporate a consideration of prolonged natural history of the disease and the risk for progression to disseminated, potentially fatal disease.

1.2.5 Treatment of prostate cancer

Currently, there are various therapeutic approaches for treating PCa. Choosing the optimal treatment regime for PCa patients depend on their age, general health and disease stage. Treatment approaches include the following: 1) watchful waiting/active surveillance for stage I; 2) Radical prostatectomy and/or radiation therapy (external beam or brachytherapy) for stage II; 3) Radiation with androgen deprivation therapy (ADT) for stage III; and 4) ADT for stage IV (Heidenreich, 2011; Mottet et al., 2011). Newer treatments are being constantly developed, and improvements are continuously being made in terms of how current and emerging treatments are applied (Figure 1.9).

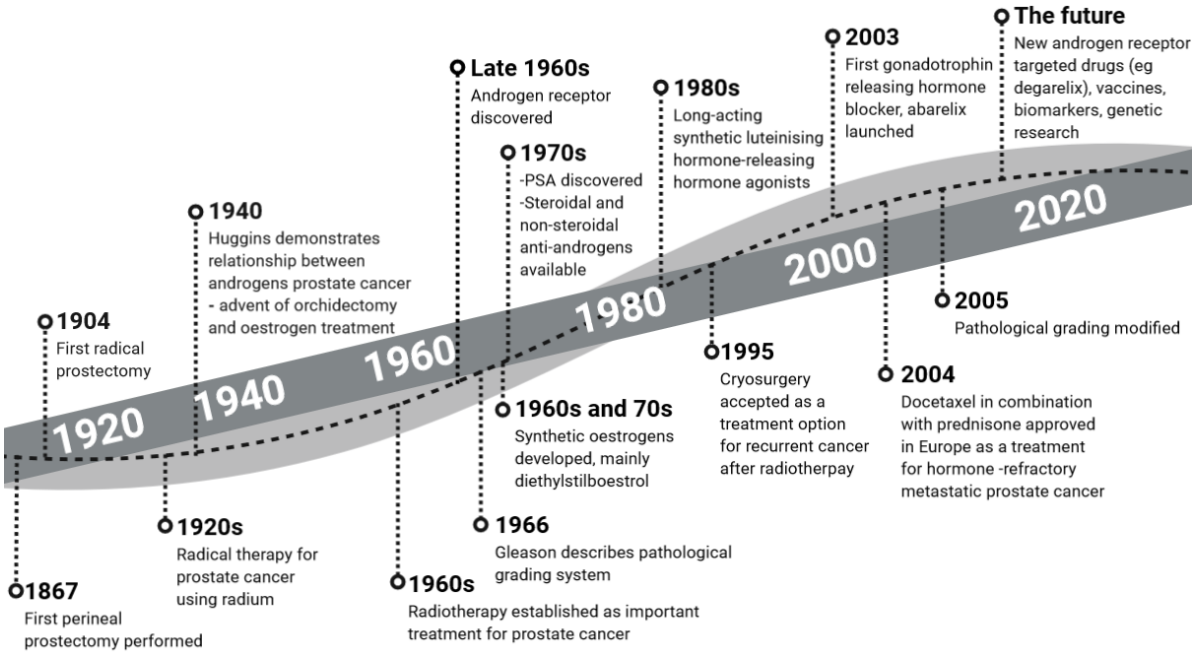

Figure 1.9: Timeline with the key milestones in historical development of treatment of PCa (Drudge-Coates, 2010). Created with BioRender.com

1.2.5.1 Treatment of localized and locally advanced PCa

Treatment and management decisions for localized and advanced PCa are based on disease risk stratification. Low-risk cancers are often slow growing, clinically insignificant and may not require active intervention (O'Donnell & Parker, 2008). Side effects of invasive treatment such as surgery/radiation therapy can have a more severe impact on quality of life than the cancer itself, particularly in an older patients with low-grade disease. In such cases, active surveillance for signs of PCa progression (through PSA testing, DRE, serial biopsies and radiological examination) is regarded as the best option to avoid active intervention in patients with tumours that are not likely to affect quality or length of life (Morash et al., 2015). For intermediate grade/stage disease that is confined to the primary tumour site,

radical prostatectomy or radiation therapy are the standard treatments with curative intention (Hasegan, 2014; Pisansky, 2005). For higher risk group patients, radical prostatectomy in combination with radiation therapy improves overall survival (Jang et al., 2018).

1.2.5.2 Systemic treatment of metastatic prostate cancer

Despite of high post-treatment survival rates, a significant proportion of cases (27–53%) develop biochemical recurrence (BCR) after primary curative therapy, either due to local disease recurrence or metastasis (Artibani, Porcaro, De Marco, Cerruto, & Siracusano, 2018; Van den Broeck et al., 2020). A subset of men with BCR are characterized by high metastatic potential and require early aggressive clinical intervention whereas others will have local recurrence and may be curable with salvage treatment. Overall, 10-20% of men with PCa develop metastatic disease after treatment and approximately 5% of men also have metastatic disease when they are diagnosed (National Cancer Control Indicators, 2019; Merseburger, Bellmunt, Jenkins, Parker, & Fitzpatrick, 2013).

1.2.5.2.1 Treatment of castration sensitive PCa

Hormonal manipulation to decrease the circulating androgen levels, commonly referred as ADT, reduces circulating testosterone level by 90-95% and is the primary treatment strategy for metastatic PCa (Norris et al., 2017) (Figure 1.10). ADT causes cancer regression and a decrease in serum PSA in the vast majority of PCa patients. ADT can be achieved either by surgical (orchitectomy; removal of testicles) or chemical castration. Orchiectomy was regarded as most

effective ADT but had physical, emotional and psychological side-effects in men. Thus, orchiectomies have now been replaced in favour of luteinizing hormone releasing hormone (LHRH) agonists and antagonists. LHRH agonists bind to their receptors in the pituitary and increase lutenizing hormone (LH) and follicule stimulating hormone (FSH), which stimulates testosterone production in the testes and the adrenal gland; as such, LHRH agonists are also known as gonadotrophin-releasing hormone (GnRH) analogues. Constant LHRH stimulation with GnRH analogues eventually results in significantly reduced production of LH/FSH as a result of a feedback mechanism, leading to decrease circulating testosterone levels (Labrie et al., 1980; Labrie et al., 2005). LHRH agonists can be detrimental to some men due to the initial rise in circulating testosterone level, or 'flare', upon exposure. Some of the side effects of 'flare' phenomenon includes erectile dysfunction, hot flashes, urinary retention, ureteral obstruction, anaemia and muscle wasting, (Thompson, 2001). In these patients, LHRH antagonists, which competitively bind to LHRH receptors and prevent the release of LH / FSH, are a safer therapeutic approach (Gordon & Hodgen, 1992).

Beside surgical and chemical castration, anti-androgen also known as AR antagonists are used for the treatment of advance PCa. Anti-androgens are a class of steroidal or non-steroidal molecules that inhibit AR signalling by competitively preventing binding of endogenous androgens to the AR (Chen, Clegg, & Scher, 2009). Anti-androgens are often used in combination with ADT to improve treatment efficacy (Yang et al., 2019). Commonly used anti-androgens are Bicalutamide, Nilutamide and Flutamide.

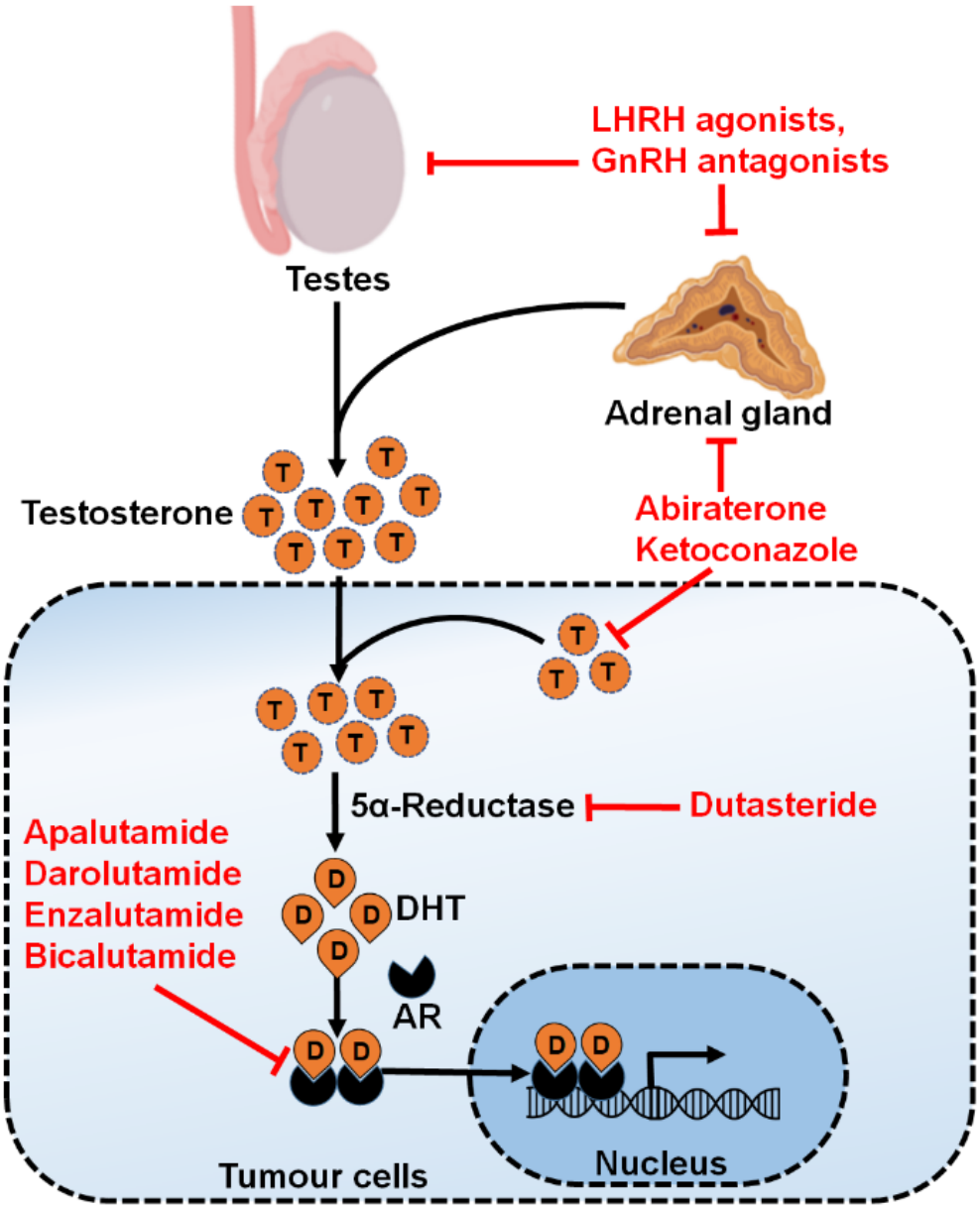

Figure 1.10: Current agents (red) that target androgen signalling axis in PCa (AR, androgen receptor; DHT, dihydrotestosterone; GnRH, gonadotropin-releasing hormone; LHRH, luteinizing-hormone –releasing hormone; T=testosterone)(Raj, Selth, Day, & Tilley, 2015). Apalutamide is used in patients with castrate-resistant prostate cancer (CRPC), who present with rising PSA levels, despite appropriate ADT (Alkhudair, 2019). Currently, a new generation of anti-androgen drugs are available and further new drugs are under clinical study to test their effectiveness in patient with CRPC.

Initial responses to ADT and first generation anti-androgens are usually very good, however all patients eventually relapse (most after approximately 18-24 months) and develop an incurable and lethal form of the disease called castrate-resistant PCa (CRPC) (Butler, Centenera, & Swinnen, 2016; Pienta & Bradley, 2006; Scher, Buchanan, Gerald, Butler, & Tilley, 2004; S. Sun et al., 2010). While several oncogenic pathways can contribute to castration-resistance, AR remains the most important driver in this disease context (Figure 1.11) (Norris et al., 2017).

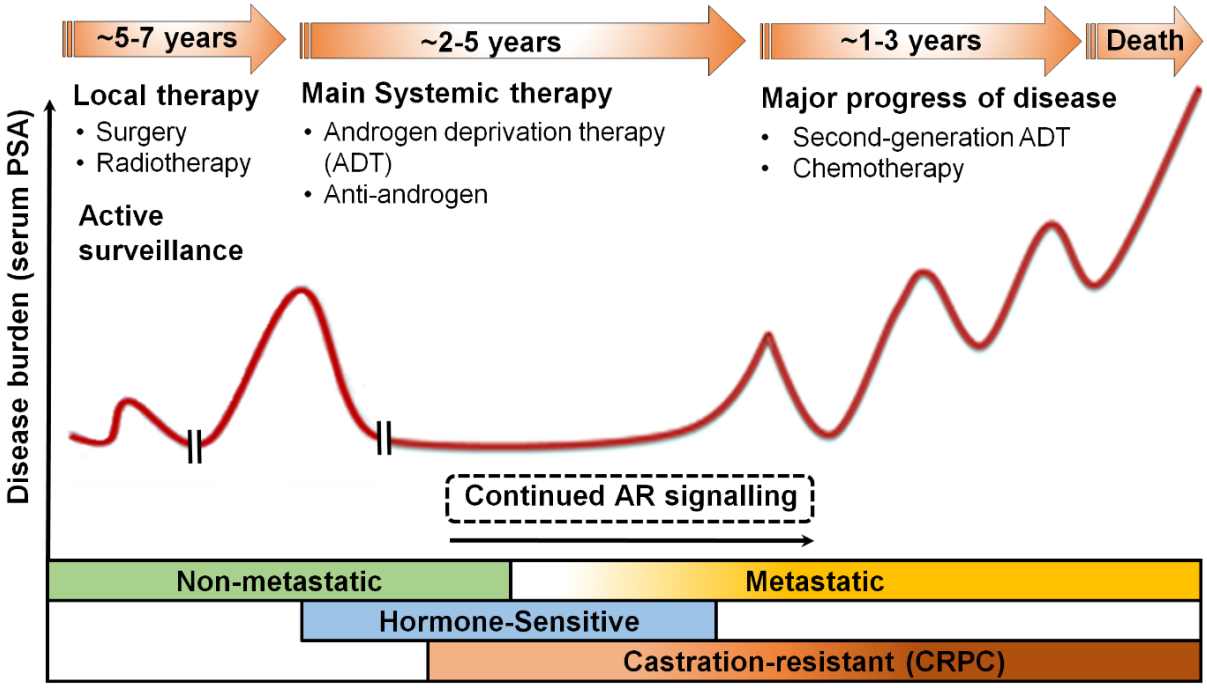

Figure 1.11: Disease progression and treatment option in PCa.

[Image concept-(Kohli & Tindall. Myoclin Proc 2010; 85:77-86]

Treatment of CRPC

The continued role of AR in CRPC led to the development of so-called second generation anti-androgens (Tran et al., 2009), which are more potent than the first-generation agents. Second-generation anti-androgens include Enzalutamide, Darolutamide and Apalutamide (Antonarakis, 2013; Rathkopf et al., 2017), all of which significantly improve overall survival and progression free survival in men with CRPC (Chong, Oh, & Liaw, 2018; Linder, van der Poel, Bergman, Zwart, & Prekovic, 2018).

Chemotherapy, radiopharmaceuticals, and immunotherapy are other additional treatment modalities for CRPC and mCRPC. Docetaxel and cabazitaxel are both taxane chemotherapies that are improve overall survival in men with CRPC (Powers et al., 2020). Radium-223 dichloride is a calcium mimetic that emits cytotoxic alpha radiation, which is incorporated in stroma formed by bone metastases during treatment and is associated with improved outcomes for men with bone metastatic disease (Parker et al., 2013). Sipuleucel-T is a dendritic cell vaccine is used to treat asymptomatic or minimally symptomatic CRPC.

Table 1.4. Agents currently available in Australia for the treatment of PCa. Reproduced, with permission from Reeves and Corcoran *et al.* (Reeves & Corcoran, 2020).

Agent	Mechanism of action	Adverse effects
Chemotherapy		
Docetaxel	Taxane chemotherapy	Myelosuppression, neuropathy, fatigue, nausea/vomiting/diarrhoea, peripheral oedema
Cabazitaxel		
Androgen signalling-targeted inhibitor		
Abiraterone	CYP17A1 inhibitor (prevents androgen synthesis)	Hypertension, hypokaelaemia, fluid retention, cardiac disorders, liver function test abnormalities (low-dose prednisolone is co-administered to reduce mineralocorticoid excess)
Enzalutamide	AR inhibitor	Fatigue, seizures, back pain, arthralgia, peripheral oedema, headache, hypertension
Apalutamide		Hypertension, rash, gastrointestinal upset, fatigue, hypothyroidism, fracture, falls, QT prolongation

1.2.6 Mechanisms of resistance to ADT

1.2.6.1 Reactivation of AR signalling

The mechanisms for the development of CRPC has been extensively studied in the last few decades (Chandrasekar et al., 2015). It is understood that androgen dependent PCa cells undergo specific genetic and epigenetic changes to adapt to the androgen depleted microenvironment (Ahmed & Li, 2013; Zong & Goldstein, 2013). Persistent AR signalling in CRPC is frequently due to AR gene amplification, which occurs at low frequency (~1%) in primary tumours but at high frequency (45-54%) in CRPC (Abida et al., 2019; Cancer Genome Atlas Research, 2015; Charlie D Chen et al., 2004; Catherine S Grasso et al., 2012; Koivisto et al., 1997; Dan Robinson et al., 2015; Taplin et al., 1995; Visakorpi et al., 1995). Increased AR expression promotes resistance to ADT by sensitizing cells to low levels of serum androgen (Visakorpi et al., 1995) and various studies have linked the overexpression of AR with the development of CRPC (C. D. Chen et al., 2004; Holzbeierlein et al., 2004; Stanbrough et al., 2006). The incidence of AR gene amplification is between 20 and 33% in CRPC patients (Hu, Denmeade, & Luo, 2010).

Additionally, various point mutations have been identified in the *AR* gene itself (Sack et al., 2001; Suzuki et al., 1996), which occur in a proportion of CRPC tumour cells, are also important in resistance to ADT (Steinkamp et al., 2009). The rate of AR mutations accounts for 5-30% of post-treatment tumours but infrequently in primary PCa prior to treatment (Coutinho, Day, Tilley, & Selth, 2016). CRPC-associated AR mutations mostly occur within the ligand binding domain of the AR where they promote promiscuous binding and activation by alternative ligands such

as estrogens, progesterone or anti-estrogens (Eisermann, Wang, Jing, Pascal, & Wang, 2013; Lallous et al., 2016).

Gain-of-function mutations enabling the AR to recover activity in the hypoandrogen environment which have been associated with the progression to CRPC (Feldman & Feldman, 2001), this include mutations, deletions and inversions at the ligand binding site leading to ligand-independent activation (Nyquist et al., 2013), and gene amplifications. Other mechanisms that maintain AR activity in the castrate environment include active AR variants (ARVs). These AR-Vs are alternately spliced isoforms of the AR mRNA that encode the N-terminal transactivating domain (NTD) and DNA-binding domain (DBD) but lack the C-terminal ligand binding domain (Dehm & Tindall, 2011; Y. Qu et al., 2015). Approximately 20 AR-Vs have been identified in cell lines and clinical specimens, of which several are constitutively active and can signal in the absence of androgen (Jernberg, Bergh, & Wikström, 2017; Kallio et al., 2018).

Another strategy adopted by PCa in response to ADT is increased intratumoral production of androgen production via upregulation of several steroidogenic enzymes including cytochrome P (CYP) 17A1, fatty acid synthase (FASN), hydroxysteroid dehydrogenase (HSD) 3B1, HSD17B3, CYP19A1, SRD5A1, and UGT2B17 in CRPC (Montgomery et al., 2008). These enzymes enhance the conversion of intratumoral androgen precursors into androgens to activate AR (Chandrasekar et al., 2015; Locke et al., 2008). Cholesterol is a major precursor for androgens and its levels influence PCa progression (Armandari, Hamid, Verhaegh, & Schalken, 2014), Thus, lipid metabolism is associated with the progression of CRPC. Drugs targeting intratumoral and adrenal androgen biosynthesis (e.g. abiraterone acetate) effectively suppress CRPC growth and are

used in this clinical context (W. Kim et al., 2014; Leibowitz-Amit et al., 2014; Mostaghel, 2014; Zobniw, Causebrook, & Fong, 2014).

1.2.6.2 "AR indifferent" prostate cancer

A subpopulation (20-25%) of patient display independent mechanism of anti-androgen resistance and progress to an "AR indifferent" state in which AR expression may or may not be not be retained (Eric G Bluemn et al., 2017). The major "AR indifferent" prostate cancer subtypes is neuroendocrine prostate cancer (NEPC) (L. Ellis & Loda, 2018). NEPC develops as a transdifferentiation from prostate adenocarcinoma, in response to ADT and/or treatment with inhibitors targeting AR signalling pathways (Lipianskaya et al., 2014). During NEPC development, cells lose their granular structure and demonstrate small cell neuroendocrine-like morphology, positive for typical neuroendocrine markers such as neurospecific enolase (NSE), synaptophysin (SYP), and chromogranin A (AHGA) but may to may not affect AR and AR-regulated gene expression (Ather, Abbas, Faruqui, Israr, & Pervez, 2008). NEPC that arose after failure of second generation AR signalling inhibitors (i.e. Abiraterone, Enzalutamide) is referred to as treatment emergent NEPC which is very aggressive and causes death of patient within 2 years of diagnosis (Davies, Beltran, & Zoubeidi, 2018). Recently, clinical and genomic profiling data suggest that NEPC may also originate *de novo* from small population of prostatic neuroendocrine cells but this is very rare (~1%) (Epstein et al., 2014; Grigore, Ben-Jacob, & Farach-Carson, 2015; Santoni et al., 2014).

Emerging evidence suggests treatment emergent NEPC is the consequence of an adoptive response to ADT via lineage/cellular plasticity and activation of

alternative pathways, thereby sustaining tumor growth independently from AR (Aggarwal, Zhang, Small, & Armstrong, 2014; L. Ellis & Loda, 2018; Le Magnen, Shen, & Abate-Shen, 2018; Watson, Arora, & Sawyers, 2015). Since AR signalling is required for epithelial cell differentiation during prostate development, inhibition of AR-driven pathway likely initiates developmental reprogramming of prostate adenocarcinoma to neuroendocrine tumours through a transdifferentiation mechanism. Thus, ADT has been shown to contribute to the emergence of NEPC via upregulation of AR-repressed genes that can promote transdifferentiation (Komiya et al., 2013). For example, *SOX2* is directly repressed by the AR, promotes lineage plasticity in NEPC (Mu et al., 2017). *BRN2,* which is also a neural transcription factor repressed by AR that is upregulated by the AR antagonist Enzalutamide (Bishop et al., 2017). BRN2 is required for treatment emergent NEPC and acts partly by regulating SOX2 (Bishop et al., 2017). Furthermore, multiple genetic and epigenetic and transcriptional events likely facilitate plasticity and transdifferentiation in treatment emergent NEPC. Loss of tumour suppressors *PTEN*, *RB1* and *TP53* and amplification of *MYCN* and *AURKA* are some of the common genetic events (Mosquera et al., 2013; H.-L. Tan et al., 2014) which enable lineage switching (Ku et al., 2017). Several cell-cycle genes (i.e. UBE2C, cyclin D1, Src family kinase-FYN, and polo-like kinase PLK1) have also been shown to be frequently amplified and/or overexpressed in NEPC, thus supporting their role in driving uncontrolled NEPC growth and proliferation (Grobholz et al., 2005; Gururajan et al., 2015; Pernicová et al., 2014). Amplification of *MYCN* has been shown to drive progression to NEPC by activation of an EZH2 mediated transcriptional program (Dardenne et al., 2016). EZH2 is a histone

methyltransferase that regulates cell pluripotency by altering gene expression via methylation of histone H3 lysine 27 (H3K27) (Dardenne et al., 2016).

Recently, profiling of metastatic CRPCs revealed another subtype or AR indifferent PCa, called double negative PCa (DNPC). DNPC subtype is negative for both AR and NEPC markers which has been proposed to be a transition state to NEPC (Eric G Bluemn et al., 2017; W. Wang & Epstein, 2008). DNPC arises in patients after treatment with more effective AR antagonists such as enzalutamide and abiraterone and the *In vitro* work showed that these DNPCs rely on FGF and MAPK activity for growth and targeting which allows these tumours to bypass the requirement for AR signalling (Eric G Bluemn et al., 2017; E. G. Bluemn et al., 2017). Although novel molecular targeting therapy against EZH2 and AURKA are currently under development, the treatment option for the AR-indifferent PCa are limited to chemotherapy (Akamatsu, Inoue, Ogawa, & Gleave, 2018).

1.3 Normal prostate metabolism

The major function of the normal prostate gland is to produce prostatic fluid which contains high concentration of zinc, citrate and PSA (enzyme responsible for liquefying semen). The capacity of producing and secreting an enormous quantity of citrate is the unique feature of the prostate gland, which is almost 240-1300 fold higher than that of plasma citrate levels (Leslie C. Costello & Franklin, 1991; L. C. Costello & Franklin, 2000; Kavanagh, 1985). The normal prostate tissues are further characterized by the ability to uptake and accumulate large concentrations of zinc (L. C. Costello, Feng, Milon, Tan, & Franklin, 2004; L.C. Costello & Franklin, 1998). The reason behind high concentrations of citrate production is high concentrations of zinc (~0.8–1.5 mM) which disrupts TCA cycle by inhibiting mitochondrial (m-) aconitase, a key enzyme of TCA that converts citrate to isocitrate (L. C. Costello, Franklin, Feng, Tan, & Bagasra, 2005) resulting in the accumulation and secretion of citrate in the prostate gland. Thus, citrate is mainly an end product of metabolism which is secreted as a major component of prostatic fluid as a result of a truncated TCA cycle (Figure 1.12). By contrast, in “typical” cells, citrate is an essential intermediate of TCA cycle which could either be utilized to produce ATP through mitochondrial oxidation or shuttled out of mitochondria into cytoplasm where it is cleaved by enzyme citrate lyase (ACYL) to produce acetyl CoA for fatty acid synthesis. The complete oxidation of citrate yields 12 mol of ATP/mol of citrate and 24 mole of ATP/mole of glucose. By accumulating citrate, normal prostate epithelial cells appear to halt the TCA cycle and therefore act very different to the majority of cells in the body in the production of ATP. Although, the function of citrate as a component of prostatic fluid is virtually unknown, its likely to contribute the seminal fluid buffering capacity, chelation of calcium, zinc and other cations, and as an

energy source to maintain sperm viability and/or for capacitation processes (ARVER, 1982; Ford & Harrison, 1984; Hicks, Martínez-Manautou, Pedron, & Rosado, 1972; Hori, Masuda, Kobayashi, & Kawakami, 2017; Medrano et al., 2006; Searcy & Simms, 1967; Tomlins et al., 1998).

There are few studies that have focused on role of AR in normal prostate cell metabolism (L. C. Costello, Liu, & Franklin, 1996; L.C. Costello, Y. Liu, J. Zou, & R.B. Franklin, 2000) and were focused on citrate metabolism and fatty acid synthesis. Studies conducted with rat ventral prostate (VP) epithelial cells and an in-vivo castration study demonstrated m-aconitase as a regulatory and regulated enzyme in prostate epithelium and hence, citrate oxidation (Leslie C. Costello, Liu, & Franklin, 1995). Androgens were found to induce pyruvate oxidation by increasing in the expression of pyruvate dehydrogenase E1 component subunit alpha (*PDHE1α*) resulting in an increase in acetyl-CoA.(L. C. Costello, Y. Liu, J. Zou, & R. B. Franklin, 2000). In addition, androgens were also reported to regulate amino acid metabolism by regulating the genes responsible for aspartate uptake and transamination [e.g. aspartate transporter (*EAAC1*) and aspartate aminotransferase (*mAAT*) genes] (L. C. Costello, Akuffo, & Franklin, 1988; L. C. Costello et al., 2000; R.B. Franklin, Brandly, & Costello, 1982). Also, the evidence of increased expression of *mAAT* and *PDHE1α* in PC3 cells expressing AR (Juang, Costello, & Franklin, 1995), and in isolated pig prostate epithelial cells (Qian, Franklin, & Costello, 1993) with DHT treatment and increased *PDHE1α* expression in rat ventral prostate epithelial cells(L.C. Costello et al., 2000) with DHT treatment are some of the examples of androgen related modulation of genes expression and hence normal prostate metabolism.

Few studies have tried to relate androgen and lipid metabolic processes in normal prostate. It is documented that androgens play an essential role in regulating the expression of key enzymes involved in lipid metabolism in prostate (Butler et al., 2016). Castration of the rat or monkey results in repression of lipogenic enzymes including ATP citrate lyase (ACLY), acetyl-CoA-carboxylase (ACC), and fatty acid synthase (FASN) and decreased total prostatic lipid content. On the other hand, androgen administration after castration restored these lipogenic enzyme activities and lipid levels to baseline (Arunakaran, Aruldhas, & Govindarajulu, 1987; Arunakaran, Aruldhas, & Govindarajulu, 1990; Arunakaran, Balasubramanian, Srinivasan, Aruldhas, & Govindarajulu, 1992; H. Heemers et al., 2003; Nyden & Williams-Ashman, 1953) supporting the involvement of androgen in normal prostate lipid metabolic process.

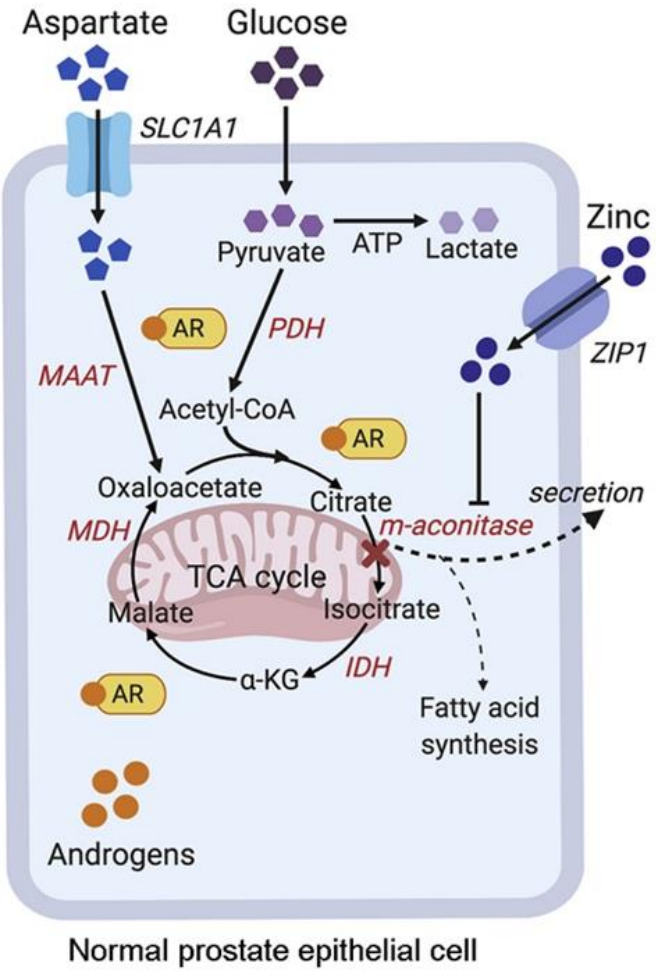

Figure 1.12: Secretion of citrate in normal prostate gland (Mah, Nassar, Swinnen, & Butler, 2019).

Abbreviations: TCA, tricarboxylic acid cycle; PDH, pyruvate dehydrogenase; MAAT, aspartate aminotransferase; AR, androgen receptor; FFAs, lipids or free fatty acids; MDH, malate dehydrogenase; a-KG, alpha ketoglutarate

1.4. Androgen and lipid metabolism in prostate cancer

Metabolic alterations in citrate production are characteristically associated with neoplastic transformation of human prostate epithelial cells (Leslie C. Costello & Franklin, 1991). During malignant transformation, the decrease in the expression of zinc transporters (ZIPs) (Desouki, Geradts, Milon, Franklin, & Costello, 2007; Renty B. Franklin et al., 2005) decreases the high level of zinc and hence, m-aconitase is no longer inhibited, thus citrate is further oxidized via TCA cycle resulting in the metabolic transformation of citrate producing cells into citrate utilizing cells (L. C. Costello et al., 2005). Thus, PCa cells are more oxidative compared to normal prostate cells and hence, reactivate the TCA cycle to oxidize citrate for energy production. In addition, instead of glucose, fatty acids become the dominant bioenergetic substrate for energy generation through the TCA cycle (Mah et al., 2019). Alternatively, citrate may be used for lipid biosynthesis through androgen-mediated activation of lipogenic enzymes which includes increased *de novo* lipogenesis, lipid uptake and lipid catabolism (J. A. Menendez & R. Lupu, 2007). Experimental studies have reported that the exposure of androgen dependent PCa cell lines to natural or synthetic androgens leads to a marked accumulation of lipid droplets in the cytoplasm, largely via increased synthesis of fatty acids and cholesterol (Johannes V Swinnen, Esquenet, Goossens, Heyns, & Verhoeven, 1997; J. V. Swinnen, Ulrix, Heyns, & Verhoeven, 1997). Highly proliferative cancer cells often have a higher demand for lipids and exhibit an abnormally active lipogenesis (Beloribi-Djefaflia, Vasseur, & Guillaumond, 2016). Since, lipid supplies energy, synthesize the cellular membrane and provide signaling molecules (Accioly et al., 2008; Dang, Chen, & Hsieh, 2019; DeBerardinis et al., 2007; Yue, Li, Lee, Lee, Shao, Song, Cheng, Masterson, Liu, Ratliff, et al.,

2014), lipids represent a diverse array of molecules having more and more important roles in PCa. Significant efforts have been made to study cellular metabolism of PCa in order to better understand the role of androgen/AR in lipid metabolic process.

1.4 AR and its influence on lipid metabolism in PCa

The development of the male urogenital tract, including the prostate, depends on an activated androgen receptor. Similarly, growth of the majority of PCa is androgen-dependent (Chodak et al., 1992; Ruizeveld de Winter et al., 1994; Sadi, Walsh, & Barrack, 1991). AR target genes contain in the regulatory regions one or more androgen response elements. AR being a transcription factor, it can regulate transcription by binding to promoter and/or enhancher regions of different genes including genes involved in lipid metabolism. In a study done by Massie *et al,* AR was identified as a core regulator of anabolic transcriptional network regulating sets of genes expression impelling cellular process in PCa. Lipid metabolic pathway was described as a major downstream target of AR signaling (Massie et al., 2011). Emerging evidence shows that AR cistrome undergoes extensive reprogramming during prostate epithelial transformation in man and this drives the normal prostate epithelium towards transformation (Pomerantz et al., 2015). Furthermore, a recent study showed that AR binding sites have a dramatically increased rate of mutations that is greater than any other transcription factors specific to only PCa. Non-coding AR binding sites are frequently mutated in PCa and can impact enhancer activities leading to the huge increase in transcriptional activities of AR (Morova et al., 2020). Furthermore, Han *et al* have associated increased AR splice variants (AR-Vs)

expression and increased lipid metabolism in PCa with therapeutic resistance suggesting AR-Vs mediated reactivation of AR signaling and lipid biosynthesis may potentially drive CRPC progression (Han et al., 2017).

1.4.1 Androgen stimulates lipid synthesis in PCa

Emerging evidences shows that increased fatty acid synthesis is an early hallmark of the prostate tumorogenesis (Johannes V Swinnen et al., 1997; Zadra, Photopoulos, & Loda, 2013). Multiple observations link upregulation of several key lipogenic enzymes in PCa development and progression (Suburu & Chen, 2012; X. Wu, Daniels, Lee, & Monaco, 2014; Zadra et al., 2013). The increased expression of the several key lipogenic enzymes including fatty acid synthase (FASN), acetyl-CoA carboxylase (ACC), and ATP citrate lyase (ACLY) indicates active lipogenesis in tumour cells (K. B. Singh & Singh, 2017). Normal cells utilize dietary lipids predominantly whereas the cancer cells fulfill the majority of their fatty acid requirement through *de novo* fatty acid synthesis (Deep & Schlaepfer, 2016; Gutierrez-Pajares, Ben Hassen, Chevalier, & Frank, 2016). De novo lipogenesis refers to the biochemical process of synthesizing fatty acids from acetyl CoA (acetyl-CoA, generated from citrate or acetate). Acetyl CoA, the building block of de novo lipogenesis is primarily converted to malonyl-CoA, which is catalyzed by the enzyme ACC and is the rate limiting step in fatty acid synthesis (Luo et al., 2017). FASN then couples acetyl-CoA and malonyl-CoA to convert long chain saturated fatty acids (mainly palmitic acid, C16:0) which can be further converted to monounsaturated fatty acid species by stearoyl-CoA desaturase (SCD) by introducing a cis-double bond to the acyl chain.

Long and very long chain fatty acids as well as polyunsaturated fatty acids play an important role in biological activities in PCa. De novo synthesized fatty acids and or dietary fatty acids are elongated to synthesize (saturated/ poly unsaturated) long chain and very long chain fatty acids by elongases (ELOVLs, a class of enzymes with seven different family members having specificities for chain length and saturation level) (Butler et al., 2016).

Fatty acid synthetic enzymes function together with ELOVLs on the same pathway involving fatty acid metabolism. ELOVLs are over expressed in PCa and a recent study by Kenji *et al* showed drastic attenuation of PCa cell growth with knockdown of ELOVL7 (Tamura et al., 2009) which further strengthens its important role in PCa growth and progression. In addition, PCa cells promote saturated fatty acids and mono-unsaturated fatty acids–rich in phospholipids that partition into detergent-resistant lipid rafts to markedly alter signal transduction cascades, vesicular trafficking and cell migration (Staubach & Hanisch, 2011; Johannes V. Swinnen et al., 2003).

The synthesized fatty acids are then esterified to phospholipids and are incorporated into the lipid membrane by the proliferating tumor (L. Liu et al., 2015; X. Wu et al., 2014). Rysman *et al.* reported the protective function of the *de novo* lipogenesis from lipid peroxidation and subsequent cell death due to endogenous and exogenous stress like reactive oxygen species and chemotherapy drugs (Willemarck et al., 2010). Supporting this biology, some reports claim that genetic or pharmacologic inhibition of key fatty acid synthesis enzymes, including FASN, ACC, and ACLY, produce anticancer effects in xenografted and cultured PCa cell models (Beckers et al., 2007; Brusselmans, De Schrijver, Verhoeven, & Swinnen,

2005; Hatzivassiliou et al., 2005; Kridel, Axelrod, Rozenkrantz, & Smith, 2004). Inhibition of key enzymes disturbs the phospholipid composition of cellular membrane and impacted on PCa progression. A recent study done by Scott and colleagues has shown that inhibiting ACC1 activity by using the small molecule TOFA reduces the formation of invadopodia and prevents invasion by the cancer cells (Scott et al., 2012). Other studies have reported that lipid-lowering drug (e.g. statins) have been associated with a reduced incidence of PCa, and in particular advanced/aggressive tumours (Lehman, Lorenzo, Hernandez, & Wang, 2012; Lustman, Nakar, Cohen, & Vinker, 2014). In addition, increase in the biochemical recurrence free survival rate among statin users was reported in a large prospective study (P. Tan et al., 2016). Similarly, patients with lower levels of circulating lipids are less likely to have a high-grade tumor (Mondul, Clipp, Helzlsouer, & Platz, 2010), whereas higher total cholesterol levels are positively associated with risk of PCa development (Kitahara et al., 2011). Moreover, recent reports have demonstrated the evidence of more aggressive disease at diagnosis and a higher rate of recurrence following surgery in obese men (Balaban, Lee, Schreuder, & Hoy, 2015; R. A. Taylor, Lo, Ascui, & Watt, 2015). High fat diet can induce lipid accumulation in the prostate tumor which can promote metastasis in a *Pten*-null mouse model of PCa (M. Chen et al., 2018). Taken together, these findings support an essential role of lipid metabolism in the development and progression of PCa.

In parallel with lipogenesis, lipolysis has also been shown to be elevated in multiple human cancers (Yue, Li, Lee, Lee, Shao, Song, Cheng, Masterson, Liu, & Ratliff, 2014). Androgens have been found to have essential role in lipid biosynthesis by stimulating the expression of genes encoding several enzymes involved in lipid synthesis, binding, uptake, metabolism and transportation (Barfeld,

Itkonen, Urbanucci, & Mills, 2014; Massie et al., 2011; J. Swinnen, P. P. Van Veldhoven, M. Esquenet, W. Heyns, & G. Verhoeven, 1996; J. V. Swinnen et al., 1997), including ACC, FASN, SCD, and ELOVLs (Butler et al., 2016; Massie et al., 2011; Nelson et al., 2002; Ngan et al., 2009; J. V. Swinnen, P. P. Van Veldhoven, M. Esquenet, W. Heyns, & G. Verhoeven, 1996).

1.4.2 Androgen and lipid uptake

Exogeneous lipid can be derived from dietary lipoproteins in the circulation, which are hydrolyzed by lipoprotein lipase (LPL) to free fatty acids, or be released by lipolysis from stores in local adipose tissue depots that comprises a major component of the tumor microenvironment (Ribeiro et al., 2012). The increase in the activities of LPL (Kuemmerle et al., 2011) and amplification of genes encoding carnitine palmitoytransferase 1A (CPT1A), the rate limiting enzyme for the transport of fatty acids in the mitochondria supports the active lipid uptake in PCa (Robinson et al., 2015; Valentino et al., 2017). Besides, the prostate is gland is surrounded by peri-prostatic adipose tissue which can supply ample amounts of fatty acids (Z. D. Nassar et al., 2018; Watt et al., 2019) required for proliferation and invasion of PCa (Tousignant et al., 2019; Watt et al., 2019). In line with this finding, a recent study has demonstrated association of PCa cell migration with obesity. PCa cells co-cultured with peri-prostatic derived adipocytes from obese mice showed enhanced migratory properties compared with lean mice (Laurent et al., 2016) suggesting that obesity induced secretory pattern of mature adipocytes plays an important role in such migration.

AR signaling is generally considered to regulate lipolysis in the adipose tissue (O'Reilly, House, & Tomlinson, 2014) and increase cellular uptake of

exogenous lipids by PCa cell (Butler et al., 2016; Nieman, Romero, Van Houten, & Lengyel, 2013). A recent study in cultured patient-derived prostate tumor explants, PCa cells and spheroids has reported that exogeneous lipids are the major contributor of lipid biosynthesis and β-oxidation in PCa (Balaban et al., 2019). It is also reported that AR-mediated induction of several lipid transporters in PCa cells significantly increases cellular lipid uptake in AR-positive PCa cells (Tousignant et al., 2019). Some of the examples that support androgen mediated lipid uptake are i) expression of transport protein FABPpm in androgen-responsive PCa cells (Pinthus et al., 2007) ii) increases in the expression of CD36 (transporter of exogenous fatty acid into the cells) with DHT in PCa cells and abrogated by antiandrogen (Enzalutamide) treatment (Tousignant et al., 2019). In addition, the expression of those lipid transporters have been associated with PCa progression. Watt and colleagues further demonstrated that blockade of CD36 reduces fatty acid uptake, results in reduction of cancer-mediated lipogenesis and accumulation of oncogenic lipid molecules required for signaling, finally reducing growth and progression of PCa cells (LNCaP, PC3) and PDX derived from organoids (Watt et al., 2019).

1.4.3 β-oxidation and prostate cancer

PCa cells differ from many other benign and normal cells, in that they predominantly utilize fatty acids as energetic rather than glucose via beta-oxidation (L. Liu et al., 2015; Y Liu, Zuckier, & Ghesani, 2010; X. Wu et al., 2014) . As the energy demands within rapidly dividing cancer cells are much higher than that for normal cells, PCa cells utilize fatty acids for ATP/ energy generation via β-oxidation.

Overexpression of CPT1 (rate limiting enzyme for mitochiondrial fatty acid oxidation) in several cancers including PCa (Y. Liu, 2006; Q. Qu, Zeng, Liu, Wang, & Deng, 2016; Schlaepfer et al., 2014) strengthen this phenomenon. In addition, the intense overexpression of peroxisomal enzyme, a-methylacyl-CoA racemase (AMACR) required for oxidation of branched chain fatty acids in PCa suggests that fatty acid is a source of energy in PCa (Lloyd et al., 2013). Inhibition of fatty acid oxidation targeting CPT1 by Etomoxir (irreversible chemical inhibitor) in PCa cells (LNCaP and VCaP) suppressed the androgen mediated PCa cell growth (Tennakoon et al., 2014). A recent study claims that the inhibition of mitochondrial fatty acid oxidation causes toxic lipid accumulation leading to ER stress and apoptosis/death of PCa cells (Schlaepfer et al., 2014). Thus, several lines of compiling evidences show a crucial role of fatty acid oxidation in PCa cell survival and driving oncogenic pathways associated with tumor progression and metastasis(Park et al., 2016).

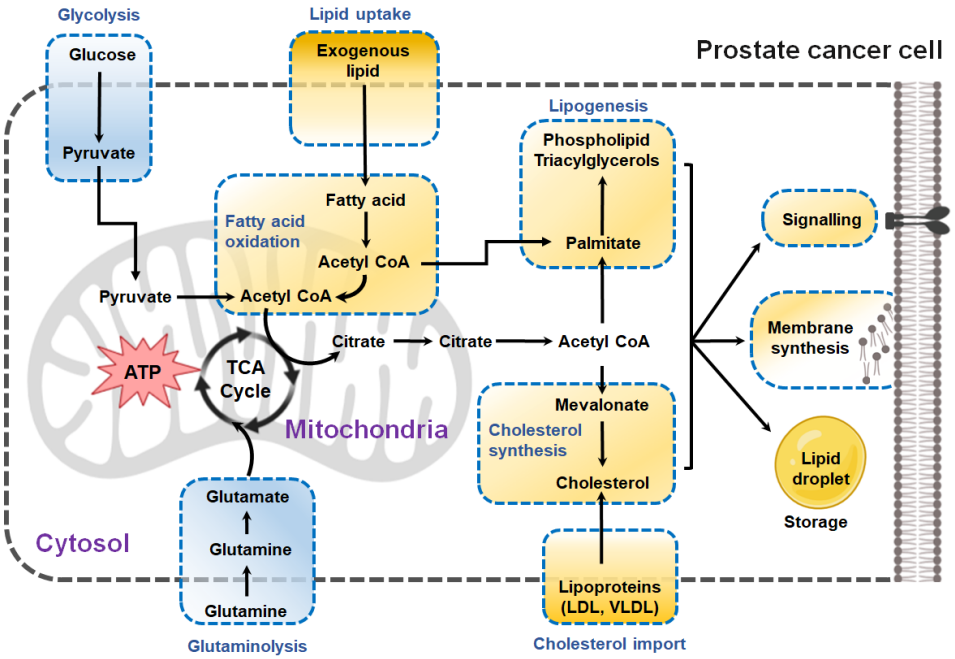

Figure 1.13: A simplified diagram showing major altered lipid metabolic pathway (yellow) in PCa. Created with BioRender.com

Not only is androgen signalling indispensable to prostate development and function, it's a key driver for PCa initiation and progression. Increased AR activity is associated with PCa development and progression to castration resistant prostate cancer. There are compelling evidences that androgen regulates the major lipid metabolism in PCa which play vital role in PCa growth and progression. Despite these successes, very few AR target genes have been identified and characterized. We believe that the aspect of AR function in lipid metabolic process is complex and very little is currently known about how AR regulates the lipid metabolic process in PCa. Therefore, this project will try to identify AR target lipid metabolic genes through cistromic, transcriptomic and metabolomics approach in order to understand the molecular mechanisms by which the AR regulates lipid metabolism in PCa. We hypothesised that identifying AR-regulated genes and associated signalling pathways, would be crucial to understanding its role in PCa metastasis and progression.

As ADT therapy fails to treat metastatic PCa at this stage, the identification and characterization of androgen-responsive lipid metabolic genes can potentially lead to the discovery of novel biomarkers and approaches for PCa diagnosis and treatment. Therefore, identification and characterization of androgen-responsive genes can potentially lead to the discovery of novel biomarkers for PCa diagnosis and approaches for better treatment options. Thus, the broad aim of the project is to understand the underlying molecular mechanism by which AR regulates the lipid metabolism.

Another class of transcription factor, SREBPs, are masters regulator of lipid homeostasis by controlling the expression of a range of enzymes required for endogenous cholesterol, fatty acid, triacylglycerol and phospholipid synthesis (H. V. Heemers, Verhoeven, & Swinnen, 2006). AR stimulates lipid metabolism indirectly through activating SREBP (Johannes V Swinnen et al., 1997). A recent study has reported extensive reprogramming of AR cistrome during PCa transformation leading to the gain of large number of AR binding sites in prostate tumour tissue as compared to non-malignant tissues influencing differential expression of large number of gene in PCa tissue (Pomerantz et al., 2015). The reprogramming of AR cistrome has been recapitulated in PCa cell lines (LNCaP and VCaP cell) after activation of AR with R1881 (Massie et al., 2011; Pomerantz et al., 2015). Massie *et al* integrated detailed genomic data with metabolomic profiling and identified an anabolic transcriptional network regulating set of genes expression that regulates the cellular processes in PCa cells (Massie et al., 2011). Upregulation of lipid biosynthetic pathways (e.g., FASN and ACACA); glycolytic pathway (e.g., GLUT1, HK1/2 and PFKFB2); cell-cycle regulators (e.g., CDC2 and CDC25A); and master regulators of these metabolic processes (e.g., MTOR and CAMKK2) were identified as major transcriptional changes (Massie et al., 2011) identifying AR as core regulator and lipid metabolic pathway as major downstream target of AR signalling (Massie et al., 2011). In addition, recent study have demonstrated that androgen induces mTOR relocalization to the nucleus to drive androgen mediated metabolic reprogramming in PCa cells (Audet-Walsh et al., 2017). Meanwhile, SREBP-1 is the downstream effector of AR/mTOR signalling axis that maintains the balance between citrate consumption for ATP production from mitochondria and substrate for FASN in the cytoplasm (Audet-Walsh et al.,

2018), this suggests the expression of lipid metabolic genes might not be controlled by a classical direct mechanism of androgen action, i.e. mediated by direct interaction of the AR with AREs in the affected genes, but rather through an indirect mechanism involving a common intermediary factor (Figure 1.15).

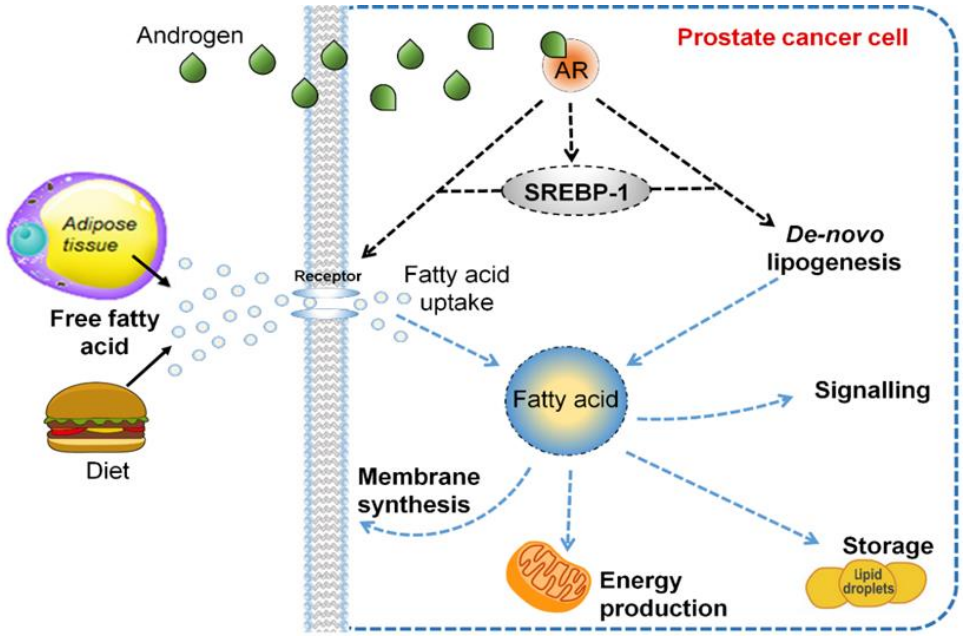

Figure 1.15: Lipid metabolism regulated by AR through SREBP (Butler et al 2016)

Most of the previous studies have reported increased activities of both transcription factors AR and SREBP-1 with increased common downstream targets. Therefore, it is very essential to elucidate the role of AR, SREBP-1 and their interplay to promote growth and progression of the PCa. Lipid metabolism may be regulated in a complex manner by mutual interaction of SREBP-1 and AR to exert their own functions more efficiently. Genome-wide analysis, *in vitro*, and *in vivo* studies have demonstrated the multiple function of SREBPs in mediating various cellular processes but very little knowledge exists regarding the molecular mechanism of AR and SREBP-1 interplay and regulation of lipid metabolomic genes

and the identification of the commonalities could possibly identify a novel target that could be more effective in a drug-resistant context in the treatment of PCa.

Nevertheless, AR signalling is also believed to regulate lipid metabolism via interplay with various other transcription factors besides SREBPs, including peroxisome proliferator-activated receptor gamma (PPARγ) and signal transducer and activator of transcription-3 (STAT3). Furthermore, increased AR activity has been associated with the activities of these transcriptional factors, but in most cases, the mechanisms underlying the interplay are not clear (Audet-Walsh et al., 2018). Thus androgen may co-ordinately stimulate the expression of battery of lipid metabolic genes.

1.5 Hypothesis and aims:

The specific aims of this project were as follow

Aim 1: Identify novel AR-regulated genes involved in regulating the lipidome.

Aim 2: Evaluate the consequences of AR-mediated regulation of lipid-related genes on PCa growth and progression

Aim 3: Elucidate how transcription factors SREBP-1 cooperate AR function to regulate genes involved in lipid metabolism

CHAPTER 2: MATERIALS AND METHODS

2 Materials and methods

2.1 Materials

Table 2.1: Common chemicals and reagents

Reagent	Supplier	Catalogue #
1kb gene ladder 17AAG	Thermo Fisher National Cancer Inst. Cole Parmer	SM0313
100 bp DNA ladder	New England Biolabs	N3231S
Agarose, analytical grade	Sigma Aldrich	A6013
Bradford assay reagent	BioRad	500-0006
BSA (bovine serum albumin)	Sigma Aldrich	A9647
Chloroform	Sigma Aldrich	C2432
Cover slips	HD Scientific Supplies	----------
Criterion precast gel (4-12%)	BioRad	567-1084
DMSO (dimethyl sulfoxide)	BDG Laboratory Supplies	D2650
DynaBeads	Invitrogen	112.03D
Eosin	Australian Biostain P/L	AEPA
Ethanol, general use	Chem Supply	EA061
Ethanol, molecular grade	Sigma Aldrich	E7023
FBS (fetal bovine serum)	Sigma Aldrich	12003C
Formaldehyde	Chem Supply	FA010
Haematoxylin	Australian Biostain P/L	AHLMA
Inactivation buffer (supplied with Turbo free)	Ambion Inc.	AM1907
iScirpt cDNA synthesis kit	BioRad	170-8891
iQ SYBR Green Supermix	BioRad	170-8885
Lipofectamine 2000	Invitrogen	11668-019
Matrigel	Corning Scientific	BD 354234
Methanol	Chem Supply	MA004
Nitrocellulose membrane (0.4 µm)	BioRad	162-0115

Nuclear free water	Ambion Inc.	AM9937
PBS (phosphate buffered saline)	Sigma Aldrich	D8537
Ponceau S	Sigma Aldrich	P3504
Propidium Iodide	Sigma Aldrich	P4864
QIAquick Plasmid Midiprep Kit	QIAGEN	12143
QIAquick Plasmid Miniprep Kit	QIAGEN	27106
Restriction Digest enzymnes and buffer	New England Biolabs	----------
RPMI 1640 liquid media	Sigma Aldrich	R8758
SDS (sodium dodecyl sulphate)	Sigma Aldrich	75746
siRNA ACSM1- 1	Ambion	s12458
siRNA ACSM1- 2	Ambion	s12459
siRNA ACSM1- 3	Ambion	s12460
siRNA ACSM3- 1	Ambion	s41984
siRNA ACSM3- 2	Ambion	s41985
siRNA ACSM3- 3	Ambion	s41986
siRNA AR	Ambion	s16858
Skim milk powder	Coles Brand	----------
Triton-X 100	Sigma Aldrich	T8787
TRIZOL Reagent	Sigma Aldrich	T9424
Trypsin EDTA solution	Sigma Aldrich	T4049
Tween 20	Sigma Aldrich	P7949
Lipofectamine RNAiMax	Thermo Fisher Scientific	13778150
Optimem	Thermo Fisher Scientific	31985070
Lipoic acid	Sigma Aldrich	
Oleic acid	Sigma Aldrich	
Octanoic acid	Sigma Aldrich	24892539
Lauric acid	Sigma Aldrich	24901204
Decanoic acid	Sigma Aldrich	

Ferrostatin-1	Sigma Aldrich	Cat#:SML0583
Deferoxamine	Sigma Aldrich	Cat#: D9533
NAC	Sigma Aldrich	
Trolox	Sapphire Bioscience; Redfern, NSW, AUS	
Erastin	Sigma Aldrich	Cat#: E7781
ML210	Tocris Bioscience	Cat#: 6429
FIN56	Tocris Bioscience	Cat#: 6280

Table 2.2: mRNA Primers

Primer	Sequence	Use
AR_exon1_2_F	CCACTTGTGTCAAAAGCGAAAT	qRT-PCR
AR_exon1_2_R	ATAGTCAATGGGCAAAACATGG	qRT-PCR
ACACA_mRNA_F – set 1	TTCACTCCACCTTGTCAGCGGA	qRT-PCR
ACACA_mRNA_R – set 1	GTCAGAGAAGCAGCCCATCACT	qRT-PCR
ACACA_mRNA_F – set 2	TCCACTTGGCTGAGCGATTG	qRT-PCR
ACACA_mRNA_R – set 2	CAAGTCAGCAAACTGCACGG	qRT-PCR
ACSM1_mRNA_F	CTGCTCTACGAGAACTATGGGC	qRT-PCR
ACSM1_mRNA_R	CTGTGTTAGGTGGCAGGATGCT	qRT-PCR
ACSM1_mRNA_F – set 2	CCAGGAAGTAGGAAATTACG	qRT-PCR
ACSM1_mRNA_R – set 2	GGGTATTTCAACAATGTCTG	qRT-PCR
ACSM2A_mRNA_F	CAGAAGGAGACATTGGCATCAGG	qRT-PCR
ACSM2A_mRNA_R	AGTCTCCTCGAATGTTGGCTGC	qRT-PCR
ACSM2B_mRNA_F	CAGAAGGAGACATTGGCATCAGG	qRT-PCR
ACSM2B_mRNA_R	AGTCTCCTCGAATGTTGGCTGC	qRT-PCR
ACSM3_mRNA_F	CTGGGCAAAGTCTGCATGGAGT	qRT-PCR
ACSM3_mRNA_R	AGTTGGTGCTGAACAGAAGACTG	qRT-PCR
ACSM3_mRNA_F – set 2	GGACAGACTGAAACGGTGCT	qRT-PCR
ACSM3_mRNA_R – set 2	GCCAAATGGTCGGTTGGGTA	qRT-PCR
ACSM4_mRNA_F	GTTCACCCTCTGCGGAAGGTAT	qRT-PCR
ACSM4_mRNA_R	GCCAGGAAGAAAACACACTGCC	qRT-PCR
ACSM5_mRNA_F	CCATCTTTCGGCTGCTTGTGCA	qRT-PCR
ACSM5_mRNA_R	CAGTCTGGTGTTTCCACTTCTCC	qRT-PCR
FASN_mRNA_F	TCTCCGACTCTGGCAGCTT	qRT-PCR
FASN_mRNA_R	GCTCCAGCCTCGCTCTC	qRT-PCR

GADPH_R	GGCATGGACTGTGGTCATGAG	qRT-PCR
GAPDH_F	TGCACCACCAACTGCTTAGC	qRT-PCR
HMGCR_mRNA_F	GACGTGAACCTATGCTGGTCAG	qRT-PCR
HMGCR_mRNA_R	GGTATCTGTTTCAGCCACTAAGG	qRT-PCR
HMGCS1_mRNA_F	AAGTCACACAAGATGCTACACCG	qRT-PCR
HMGCS1_mRNA_R	TCAGCGAAGACATCTGGTGCCA	qRT-PCR
KLK3_F	CAGAGGAGTTCTTGACCCCAA	qRT-PCR
KLK3_R	ACAGCATGAACTTGGTCACCTT	qRT-PCR
LDLR_mRNA_F	GAATCTACTGGTCTGACCTGTCC	qRT-PCR
LDLR_mRNA_R	GGTCCAGTAGATGTTGCTGTGG	qRT-PCR
SCD_mRNA_F	CCTGGTTTCACTTGGAGCTGTG	qRT-PCR
SCD_mRNA_R	TGTGGTGAAGTTGATGTGCCAGC	qRT-PCR

Table 2.3: ChIP Primers

Primer	Sequence	Use
ACACA_Peak_1_ChIP_F	ACCAGTCCTGGGTAGGAACA	ChIP PCR
ACACA_Peak_1_ChIP_R	ACACTGGAGGAGAGCTGTTG	ChIP PCR
ACACA_Peak_2_ChIP_F	GGCCAAGAGGTCTGGGAAAT	ChIP PCR
ACACA_Peak_2_ChIP_R	GCTGAGGCCAATAAAACCGC	ChIP PCR
ACACA_Peak_3_ChIP_F	CCCCTTCCTCGTGTTTGATA	ChIP PCR
ACACA_Peak_3_ChIP_R	AGAGCTGTATGCCTGGAGGA	ChIP PCR
ACACA_Peak_4_ChIP_F	CCCTCAGCAAAGGAGTACCA	ChIP PCR
ACACA_Peak_4_ChIP_R	GAGCTTCTTCCCTTCCCCTA	ChIP PCR
ACACA_Peak_5_ChIP_F	TCAGAGCCCTTCCTGAGTGA	ChIP PCR
ACACA_Peak_5_ChIP_R	GTCTATCACTGGGGTTCAAGACA	ChIP PCR
ACSM1/3_Peak_1_ChIP_F	TGGTAGAGCAACTCGCCTTT	ChIP PCR
ACSM1/3_Peak_1_ChIP_R	TATGATTGGCCCAGCTTAGG	ChIP PCR
ACSM1/3_Peak_2_ChIP_F	AACAACACGGGCTCAAATTC	ChIP PCR
ACSM1/3_Peak_2_ChIP_R	TACTTGTCCGTGCTGAATGC	ChIP PCR

ACSM1/3_Peak_4_ChIP_F	CAGCCTCACGAAAGCCAGAAA	ChIP PCR
ACSM1/3_Peak_4_ChIP_R	TTAGCCCTGGGAAGAACTTGTG	ChIP PCR
ACSM1/3_Peak_5_ChIP_F	AGGCTCACCAACTGTGGACT	ChIP PCR
ACSM1/3_Peak_5_ChIP_R	AACTGGTTTTGGCAGGTTTG	ChIP PCR
FASN_2_ChIP_F	GCTGCTCGTACCTGGTGAG	ChIP PCR
FASN_2_ChIP_R	GATGGCCGCGGTTTAAATA	ChIP PCR
FASN_ChIP_F	GAGAGCGGAGGATGAGGAG	ChIP PCR
FASN_ChIP_R	TAGAGGGAGCCAGAGAGACG	ChIP PCR
FASN_PCa_ChIP_F	TGGACTGTAACGTTCCCTGC	ChIP PCR
FASN_Pca_ChIP_R	ACCCAGGGCTTTCGTTCATT	ChIP PCR
HMGCR_ChIP_F	CTCTCCCGCGCTAGTAACTG	ChIP PCR
HMGCR_ChIP_R	ACTAGGGCCTGCCTATTGGT	ChIP PCR
HMGCS1_2_ChIP_F	TAGTCAAGGACACCGCCTCT	ChIP PCR
HMGCS1_2_ChIP_R	TATAAAGCTGGTGGCGAAGG	ChIP PCR
HMGCS1_ChIP_F	AGAGGCGGGGACAAAGTCT	ChIP PCR
HMGCS1_ChIP_R	CCCGCATCTCCTCTCACTTA	ChIP PCR
KLK3_ChIP(Prom)_F	GCCTGGATCTGAGAGAGATATCATC	ChIP PCR
KLK3_ChIP(Prom)_R	ACACCTTTTTTTTTCTGGATTGTTG	ChIP PCR
LDLR_P1_ChIP_F	ATGCGTTTCCAATTTTGAGG	ChIP PCR
LDLR_P1_ChIP_R	ACCTCACTGCAAGAGGAGGA	ChIP PCR
LDLR_P2_ChIP_F	CCGGGACCCTCTCTTCTAAC	ChIP PCR
LDLR_P2_ChIP_R	GACTGCACCCAACTCAGGAT	ChIP PCR
LDLR_PCa_ChIP_F	CGATGTCACATCGGCCGTTCG	ChIP PCR
LDLR_PCa_ChIP_R	CACGACCTGCTGTGTCCTAGCT	ChIP PCR
NC2_F	GTGAGTGCCCAGTTAGAGCATCTA	ChIP PCR
NC2_R	GGAACCAGTGGGTCTTGAAGTG	ChIP PCR
SCD_ChIP_F	TGGAAGAGAAGCTGAGAAGG	ChIP PCR
SCD_ChIP_R	TTCTGTAAACTCCGGCTCGT	ChIP PCR

Table 2.4: Antibodies

Primary antibody	Secondary	Catalogue No.	Company
AR (ChIP grade)	Rabbit	ER179, Ab108341	Abcam
AR	Rabbit	N20, SC-816	Santa Cruz Bio.
ACSM1	Rabbit	SAB1301678	Sigma-Aldrich
ACSM3	Mouse	sc-377173 (G8)	Santa Cruz
Actin; beta	Mouse	AC-15, Ab6376	Abcam
Anti-lipoic acid	Rabbit	ab58724	Abcam
a-Tubulin	Mouse	05-829	Millipore
DLAT	Mouse	12362S	Cell Signalling Tech
DLST	Rabbit	11954S	Cell Signalling Tech
GAPDH	Mouse	MAB374,	Millipore
GPX4	Rabbit	ab41787	Abcam
Lipoic acid	Abcam	Rabbit	Abcam
MDA	Rabbit	ab6463	Abcam
SREBP-1	Rabbit	H160, sc8984	Santa Cruz
SREBP-1	Mouse	E4, sc17755	Santa Cruz
SREBP-1	Mouse	2A4, sc13551	Santa Cruz
SREBP-1 (ChIP grade)	Mouse	2A4, sc13551	Santa Cruz
Secondary antibody	Source	Catalogue No.	Company
Immunoglobulins, biotinylated: Anti-Mouse	Goat	E0433	DAKO
Immunoglobulins, biotinylated: Anti-Rabbit	Goat	E0432	DAKO

Table 2.5: Reagents for metabolomics experiment

Reagents	Supplier	Product code
Methanol (LC Grade for metabolomics) Optima, 1L, CAS No. 67-56-1	Thermo Fisher	FSBA456-1/Each
Chloroform GR for analysis	Merck	1024421000
Water for chromatography LiChrosolv® - 1 l	Merck	1153331000
Nunclon Multidishes - 6 well plate, Poly-D-lysine coated	Sigma	Z720798-20EA
MES Sodium Salt	Sigma	M3885-25G
(1S)-(+)-10-Camphorsulfonic acid	Sigma	C2107-5G

2.2 Methods

2.2.1 Cell culture

2.2.1.1 Maintaining and Passaging Cells

The human PCa cells lines LNCaP, 22Rv1, VCaP, were obtained from American Type Culture Collection (ATCC). Cell Bank Australia performed verification of all cells lines in 2010 and 2016 via short-tandem repeat profiling. LNCaP, 22Rv1, V16D and MR49F cells were maintained in RPMI-1640 containing 10% FBS; the media for growth of MR49F cells was additionally supplemented with 10uM enzalutamide. VCaP cells were maintained in Dulbecco's Modified Eagles's medium (DMEM) containing 10% FBS, 1% sodium pyruvate, 1% MEM non–essential amino acids, and 0.1 nM 5α-dihydrotestosterone (DHT).

To prepare cells for storage in liquid nitrogen, fully confluent T75 flasks were collected using trypsin followed by centrifugation at 450 rcf for 5 minutes. Cell pellets were resuspended in 1.5 mL of cells line specific media and 1.5 mL of freezing mix (40% DMSO, 40% FBS, 20% culture) media on ice. One mL of cell: freeze mix suspension was added to each cryovial, labelled approximately and placed in isopropanol filled Mr. Frosty freezing container at -80°C. Once cells were adequately frozen they were transferred to liquid nitrogen for long term storage.

Human PCa cell lines obtained from liquid nitrogen stores were thawed quickly by gentle agitation in a 37°C water bath then missed with 9mL cell line specific culture medium. Cells were centrifuged at 450 rcf for 5 minutes and pellets were resuspended in 10 mL cell line specific culture media and placed directly into a T25

flask overnight at 37°C with 5% CO2. Cells were passaged to a T75 flask the following day and were then passaged a second time prior to use in experiments.

2.2.1.2 Charcoal Stripping of Foetal Calf Serum

50 mL of dextran coated charcoal (DCC) per 50 mL falcon tube was centrifuged at 3200 rcf for 30 minutes and supernatant was discarded. 50 mL of FCS was added to each charcoal pellet and tubes were incubated for 2 h with rotation at room temperature (r.t) to adsorb steroids from the FBS. Tubes were then centrifuged at 3200 rcf for 30 minutes and the supernatants were transferred to fresh 50 mL tubes with charcoal pellets prepared as above. The incubation and centrifugation steps were repeated and the supernatants were combined, filter sterilised and stored at -20°C.

2.2.2 Preparation of Steroid Stocks

DHT stocks (10^{-2} M) were prepared in 100% EtOH and stored at -20°C in glass vials. DHT was diluted further in specific culture medium as required for use in experiments.

2.2.3 Preparation of Enzalutamide stock

Enz stocks (50mM) were prepared in 100% DMSO and stored at -20°C in glass vials. ENZ was diluted further in specific culture medium as required for use in experiments.

2.2.4 Trypan blue exclusion test of cell viability

Cell viability is calculated as the number of viable cells divided by the total number of cells within the grids on the haemocytometer. If cells take up trypan blue they are considered non-viable. First, using a haemocytometer, the cells density of the cell line suspension was determined. Second, 20µL of trypan blue stock solution was added to 20 µL of cell suspension and loaded on a haemocytometer to examine the cells under microscope, immediately. Finally, the number of blue stained cells and the total number of cells are counted into the following formula.

%viable cells= [1.0-(Number of blue cells ÷ Number of total cells)] X 100

2.2.5 Cell line transfection

The human ACSM1 and ACSM3 Silencer® Select Pre-designed small interfering RNAs (siRNAs) and control siRNA were purchased from by Ambion® by Life Technologies. Three siRNA were tested for ACSM1 and ACSM3 and the most two effective were selected for our experimentation: siACSM1-1 (s41984), siACSM1-2 (s41985), siACSM3 (s12459) and siACSM3 (s12460). The siRNAs at a concentration of 10nM were reverse transfected using Lipofectamine RNAiMAX transfection reagent (Invitrogen) according to the manufacturer's protocol. ACSM1 and ACSM3 downregulation was confirmed on mRNA and protein levels.

2.3 Organoid culture

2.2.4.1 Reviving, maintaining, passaging and freezing of organoids

The organoid cell lines 201.1 Dura representing prostate adenocarcinoma was obtained from the Melbourne Urology Research Alliance (MURAL) and are described in (Lawrence et al. 2018). Organoid cell line was generated from patient derived xenografts (PDX) of CRPC metastases from rapid autopsy specimens. The 201.1 Dura line was derived from metastases in the dura matter (Lawrence et al. 2018).

201.1 Dura cells were seeded in growth factor reduced, phenol red-free, LDEV-free Matrigel (Corning). 201.1 organoids were cultured in advanced DMEM/F-12 media (Gibco) containing 0.1ml Primocin (Invivogen), 2 mM Glutamax (Sigma), 10mM HEPES (Sigma), 1nM DHT (Sigma), 1.25mM N-acetylcysteine (Sigma), 5nM NRG1 Heregulinβ-1 (Peprotech), 500 nM A83-01, 10 mM nicotinamide (Sigma), 10μM SB202190 (Sigma), 2% B27 (Thermo), 10ng/ml FGF10 (Peprotech), 5ng/ml FGF2 (Peprotech), 1μM prostaglandin E2 (Tocris), 10% noggin conditioned media and 10% R-spondin conditioned media. 10μM Y-27632 dihydrochloride (Selleck Chemicals) was added to culture medium during organoid establishment and following passage.

For revival, frozen vials were thawed in a 37°C water bath. Cell suspension was centrifuged at 1200rpm for 4 minutes, pellet was washed with organoid culture media. Pellets were resuspended in growth factor reduced Matrigel (Corning) at a concentration of 100,000-50,000 cells per 30μl of Matrigel in 24 well plates. Plates were inverted at 37°C for 15 minutes to allow Matrigel to solidify, then overlaid with

500mL of human organoid culture medium containing 10μM Y27632. Media was replaced every 3-4 days.

At the time of passage, organoids were washed in PBS, 250μl of TrypLE (GIBCO) was added and Matrigel broken up by pipetting. Plates were incubated at 37°C for 5 minutes. Once the Matrigel was digested, the cells were transferred to 1.5ml Eppendorf tubes and centrifuged to form a pellet, washed and reseeded in Matrigel.

For freezing organoids, cells were digested out of Matrigel as described above and pelleted. Pellets were resuspended in freezing media (90% human organoid culture medium containing 10μM Y27632, 10% DMSO). 1ml of suspension was added to each labelled cryo-vial, and placed in an isopropanol filled freezing container at -80°C. Cells were transferred to liquid nitrogen once frozen.

2.3.1 Organoid transfection

Organoid transfections were carried out as described (Broutier et al. 2016). Organoid cells were digested out of Matrigel discs as described above, counted and resuspended to an appropriate concentration in 450μl of organoid culture media. The transfection mix was prepared by adding 25μl of Opti-MEM per tube to two 1.5ml microcentrifuge tubes for each transfection condition. 6.25μl of siRNA at 20mM (for a final concentration of 250nM) was added to one of the tubes and 1.5μl of RNAiMAX reagent to the other tube and incubated at room temperature (RT) for 5 minutes. The contents of the two tubes were mixed together and incubated at RT for a further 5-15 minutes. 50μl of the transfection mixture was added to 450μl of single cell suspension and centrifuged in a pre-warmed centrifuge at 32°C, 600g for

1h. Cells were then incubated in a tissue culture incubator at 37°C for 4h. Cells were collected in a 1.5ml centrifuge tube and centrifuged at 1200rpm for 5 minutes at RT. Pellet was resuspended in 90ul Matrigel and seeded out in 30ul Matrigel discs. Plates were inverted at 37°C for 15 minutes to allow Matrigel to solidify, then overlaid with 500mL of human organoid culture medium.

Organoid forming efficiency was assessed as described previously (Lawrence et al. 2018). At seven days post transfection, ≥5 sets of images were taken per treatment. Images were taken at different depths in order to get all the organoids for each field of view. Number of organoids per μm^2 was determined by manually counting number of organoids from each field of view and dividing by area. Images of the Matrigel disc were taken at 2x magnification with scale bar and diameter was estimated using measure function in ImageJ. Average number of organoids per μm2 was multiplied by area of disc to estimate average number of organoids per disc. Organoid forming efficiency was calculated as average number of organoids divided by number of cells originally seeded.

2.3.2 Organoid viability using Cell Titer-Glo

Organoid cells were transfected as described above. Briefly, organoid were collected and 50,000 cells were resuspended in 450μl of organoid culture media and 50μl of transfection mix containing RNAiMAX with 50, 100, 250 and 500nM siACSM1/3 or siControl. Cells were centrifuged in a pre-warmed centrifuge at 32°C, 600g for 1h. After centrifuging, cells were incubated in a tissue culture incubator at 37°C for 2-4 hrs and then collected in 1.5ml centrifuge tubes by centrifugation at 300 g for 5 minutes at room temperature. Cell pellets were resuspended in 5 μl

Matrigel and seeded out in 10µl matrigel discs in 96-well plates. Plates were inverted and incubated at 37°C for 15 minutes to allow Matrigel to solidify, then overlaid with 100µL of organoid culture medium.

Organoid viability was assessed at 7 days post-transfection using the Cell Titer-Glo® Luminescent Cell Viability Assay kit (Promega). Media was removed from wells and 70µl fresh media was added to each well. 80µl of Cell Titer-Glo reagent was added to each well and contents of the well were mixed by pipetting up and down several times. Plate was wrapped in foil and contents were then mixed on an orbital shaker for 5 minutes. The plate was incubated at room temperature for 25 minutes. Luminescence was measured using a BMG Lumistar Optima luminometer.

2.4 Western blotting

2.4.1 Preparation of cell lysates:

Cells were washed with 1x PBS and removed from culture plates by scraping in 100 µL RIPA lysis buffer per well of a 6-well plate. Cell lysates were centrifuged for 10 minutes at 10000 rcf at 4°C and supernatant containing protein was collected and stored at -80°C.

2.4.2 Cellular Fractionation

Cells were plated in 10 cm plates [$1x10^6$ cells per plate] in cell-line specific medium overnight at 37°C and 5% CO2 prior to undergoing the indicated treatment. Cells were collected using trypsin and an equal number of cells were collected from each sample. One half of the cells was resuspended in 100 µL lysis buffer 1 (LB1: 50 mM Hepes-KOH pH7.5,140 mM NaCl, 1 mM EDTA, 10% Glycerol, 0.5% NP-40. 0.25% TX-100) containing protease inhibitor cocktail (Sigma) and kept for whole cell lysate. The other half of each sample was processed through a series of lysis/centrifugation steps to separate cytoplasmic and nuclear fractions. First, cells were resuspended in 100 µL of LB1 containing protease inhibitor cocktail (Sigma) and centrifuged at 9300 rcf for 10 s. The supernatant from this step was kept as the cytoplasmic fraction. Remaining pellets were washed in 1 mL of LB2 (10 mM Tris-HCl pH 8.0, 200 mM NaCl, 1 mM EDTA, 0.5 mM EGTA) containing protease inhibitor cocktail (Sigma), centrifuged and resulting supernatant was discarded. The nuclear pellets were resuspended in 100 µL LB3 (10mM Tris-HCl pH8.0, 100mM NaCl, 1mM EDTA, 0.5mM EGTA, 0.1% Na-Deoxycholate, 0.5% N-lauroylsarcosine) containing protease inhibitor cocktail (Sigma Aldrich). Both nuclear and whole cell fractions

were sonicated on high (Diagenode Life Research Bioruptor Millenium 3 XD10) 10 times for 30 s with 1 minute rest on ice between sets to extract nuclear proteins. Samples were centrifuged at 15700 rcf for 10 minutes and protein supernatant was collected then frozen for later analysis by 4-15% criterion gel and western blot.

2.4.3 Bradford Assay

Total protein concentration of cell lysates was determined via Bradford assay. Microtiter plates were set up as follows in clear, untreated, flat bottomed 96 well microtiter plates with lids (Cole Parmer, Cat no: KH-01728-01). “S” indicates standard and subscript numbers indicate µl of 1 mg/mL BSA added to each standard well and (A-H) letters indicate samples in duplicate sample wells to which 1 µl of sample was added per well. 20% Bradford reagent was added to every well to a total volume of 200 µl. The plate was mixed and incubated at RT for 5 minutes before being read at 595 nm on a PolarStar microplate reader.

2.2.4.3. Sodium Dodecyl Sulfate Polyacrylamide Gel Electrophoresis (SDS-PAGE)

BioRad precast SDS-PAGE gels were run using 20 µg of total protein per well unless indicated otherwise. Protein lysates were mixed 5:1 with 6x load dye and heated at 95°C for 5 minutes prior to gel loading. The SDS-PAGE running apparatus was filled with 1x SDS-running buffer (BioRad). To examine fibronectin expression, protein lysates were run on 4-15% gradient gels at constant voltage (80 V) for 15 minutes followed by 150 V for 2h. To detect all other proteins, lysates were run on 10% or 4 – 12% gels at constant voltage (120 V) for 90 minutes.

2.4.4 Western transfer and Immunoblot

Proteins were transferred from SDS-PAGE gel to nitrocellulose membrane using a BioRad transfer apparatus (miniPROTEAN®Tetra Cell or Criterion™ Cell) filled with 1x Transfer Buffer. Transfer of proteins from SDS-PAGE gel to nitrocellulose membrane was run using a BioRad Criterion™ Blotter at constant amperage (400 mA) for 60 minutes. Nitrocellulose membranes were then blocked for 60 minutes or overnight at 4°C on a rocking tray using 3% skim milk powder or 3% Bovine Serum Albumin (BSA) dissolved in 1x TBST. Membranes were probed using primary and HRP-conjugated secondary antibodies as indicated in table 2.4. HRP-conjugates were detected using ECL solution and imaged on a BioRad Chemidoc MP imaging system and processed using Image Lab Software. Densitometry analysis of the protein expression was normalized with loading control and compared.

Table 2.6: Western blot buffers

Buffer Name	**Buffer Components**
Loading Buffer (6x) for western blot	0.27M Tris base 10.3% SDS 35% Glycerol 6% β-mercaptoethanol 0.05% bromophenol blue
RIPA (Radioimmunoprecipitation assay) Buffer	10 mM Tris base 150 mM NaCl 1 mM EDTA 1% Triton X-100 Volume to 500 mL with water pH 7.4
Running Buffer (10x)	77.5 g Tris base 360 g Glycine 25 g SDS Volume to 2.5 L with water
TBS (Tris-buffered saline) (10x)	151.5 g Tris base 219 g NaCl Volume to 2.5 L with water pH 7.4
TBST (Tris-buffered saline, 0.1% Tween 20) (1x)	2.5 mL Tween20 250 mL 10x TBS Volume to 2.5 L with water

Transfer Buffer (10x)	77.5 g Tris base 360 g Glycine Volume to 2.5 L with water
Ponceau S Stain	2 g Ponceau S 30 g Trichloracetic Acid 30 g Sulfosalycylic Acid Volume to 100 mL with water
Tris-HCl, pH 6.5, 7.5, 8.1	121.1 g Tris Volume to 800 mL with water pH to desired level with concentrated HCl Volume to 1 L with water

2.5 Quantitative polymerase chain reaction (RT-qPCR)

2.5.1 RNA isolation

PCa cell lines are plated in 6-well plates at $1X10^5$ cells per well in 2 mL of growth medium as specified in section 2.2.1.1. and incubated at 37ºC and 5% CO_2 for 24 hrs to adhere to culture plates. The cells were treated with different drugs/steroids and transfection of siRNA to knockdown different genes as per the experimental plan.

Cells were washed with 1x PBS and collected using 1.0 mL Trizol per well. Chloroform isolation and isopropanol precipitation were used to extract RNA from cell lysates. Trizol samples were mixed with 200 µl of chloroform and shaken vigorously for 15 s then left to incubate for 3 minutes at RT. Samples were then centrifuged at 12000 rcf at 4°C for 15 minutes and the clear aqueous layer was collected, taking care not to disrupt the interphase layer (which contains DNA). The aqueous layer was mixed with 500 µl isopropanol, mixed and incubated for 10 minutes at RT. RNA was pelleted by centrifugation at 12000 rcf at 4°C for 10 minutes, washed in 75% EtOH and resuspended and dissolved in RT-PCR grade water. RNA concentrations were determined by spectrophotometry using a Thermo Scientific NanoDrop 2000.

2.5.2 DNase treatment

RNA samples were DNase treated using TURBO DNA-free™ DNase Treatment kits (Ambion cat#AM1907). RNA (1 to 2 µg) was diluted in RNase free water to a total volume of 44 µl, gently mixed with 5 µl of 10xTurbo DNAse Buffer with 1 µl

TURBO DNasefree and incubated at 37°C for 30 minutes. 5 µl of DNase inactivation reagent was gently mixed into each sample and repeatedly mixed 2 to 3 times over an incubation period of 5 minutes at RT. Inactivation reagent was removed by centrifugation of samples at 10000 rcf for 1.5 minutes and subsequent collection of supernatant being sure not to disrupt inactivation reagent. To ensure thorough mixing, samples were incubated at 55°C for 10 minutes, flicking twice or thrice during this time. RNA concentrations were determined using Nanodrop.

2.5.3 Reverse Transcription

Reverse transcription of RNA samples was performed following DNase treatment using iScript™ Reverse Transcription kits. RNA (1000 ng) was prepared in a 1:5 mix with iScript master mix, including one control containing all products except reverse transcriptase and a second control containing all products except RNA. RNA-iScript samples were incubated at RT for 5 minutes, 42°C for 30 minutes and 85°C for 5 minutes. Resultant cDNA samples were diluted 1:5 and stored at -20°C.

2.2.5.4 Quantitative Reverse Transcriptase Polymerase Chain Reaction (qRT-PCR)

RNA expression was examined via qRT-PCR using a BioRad C1000 Thermal Cycler and CFX384™ Real-Time System. RNA expression of target genes was measured and expression was expressed relative to reference genes as indicated. Samples were prepared by mixing 0.5 µl forward primer (5 pmol per µl), 0.5 µl reverse primer (5 pmol per µl), 5 µl iQ SYBR Green Supermix, 2 µl RNase free water, and 2 µl cDNA. Three biological and three technical replicates were

performed for all reactions. qRT-PCR reaction followed 3 minutes 95°C x1 followed by 40x 15 sec 95°C, 15 sec 55°C, 30 sec 72°C and finally 1 minute 95°C x1, 1 minute 55°C x1 and 70x 10 sec 60°C. Data were analysed using CFX Manager Software Version 3.0 (Bio-Rad Laboratories, Inc.).

2.6 Immunohistochemistry

2.6.1 Preparation of sections

Paraffin embedded human PCa sections (3 μm) were cut using a microtome and collected on Superfrost Ultra-plus slides. Slides were placed on a heating block at 62°C for a minimum of 2 hrs prior to beginning the staining procedure. Slides were de-waxed in three 5 minutes washes of 100% xylene. Xylene was cleared by dipping slides 10 times each in 3 pots of 100% EtOH, then the slides were rehydrated and stained for haematoxylin/eosin (H&E) or immunohistochemistry using primary antibodies directed at specific proteins of interest.

2.6.2 Haematoxyllin and Eosin (H&E) staining

For H&E staining, slides were washed for 2 minutes in running tap water, stained for 4 minutes in 1:2 Haematoxylin then rinsed in running tap water for 2 minutes or until the water ran clear. Slides were differentiated with 0.3% acid alcohol by dipping into the solution twice. Slides were again rinsed in running tap water for 3 minutes, counterstained with Eosin for 1 minute and rinsed one final time in running tap water until the water ran clear. Finally, slides were dehydrated and cleared in ethanol by

dipping 10 times each in 3 separate pots followed by 3 times 5 minutes incubation in xylene and coverslips were sealed using DPX mounting media. Scanning of all slides was completed using a Nanozoomer digital slide scanner (Hamamatsu). Images were viewed with NDPview software.

2.6.3 Immunohistochemistry

Slides were washed twice for 3 minutes in PBS then endogenous peroxidase activity was blocked with 0.3% H_2O_2 for 5 minutes. Antigen retrieval was completed in citrate buffer (0.525 g in 250 mL RO-water, pH 6.5) using a Biocare Medical Decloaking Chamber V3.7.2.2 for 15 minutes at 95°C and 2.5 psi. Slides were then blocked in 5% goat serum for 30 min at RT, and incubated with primary antibody as indicated overnight at 4°C. Secondary biotinylated antibody was added to slides at a dilution of 1:400 in blocking solution for 1 hr at RT followed by HRP-strepdavidin at 1:500 for 1 hr at RT. Freshly mixed DAB: H_2O_2 was added to slides for exactly 6 minutes. Slides were counterstained in fresh 1:5 haematoxylin for 1.5 minute. Slides were dehydrated and cleared in ethanol by dipping 10 times each in 3 separate pots followed by 3 times 5 minutes incubation in xylene. Coverslips were sealed using DPX. Scanning of all slides was completed using a Nanozoomer digital slide scanner (Hamamatsu). Images were viewed with NDP view software and quantified using ALLRED score (Choudhury, Yagle, Swanson, Krohn, & Rajendran, 2010) compared and correlated with different proteins.

2.6.3.1 Scoring System

Semi-quantitative system that takes into consideration the proportion of positive cells and staining intensity was performed following the ALLRED scoring system guidelines. To obtain the final scores, individual scores of the percentage of positive cancer cell nuclei (0–5) and the staining intensity (0–3) The proportion and intensity were then summed to produce total scores of 0 to 8 (Choudhury et al., 2010; Collins, Botero, & Schnitt, 2005).

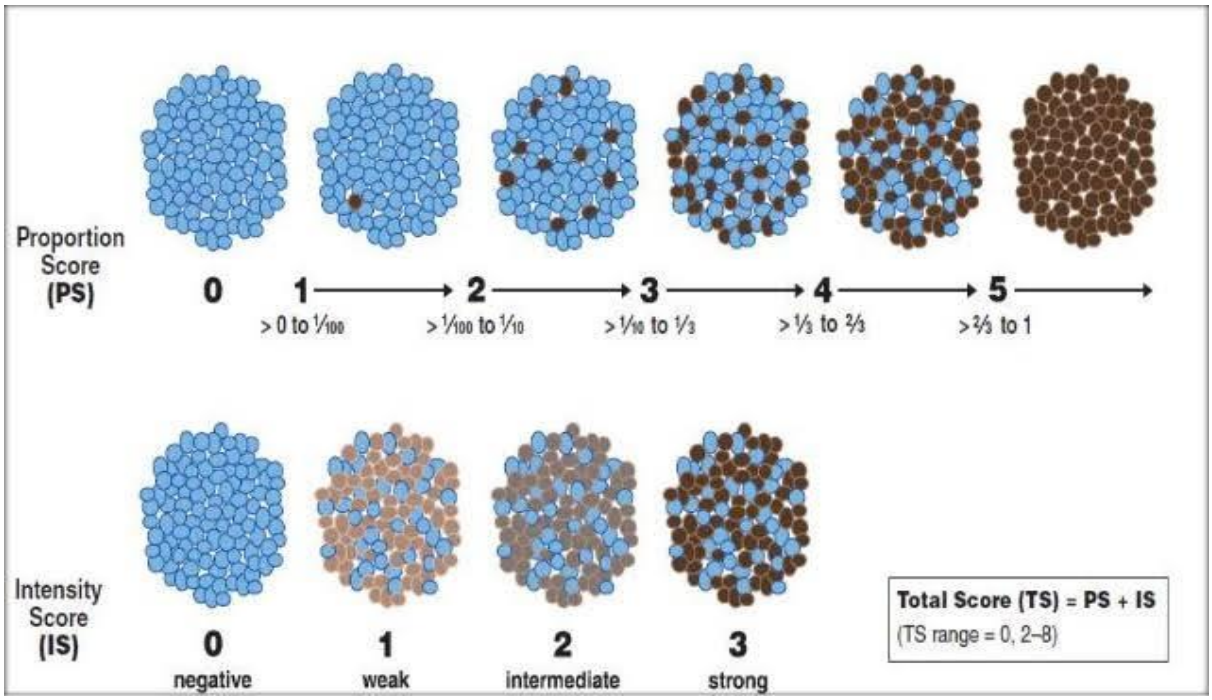

Figure 2.1: Allred scoring system for androgen receptor/ACSM1/ACSM3 scoring

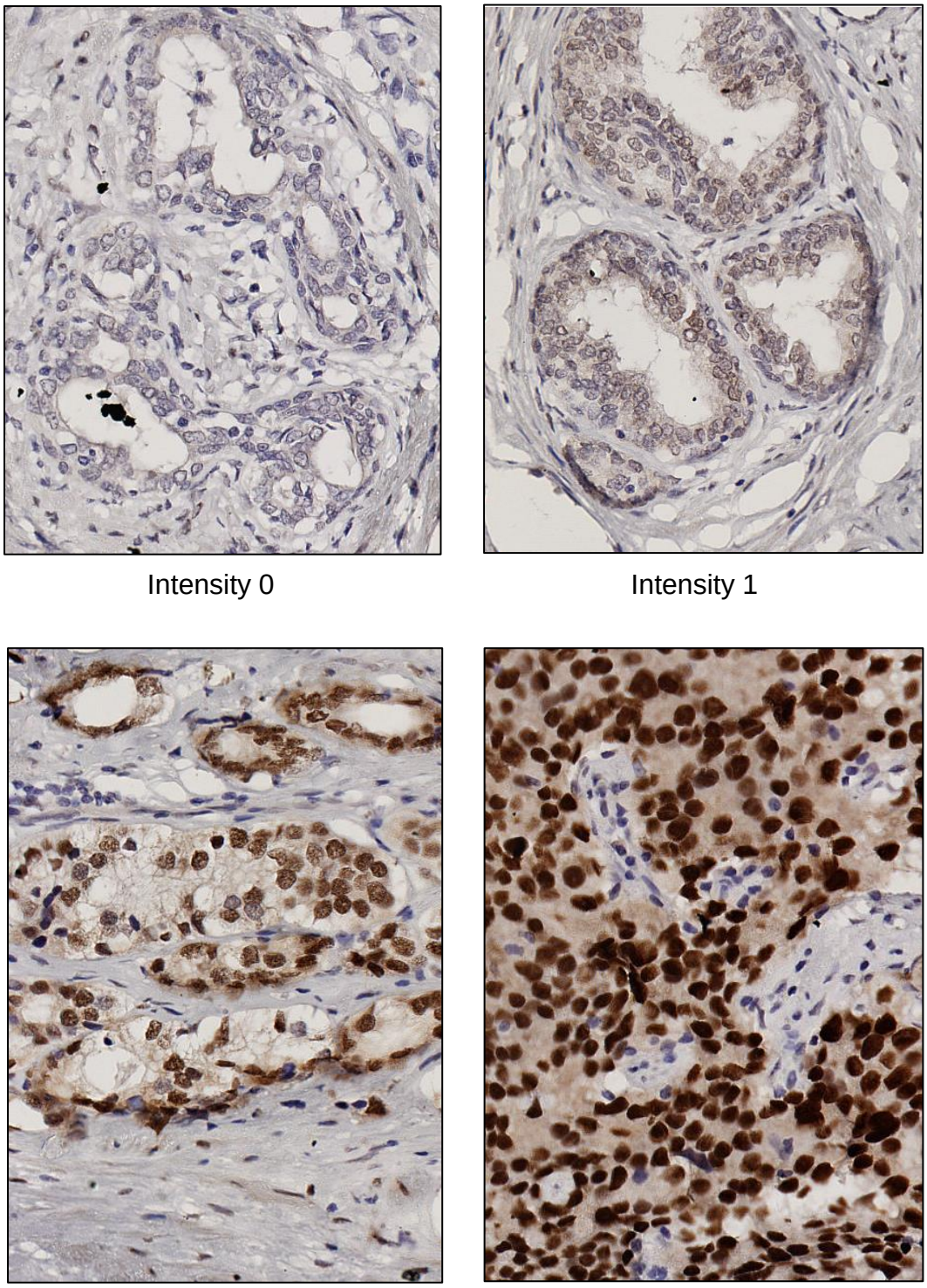

Figure 2.2: ALLRED intensity score references (AR staining prostate progression TMA)

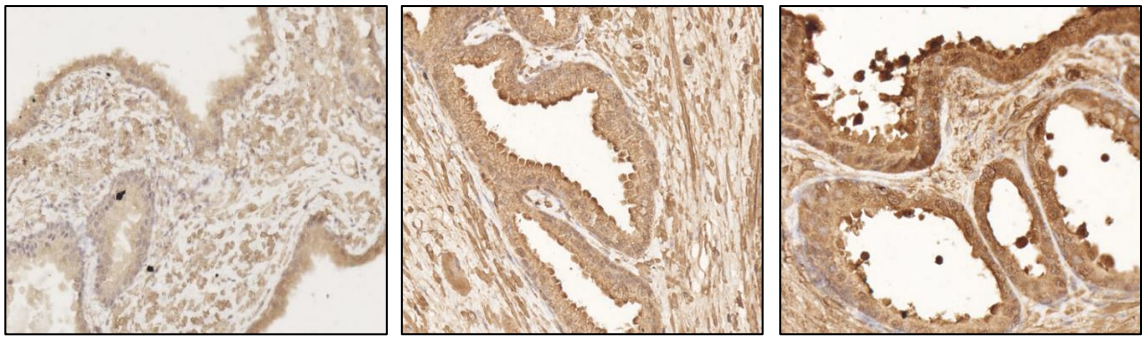

Intensity 1 Intensity 2 Intensity 3

Figure 2.3: ALLRED intensity score references (ACSM1 staining prostate progression TMA)

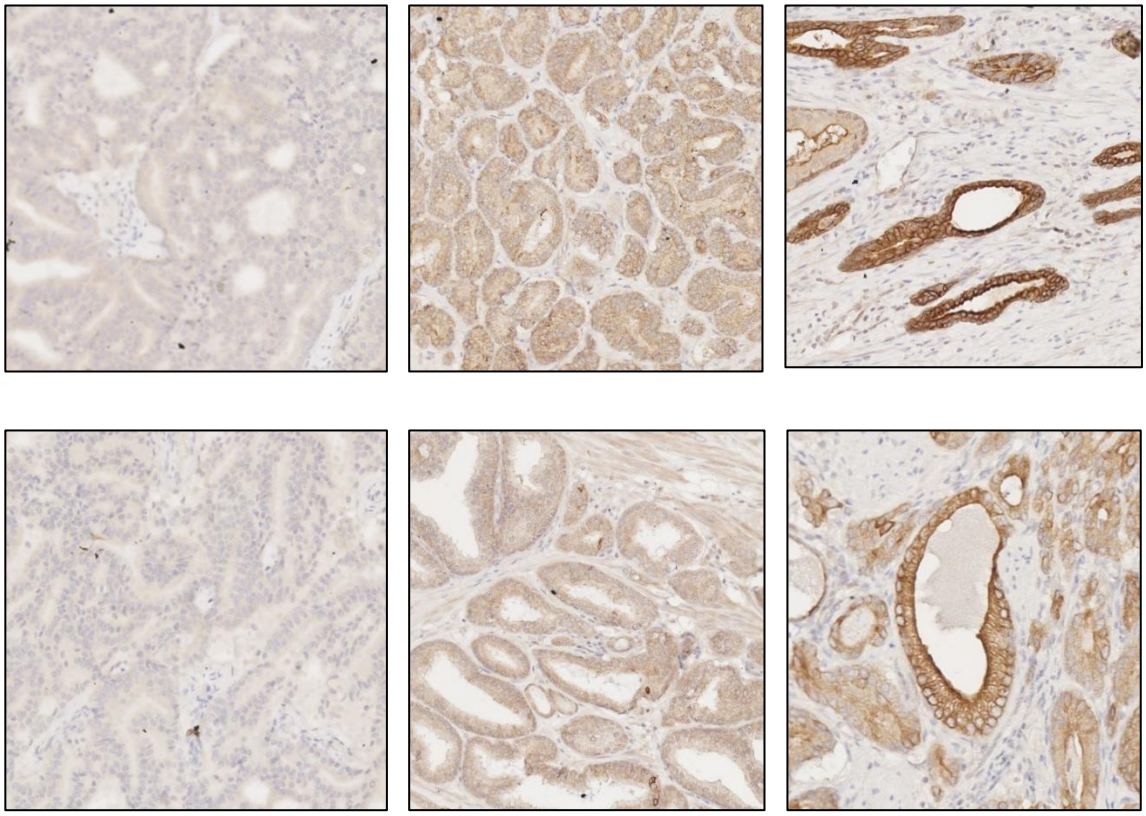

Intensity 1 Intensity 2 Intensity 3

Figure 2.4: ALLRED intensity score references (ACSM3 staining prostate progression TMA)

2.7 Androgen Receptor Chromatin Immuno-precipitation coupled with Quantitative Polymerase Chain Reaction (AR ChIP-PCR)

LNCaP cells were seeded at $3x10^6$ cells/plate in 15cm plates in RPMI 1640 + 10% FBS and allowed to grow for 3 days prior to fixation. The cells were treated with 10nM DHT for 4 hrs and cross-linked with formaldehyde. ChIP was then performed as described previously (Paltoglou et al., 2017). For ChIP-qPCR, 2 µl of DNA was used in 10 µl PCR reactions.

2.7.1 ChIP Primer design and validation

The Integrative Genomics Viewer (IGV) software was used to visualize the AR binding sites (peaks). The peak co-ordinates of the identified AR binding peaks were obtained from the dataset using IGV software. The DNA sequence of the peak co-ordinates was obtained using UCSC online genome browser [https://genome.ucsc.edu/ , Feb. 2009 (GRCh37/hg19) Assembly]. With reference the DNA sequence of the peak coordinates the primers were designed using Primer3Plus – Bioinformatics online tool (www.bioinformatics.nl/primer3plus) which was further confirmed using NCBI Primer Blast online tool to make sure that the primers are specific PCR template.

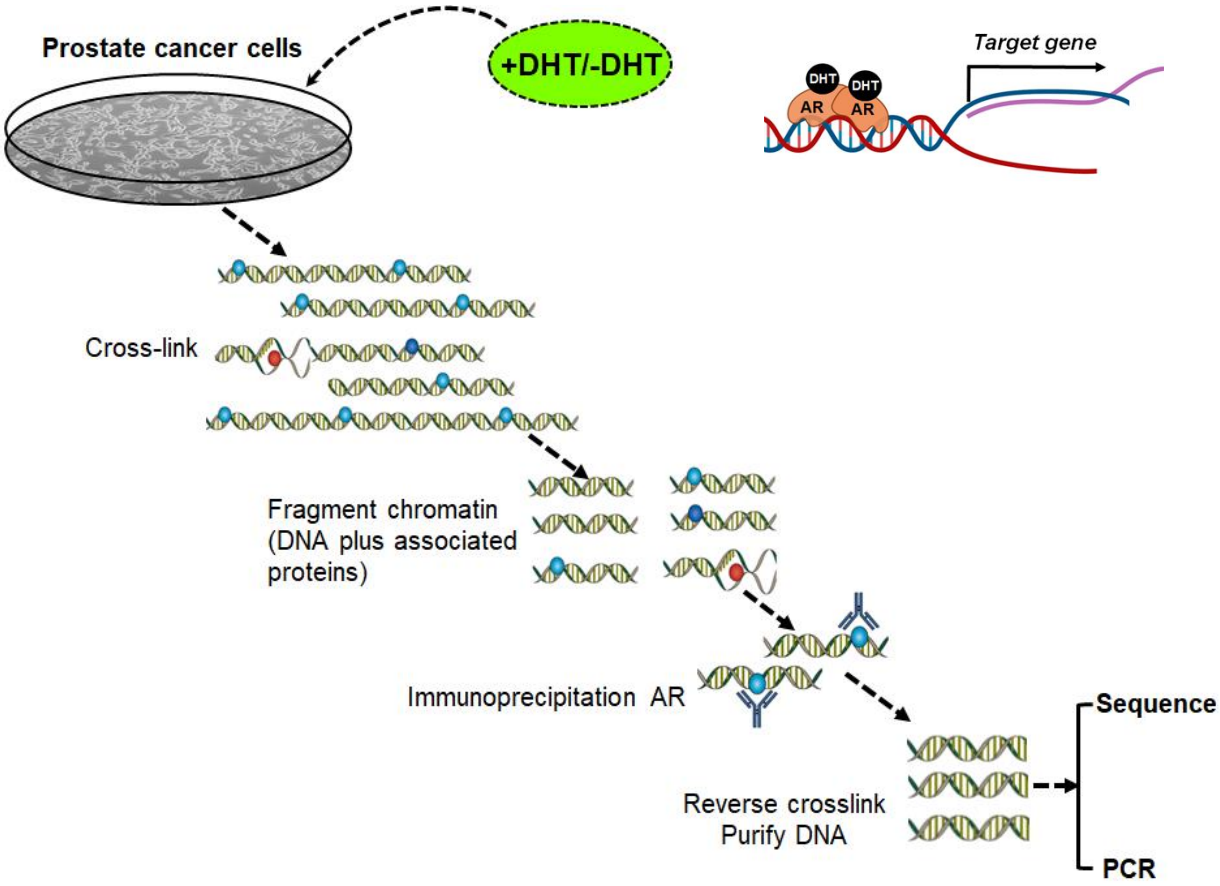

Figure 2.5: Diagrammatic representation of AR-ChIP PCR/Sequence.

Table 2.7: The buffers used for the ChIP protocol are as follow

a) Solution A

Final Concentration	**Stock concentration**	**Volume for 80ml**
1% Formaldehyde	40%	2ml
50mM HEPES-KOH, pH 7.5	0.5M	8ml
100mM NaCl	5M	1.6ml
1mM EDTA	0.5M	160µl
0.5mM EGTA	0.1M	400µl
water		67.84ml
TOTAL		80ml

b) Block solution

Final Concentration	**Volume for 50ml**
0.5% BSA	250mg
PBS	to 50ml

c) LB1

Final Concentration	Stock concentration	Volume for 100ml	Volume for 10ml
50mM HEPES-KOH, pH 7.5	0.5M	10ml	1ml
140mM NaCl	5M	2.8ml	280µl
10% glycerol	100%	10ml	1ml
1mM EDTA	0.5M	200µl	20µl
0.5% NP-40	100%	500µl	50µl
0.25% Triton X-100	100%	250µl	25µl
water		76.25ml	7.63ml
TOTAL		100ml	10ml

d) LB2

Final Concentration	Stock concentration	Volume for 100ml	Volume for 10ml
10mM Tris-HCl, pH 8.0	0.5M	2ml	200µl
200mM NaCl	5M	4ml	400µl
1mM EDTA	0.5M	200µl	20µl
0.5mM EGTA	0.1M	500µl	50µl
water		93.3ml	9.33ml
TOTAL		100ml	10ml

e) LB3

Final Concentration	Stock concentration	Volume for 50ml	Volume for 10ml
10mM Tris-HCl, pH 8.0	0.5M	1ml	200µl
100mM NaCl	5M	1ml	200µl
1mM EDTA	0.5M	100µl	20µl
0.5mM EGTA	0.1M	250µl	50µl
0.1% Na-Deoxycholate	5%	1ml	200µl
0.5% *N*-laurylsarcosine	5%	5ml	1ml
water		41.65ml	8.3ml
TOTAL		50ml	10ml

f) RIPA buffer

Final Concentration	Stock concentration	Volume for 100ml	Volume for 50ml
50mM HEPES-KOH, pH 7.5	0.5M	10ml	5ml
500mM LiCl	5M	10ml	5ml
1mM EDTA	0.5M	200µl	100µl
1% NP40	100%	1ml	500µl
0.7% Na-Deoxycholate	5%	14ml	7ml
water		64.8ml	32.4ml
TOTAL		100ml	50ml

g) TBS

Final Concentration	Stock concentration	Volume for 50ml	Volume for 10ml
20mM Tris-HCl, pH 7.6	0.5M	2ml	400µl
150mM NaCl	5M	1.5ml	300µl
water		46.5ml	9.3ml
TOTAL		50ml	10ml

h) Elution Buffer

Final Concentration	Stock concentration	Volume for 10ml
50mM Tris-HCl, pH 8.0	0.5M	1ml
10mM EDTA	0.5M	200µl
1% SDS	10%	1ml
water		7.8ml
TOTAL		10ml

2.8 Proximity-ligation assay– Fluorescence Detection

Proximity-ligation assay (PLA) was performed following the manufacturer`s instructions (Olink Bioscience). In brief, (~200,000) LNCaP cells were seeded in the sterile coverslip placed in 6 well plate with 2 mL of media. After 48 h cells were treated with DHT for 16 hrs and fixed with paraformaldehyde and permeabilized using 0.1% TritonX at room temperature. The cells were stained with anti-AR (Abcam, ER179) and anti-SREBP-1 ((Santa Cruz Biotechnology, sc2A4). PLA was performed using Duolink® In Situ PLA Probe Anti-Mouse PLUS and using Duolink® In Situ PLA® Probe Anti-Rabbit MINUS following the manufacturer`s instructions (Sigma, 92001 and 92005).

Imaging was performed using Olympus FV3000 Confocal Microscope (FLUOVIEW FV3000 series) and analyzed by ImageJ software. Signal of 300 cells were analyzed per experiment.

2.8.1 Principle of PLA assay:

Principle of the PLA assay. Firstly, the samples are incubated with two primary antibodies which bind to the proteins of interest. Secondly, two secondary antibodies conjugated with oligonucleotides (PLA probe PLUS and PLA probe MINUS) are added to the reaction. Thirdly, the oligonucleotides in the Ligation solution will hybridize to the two PLA probes and join to a closed circle by Ligase if they are in close proximity. Fourthly, in the amplification step, the oligonucleotide arm of one of the PLA probes acts as a primer for a rolling-circle amplification (RCA) reaction with the ligated circle as the template, generating the concatemeric product

with Polymerase. The fluorescently labelled oligonucleotides in the Amplification solution will hybridize to the RCA product. The signal is visible as a distinct fluorescent spot by fluorescence microscopy

Antibodies used for PLA:

- SREBP-1, Santa-Cruz sc2A4, Mouse, 1/400
- AR, LS-Bio B3326, Rabbit, 1/400

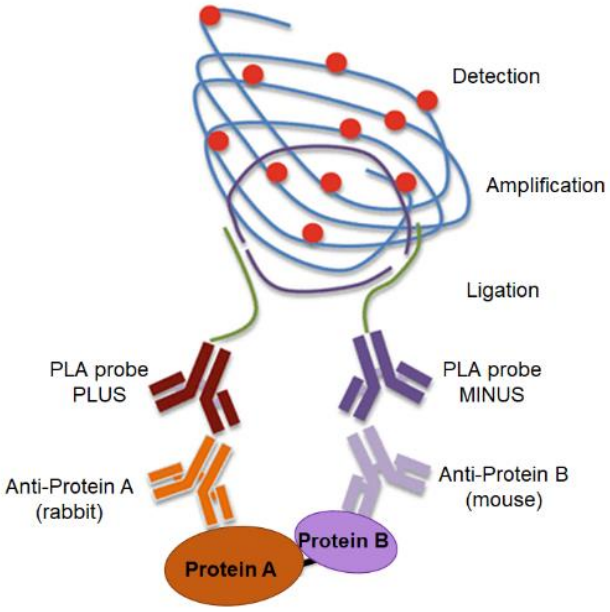

Figure 2.6: Diagrammatic representation of working principle of PLA assay (Ristic et al. 2016).

Source: https://link.springer.com/protocol/10.1007/978-1-4939-3756-1_17

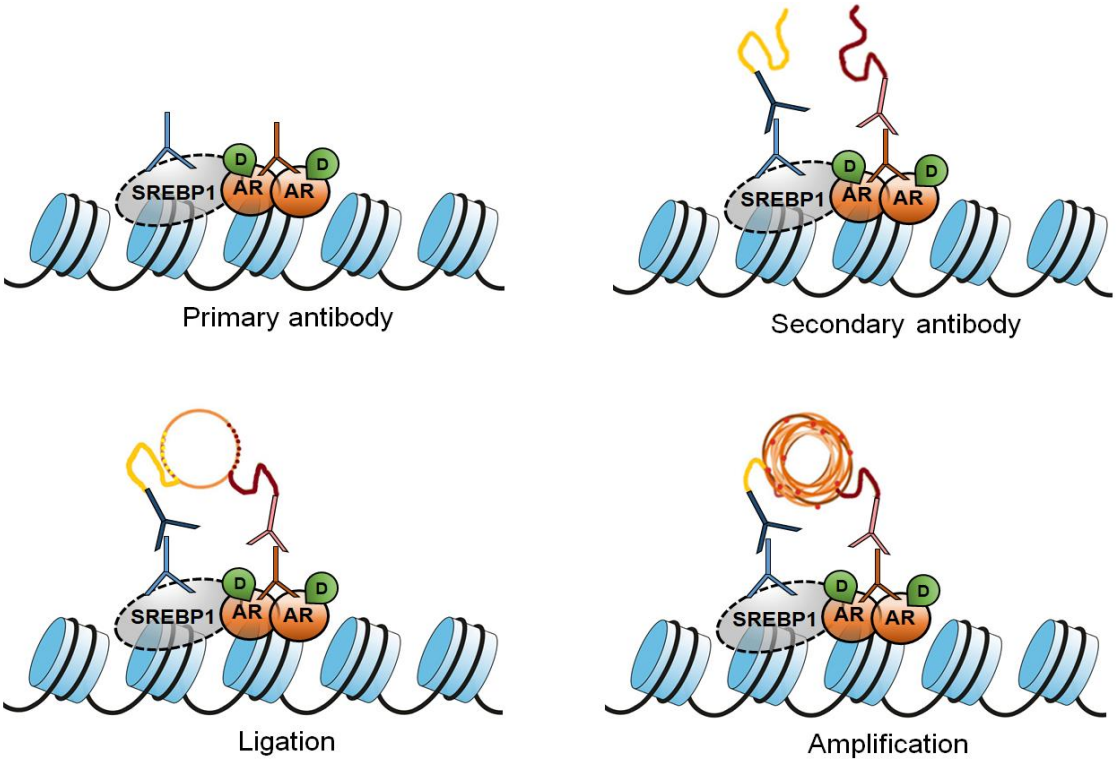

Figure 2.7: Diagrammatic representation of proposed interaction between AR and SREBP-1 and detection of interaction through PLA.

2.9 Malondialdehyde (MDA) assay

Lipid peroxidation in tissue cultures was measured in cells that were grown to 70-80% confluence on 100 mm tissue culture dishes containing complete DMEM: F12 medium. After treatment, cells were washed with ice-cold PBS, scraped into cold PBS and centrifuged for 5 minutes at 15000 rpm to obtain cell pellets that were frozen at -80^{o}C. Pellets were then thawed and homogenized in 250ul 1% Sodium dodecyl sulfate (SDS), and the homogenate was taken and 1ml 20% trichloroacetic acid (TCA; Sigma, USA),2ml 0.8% TBA (ACROS, USA) and 250ul 1% phosphoric acid were added.

The mixture was then boiled for 1 h, cooled on ice and then extracted with 1ml butanol. The mixture was centrifuged at high speed for 15 minutes, and the

absorbance of the upper phase was then measured at 530 nm with Jasco-V-530 spectrophotometer. Absorbance was converted to nmole/mg protein MDA using a standard curve that was generated with 1, 1, 3, 3- tetra ethoxypropane (TEP; Sigma, USA).

In addition to the chemical method of estimating MDA in the samples. MDA was also detected using specific antibody in western blot after ACSM1/3 knockdown in PCa cell lysate.

2.10 3D Spheroid Growth Assay

LNCaP cells were transfected with siRNA in 6-well plates for 48 hrs. Cells were collected and prepared at a concentration of 7.5 x 10^4 cells/ml. Cell suspensions (1500 cells in 20µl) were pipetted onto 96 well plate (Corning® Spheroid Microplates) and incubated at 37°C for 5 days. Photos of the formed spheres were captured, and the sphere volume was determined using ReViSP software (Piccinini, Tesei, Arienti, & Bevilacqua, 2015).

2.11 Colony formation assay

ACSM1/3 knockdown in LNCaP cells (siACSM1/3**)** or negative control cells (siControl) were prepared in a single-cell suspension before being plated in 6-well plates (500 cells/well). Cells were incubated for 2 weeks at 37°C and medium was replenished every 3-4 days. After 3 weeks, cells were washed with PBS, fixed with

4% paraformaldehyde and stained with 1% crystal violet for 30 minutes. Colonies were counted manually, and results were reported as number of colonies ± SEM.

2.12 Seahorse Extracellular Flux Analysis

Cells were plated on XF96 well cell culture microplates (Agilent) at equal densities in substrate-limited medium (DMEM with 0.5mM glucose, 1.0mM glutamine, 0.5mM carnitine and 1% FBS) and incubated overnight. One hour before the beginning of OCR measurement, the cells were changed into FAO Assay Medium (111mM NaCl, 4.7mM KCl, 2.0mM MgSO4, 1.2mM Na2HPO4, 2.5mM glucose, 0.5mM carnitine and 5mM HEPES). After baseline OCR is stabilized in FAO Assay Medium, 200μM of linoleic-acid (LA) or palmitic acid (PA) were added before initializing measurements. Extracellular flux analysis was performed using the Seahorse XF Cell Mitochondrial Stress Test kit (Seahorse Bioscience) according to the manufacturer's protocol. Extracellular flux experiments were performed on a Seahorse XF96 Analyzer and results were analysed using Seahorse Wave software for XF analyzers. The OCR values were normalized to cell numbers in each well.

2.13 Total ATP assay

LNCaP cells were transfected with siACSM1 and siACSM3 for 72 hrs in 96 well plate format. Total cellular ATP levels measurement were made according to manufacturer's instructions (Luminescent ATP Detection Assay Kit, ab113849) and

normalized to the total cellular DNA content / cell number in each well determined by CyQUANT™ Cell Proliferation Assay kit (ThermoFisher Scientific).

2.14 Lipoylation profile

Anti-DLAT and anti-DLST antibody were used to identify specific protein subunit of a-ketoglutyrate dehydrogenease and pyruvate dehydrogenase respectively which requires lipoylation for its activities. Anti-lipoic acid antibody was used to identify all the proteins that are lipoylated. Lipoylated DLAT and DLST was accessed using anti-lipoic acid antibody after knockdown of ACSM1/3.

2.15 Mitochondrial ROS Measurement

LNCaP cells were transfected with siRNA for 96 hrs in 6-well plates. Cells were collected into fluorescence-activated cell sorting (FACS) tubes and stained with 2.5mM of MitoSOX™ Red stain (Thermo Fisher Scientific, VIC, Australia) for 30 minutes in a 37°C water bath. Cells were centrifuged at 1,500rpm for 5 minutes, washed twice with 500µl of PBS, and resuspended in 500µl of pre-warmed PBS before the samples are read on a BD FACSymphony™ flow cytometer.

2.16 Seahorse Extracellular Flux Analysis

Cells were plated on XF96 well cell culture microplates (Agilent) at equal densities in substrate-limited medium (DMEM with 0.5mM glucose, 1.0mM glutamine, 0.5mM carnitine and 1% FBS) and incubated overnight. One hr before the beginning of

OCR measurement, the cells were changed into FAO Assay Medium (111mM NaCl, 4.7mM KCl, 2.0mM $MgSO_4$, 1.2mM Na_2HPO_4, 2.5mM glucose, 0.5mM carnitine and 5mM HEPES). After baseline OCR is stabilized in FAO Assay Medium, 200μM of palmitic acid (PA) was added before initializing measurements. Extracellular flux analysis was performed using the Seahorse XF Cell Mitochondrial Stress Test kit (Seahorse Bioscience) according to the manufacturer's protocol. Extracellular flux experiments were performed on a Seahorse XF96 Analyzer and results were analysed using Seahorse Wave software for XF analyzers. The OCR values were normalized to cell numbers in each well.

2.17 Glutathione assay

Cell density for day 3, 5 and 7 was optimized for the experiments. 4.0 X 10^5, 1.5 X 10^5 and 0.8 X 10^5 of cells were seeded per well for day 3, 5 and 7 harvesting. The 6 well plates were coated with poly L-lysine before seeding cells. Cells were transfected with 10nM of siRNA to knockdown *ACSM1 / ACSM3* with Control. At day 3, 5 and 7, cells were collected by scrapping and prepared for measurement of glutathione (GSH+GSSG) using the Cayman Chemical Glutathione Assay Kit (Cayman Chemical) according to the manufacturer's protocol. The GSH and GSSG concentration were calculated using a standard curve and normalized to the total protein level in each sample. Three independent biological replicates were performed for each condition.

2.18 Lipidomics assay

2.18.1 GCMS analysis of the sample

Cells were plated in 6 well plate and transfected with siRNA to knockdown ACSM1/ACSM3 with control and harvested on day 5, 6 and 7. On the day of harvest the cell containing plates were removed from the incubator and placed on ice. 1.0 mL of media was collected from the each well in the pre-labelled clean 1.5 mL Eppendorf vial and stored at -80°C. The remaining media was discarded and cells were washed with cold PBS for 3 times. Cells were collected by scraping followed by centrifugation at 450 rcf for 5 minutes. The cell pellets were frozen for long term storage before extracting fatty acids/lipids for analysis.

Total fatty acid extraction and analysis was done in 3 different steps

- Extraction of fatty acids from the sample matrix
- Derivatization /methylation of the fatty acids
- GC–MS analysis

On the day of lipid extraction, the samples (cell pellet and media) were thawed at room temperature and following protocol was followed to extract lipid from the samples for analysis.

Table 2.8: Protocol for fatty acid extraction for GC-MS analysis

Reagents:	**Cell pallet**	**Media**
Sample	Cell pellet	1.0 mL
Normal saline	1.5 mL	0.5 mL
Isopropanol (IPA + 0.005%BHA)	2.0 mL	-
Methanol	-	2.0 mL
Resuspend cell suspension / media and brief vortex Stand in room temperature for 10 minutes with brief vortex in between		
Chloroform	4.0 mL	4.0mL
After addition of Chloroform, give brief vortex Centrifuge at 1500 RPM for 10 minutes Separate the lower phase into new tubes Dry the content using nitrogen vapour		
Sulphuric acid	2.0 mL	2.0 mL
For the methylation, sulphuric acid was added Brief verted and incubated at for 2 hrs with brief vortex in between		
Water	250 µL	250 µL
Heptene	0.6mL	0.6mL
Brief vortex Collect the upper heptane layer in the next tube to inject in GCMS		

The hepten layer was collected in 1.0 mL tubes and injected in the GCMS to detect the peaks. The peaks were identified using standard peaks. The relative quantity of the individual fatty acid was determined and compared with different treatment groups.

2.18.2 Lipidomics analysis

Cell density for day 4 and 6 was optimized for the experiments to harvest equal numbers of cells from the each treatment in 6-well plate set up. As the knockdown slows down cell growth of LNCaP cells, the seeding density of the cells in siACSM1 and siACSM3 knockdown wells was higher than control group but the numbers of the cells on day of harvest (cells counted using coulter counter) was approximately equal. The different seeding density of the cells in the different treatment groups are listed in the table below.

Table 2.9: Seeding density for lipidomic analysis of the cells after knockdown of ACSM1 and ACSM3 in LNCaP cells

Treatment	Seeding density for different day cell harvest	
	Day 4	Day6
siNC	1.0 X 10^5 cells/well	8.0 X 10^4 cells/well
siACSM1	1.5 X 10^5 cells/well	1.2 X 10^5 cells/well
siACSM3	1.5 X 10^5 cells/well	1.2 X 10^5 cells/well

On the day of harvest the cell containing plates were removed from the incubator and placed on ice. Media was removed and cells were washed with cold PBS or physiological saline for 3 times. The cells scrapped and collected in 1.5 ml tubes by centrifugation at 20000g for 5 minutes. The supernatant was removed and the cell pellet were frozen at -80°C for storage. Finally the samples were shipped in dry for analysis.

2.19 Metabolomics

Table 2.11: Buffers for metabolomics

Buffer Preparation:
1. MeOH: H_2O (1:1) Required per well: 0.6 mL (Calculate total amount required for the experiment) To prepare **20 mL** (10 mL of LC grade Methanol + 10 mL LC grade H_2O) Add internal standards C2107 (1S)-(+)-10-Camphorsulfoniuc acid (Cf = 0.25uM), and M3885 MES sodium salt (Cf+5uM) to the MeOH:H_2O solution
2. Internal Standards: **2.a. (1S)-(+)-10-Camphorsulfoniuc acid (25mM STOCK)** MW = 232.30 Prepare 25mM STOCK using LC grade H_20 Weigh 0.5g + 86.25ml LC grade H_20 **2.b. MES sodium salt (5mM)** MW = 217.22 Prepare 5mM STOCK using LC grade H_20 Weigh 0.1g + 92ml LC grade H_20 *Make serial dilution to get the final concentration.*
3. NaCl Saline Buffer: Required conc: 0.9% w/v NaCl in LC grade H20 4.5g in 500ml LC grade H_20
4. Chloroform LC Grade Aliquot 50 ml and place at -80C overnight.

LNCaP cells were transfected with siRNA for 48 hrs in RPMI (phenol red free) with 10% FBS supplemented with 2.0mM glucose in 6-well plates. To harvest cells pellet and media, the plates were placed in sufficient volumes of ice to cover the surface

of the plate. Cells were washed twice with 5 ml cold NaCl saline and 300µl of ice cold methanol:chloroform (MeOH:CHCl3) extraction solvent containing the internal standards (0.5µl/samples) was added onto each well and scrapped to collect cells into 15ml falcon tubes. Additional 300 µL MeOH:CHCl3 was added to rinse the well to collect the remaining cells. 1.5 ml of chloroform was added in each tube, vortexed and incubated on ice for 5 minutes. The tubes were centrifuged at 4°C for 5 minutes at 16,100g and the top aqueous layer was then transferred into a fresh 1.5ml Eppendorf tube and allowed to dry in a Speedvac. Dried samples were derivatised with 20µl methoxyamine (30mg/ml in pyridine, Sigma Aldrich) and 20µl N,O-Bis(trimethylsilyl) trifluoroacetamide (BSTFA) + 1% Trimethylchlorosilane (TMCS). The derivatised samples were analysed using GC QQQ targeted metabolomics as described in (Best et al., 2018).

2.20 Lipid Peroxidation Analysis by Imaging

For imaging, LNCaP cells following ACSM1 and ACSM3 knockdown were plated at 2.5 x 10^3 cells/well in a 8-well chamber slide. Cells were then washed with Hank's balanced salt solution (HBSS) and incubated with 5µM BODIPY-581/591 C11 stain (Thermo Fisher Scientific). Cells were washed and fixed with 4 % paraformaldehyde (PFA), and mounted with Prolong Gold anti-fade solution with DAPI (Thermo Fisher Scientific). Cells were imaged at 60 X magnification using a Olympus FV3000 Confocal Microscope. Quantification of BODIPY-C11 stain was performed using ImageJ analysis software.

2.21 Lentiviral transduction of cells

SMARTvector Inducible Lentiviral shRNA vectors for ACSM1, ACSM3 and Non-targeting shRNA Control (glycerol stock *E. coli*) were obtained from Dharmacon (catalogue numbers V3SH11252-225482707 and V3SH11252-224860261). For over-expression of ACSM1 and ACSM3 in PCa cells, linear dsDNA fragments containing codon-optmised ACSM1 and ACSM3 cDNA sequences were cloned into Gateway entry vector (pDONR221) and then transferred into pJS64 destination vector. The sequence of the inserts was verified by Sanger sequencing at AGRF. Viral supernatants were prepared by transfection of HEK293T cells with the vector plasmids and packaging plasmids (psPAX2 Addgene 12259 and pMD2.G Addgene 12260). The transfection was performed with polethylenimine (PEI MAX Transfection Grade Linear Polyethylenimine Hydrochloride, 24765-1, Polysciences) as described previously (Das et al., 2017). After 48 hrs, supernatants were filtered through 0.45 µm and 0.22 µm syringe filters and then concentrated ~100-fold using Vivaspin 100 kDa cut-off columns by centrifugation at 3000 g at 10°C for 6 hrs. Concentrated virus was stored at -80° C. For transduction, luciferase-tagged LNCaP cells (for shRNA viruses) and untagged LNCaP cells (for over-expression vectors) were seeded at 1.25 x 10^5 cells in 6 well plates and the following day were transduced with concentrated lentivirus for a period of 3 days. Puromycin (1.0 µg per mL) was added to select for transduced cells for an additional 3 days. Cells transduced with shRNA constructs were grown in 2ug µg per ml of doxycycline to induce expression of shRNAs.

2.22 Animal experiments

All animal procedures were were approved by the University of Adelaide Animal Ethics Committee (approval number M-2019–037) and carried out in accordance with the guidelines of the National Health and Medical Research Council of Australia. LNCaP-NC and LNCaP-shACSM3 cell suspensions (1×10^6 cells in 10 µl PBS) were injected intraprostatically in 8-week old NOD/SCID male mice. Whole-body imaging to monitor luciferase-expressing LNCaP cells was performed at day 3 of the injection and once weekly thereafter using an IVIS Spectrum *in vivo* Imaging System (PerkinElmer). D-luciferin (potassium salt, PerkinElmer) was dissolved in sterile deionized water (0.03 g/ml) and injected subcutaneously (3 mg/20 g of mouse body weight) before imaging. Bioluminescence was reported as the sum of detected photons per second from a constant region of interest.

2.23 Statistical analysis

All the experiments were performed at least three times. Results were statically analysed using GraphPad Prism 7.02 software. Error bars represent the standard error of the mean (SEM). Scatter plots were analysed using student's t test which were two-tailed and unpaired, with statistical significance accepted at $p<0.05$. Detailed methods for statistical analysis are included in figure legends or in the individual Chapter methods.

CHAPTER 3. IDENTIFICATION OF NOVEL AR-REGULATED LIPID METABOLIC GENES IN PROSTATE CANCER

3 Identification of novel AR regulated lipid metabolic genes in prostate cancer

3.1 Anatomy and Physiology of Prostate Gland

Dysregulated lipid metabolism is a hallmark of PCa (Barfeld et al., 2014; Rysman et al., 2010). An emerging concept is that AR plays a major role in lipid metabolism by directly regulating genes that are involved in this process (Butler et al., 2016). Direct regulation refers to a process whereby AR directly binds to cis-regulatory elements that regulate the expression of a particular gene, as opposed to indirect regulation in which the gene is regulated via downstream effects. The specific cis-regulatory elements that AR binds to and regulates are referred to as androgen response elements (AREs). It is often challenging to identify whether a particular gene is directly regulated by AR because AREs are often found in gene enhancers that are very distal, often greater than tens of kilobases, from the genes that they regulate (D. Wu, Zhang, Shen, Nephew, & Wang, 2011). This is distinct from other transcription factors, such as Sp1 (stimulatory protein 1), SREBP (sterol-regulatory-elementbinding protein), NF-Y (nuclear factor-Y), and USF (upstream stimulatory factor) that normally bind to gene promoters (M. R. Briggs, Kadonaga, Bell, & Tjian, 1986; Dorotea, Koya, & Ha, 2020; Teran-Garcia et al., 2007)

In this chapter, I describe a relaFtively unbiased strategy to identify novel direct AR-regulated genes involved in lipid metabolism. Further investigation into a subset of these genes is described in the following chapter.

3.2 Methods

3.2.1 Selection of Candidate genes

To identify novel downstream mediators by which AR regulates lipid metabolism in PCa, we manually curated a list of 178 genes encoding enzymes with a putative role in lipid metabolic processes. The gene list was created by combining the Kyoto Encyclopedia of Genes and Genomes (KEGG) "lipid metabolism" pathway (Kanehisa, Furumichi, Tanabe, Sato, & Morishima, 2017), the REACTOME "Metabolism of lipids" pathway (Fabregat et al., 2017), the Gene Ontology "lipid metabolic process" (www.geneontology.org) and manual addition of select genes not present in those groups but with published putative roles in fatty acid metabolism. The curated gene list was then subjected to a series of filtering steps (Figure 3.1) to identify those regulated by AR and with a potential oncogenic role in PCa. Our gene filtration pipeline encompasses 3 different criterion which are discussed below.

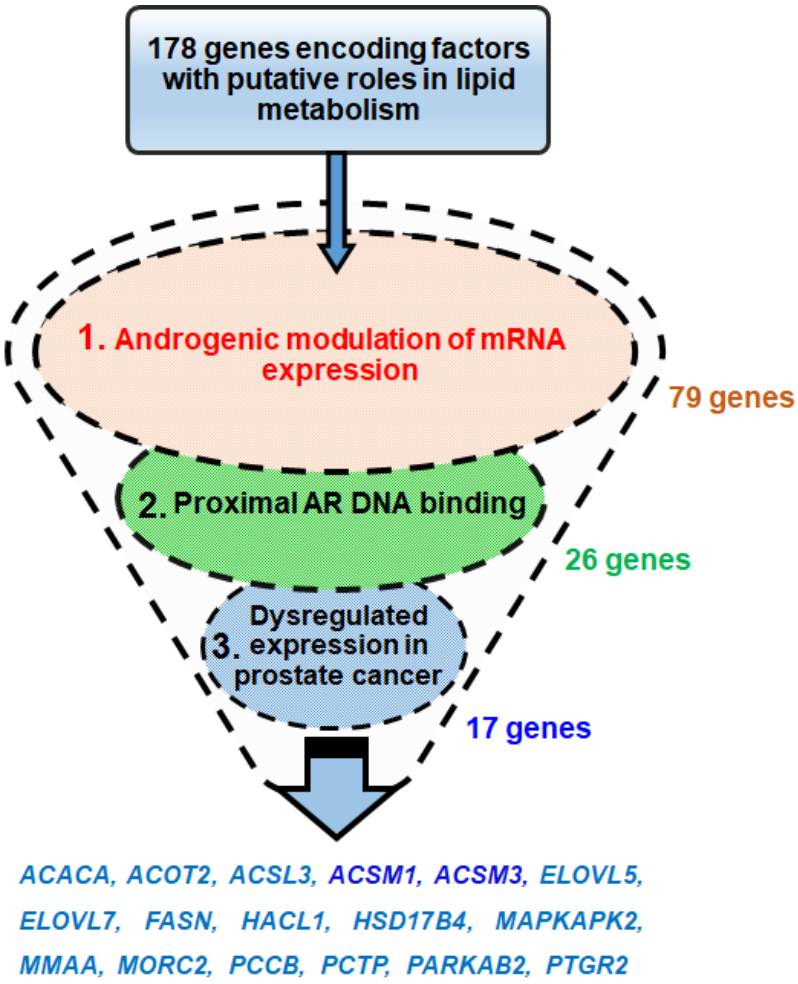

Figure 3.1: Schematic illustration of filtering methods to select the candidate genes for subsequent validation.

3.2.1.1 Criterion 1: Androgenic regulation of mRNA expression.

The androgen-sensitive PCa cell line LNCaP is the most frequently used model for identification of genes regulated by the AR signalling axis (Jin, Kim, & Yu, 2013) Thus, we selected two gene expression datasets in which LNCaP cells had been treated with androgens: 1) GSE7868: expression profiling by cDNA microarray after 0, 4 hrs and 16 hrs of treatment with DHT; 2) GSE22606: expression profiling by microarray after 0 and 48 hrs of R1881 treatment. Students t tests (for GSE22606) or ordinary one way ANOVA tests (for GSE7868) were used to compare the differential gene expression between different treatment groups. We included genes that had a significant change (in either or both) datasets and discarded genes that showed an opposite pattern of regulation in the 2 datasets.

3.2.1.2 Criterion 2: Proximal AR-DNA binding

Androgenic gene regulation does not necessarily identify genes that are directly regulated by AR. In some cases, AR regulates the expression of genes through different transcription factors regulation which is an indirect effect of the androgen treatment. Therefore, we used AR genome-wide DNA binding data to identify genes with proximal AR binding sites. The data was generated by ChIP-seq, a method that interrogates genome-wide physical binding between DNA and a specific protein of interest. Specific DNA sites in direct physical interaction with the protein of interest (transcription factors) can be isolated by chromatin immunoprecipitation (ChIP), and identified by next-generation sequencing (ChIP-seq). In this method, AR is immunoprecipitated with a specific antibody and co-

precipitating DNA, with AR binding sites identified as areas with enriched DNA sequences.

The dataset we used was Pomerantz et al dataset (GSE56288), which is comprised of AR ChIP-seq from 13 independent PCa tissue and 7 histologically normal samples (where 6 tumours had matched normal samples) (Pomerantz et al., 2015). We first generated a consensus peak set for the 13 tumours; more specifically, a peak had to be present in all 13 tumours to be included in this set. To do this, we used Diffbind (Ross-Innes et al., 2012) (dba.peakset command, minOverlap=13).

To the best of our knowledge, there is no clear-cut demarcation of the genomic window of AR binding to regulate its direct targets. Therefore, in this study we considered genes to be candidate direct targets if an AR binding site was detected within 100 kb of the transcriptional start site (TSS), a cutoff that has been used in the past (Q. Wang, Carroll, & Brown, 2005; L. Wu et al., 2014). Using the consensus Pomerantz peak set described above, we identified all genes that had an AR binding site with 100 kb of the TSS. This was done using CisGenome software (http://www.biostat.jhsph.edu/~hji/cisgenome/ (Ji et al., 2008)) ("Annotate with Neighbouring genes" tool, maximum distance 100,000 bp). The Integrative Genomics Viewer (IGV) (Robinson et al., 2011) software was used to visually inspect AR binding peaks proximal to the TSS of candidate genes. Only genes with AR peaks present in all the tumour tissues from Pomerantz et al were selected for the next filtering step.

We also used AR ChIP-seq data from VCaP cells (GSE55064) (Asangani et al., 2014) as another indicator of the relevance of these binding events. This AR ChIP-seq data from VCaP cells consist of samples treated with vehicle and 10nM DHT treatment after VCaP cells were grown in charcoal-stripped serum containing media. The enrichment of the binding sites were confirmed with DHT treatment but the VCaP data was not used to filter genes.

3.2.1.3 Criterion 3: Dysregulated expression in PCa.

We reasoned that AR-regulated genes with an important role in oncogenic lipid metabolism would be dysregulated in PCa compared to the normal prostate. Thus, we evaluated candidate direct AR target genes (i.e. genes that passed the first 2 filtering steps) in 3 distinct clinical transcriptomic datasets cohorts: TCGA ("The Molecular Taxonomy of Primary Prostate Cancer," 2015); MSKCC (D. Robinson, E. M. Van Allen, et al., 2015b); and CPGEA (J. Li et al., 2020). The TCGA dataset consists of RNA-seq data of lipid metabolism genes from prostate tumours (n=52) and matched normal prostate tissues (n=52) lipid metabolic gene expression in PCa. The MSKCC cohort consists of microarray expression data (Agilent 244K aCGH) for normal (n=29) and primary prostate tumours (n=131) and metastatic (n=19) PCa data. The CPGEA cohort consists of 208 patient-matched pairs of primary tumours and matched healthy control tissues from Chinese patients.

For TCGA and MSKCC, the normalized gene expression data was obtained from cBioportal (www.cbioportal.org). For CPGEA, normalized gene expression data was obtained from http://bigd.big.ac.cn/gsa-human/. Differential gene expression between tumour and normal tissues was determined using a paired ‘t’ test in TCGA, MSKCC and CPGEA dataset. Genes that were significantly altered

(in the same direction) in at least two of the three datasets were included, whereas genes exhibiting an opposite pattern of regulation in any of the datasets were excluded.

3.3 Result

Of the 178 genes with known or putative roles in lipid metabolism, 79 (44%, n=79) were modulated by androgen treatment in LNCaP cells (Table 3.1) and 26 of these had evidence of AR binding events proximal to their TSS (Table 3.2). Thus, 26/178 (14.6%) are putative direct targets of the AR transcription factor. Out of these, 17 exhibited consistent dysregulation in cancer vs normal tissues shown in Table 3.3. For these 17 genes, androgen regulation in LNCaP cells, AR binding and expression in prostate cancer patient cohorts are shown in Figures 3.2 - 3.18. Supplementary table S3.1 - S3.3 consist of results of data mining process and **Error! Reference source not found.** consist of functions or proposed functions of the final 17 genes.

Table 3.1: List of genes involved in lipid metabolism that are modulated by androgen in LNCaP cells

S.No.	Gene name	GSE7868			GSE22606	
		Regulation and time points			Regulation at 48 hrs	
		Reg	4 hrs (p value)	16 hrs (p value)	Reg	p value
1	*ABCC1*	1	0.219	0.0012	1	0.0001
2	*ABCD1*	0	0.8329	0.4785	-1	0.0023
3	*ACAA1*	1	0.9546	0.0047	1	0.0001
4	*ACACA*	1	0.0924	0.0001	1	0.0001
5	*ACAD11*	0	0.8323	0.3283	-1	0.0038
6	*ACADM*	0	0.4834	0.89	1	0.0005
7	*ACADVL*	0	0.9313	0.7249	1	0.0086
8	*ACBD5*	0	0.1727	0.1516	-1	0.0099
9	*ACBD6*	-1	0.7704	0.0226	-1	0.0005
10	*ACLY*	1	0.4369	0.0001	1	0.0001
11	*ACOT1*	0	0.9876	0.7639	1	0.0379
12	*ACOT2*	0	0.9876	0.7639	1	0.0379
13	*ACOT7*	0	0.1541	0.6986	1	0.0008
14	*ACOT8*	0	0.6136	0.9166	1	0.0018
15	*ACOT9*	0	0.5061	0.2002	1	0.0003
16	*ACOX1*	0	0.1827	0.1166	1	0.0197
17	*ACOX3*	1	0.0407	0.0392	1	0.0019
18	*ACSL3*	1	0.101	0.0007	1	0.0001
19	*ACSM1*	0	0.5393	0.9684	1	0.0001
20	*ACSM3*	1	0.8656	0.05	1	0.017
21	*ALDH3A2*	0	0.1503	0.5892	1	0.0141
22	*AMACR*	1	0.5818	0.0132	1	0.0001
23	*CPT2*	0	0.8673	0.1489	1	0.0237
24	*CROT*	0	0.1298	0.1588	1	0.0001
25	*CYP2C19*	0	0.6474	0.6067	1	0.0041
26	*CYP2C9*	0	0.6857	0.3581	-1	0.0273
27	*CYP2J2*	0	0.8819	0.9879	-1	0.0214

28	*CYP2U1*	1	0.0008	0.0779	1	0.0001
29	*CYP4A22*	0	0.9011	0.6213	1	0.0388
30	*CYP4B1*	1	0.0308	0.9587	0	0.6564
31	*DBI*	1	0.8726	0.0096	0	0.9999
32	*DECR1*	-1	0.7262	0.0302	-1	0.0003
33	*ECHS1*	0	0.8997	0.6245	-1	0.0163
34	*ECI1*	0	0.8983	0.9038	1	0.0001
35	*ECI2*	1	0.0695	0.0084	1	0.0001
36	*ELOVL1*	1	0.0444	0.0014	1	0.0001
37	*ELOVL2*	0	0.8907	0.2161	1	0.0238
38	*ELOVL5*	1	0.0672	0.0001	1	0.0001
39	*ELOVL7*	1	0.0348	0.0003	1	0.0001
40	*EPHX2*	1	0.9986	0.0485	1	0.0199
41	*FAAH*	0	0.6077	0.2284	1	0.2323
42	*FADS1*	0	0.7768	0.9594	1	0.0001
43	*FADS2*	0	0.0382	0.1064	1	0.0004
44	*FAM213B*	0	0.8756	0.566	-1	0.0101
45	*FASN*	1	0.9964	0.03	1	0.0002
46	*HACD2*	0	0.6324	0.3858	1	0.0001
47	*HACL1*	-1	0.0025	0.0001	-1	0.0001
48	*HADHB*	-1	0.0935	0.0107	-1	0.0001
49	*HPGD*	1	0.7768	0.9594	1	0.0001
50	*HSD17B4*	1	0.6417	0.0013	0	0.115
51	*LTA4H*	-1	0.0082	0.0014	-1	0.0001
52	*MAPKAPK2*	0	0.9303	0.378	1	0.0057
53	*MCEE*	0	0.3735	0.0554	1	0.0016
54	*MID1IP1*	0	0.1291	0.1738	-1	0.0068
55	*MMAA*	1	0.3774	0.001	1	0.0001
56	*MORC2*	0	0.9272	0.9988	-1	0.0022
57	*MUT*	0	0.4519	0.076	-1	0.0006
58	*NUDT19*	0	0.8311	0.4027	-1	0.0009
59	*OLAH*	0	0.6178	0.4035	1	0.0461
60	*PCCB*	-1	0.2121	0.0116	-1	0.001
61	*PCTP*	0	0.8897	0.8224	1	0.0001
62	*PHYH*	-1	0.9881	0.0582	-1	0.0002

63	*PON1*	1	0.0487	0.098	0	0.7928
64	*PON2*	-1	0.1345	0.0041	-1	0.0002
65	*PPARD*	0	0.9976	0.6282	-1	0.0214
66	*PPT11*	-	-	-	1	
67	*PRKAB2*	0	0.1907	0.8147	1	0.0004
68	*PRKAG2*	0	0.9642	0.9788	-1	0.0024
69	*PTGES2*	0	0.994	0.5381	-1	0.0084
70	*PTGIS*	1	0.449	0.0183	0	0.6553
71	*PTGR1*	1	0.1794	0.0226	0	0.6166
72	*PTGR2*	0	0.9963	0.8514	1	0.0003
73	*RXRA*	0	0.1045	0.313	-1	0.0001
74	*SCD*	0	0.5616	0.0583	1	0.0002
75	*SLC22A5*	1	0.5567	0.2404	1	0.0006
76	*SLC25A17*	-1	0.1641	0.0075	0	0.6694
77	*SLC25A20*	1	0.132	0.012	1	0.0001
78	*SLC27A2*	0	0.0156	0.1493	-1	0.0073
79	*THEM4*	0	0.9487	0.7405	-1	0.0007

Abbreviation: Reg, Regulation pattern; 1, Upregulation; -1 down regulation; 0, No change.

Table 3.2: List of genes that are androgen modulated and have AR binding sites proximal to the TSS. Base pair, bp.

Gene name	Distance from TSS (bp)
ABCC1	-29459
ACACA	-22605
ACADVL	35292
ACBD6	-26064
ACOT2	91643
ACOX3	88713
ACSL3	-74582
ACSM1	-13004
ACSM3	-59730
CROT	-982
DBI	-477
ELOVL5	-84792
ELOVL7	16842
FASN	36578
HACL1	-72082
HSD17B4	49389
MAPKAPK2	-89291
MMAA	60695
MORC2	-87412
PCCB	93424
PCTP	-20008
PHYH	-99875
PRKAB2	48774
PTGR1	-6108
PTGR2	93399
SLC25A20	13013

Table 3.3 The list of candidate genes fulfilling all 3 criteria.

Figure	Gene symbol	Gene Name	Androgen treatment in LNCaP cells	Tumour gene expression compared to normal
3.2	*ACACA*	*Acetyl-CoA carboxylase 1*	↑	↑
3.3	*ACOT2*	*Acyl-coenzyme A thioesterase 2, mitochondrial*	↑	↓
3.4	*ACSL3*	*Long-chain-fatty-acid--CoA ligase 3*	↑	↑
3.5	*ACSM1*	*Acyl-coenzyme A synthetase ACSM1, mitochondrial*	↑	↑
3.6	*ACSM3*	*Acyl-coenzyme A synthetase ACSM3, mitochondrial*	↑	↑
3.7	*ELOVL5*	*Elongation of very long chain fatty acids protein 5*	↑	↑
3.8	*ELOVL7*	*Elongation of very long chain fatty acids protein 7*	↑	↑
3.9	*FASN*	*Fatty acid synthase*	↑	↑
3.10	*HACL1*	*2-hydroxyacyl-CoA lyase 1*	↓	↑
3.11	*HSD17B4*	*Peroxisomal multifunctional enzyme type 2*	↑	↑
3.12	*MAPKAPK2*	*MAP kinase-activated protein kinase 2*	↓	↓
3.13	*MMAA*	*Methylmalonic aciduria type A protein, mitochondrial*	↑	↑
3.14	*MORC2*	*ATPase MORC2*	↑	↑
3.15	*PCCB*	*Propionyl-CoA carboxylase beta chain, mitochondrial*	↓	↑
3.16	*PCTP*	*Phosphatidylcholine transfer protein*	↑	↑
3.17	*PRKAB2*	*Protein Kinase AMP-Activated Non-Catalytic Subunit β2*	↑	↓
3.18	*PTGR2*	*Prostaglandin reductase 2*	↓	↑

Abbreviation: ↑, upregulated gene expression; ↓, downregulated gene expression compared to vehicle/normal prostate.

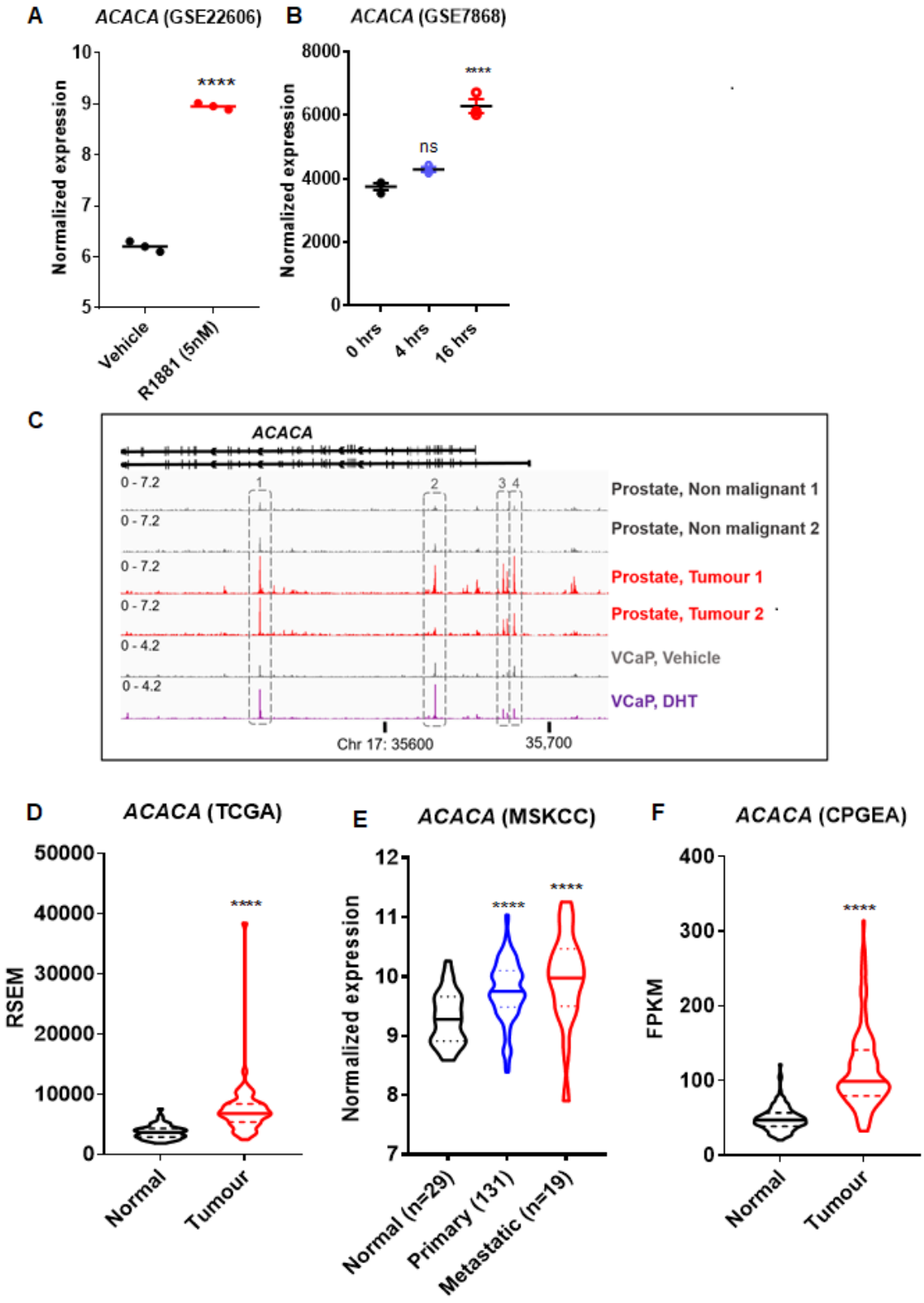

Figure 3.2: *ACACA* is a candidate direct AR target gene that is dysregulated in prostate cancer. Expression of *ACACA* in response to: (A) Vehicle or R1881

(5nM) treatment (B) DHT (1nM) in cells grown in charcoal-strippd serum; error bars are SEM. Differential expression was evaluated using unpaired t tests (*, $p < 0.05$; **, $p < 0.01$; ***, $p < 0.001$; ****, $p < 0.0001$). (C) ChIP-seq data showing AR DNA binding near the *ACACA* gene in non-malignant and prostate tumour samples ((GSE56288, (Pomerantz et al., 2015)) and VCaP cells (GSE55064), (Asangani et al., 2014)). The grey dotted box indicates AR binding peaks. D-F) ACACA expression is elevated in primary prostate cancer (1° Cancer). The TCGA dataset comprises 52 patient-matched non-malignant and cancer samples. Violin plots show minimum and maximum (bottom and top lines, respectively) and mean (line within the boxes) values. Paired (TCGA and CPGEA) or unpaired (MSKCC) t tests were used to compare expression in non-malignant versus cancer tissues. RSEM, a quantitative value produced by RNA-Seq by Expectation Maximization; FPKM, fragments per kilobase of exon per million mapped reads.

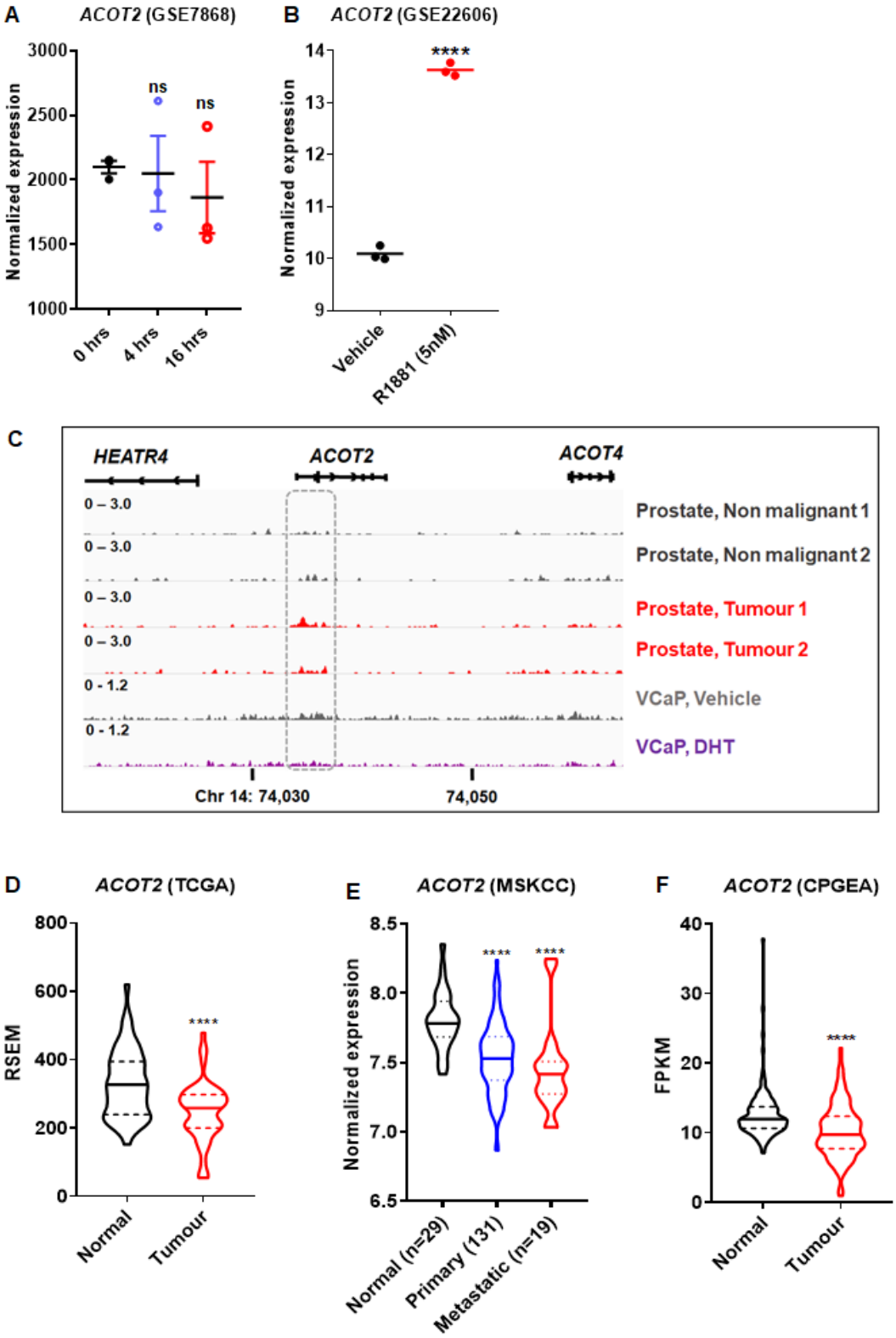

Figure 3.3: *ACOT* is a candidate direct AR target gene that is dysregulated in prostate cancer. Results in each panel are as described in Figure 3.2**.**

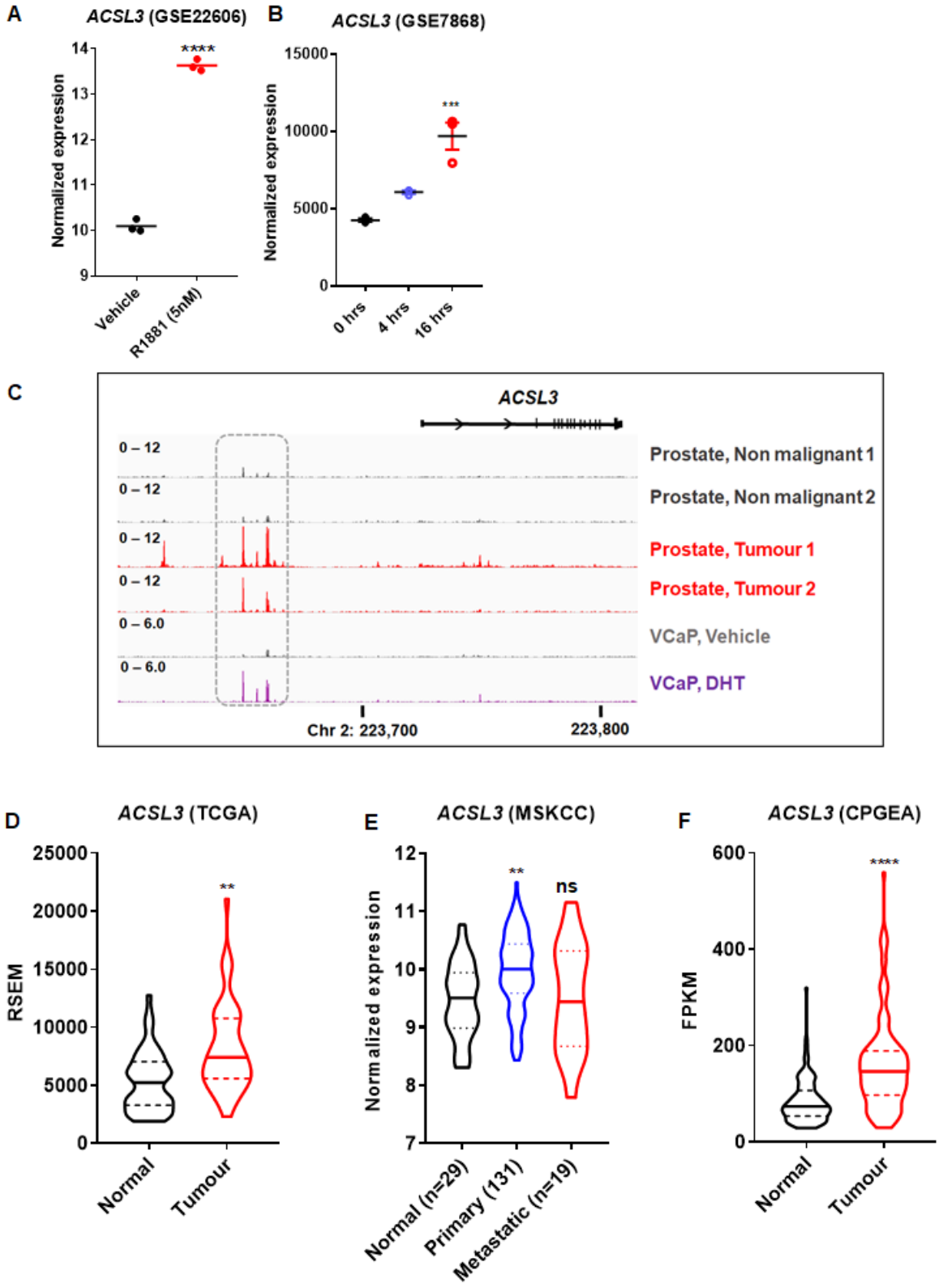

Figure 3.4: *ACSL3* is a candidate direct AR target gene that is dysregulated in prostate cancer. Results in each panel are as described in Figure 3.2**.**

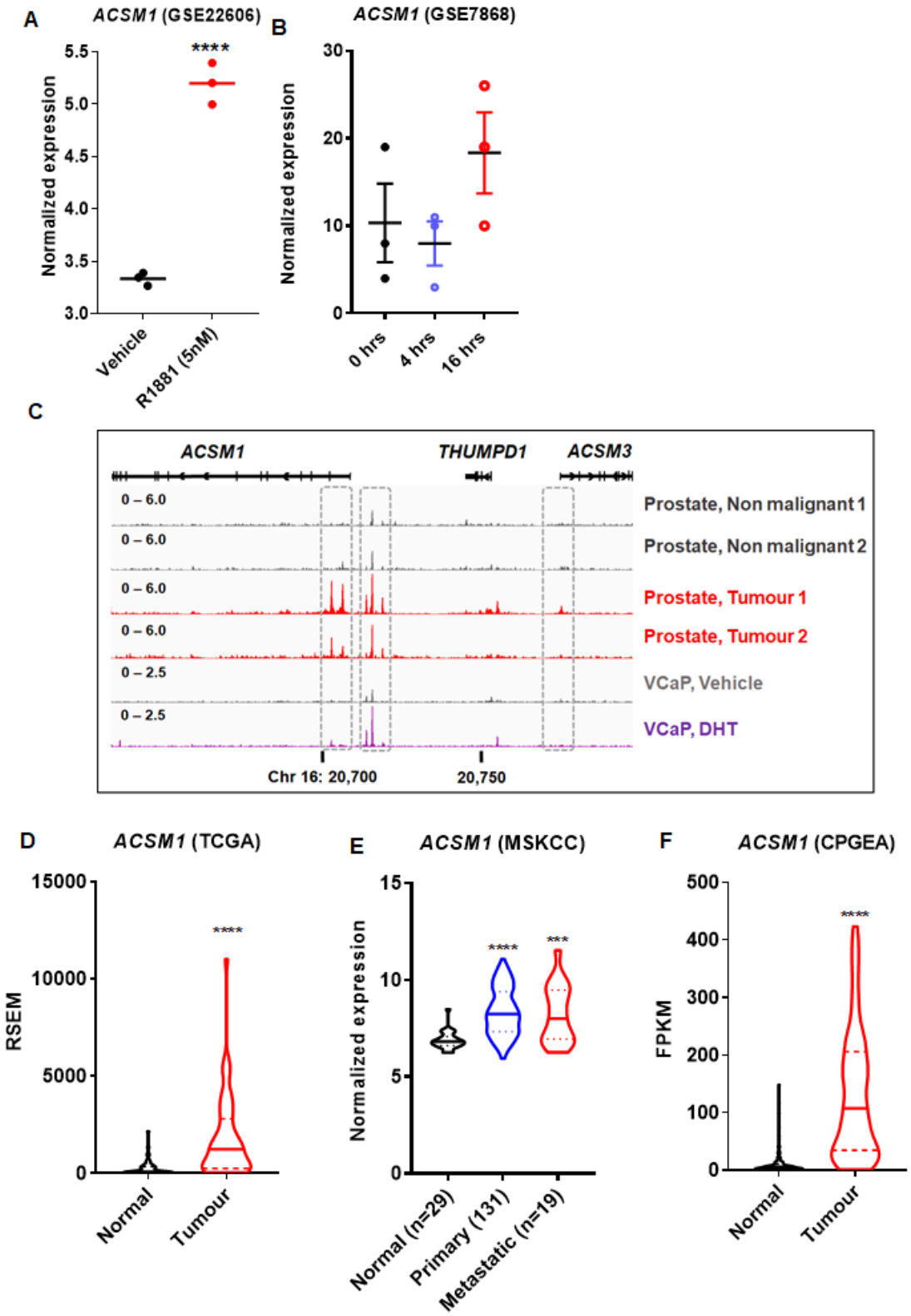

Figure 3.5: *ACSM1* is a candidate direct AR target gene that is dysregulated in prostate cancer. Results in each panel are as described in Figure 3.2**.**

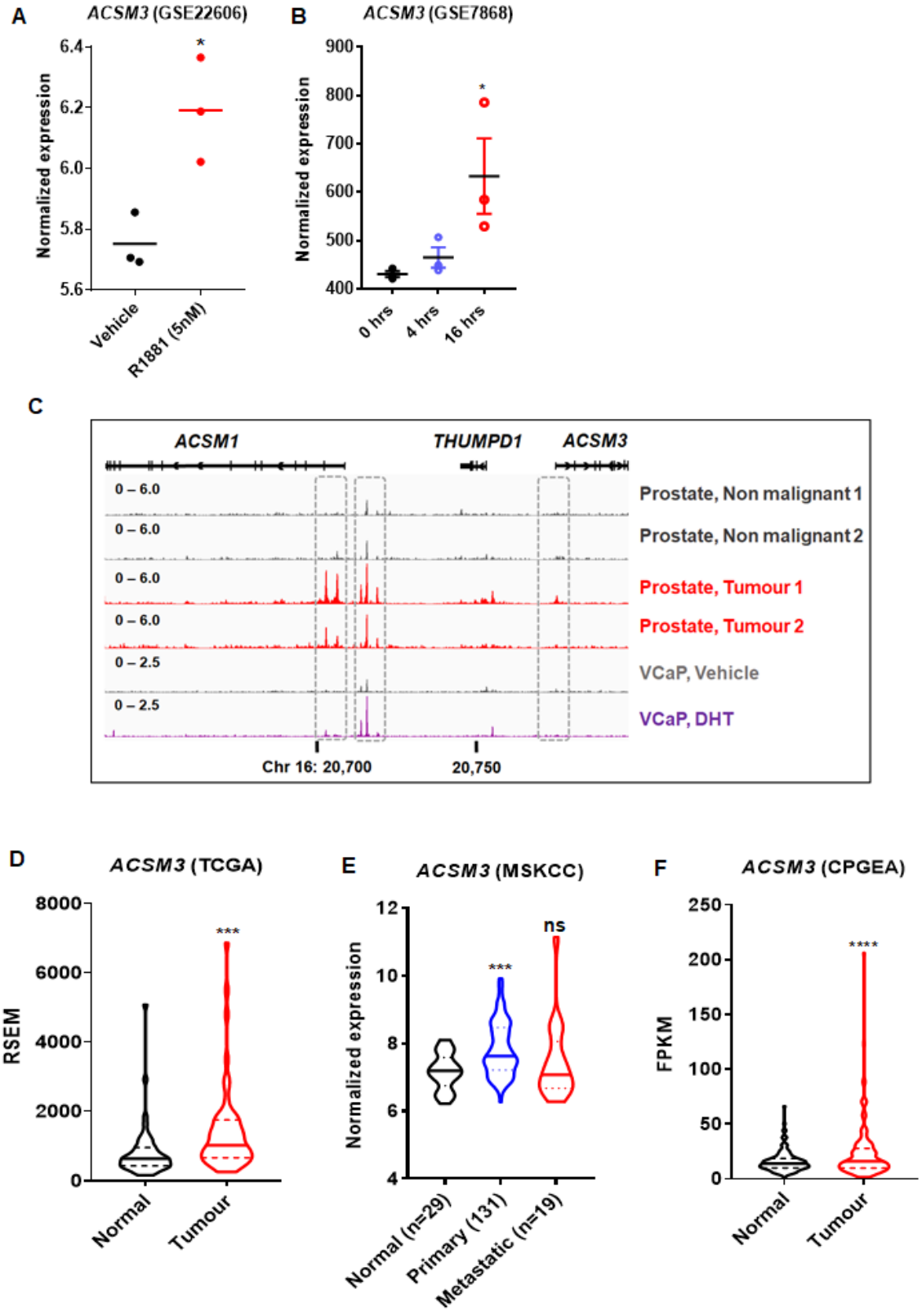

Figure 3.6: *ACSM3* is a candidate direct AR target gene that is dysregulated in prostate cancer. Results in each panel are as described in Figure 3.2**.**

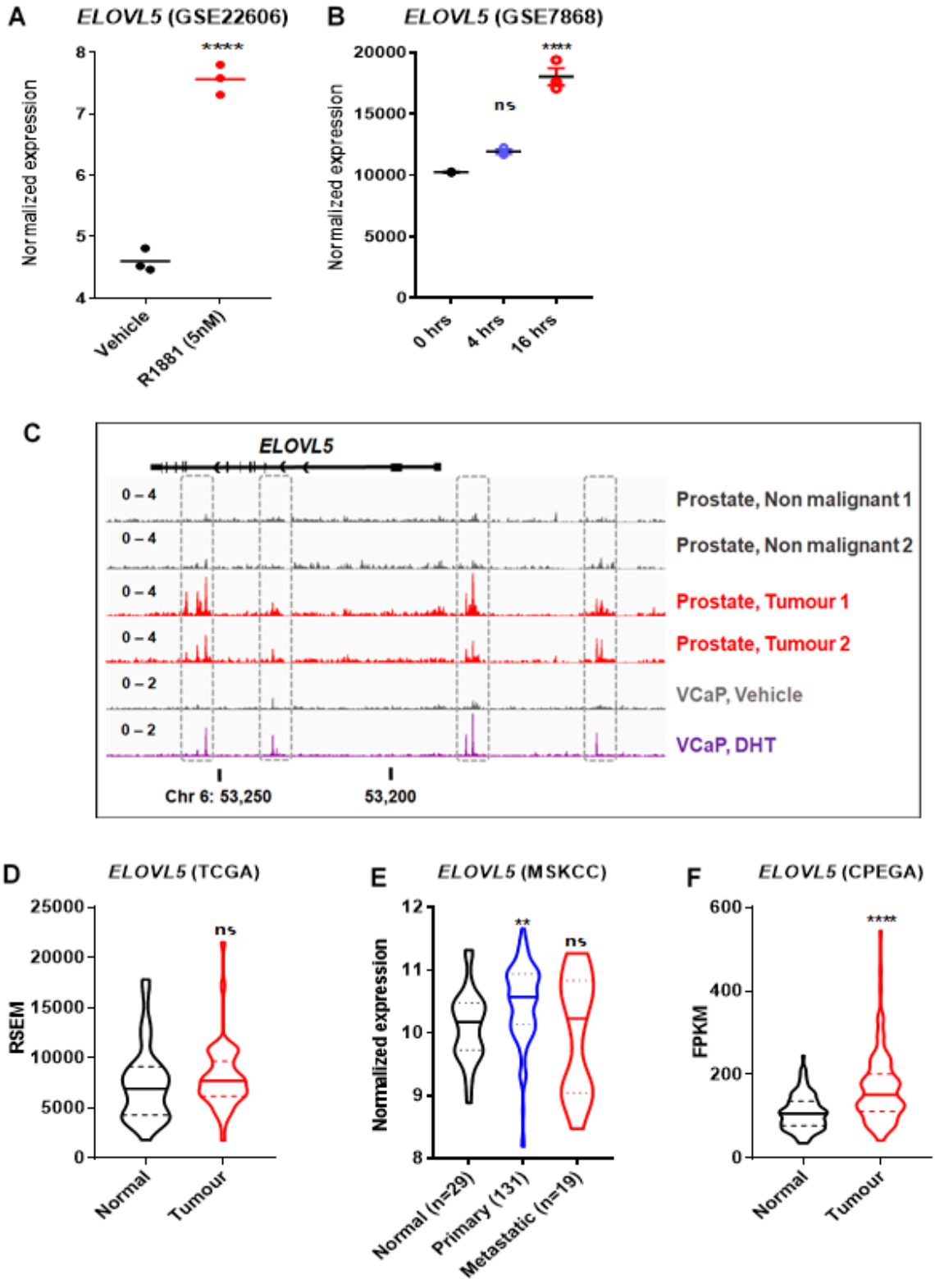

Figure 3.7: *ELOVL5* is a candidate direct AR target gene that is dysregulated in prostate cancer. Results in each panel are as described in Figure 3.2**.**

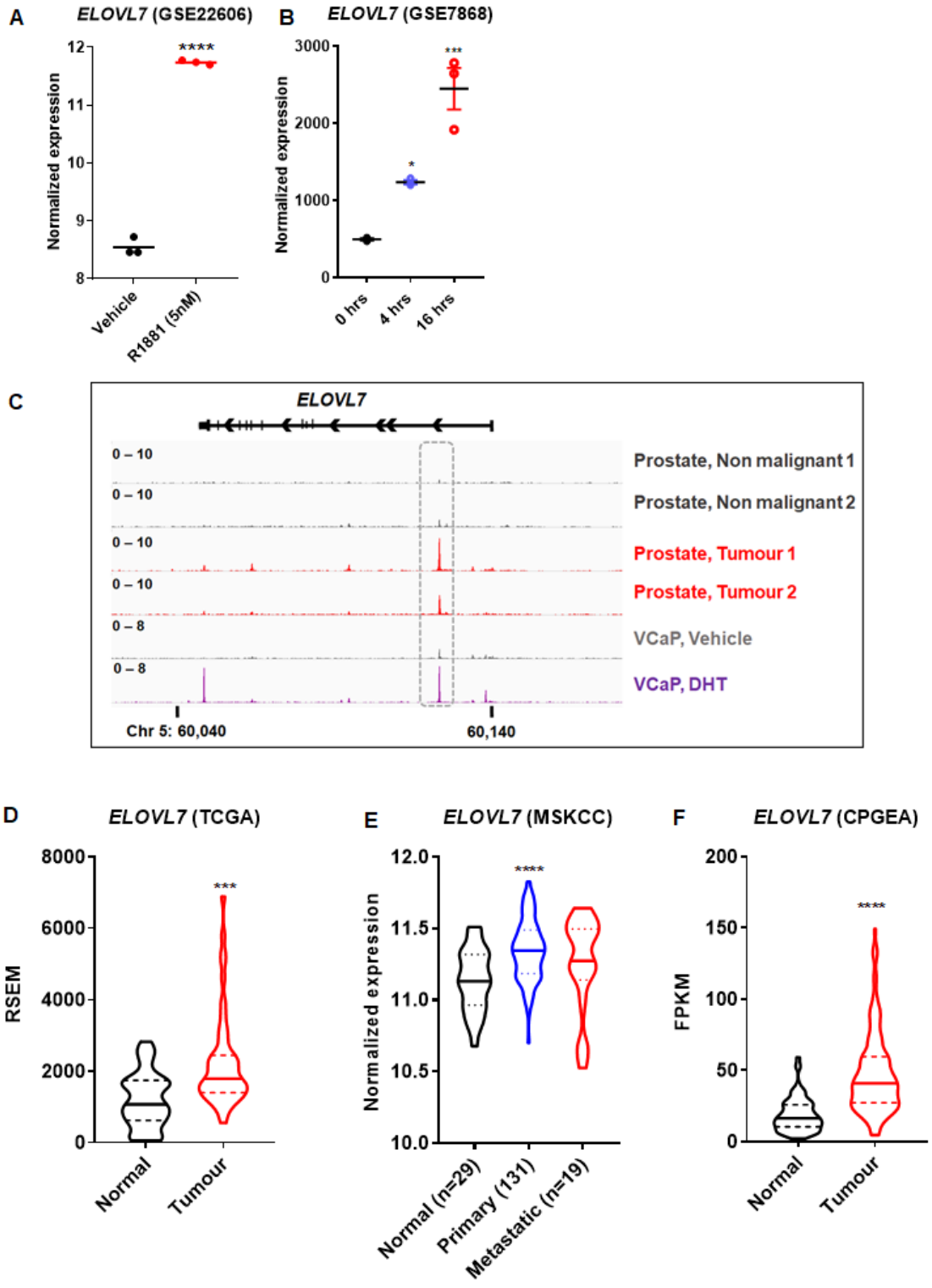

Figure 3.8: *ELOVL7* is a candidate direct AR target gene that is dysregulated in prostate cancer. Results in each panel are as described in Figure 3.2**.**

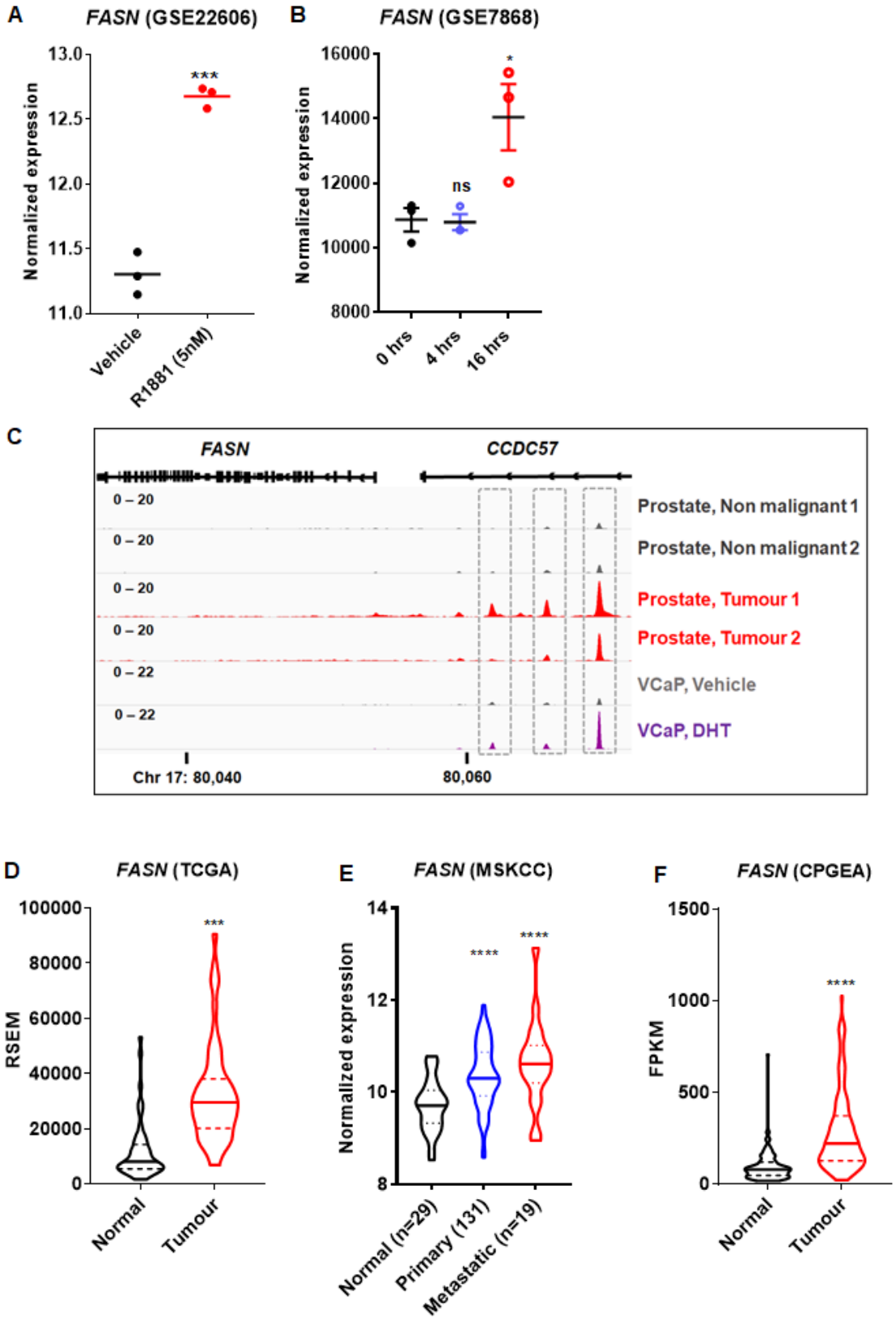

Figure 3.9: *FASN* is a candidate direct AR target gene that is dysregulated in prostate cancer. Results in each panel are as described in Figure 3.2**.**

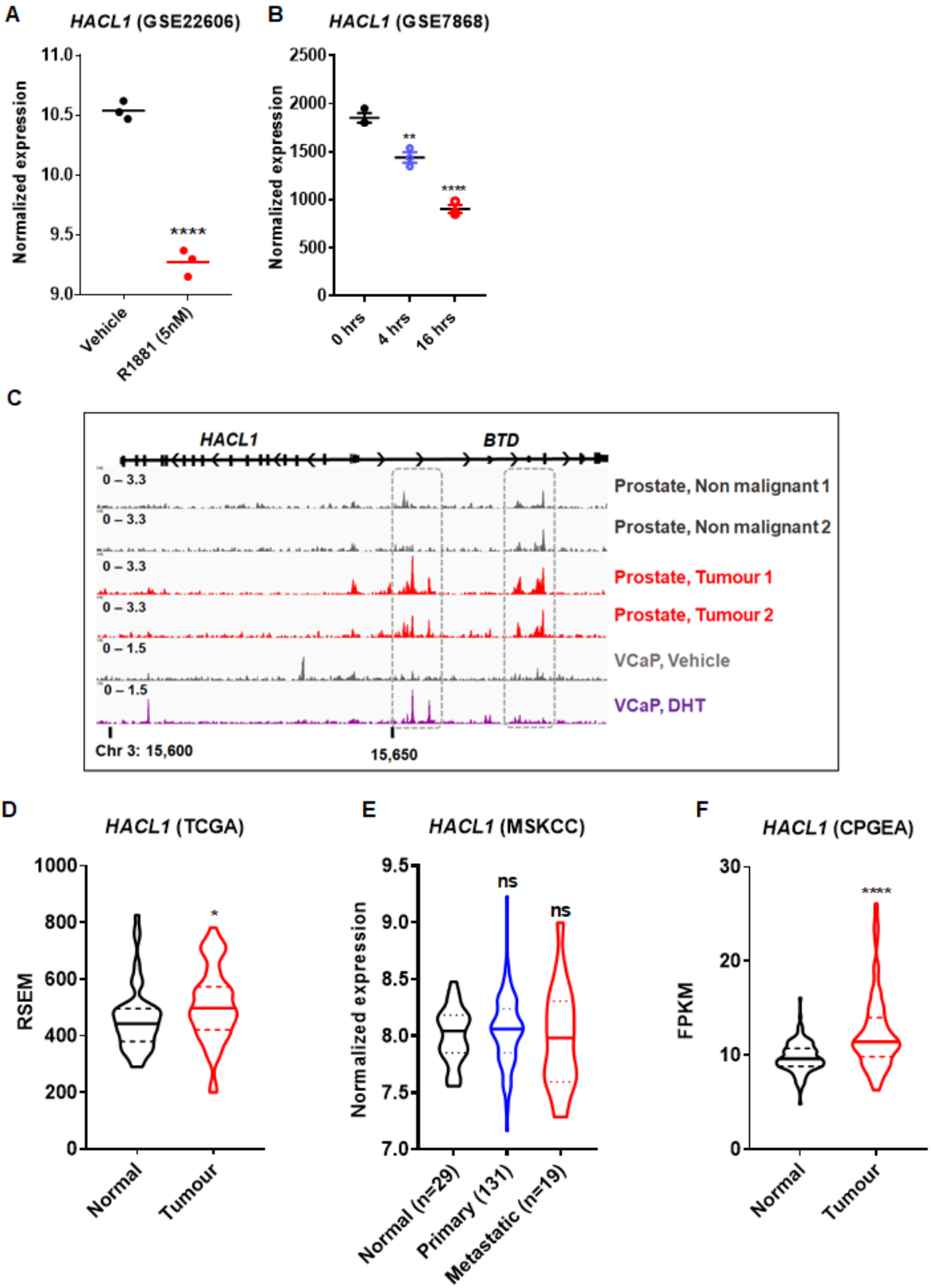

Figure 3.10: H*ACL1* is a candidate direct AR target gene that is dysregulated in prostate cancer. Results in each panel are as described in Figure 3.2**.**

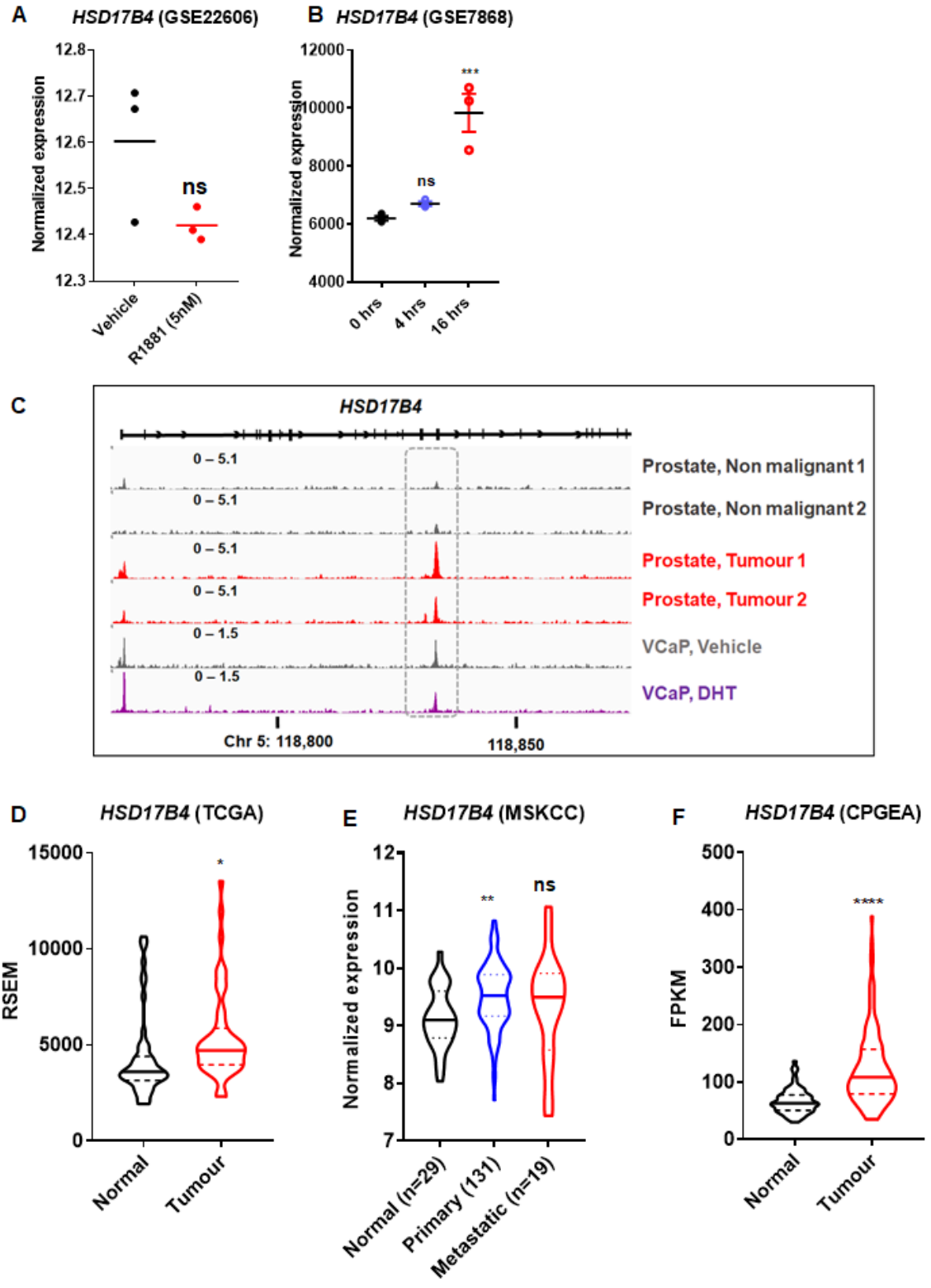

Figure 3.11: *HSD17B4* is a candidate direct AR target gene that is dysregulated in prostate cancer. Results in each panel are as described in Figure 3.2**.**

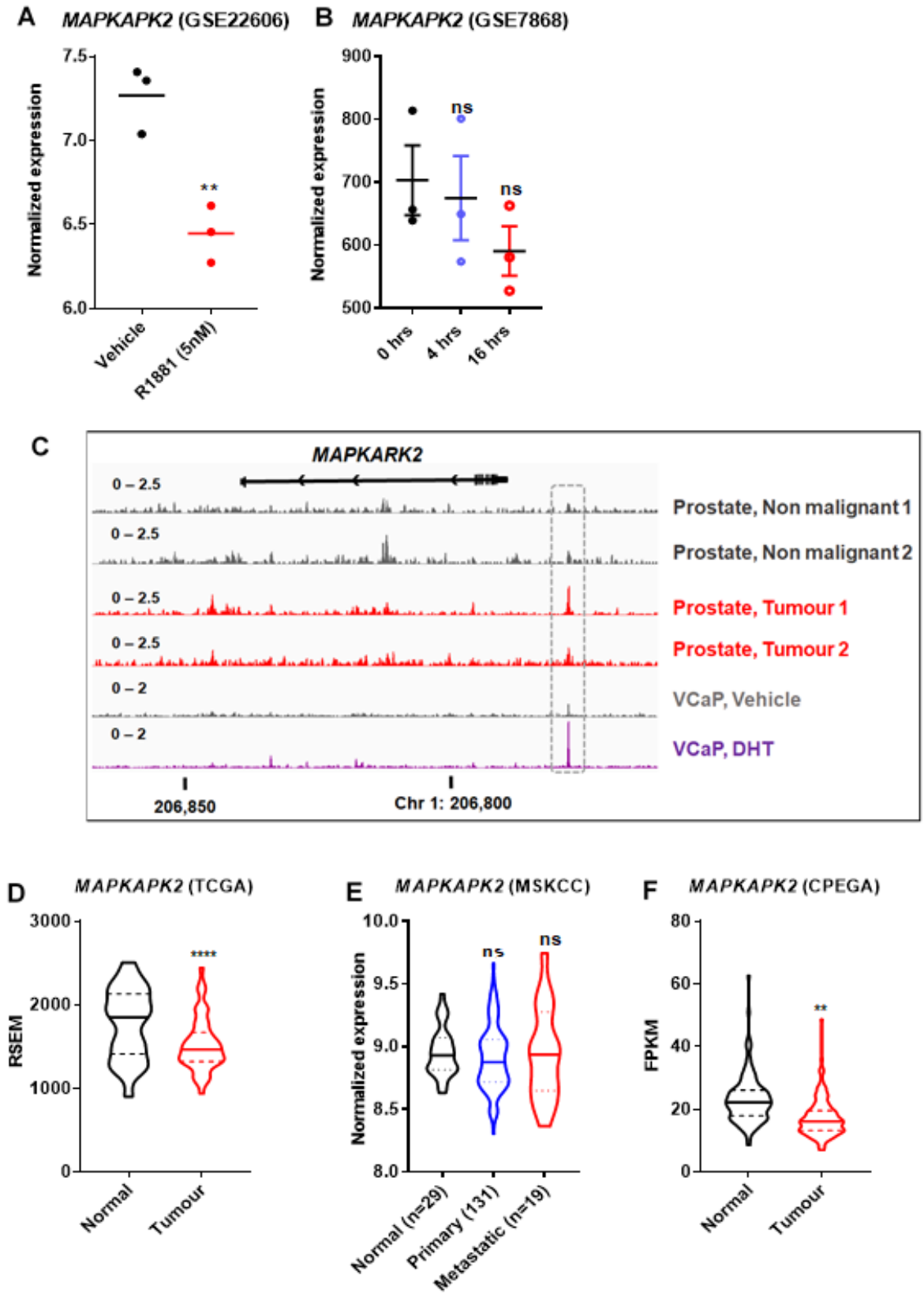

Figure 3.12: *MAPKAPK2* is a candidate direct AR target gene that is dysregulated in PCa. Results in each panel are as described in Figure 3.2**.**

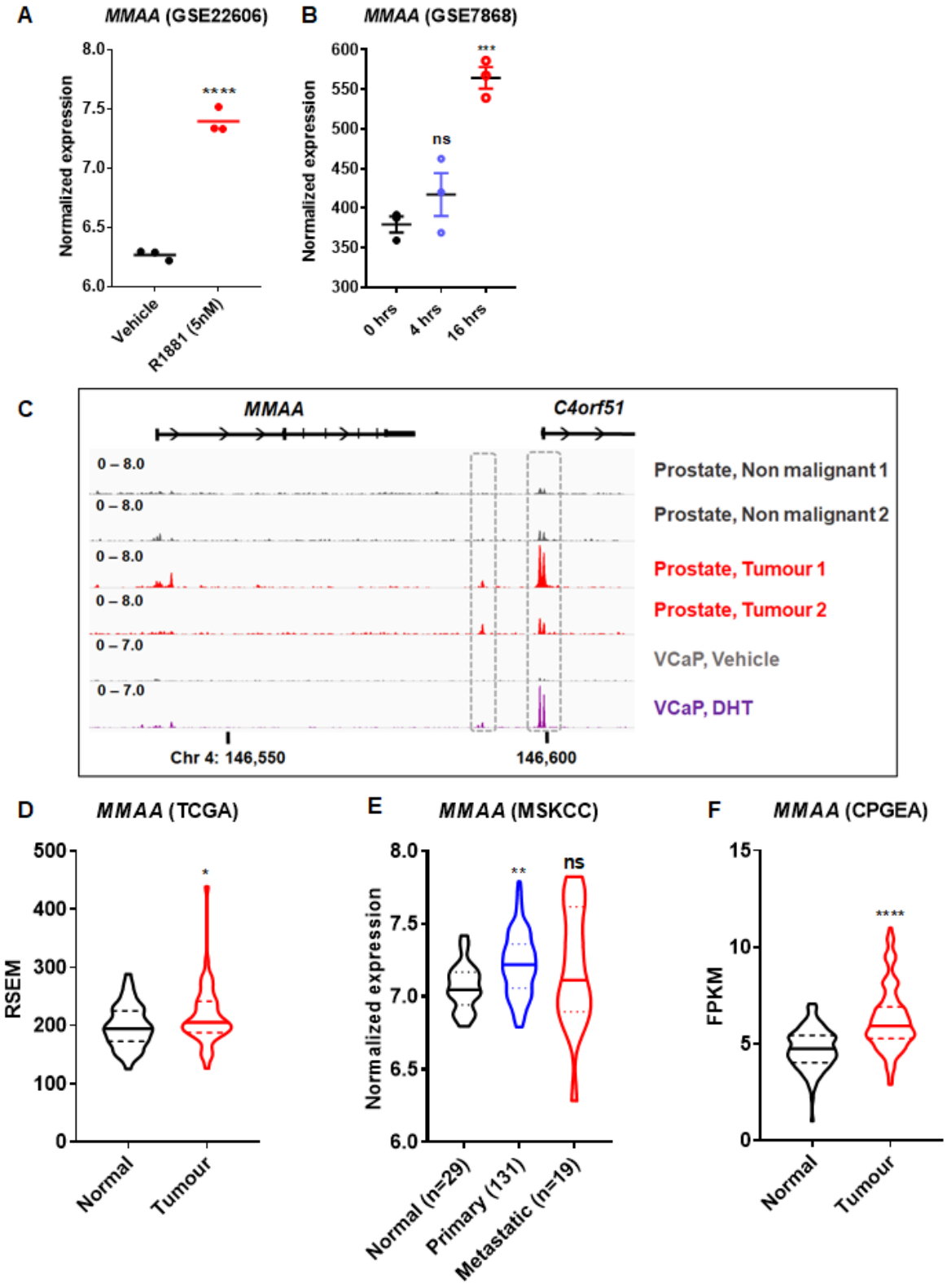

Figure 3.13: *MMAA* is a candidate direct AR target gene that is dysregulated in prostate cancer. Results in each panel are as described in Figure 3.2**.**

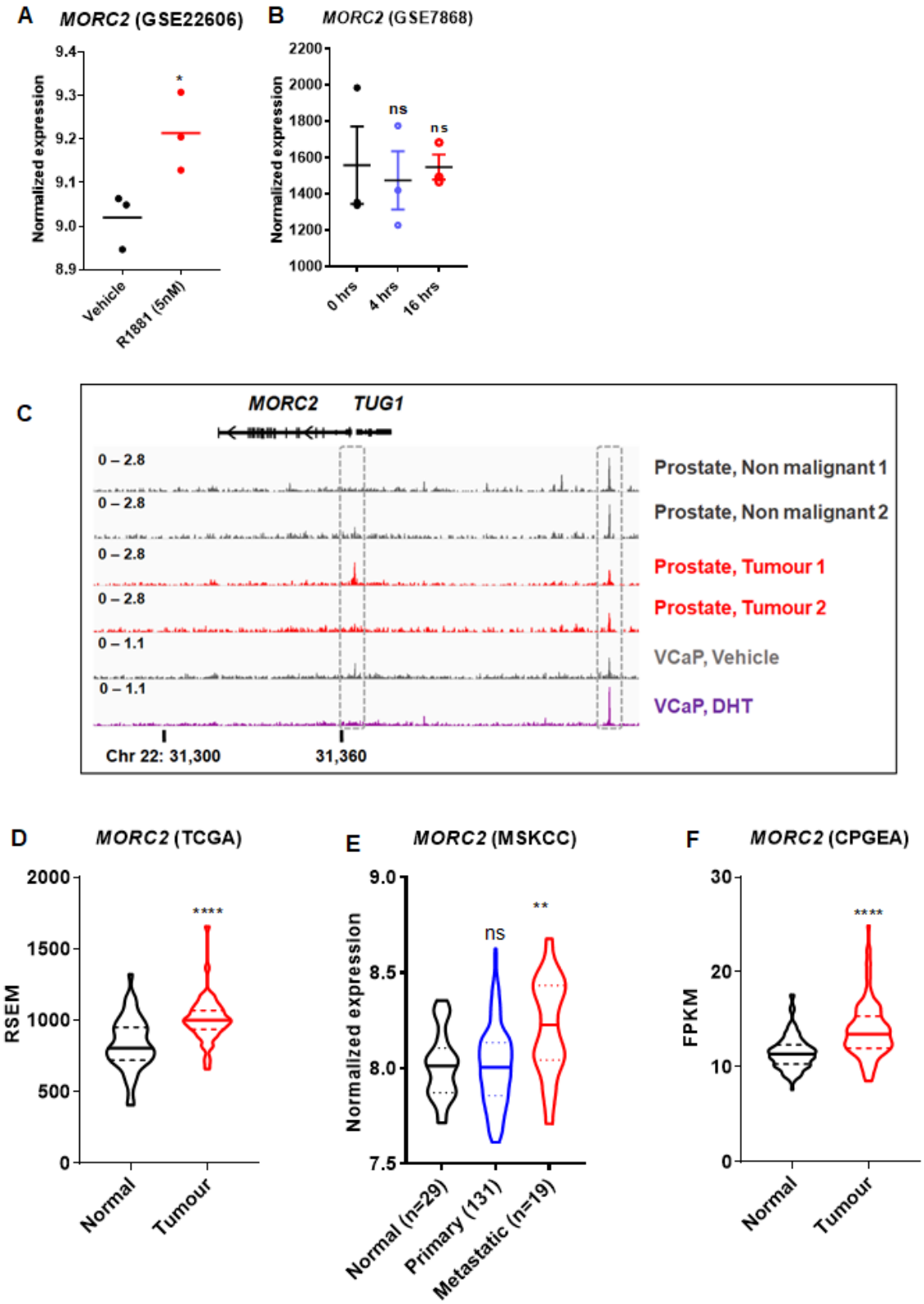

Figure 3.14: *MORC2* is a candidate direct AR target gene that is dysregulated in prostate cancer. Results in each panel are as described in Figure 3.2**.**

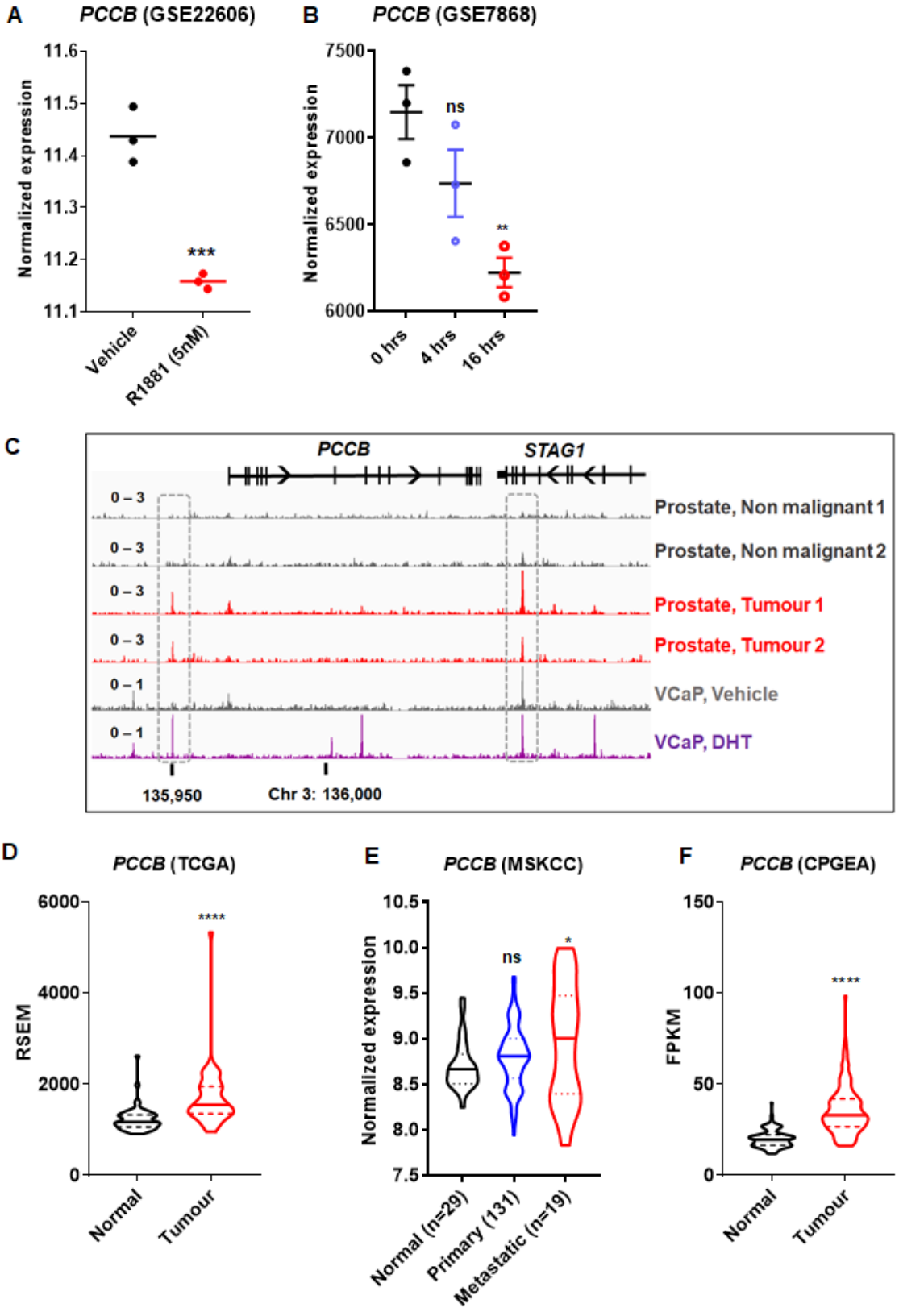

Figure 3.15: *PCCB* is a candidate direct AR target gene that is dysregulated in prostate cancer. Results in each panel are as described in Figure 3.2.

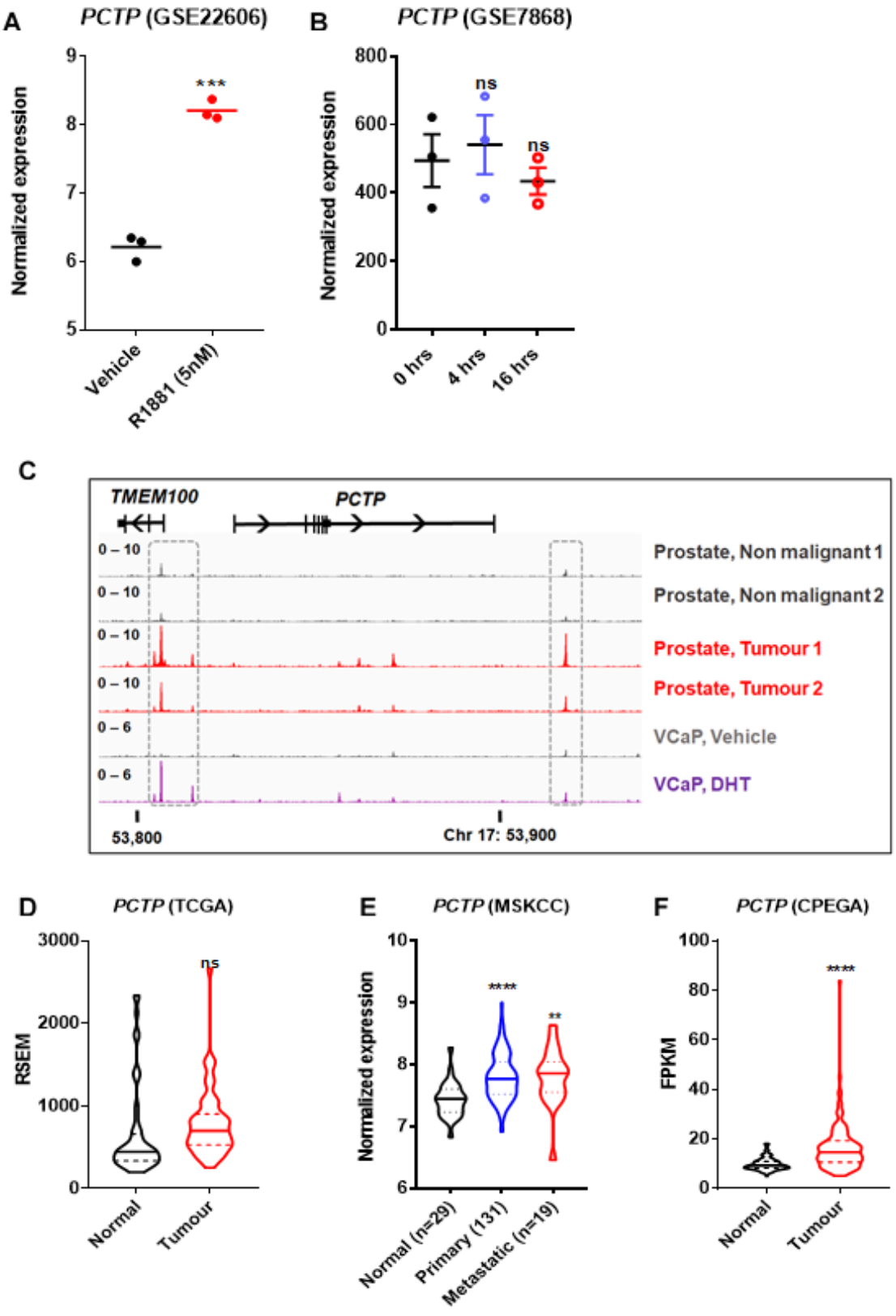

Figure 3.16: *PCTP* is a candidate direct AR target gene that is dysregulated in prostate cancer. Results in each panel are as described in Figure 3.2**.**

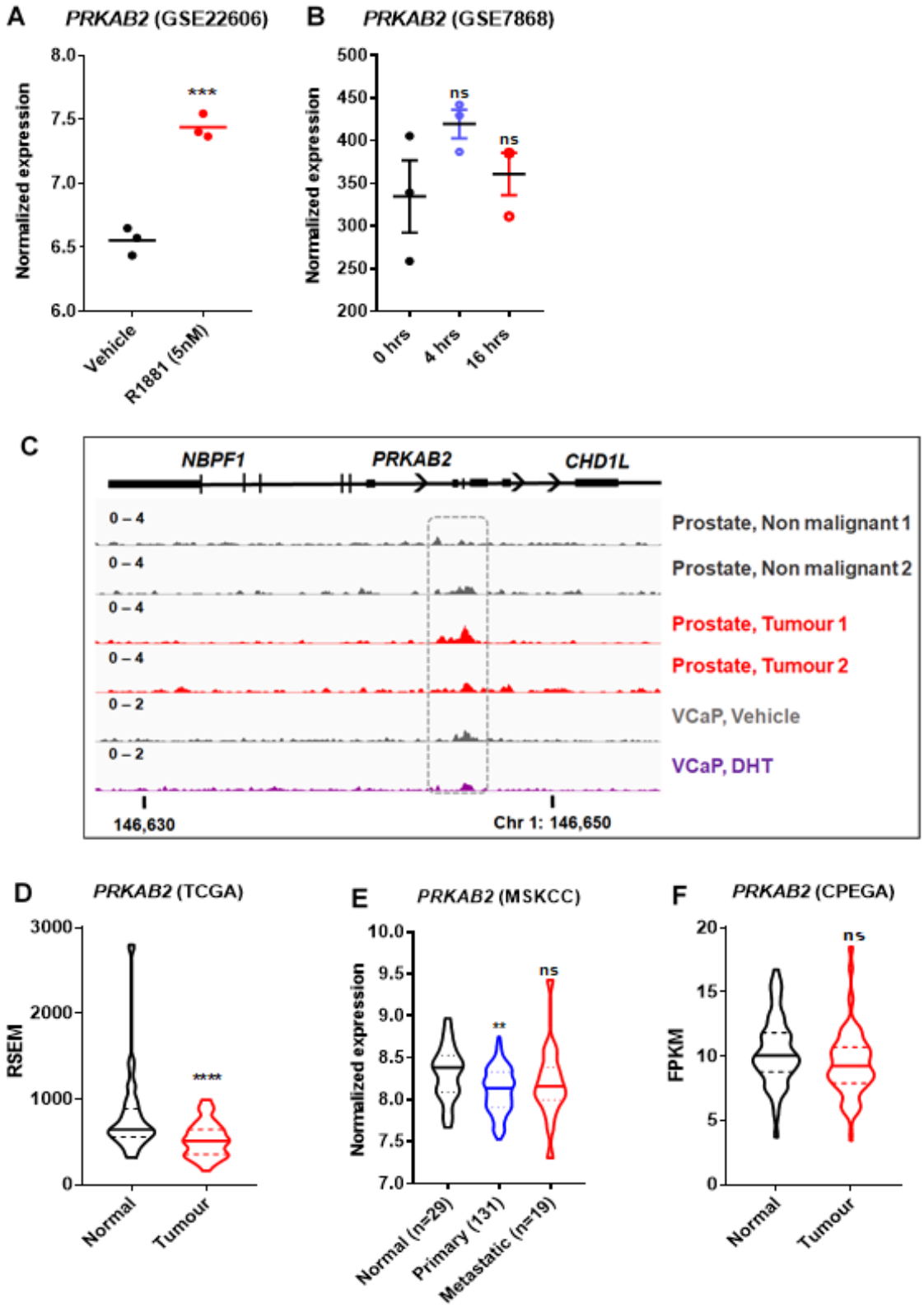

Figure 3.17: *PRKAB2* is a candidate direct AR target gene that is dysregulated in prostate cancer. Results in each panel are as described in Figure 3.2**.**

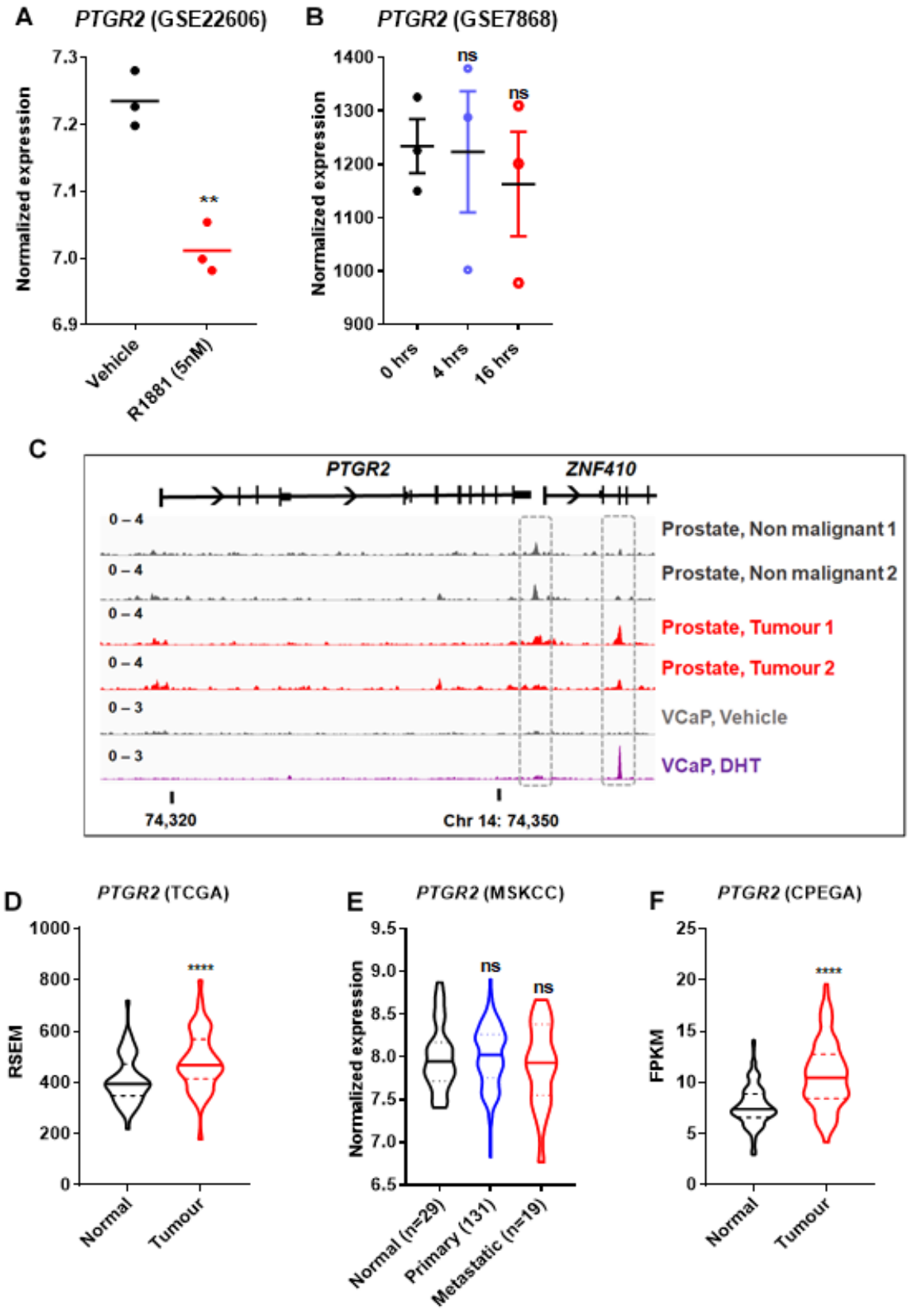

Figure 3.18: *PTGR2* is a candidate direct AR target gene that is dysregulated in prostate cancer. Results in each panel are as described in Figure 3.2**.**

3.4 Discussion

In this chapter, we applied a systematic approach to identify putative direct AR target genes that may play a role in dysregulated lipid metabolism in PCa, which identified 17 putative candidate genes. Some of those genes were previously identified as direct AR target genes including ACACA (H. V. Heemers et al., 2006; J. V. Swinnen et al., 1997), FASN (Migita et al., 2009; U. S. Shah et al., 2006; J. V. Swinnen et al., 1997), ACSL3 (Han et al., 2017), ELOVL2, 5 (Z. Nassar et al., 2019), and ELOVL7 (Z. Nassar et al., 2019; Tamura et al., 2009), supporting the robustness of our strategy.

Other studies have also used systematic approaches to identify AR-regulated genes with roles in metabolism. A similar systematic identification of AR-regulated metabolic genes has been performed previously in the LNCaP and VCaP (Massie et al., 2011) and VCS2 cell lines (Han et al., 2018). Our approach differed from these other studies in a number of ways. First, we used a curated list of genes predicted to encode factors involved in lipid metabolism, whereas other studies were focussed more broadly on the entire protein-coding genome. Second, we focussed on direct regulation by AR by exploiting newer tissue AR ChIP-seq data from clinical prostate tumour and matched normal tissue (GSE56288) (Pomerantz et al., 2015). The aforementioned studies also integrated androgen regulation and AR ChIP-seq data, but they both used AR ChIP-seq data from cell lines, which do not accurately recapitulate the *in vivo* situation (Pomerantz et al., 2015). Finally, we added another criterion, dysregulation in clinical prostate cancer, as another criteria to identify potentially important genes. We believe that this latter criterion is very important as it provides evidence for important pathobiolgical functions of the genes.

Our approach has a number of limitations. Firstly, we limited our evaluation of androgen regulation to a single cell line. Although we did use two distinct datasets, analysis of additional cell line models would have provided further evidence of androgenic regulation of candidate genes. It is also worth noting that the LNCaP cell line expresses an AR mutant (T878A) that is known to alter its transcriptional activity (Jernberg et al., 2017; Prekovic et al., 2016; Zhao et al., 2000); therefore, we cannot exclude the possibility that genes that passed (or did not) our gene filtering process may not be regulated by wild-type AR. Another issue with the LNCaP cell line is that it is a poor model of CRPC; it would be interesting to repeat our gene filtering process using data from a cell line model of CRPC (e.g. C4-2B;(Decker et al., 2012; Samuel E. DePrimo et al., 2002). Second, it is important to note that the steady-state level of RNA, as measured by RNA-seq and microarrays, does not always accurately mirror transcriptional activity of that gene. Thus, evaluation of nascent transcripts using a technique such as global run-on sequencing (GRO-seq) (Gardini, 2017) could have provided a better readout of androgen-regulated genes.

Finally, we limited our analysis to a list of 178 genes purported to have a role in lipid metabolism. This list was carefully curated from well-characterised databases (KEGG, REACTOME, Gene Ontology resource) as well as interrogation of the published literature. However, we cannot rule out the possibility that key players in lipid metabolism were not on this list and therefore not discoverable in our data mining pipeline. Although this is an unavoidable issue, we are confident that the 17 candidate lipid metabolic genes identified in this chapter have important roles in PCa growth and progression. Based on available functional information, the 17 genes are involved in lipid biosynthesis (*ACACA, ACOT2, ACSL3, ELOVL5,*

ELOVL7, FASN and *MORC2*), lipid oxidation/catabolism for the generation of energy (*ACSM1, ACSM3, HACL1, MMAA* and *PCCB*), cellular response to metabolic stress (*MAPKAPK2, MORC2, PRKAB2* and *PTGR2*), intratumoral steroidogenesis (*HSD17B4*) and maintain membrane integrity (*PCTP*), highlighting the diversity by which AR can potentially influence lipid metabolism in PCa.

In summary, in this chapter we identified lipid metabolic genes that are potentially AR-regulated and may influence PCa growth and progression. The function of the majority of these genes in PCa is largely unknown; in the next chapter, I will explore the role of ACSM1 and ACSM3 in more detail.

Supplementary table:

Table S3.1: List of lipid metabolic genes encoding factors with putative roles in lipid metabolism (n=178)

	Gene name	GSE7868			GSE22606	
		Regulation pattern	0-4 (p value)	0-16 (p value)	Regulation pattern	p value
1	***ABCC1***	1	0.219	0.0012	1	0.0001
2	***ABCD1***	0	0.8329	0.4785	-1	0.0023
3	***ACAA1***	1	0.9546	0.0047	1	0.0001
4	***ACAA2***	0	0.90102	0.925	0	0.6312
5	***ACACA***	1	0.0924	0.0001	1	0.0001
6	***ACACB***	0	0.5369	0.9269	0	0.4444
7	***ACAD10***	0	0.938	0.9916	0	0.1085
8	***ACAD11***	0	0.8323	0.3283	-1	0.0038
9	***ACADL***	0	0.9756	0.97	0	0.1085
10	***ACADM***	0	0.4834	0.89	1	0.0005
11	***ACADS***	0	0.3727	0.4506	0	0.7699
12	***ACADVL***	0	0.9313	0.7249	1	0.0086
13	***ACBD4***	0	0.9753	0.4001	0	0.2663
14	***ACBD5***	0	0.1727	0.1516	-1	0.0099
15	***ACBD6***	-1	0.7704	0.0226	-1	0.0005
16	***ACBD7***	-	-	-	-	-

17	***ACLY***	1	0.4369	0.0001	1	0.0001
18	***ACOT1***	0	0.9876	0.7639	1	0.0379
19	***ACOT11***	0	0.4474	0.611	0	0.9639
20	***ACOT12***	0	0.6205	0.9994	0	0.7312
21	***ACOT13***	0	0.8084	0.9082	0	0.403
22	***ACOT2***	0	0.9876	0.7639	1	0.0379
23	***ACOT4***	0	0.3086	0.2043	0	0.7522
24	***ACOT6***	0	0.939	0.8752	0	0.8254
25	***ACOT7***	0	0.1541	0.6986	1	0.0008
26	***ACOT8***	0	0.6136	0.9166	1	0.0018
27	***ACOT9***	0	0.5061	0.2002	1	0.0003
28	***ACOX1***	0	0.1827	0.1166	1	0.0197
29	***ACOX2***	0	0.9912	0.1264	0	0.3578
30	***ACOX3***	1	0.0407	0.0392	1	0.0019
31	***ACOXL***	0	0.858	0.946	0	0.8482
32	***ACSBG1***	0	0.3817	0.2353	0	0.4402
33	***ACSBG2***	0	0.0634	0.9089	0	0.9617
34	***ACSF2***	0	0.9557	0.2463	0	0.5964
35	***ACSF3***	0	0.9842	0.5913	0	0.3754
36	***ACSL1***	-1	0.1311	0.014	1	0.001
37	***ACSL3***	1	0.101	0.0007	1	0.0001
38	***ACSL4***	0	0.8202	0.9881	0	0.864

39	***ACSL5***	0	0.8534	0.1519	0	0.5811
40	***ACSL6***	0	0.3122	0.9987	0	0.1684
41	***ACSM1***	0	0.5393	0.9684	1	0.0001
42	***ACSM3***	1	0.8656	0.05	1	0.017
43	***ACSM6***	-	-	-	-	-
44	***AKR1C3***	0	0.9931	0.0544	0	0.2339
45	***ALDH3A2***	0	0.1503	0.5892	1	0.0141
46	***ALOX12***	0	0.8239	0.9111	0	0.268
47	***ALOX12B***	0	0.9312	0.9788	0	0.1962
48	***ALOX15***	0	0.5954	0.8736	0	0.1118
49	***ALOX15B***	0	0.1333	0.161	0	0.0978
50	***ALOX5***	0	0.3538	0.99	0	0.5751
51	***ALOX5AP***	0	0.5348	0.8689	0	0.4489
52	***ALOXE3***	0	0.6098	0.6655	0	0.5796
53	***AMACR***	1	0.5818	0.0132	1	0.0001
54	***AWAT1***	0	0.9909	0.9406	0	0.3208
55	***CBR1***	0	0.9938	0.9777	0	0.8622
56	***CBR4***	0	0.8297	0.972	0	0.0108
57	***CPT1A***	0	0.8235	0.9999	0	0.1514
58	***CPT1B***	0	0.9866	0.695	0	0.2701
59	***CPT2***	0	0.8673	0.1489	1	0.0237
60	***CRAT***	-1	0.9939	0.0163	1	0.0031

61	***CROT***	0	0.1298	0.1588	1	0.0001
62	***CYP1A1***	0	0.7984	0.9433	0	0.9842
63	***CYP1A2***	0	0.642	0.964	0	0.3964
64	***CYP1B1***	0	0.6936	0.1743	0	0.6268
65	***CYP2C19***	0	0.6474	0.6067	1	0.0041
66	***CYP2C8***	0	0.4388	0.6644	0	0.6755
67	***CYP2C9***	0	0.6857	0.3581	-1	0.0273
68	***CYP2J2***	0	0.8819	0.9879	-1	0.0214
69	***CYP2U1***	1	0.0008	0.0779	1	0.0001
70	***CYP4A11***	0	0.9011	0.6213	0	0.7167
71	***CYP4A22***	0	0.9011	0.6213	1	0.0388
72	***CYP4B1***	1	0.0308	0.9587	0	0.6564
73	***CYP4F11***	0	0.9618	0.2148	0	0.7316
74	***CYP4F2***	0	0.9069	0.9974	0	0.839
75	***CYP4F22***	0	0.9979	0.947	0	0.7439
76	***CYP4F3***	0	0.0893	0.9784	0	0.7537
77	***CYP4F8***	0	0.5721	0.7919	0	0.3974
78	***CYP8B1***	0	0.4293	0.2948	0	0.1028
79	***DBI***	1	0.8726	0.0096	0	0.9999
80	***DECR1***	-1	0.7262	0.0302	-1	0.0003
81	***DECR2***	0	0.6835	0.9194	0	0.0324
82	***DPEP1***	0	0.8946	0.7912	0	0.5631

83	***DPEP2***	0	0.8444	0.9895	0	0.3259
84	***DPEP3***	0	0.8168	0.4767	0	0.3454
85	***ECHS1***	0	0.8997	0.6245	-1	0.0163
86	***ECI1***	0	0.8983	0.9038	1	0.0001
87	***ECI2***	1	0.0695	0.0084	1	0.0001
88	***EHHADH***	0	0.0729	0.0514	0	0.4086
89	***ELOVL1***	1	0.0444	0.0014	1	0.0001
90	***ELOVL2***	0	0.8907	0.2161	1	0.0238
91	***ELOVL3***	0	0.4301	0.3229	0	0.7258
92	***ELOVL4***	0	0.999	0.9489	0	0.9571
93	***ELOVL5***	1	0.0672	0.0001	1	0.0001
94	***ELOVL6***	0	0.9217	0.8028	0	0.4357
95	***ELOVL7***	1	0.0348	0.0003	1	0.0001
96	***EPHX2***	1	0.9986	0.0485	1	0.0199
97	***FAAH***	0	0.6077	0.2284	1	0.2323
98	***FAAH2***	0	0.9978	0.886	0	0.7347
99	***FADS1***	0	0.7768	0.9594	1	0.0001
100	***FADS2***	0	0.0382	0.1064	1	0.0004
101	***FAM213B***	0	0.8756	0.566	-1	0.0101
102	***FASN***	1	0.9964	0.03	1	0.0002
103	***GGT1***	0	0.282	0.5588	0	0.2253
104	***GGT5***	0	0.3455	0.0735	0	0.4015

105	***GPX1***	0	0.8789	0.4784	0	0.6951
106	***GPX2***	0	0.6805	0.8159	0	0.5384
107	***GPX4***	0	0.2642	0.1322	0	0.4237
108	***HACD1***	0	0.7507	0.9693	0	0.4491
109	***HACD2***	0	0.6324	0.3858	1	0.0001
110	***HACD3***	0	0.5143	0.9207	0	0.1664
111	***HACD4***	0	0.4339	0.2976	0	0.71
112	***HACL1***	-1	0.0025	0.0001	-1	0.0001
113	***HADH***	0	0.1909	0.5711	0	0.0059
114	***HADHA***	0	0.1987	0.2471	0	0.0014
115	***HADHB***	-1	0.0935	0.0107	-1	0.0001
116	***HAO2***	0	0.964	0.9842	0	0.3322
117	***HPGD***	1	0.7768	0.9594	1	0.0001
118	***HPGDS***	0	0.5097	0.9966	0	0.859
119	***HSD17B12***	0	0.7808	0.9673	0	0.778
120	***HSD17B3***	0	0.991	0.9204	0	0.8389
121	***HSD17B4***	1	0.6417	0.0013	0	0.115
122	***HSD17B8***	0	0.9956	0.8721	0	0.4269
123	***LTA4H***	-1	0.0082	0.0014	-1	0.0001
124	***LTC4S***	0	0.6048	0.397	0	0.4064
125	***MAPKAPK2***	0	0.9303	0.378	1	0.0057
126	***MCAT***	0	0.9529	0.406	0	0.5124

127	***MCEE***	0	0.3735	0.0554	1	0.0016
128	***MECR***	0	0.9515	0.5319	0	0.0695
129	***MID1IP1***	0	0.1291	0.1738	-1	0.0068
130	***MLYCD***	0	0.9953	0.9749	0	0.6251
131	***MMAA***	1	0.3774	0.001	1	0.0001
132	***MORC2***	0	0.9272	0.9988	-1	0.0022
133	***MUT***	0	0.4519	0.076	-1	0.0006
134	***NDUFAB1***	0	0.4556	0.0601	0	0.8686
135	***NUDT19***	0	0.8311	0.4027	-1	0.0009
136	***NUDT7***	0	0.3036	0.6263	0	0.2583
137	***OLAH***	0	0.6178	0.4035	1	0.0461
138	***PCCA***	0	0.1838	0.9781	0	0.7453
139	***PCCB***	-1	0.2121	0.0116	-1	0.001
140	***PCTP***	0	0.8897	0.8224	1	0.0001
141	***PECR***	0	0.6406	0.6595	0	0.0278
142	***PHYH***	-1	0.9881	0.0582	-1	0.0002
143	***PLA2G4A***	0	0.7609	0.3292	0	0.9115
144	***PON1***	1	0.0487	0.098	0	0.7928
145	***PON2***	-1	0.1345	0.0041	-1	0.0002
146	***PON3***	0	0.9181	0.7728	0	0.4512
147	***PPARD***	0	0.9976	0.6282	-1	0.0214
148	***PPT11***	-	-	-	1	

149	***PPT2***	0	0.7582	0.977	0	0.1172
150	***PRKAA2***	0	0.4986	0.5782	0	0.3634
151	***PRKAB2***	0	0.1907	0.8147	1	0.0004
152	***PRKAG2***	0	0.9642	0.9788	-1	0.0024
153	***PTGDS***	0	0.1816	0.9885	0	0.3464
154	***PTGES***	0	0.7706	0.271	0	0.1739
155	***PTGES2***	0	0.994	0.5381	-1	0.0084
156	***PTGES3***	0	0.4241	0.9479	0	0.0017
157	***PTGIS***	1	0.449	0.0183	0	0.6553
158	***PTGR1***	1	0.1794	0.0226	0	0.6166
159	***PTGR2***	0	0.9963	0.8514	1	0.0003
160	***PTGS1***	0	0.8929	0.917	0	0.3626
161	***PTGS2***	0	0.7237	0.8477	0	0.506
162	***RPP14***	0	0.9386	0.9073	0	0.1458
163	***RXRA***	0	0.1045	0.313	-1	0.0001
164	***SCD***	0	0.5616	0.0583	1	0.0002
165	***SCD5***	0	0.7611	0.1314	0	0.2729
166	***SCP2***	0	0.4666	0.7694	0	0.821
167	***SLC22A5***	1	0.5567	0.2404	1	0.0006
168	***SLC25A1***	0	0.3942	0.8987	0	0.5028
169	***SLC25A17***	-1	0.1641	0.0075	0	0.6694
170	***SLC25A20***	1	0.132	0.012	1	0.0001

171	***SLC27A2***	0	0.0156	0.1493	-1	0.0073
172	***SLC27A3***	0	0.2189	0.0583	0	0.2456
173	***TBXAS1***	0	0.9976	0.6282	0	0.2111
174	***TECR***	0	0.241	0.1375	0	0.4215
175	***TECRL***	0	0.9992	0.9935	0	0.9657
176	***THEM4***	0	0.9487	0.7405	-1	0.0007
177	***THEM5***	0	0.451	0.8413	0	0.7675
178	***THRSP***	0	0.6853	0.1477	0	0.8006

Abbreviation: 1, upregulated; -1, down regulated and 0, no significant change in gene expression

Table S3.2: List of filtered genes that are dysregulated in prostate cancer (in any of two datasets)

Gene Symbol	MSKCC				TCGA		CPGEA	
	Regulation pattern	Normal vs Primary (p-value)	Normal vs Metastatic (p-value)	Primary vs Metastatic (p-value)	Regulation pattern	p-value	Regulation pattern	p-value
ACACA	1	0.0001	0.0001	0.2671	1	0.0001	1	0.0001
ACOT2	-1	0.0001	0.0001	0.3951	-1	0.0001	-1	0.0001
ACSL3	1	0.0015	0.9714	0.0221	1	0.0001	1	0.0001
ACSM1	1	0.0001	0.0004	0.9282	1	0.0001	1	0.0001
ACSM3	1	0.0003	0.4615	0.1432	1	0.001	1	0.0014
ELOVL5	1	0.0119	0.8293	0.0062	0	0.326	1	0.0001
ELOVL7	1	0.0001	0.1801	0.2279	1	0.0001	1	0.0001
FASN	1	0.0001	0.0001	0.2736	1	0.0001	1	0.0001
HACL1	0	0.8029	0.9615	0.673	1	0.0282	1	0.0001
HSD17B4	1	0.0074	0.522	0.43	1	0.0123	1	0.0001
MAPKAPK2	0	0.6216	0.974	0.864	-1	0.0001	-1	0.0001
MMAA	1	0.0054	0.1668	0.8945	1	0.0169	1	0.0001
MORC2	1	0.9791	0.0043	0.0002	1	0.0001	1	0.0001
PCCB	0	0.45	0.0646	0.2063	1	0.0001	1	0.0001
PCTP	1	0.0001	0.0028	0.9999	0	0.1507	1	0.0001
PRKAB2	-1	0.026	0.3488	0.4859	-1	0.0001	-1	0.0008
PTGR2	0	0.9921	0.685	0.5167	1	0.0001	1	0.0001

Abbreviation: 1, upregulated; -1, down regulated and 0, no significant change in gene expression

CHAPTER 4: ACSM1 AND ACSM3 REGULATE FATTY ACID OXIDATION IN PROSTATE CANCER TO PROMOTE GROWTH AND PROTECT AGAINST FERROPTOSIS (PUBLICATION)

4 ACSM1 AND ACSM3 REGULATE FATTY ACID OXIDATION IN PROSTATE CANCER TO PROMOTE GROWTH AND PROTECT AGAINST FERROPTOSIS

This chapter includes a manuscript ready to submit for publication followed by supplementary figures and tables. This chapter makes up a significant proportion of the work completed as a part of my PhD.

4.1 Statement of Authorship

Statement of Authorship

Title of Paper	ACSM1 and ACSM3 regulate fatty acid oxidation in prostate cancer to promote growth and protect against oxidative stress
Publication Status	☐ Published ☐ Accepted for Publication ☐ Submitted for Publication ☑ Unpublished and Unsubmitted work written in
Publication Details	

Principal Author

Name of Principal Author (Candidate)	Raj K. Shrestha		
Contribution to the Paper	Conceived project, designed and performed experiments (cell and organoids culture, transfections, Western blots, qRT-PCR, ChIP-PCR, metabolomics, lipidomics, *In vivo* experiment), data mining, analysed and interpreted data, made figures, co-wrote manuscript.		
Overall percentage (%)	80		
Certification:	This paper reports on original research I conducted during the period of my Higher Degree by Research candidature and is not subject to any obligations or contractual agreements with a third party that would constrain its inclusion in this thesis. I am the primary author of this paper.		
Signature		Date	01/11/2020

Co-Author Contributions

By signing the Statement of Authorship, each author certifies that:

i. the candidate's stated contribution to the publication is accurate (as detailed above);
ii. permission is granted for the candidate in include the publication in the thesis; and
iii. the sum of all co-author contributions is equal to 100% less the candidate's stated contribution.

Name of Co-Author	Zeyad D. Nassar		
Contribution to the Paper	Assisted with cell line experiments related to lipid peroxidation assay, seahorse assay and *in-vivo* experiment		
Signature		Date	30.10.20

Name of Co-Author	Adrienne R. Hanson		
Contribution to the Paper	Assisted with cell line experiments		
Signature		Date	03-11-2020

Name of Co-Author	Richard Iggo		
Contribution to the Paper	Assisted with preparation of stable cell lines for *in vivo* experiments		
Signature		Date	29.10.2020

Name of Co-Author	Scott Townley		
Contribution to the Paper	Assisted with cell line experiments		
Signature		Date	3/11/20

Name of Co-Author	Chui Yan Mah		
Contribution to the Paper	Assisted with Seahorse assay experiment		
Signature		Date	30/10/2020

Name of Co-Author	Mohammadreza Ghodsi		
Contribution to the Paper	Assisted with cell line experiments		
Signature		Date	29.10.20

Name of Co-Author	Marie Pickering		
Contribution to the Paper	Immunohistochemistry of tissue microarray comprised of different grade of prostate cancer		
Signature		Date	30-10-20

Name of Co-Author	Lake-Ee Quek		
Contribution to the Paper	Performed metabolomics experiment and data analysis/ interpretation		
Signature		Date	29th Oct 2020

Name of Co-Author	Andrew J. Hoy		
Contribution to the Paper	Performed metabolomics experiment and data analysis/ interpretation		
Signature		Date	29 October 2020

Name of Co-Author	Wayne D. Tilley		
Contribution to the Paper	Project supervisor, assisted in data analysis and interpretation, evaluated /edited manuscript		
Signature		Date	30-10-20

Name of Co-Author	Johan Swinnen		
Contribution to the Paper	Assisted in lipidomics data analysis and interpretation		
Signature		Date	02/11/2020

Name of Co-Author	Lisa M. Butler		
Contribution to the Paper	Project supervisor, assisted in data analysis and interpretation, evaluated /edited manuscript		
Signature		Date	13/11/20

Name of Co-Author	Luke A. Selth		
Contribution to the Paper	Principal supervisor, conceived project, designed experiments, analysed data, made figures and co-wrote the manuscript		
Signature		Date	13/11/20

4.2 ACSM1 and ACSM3 regulate fatty acid oxidation in prostate cancer to promote growth and protect against ferroptosis

Running title: ACSM enzymes promote prostate cancer growth

Raj Shrestha[1,2], Zeyad Nassar[2,3], Adrienne R. Hanson[1,4], Richard Iggo[1,5], Scott Townley[1], Chui Yan Mah[2,3], Mohammadreza Ghodsi[1,2], Marie Pickering[1], Lake Ee Quek[6], Andrew J. Hoy[7], Wayne D. Tilley[1,2], Johannes V. Swinnen[8], Lisa M. Butler[1,2] and Luke A. Selth[1,2,10*]

[1]Dame Roma Mitchell Cancer Research Laboratories, Adelaide Medical School, University of Adelaide, Adelaide, SA 5005, Australia.

[2]Freemasons Foundation Centre for Men's Health, Adelaide Medical School, University of Adelaide, Adelaide, SA 5005, Australia.

[3]South Australian Health and Medical Research Institute, Adelaide, SA 5000, Australia.

[4]Flinders Health and Medical Research Institute and Flinders Centre for Innovation in Cancer, Flinders University, College of Medicine and Public Health, Bedford Park, SA 5042, Australia.

[5]Institut Bergonié Unicancer, INSERM U1218, Bordeaux, France.

[6]School of Mathematics and Statistics, Charles Perkins Centre, Faculty of Science, The University of Sydney, Camperdown, NSW 2006, Australia

[7]School of Medical Sciences, Charles Perkins Centre, Faculty of Medicine and Health, The University of Sydney, Camperdown, NSW 2006, Australia.

[8]KU Leuven - University of Leuven, LKI - Leuven Cancer Institute, Department of Oncology, Laboratory of Lipid Metabolism and Cancer, Leuven, Belgium.

*Corresponding author:

Luke A. Selth: luke.selth@flinders.edu.au

4.3 ABSTRACT

Prostate tumours are highly dependent on lipids for growth and survival. The androgen receptor (AR) is a major mediator of dysregulated lipid metabolism in prostate cancer, although the molecular mechanisms underlying this phenomenon remain to be fully elucidated. Here, we identified Acyl-CoA Synthetase Medium Chain Family Members 1 and 3 (*ACSM1* and *ACSM3*), enzymes that play a critical role in fatty acid activation, as factors that are directly regulated by AR in prostate cancer. *ACSM1* and *ACSM3* are highly upregulated in prostate tumours compared to non-malignant tissues and discriminate this cancer type in pan-cancer analyses. Knockdown of ACSM1/3 in PCa cells resulted in growth inhibition (*in vitro* and *in vivo*) and depletion of ATP, consistent with both factors having a major role in energy production via fatty acid oxidation. Mass spectrometry-based lipidomics and metabolomics revealed that loss of ACSM1/3 caused prostate cancer cells to accumulate poly-unsaturated fatty acids and switch to a glycolytic phenotype. These phenotypic changes led to mitochondrial oxidative stress and subsequent lipid peroxidation, eventually resulting in cell death. Build-up of mitochondrial reactive oxygen species was abrogated by an iron chelator, ferrostatin-1, suggesting that cell death was due to an iron-dependent form of apoptosis termed ferroptosis. Supporting this concept, over-expression of ACSM1 and ACSM3 elicited resistance to the ferroptosis inducers Erastin and ML210. Collectively, these studies uncover a novel link between AR and lipid metabolism in prostate cancer cells. Importantly, the critical role of ACSM1 and ACSM3 as key regulators of growth and protectors against ferroptosis emphasises their potential as novel therapeutic targets.

4.4 INTRODUCTION

Cancer cells have different metabolic requirements compared to normal cells, as they are highly proliferative and need to survive in a transformed microenvironment characterised by hypoxia and limited nutrient supply. Altered lipid metabolism represents one of the most common metabolic adaptations exhibited by cancer cells (Peck and Schulze, 2019). For example, cancer cells exhibit increased *de novo* synthesis and uptake of fatty acids (FAs), which are used for membrane biogenesis, energy production (via β-oxidation) and storage, and protein modification (Butler et al., 2020). Additionally, cancer cells actively stimulate mobilisation and release of stored lipids from adipocytes in the tumour microenvironment, a process called lipolysis (Laurent et al., 2016).

Prostate cancer (PCa) is characterised by and highly dependent on dysregulation of lipid metabolic pathways (Zadra and Loda, 2018), a phenomenon that is heavily influenced by the androgen receptor (AR) signalling axis (Butler et al., 2016). AR, a ligand (androgen)-activated transcription factor, is the primary oncogenic driver of PCa and the major therapeutic target in advanced and metastatic disease (Coutinho et al., 2016). AR indirectly regulates the expression of factors with major roles in lipid metabolism by enhancing the expression and activity of sterol regulatory element binding proteins (SREBPs) (Butler et al., 2016), transcription factors with a fundamental role in activating a lipogenic transcriptional program. Additionally, AR also directly regulates the expression of genes encoding factors involved in lipid synthesis, uptake and storage (Butler et al., 2016; Massie et al., 2011), one key example being fatty acid synthase (FASN) (Chan et al., 2015). Given the essential role of FAs/lipids in enhancing the growth of PCa and the

emerging realisation of their widespread and intricate interplay with AR signalling, there is increasing interest in therapeutic targeting of lipid metabolic pathways (Watt et al., 2019; Zadra et al., 2019).

The first step in utilisation of FAs - either those synthesised *de novo* or taken up from exogenous sources - is conversion to fatty acyl-CoA esters. This thioesterification process is catalyzed by a large family of enzymes called acyl-coenzyme A (acyl-CoA) synthetases (ACSs) and yields substrates for both β-oxidation and lipid synthesis (Coleman et al., 2002). The carbon chain length of FAs varies from 2 to >30, which are processed by distinct sub-families of ACSs: short-chain (C2–C4, ACCSs), medium-chain (C4–C12, ACSMs), long-chain (C12–C22, ACSLs), bubblegum (C14-C24, ACSBG), and very long-chain (C18–C26, annotated as solute carrier family 27A) (Soupene and Kuypers, 2008). Despite their central roles in cellular lipid metabolism, the normal and pathophysiological functions of many ACS enzymes, particularly the ACSMs, are poorly understood.

Here, we identify ACSM1 and ACSM3 as direct AR targets that are highly upregulated in the malignant prostate. The application of functional assays coupled with lipidomic and metabolomic experiments revealed that ACSM1/3 play crucial roles in determining the PCa cell lipidome and metabolome, which enables them to regulate oxidative stress and suppress ferroptotic cell death. Collectively, these data provide fundamental new insights into PCa lipid metabolism and reveal fatty acid activation by ACSM1/3 as a therapeutic vulnerability.

4.5 RESULTS

ACSM1 *and* ACSM3 *are AR target genes in prostate cancer*

To identify novel downstream mediators by which AR regulates lipid metabolism in PCa, we first compiled a list of 178 genes encoding factors with a putative role in this process (Table S1). Subsequently, published data (Cancer Genome Atlas Research, 2015; Heemers et al., 2011; Pomerantz et al., 2015; Taylor et al., 2010; Wang et al., 2007) was interrogated to filter the gene set by 3 criteria (Figure 1A): 1) evidence of regulation by androgen treatment in models of PCa; 2) evidence of proximal AR DNA binding proximal to transcriptional start sites (TSSs); and 3) evidence of dysregulated expression in clinical PCa. This data mining effort revealed 17 genes of interest: *ACACA*, *ACOT2*, *ACSL3*, *ACSM1*, *ACSM3*, *ELOVL5, ELOVL7*, *FASN, HACL1, HSD17B4, MAPKAPK2, MMAA, MORC2, PCCB, PCTP, PRKAB2* and *PTGR2* (Figure 1A; Table S1). The identification of known androgen-regulated genes (e.g. *ACACA* (Massie et al., 2011), *ACSL3* (Nelson et al., 2002) and *FASN* (Swinnen et al., 1997)) validated our approach. We focussed our attention on *ACSM1* and *ACSM3* (Acyl-CoA Synthetase Medium Chain Family Members 1 and 3), genes that encode enzymes reported to catalyse activation of medium chain fatty acids, since their potential roles in PCa are entirely unknown. AR-mediated upregulation of *ACSM1* and *ACSM3* was confirmed by treatment of LNCaP and VCaP cells with the potent androgen DHT, an effect that was reversed by co-treatment with the AR antagonist Enzalutamide (Figure 1B). These findings were reinforced by treating LNCaP or VCaP cells with Enzalutamide or an AR siRNA, which significantly reduced expression of *ACSM1* and *ACSM3* (Figures 1C-D). Activation or inhibition of AR also reduced protein levels of

ACSM1/ACSM3 (Figure 1E). In support of the *in vitro* data, *ACSM1* and *ACSM3* expression decreased following ADT in patient tumours (Figure 1F).

As part of our gene filtering criteria, we had noted putative AR binding sites proximal to the *ACSM1* and *ACSM3* TSSs in ChIP-seq data from prostate tumours and patient-matched normal specimens (Figure 1G). At all of these sites, it was apparent that AR binding was increased in malignant compared to non-malignant tissues. These binding events were also induced by androgen treatment in AR ChIP-seq data from the VCaP cell line model, highlighting their functional relevance (Figure 1G). We validated androgen-regulated AR binding at 5/6 of these loci by ChIP-qPCR in LNCaP cells (Figure 1H). Collectively, these data suggest that AR directly regulates the expression of *ACSM1* and *ACSM3*.

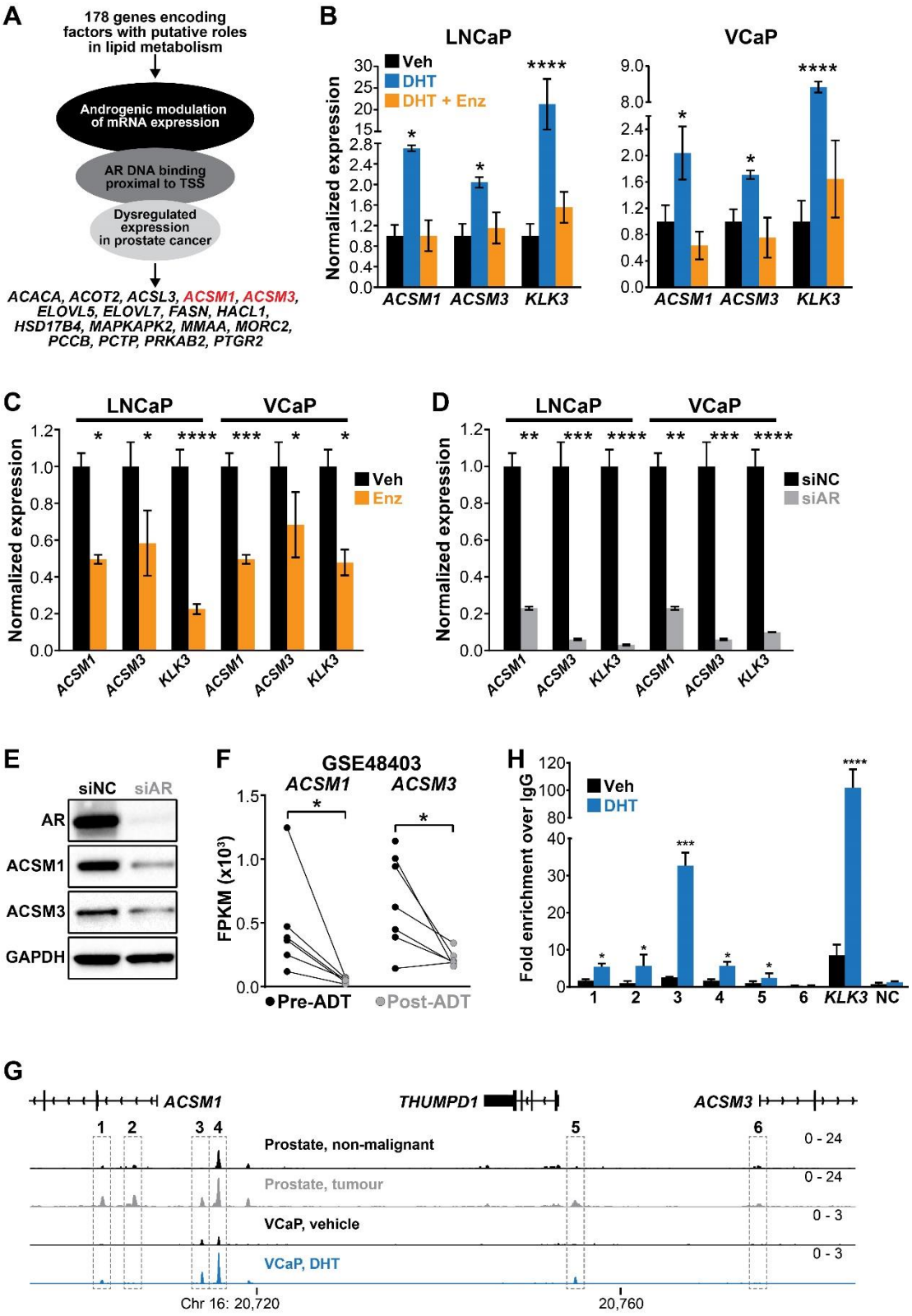

Figure 1. *ACSM1* and *ACSM3* are AR target genes in prostate cancer. (A) Schematic illustration of strategy to identify novel AR-regulated lipid metabolic genes. **(B-D)** Expression of *ACSM1* and *ACSM3* in response to: **(B)** DHT or DHT +

Enzalutamide (DHT+Enz) in cells grown in charcoal-strippd serum; **(C)** Enzalutamide (Enz) in cells grown in full serum; and **(D)** siRNA-mediated knockdown of AR (siAR). Gene expression was normalised to *GAPDH;* vehicle (Veh) or negative control siRNA (siNC) were set to 1; error bars are SEM. Differential expression was evaluated using unpaired t tests (*, $p < 0.05$; **, $p < 0.01$; ***, $p < 0.001$; ****, $p < 0.0001$). **(E)** ACSM1 and ACSM3 protein levels in response to siAR treatments were measured by immunoblotting in LNCaP cells. GAPDH was used as a loading control. **(F)** *ACSM1* and *ACSM3* mRNA expression in prostate tumours pre- and post- androgen deprivation therapy (ADT; (Rajan et al., 2014)). A Wilcoxon matched-pairs signed rank test was used to compare expression in the groups. FPKM, fragments per kilobase of exon per million mapped reads. **(G)** ChIP-seq data showing AR DNA binding near the *ACSM1* and *ACSM3* gene in non-malignant and prostate tumour samples ((GSE56288, (Pomerantz et al., 2015)) and VCaP cells (GSE55064), (Asangani et al., 2014)). The grey dotted box indicates AR binding peaks. **(H)** Evaluation of 6 putative AR binding sites (1-6; shown below the ChIP-seq tracks in G) by ChIP-qPCR. Data is represented as fold-change over an IgG control. Error bars represent SEM.

ACSM1 and *ACSM3* are highly expressed in the malignant prostate

To assess the clinical relevance of ACSM1 and ACSM3 in PCa, we examined a series of published clinical datasets. Both genes were highly upregulated in PCa compared to non-malignant prostate tissues in 3 large datasets, 2 of which (TCGA and CPGEA) represent patient-matched normal:tumour pairs (Figure 2A). Moreover, in multiple proteomic datasets, ACSM3 levels were elevated in cancer compared to non-malignant tissues (Supplementary Figure S1); ACSM1 was not evaluated in these studies. To extend upon these *in silico* analyses, we used immunohistochemistry to measure ACSM1 and ACSM3 protein expression in a tissue microarray containing non-malignant and tumour tissues from 160 men (see Materials and Methods). Both proteins were detectable in all samples: ACSM1 is ubiquitously expressed in epithelia and stroma, whereas ACSM3 expression is restricted to epithelial cells (Figure 2C, right). Consistent with the public datasets, levels of both proteins were significantly higher in tumours and associated with increasing Gleason grade (Figure 2C, left; representative images shown on right).

The ACS medium chain family is comprised of 7 genes: *ACSM1*, *ACSM2A*, *ACSM2B*, *ACSM3*, *ACSM4*, *ACSM5* and *ACSM6*. To assess if other family members have a function in PCa, we interrogated RNA-seq data from the TCGA (non-malignant and primary cancer) and SU2C (metastatic CRPC) cohorts was examined. *ACSM1* and *ACSM3* are the only family members expressed at an appreciable level in the normal prostate and primary tumours (Figure 2D, left). Although *ACSM2A*, *ACSM2B* and *ACSM5* are detectable in a subset of metastatic CRPC tumours, *ACSM1* and *ACSM3* are expressed at significantly higher levels ($p < 0.0001$ compared to all other genes; Figure 2D, right). We then evaluated the pan-

cancer distribution of *ACSM1* and *ACSM3* expression using a unified version of the TCGA dataset in which data from distinct tumour types can be compared after correction for study-specific biases (Wang et al., 2018). Notably, PCa exhibits the highest expression of both genes compared to 18 other cancer types (Figure 2E).

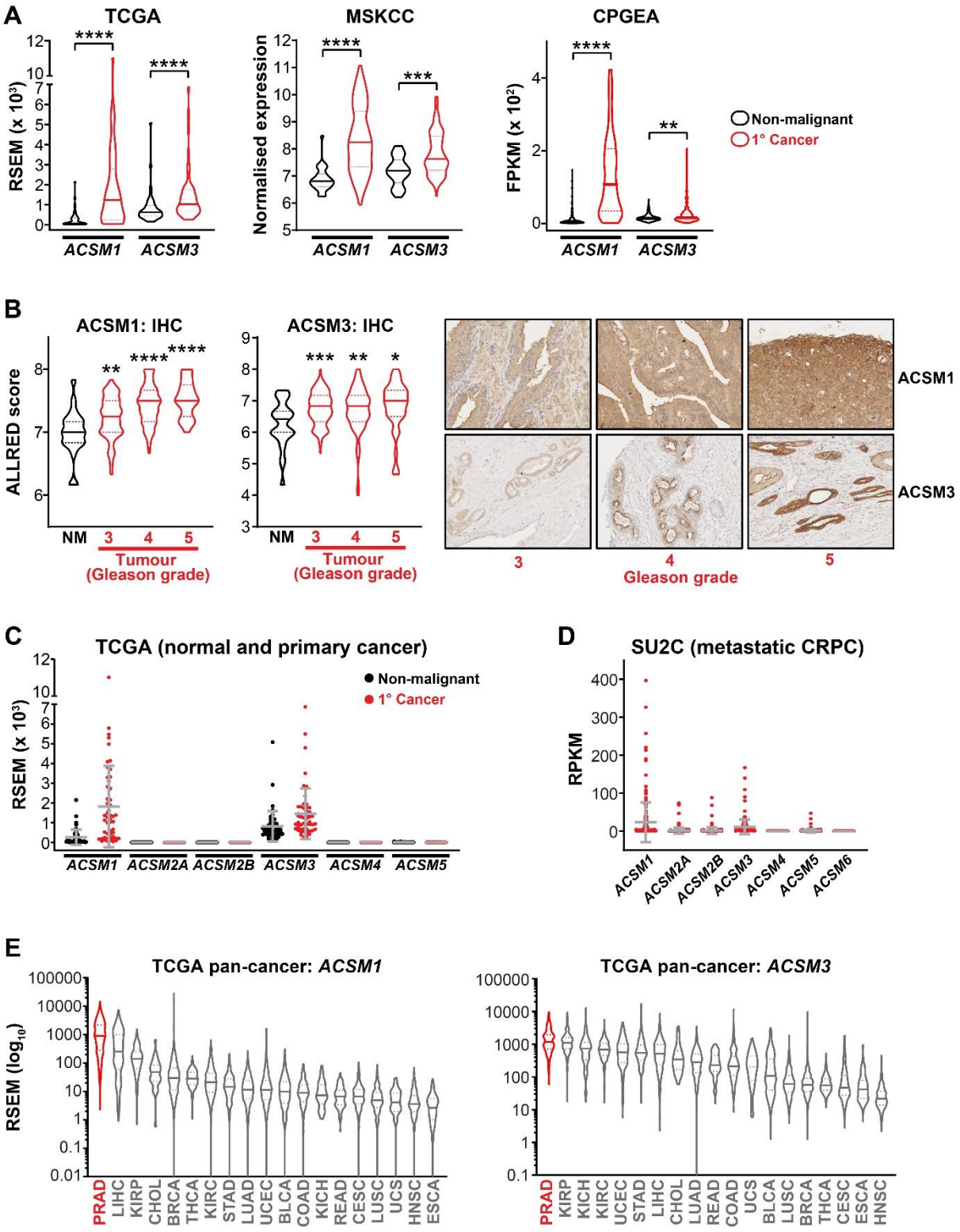

Figure 2. ACSM1 and ACSM3 are over-expressed in prostate cancer. (A) *ACSM1* and *ACSM3* expression is elevated in primary prostate cancer (1° Cancer). The TCGA dataset comprises 52 patient-matched non-malignant and cancer samples. Violin plots show minimum and maximum (bottom and top lines,

respectively) and mean (line within the boxes) values. Paired (TCGA and CPGEA) or unpaired (MSKCC) t tests were used to compare expression in non-malignant versus cancer tissues. RSEM, a quantitative value produced by RNA-Seq by Expectation Maximization; FPKM, fragments per kilobase of exon per million mapped reads. **(B)** ACSM1 and ACSM3 protein levels are associated with prostate cancer grade, as determined by IHC. Violin plots on left show minimum and maximum (bottom and top lines, respectively) and mean (line within the plot) values. One-way ANOVA was used to compare primary Gleason grade groups with non-malignant tissues. Representative IHC images are shown on the right (scale bars represent 50 μm). **(C)** Expression of ACSM family members in normal prostate and primary tumours in the TCGA cohort. **(D)** Expression of ACSM family members in metastatic CRPC in the SU2C cohort. RPKM, reads per kilobase of exon per million mapped reads. **(E)** Pan-cancer expression of *ACSM1* and *ACSM3* using a unified TCGA dataset (Wang et al., 2018).

ACSM1 and ACSM3 promote the growth of prostate cancer

The striking upregulation of ACSM1 and ACSM3 in malignancy and enrichment in prostate tumours compared to other cancer types are suggestive of important functional roles in PCa growth and progression. To identify appropriate model systems to evaluate this hypothesis, the expression of both factors was assessed in a panel of PCa cell lines. ACSM1 was robustly expressed in all 11 models tested, whereas the expression of ACSM3 was more variable and completely absent in the AR-negative cell lines (PC3 and DU145) (Figure 3A). Transient knockdown using two distinct siRNAs for each factor, both of which were highly effective at reducing cellular protein levels (Figure 3B), was used to determine whether ACSM1 and/or ACSM3 contribute to PCa growth. Targeting either factor markedly suppressed the proliferation of cell line models of castration-sensitive PCa (LNCaP, VCaP) and CRPC (22Rv1, MR49F) (Figure 3C). ACSM1 knockdown also caused inhibition of PC3 growth, but as expected ACSM3-specific siRNAs had no effect in this ACSM3-negative line (Figure 3C). Concomitant knockdown of both ACSM1 and ACSM3 did not elicit a stronger growth inhibitory phenotype that either factor alone (Figure 3C), suggesting redundancy in their function. The relevance of ACSM1 and ACSM3 in PCa tumourigenesis and growth was further demonstrated using colony formation and 3D spheroid assays, the latter chosen because it more closely mimics *in vivo* conditions than 2-dimensional cell culture. In both of these assays, loss of ACSM1 and ACSM3 had profound tumour suppressive effects (Figure 3D-E). We expanded our study of ACSM1 and ACSM3 by generating LNCaP cells stably modified to express higher levels of either factor (Figure 3F). Supporting the findings from the loss of function experiments, LNCaP-ACSM1 and LNCaP-ACSM3 cells exhibited an increased growth rate and an enhanced ability to form colonies (Figure 3G). Our

observations from the various growth assays suggested that loss of ACSM1 and ACSM3 caused cytotoxicity, which we tested using Annexin V/7-AAD assays. Annexin V binds to phosphatidylserine on the surface of cells that are undergoing multiple types of programmed cell death, including apoptosis, necroptosis and ferroptosis (Kloditz and Fadeel, 2019). Targeting of either factor caused a significant increase in cell death in multiple cell line models of PCa (Figure 3F). Collectively, these findings suggest that ACSM1 and ACSM3 are important mediators of growth and survival in PCa.

Encouraged by the *in vitro* data across a diverse range of PCa models, we investigated the requirement of ACSM1/3 in prostate cancer tumour growth *in vivo*. Luciferase-tagged LNCaP cells were engineered with lentiviruses to express doxycycline-inducible shRNAs specific for ACSM1 or ACSM3. LNCaP-shACSM3 cells exhibited robust knockdown of ACSM3 in response to doxycycline, and this shRNA-mediated knockdown recapitulated the effects on growth and colony forming ability elicited by siRNAs (Supplementary Figure S2A-C). By contrast, LNCaP-shACSM1 cells did not exhibit robust down-regulation of ACSM1 (Supplementary Figure S2A), and hence we did not proceed to *in vivo* experiments with this engineered line. LNCaP-shACSM3 cells were injected directly into the prostate and the growth of intra-prostatic xenografts was measured by monitoring of luciferase expression. After a period of 10 days to establish the xenografts, mice were fed doxycycline to induce knockdown of ACSM3. Loss of ACSM3 led to a striking decrease in the growth of LNCaP cells over a period of 48 days (Figure 3G), demonstrating that this factor is required for tumour growth in the prostate microenvironment.

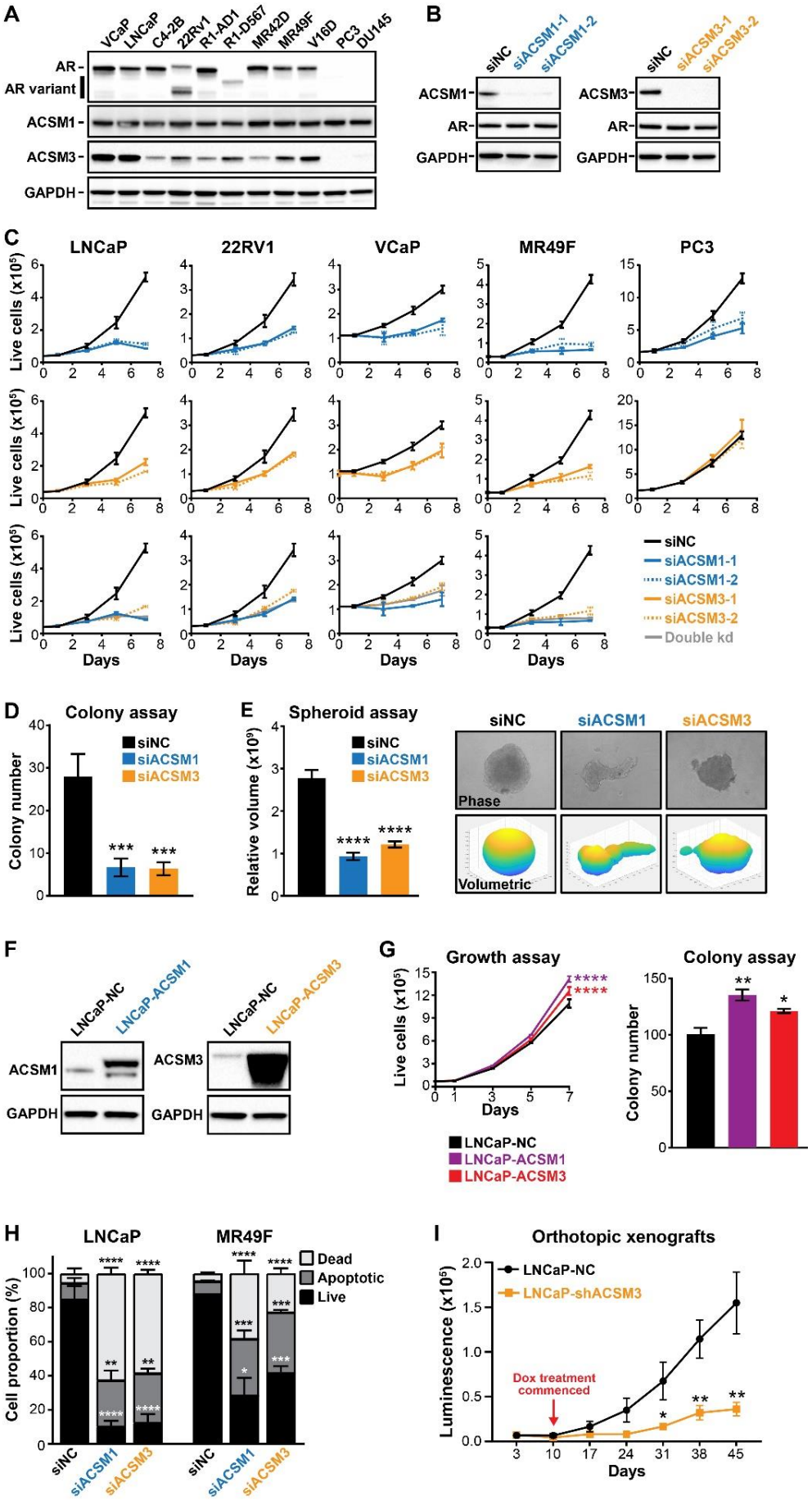
A
VCaP
LNCaP
C4-2B
22Rv1
R1-AD1
R1-D567
MR42D
MR49F
V16D
PC3
DU145
AR
AR variant
ACSM1
ACSM3
GAPDH
B
siNC
siACSM1-1
siACSM1-2
siACSM3-1
siACSM3-2
ACSM1
ACSM3
AR
GAPDH
C
LNCaP
22RV1
VCaP
MR49F
PC3
Live cells (x10⁵)
Days
siNC
siACSM1-1
siACSM1-2
siACSM3-1
siACSM3-2
Double kd
D
Colony assay
Colony number
siNC
siACSM1
siACSM3
E
Spheroid assay
Relative volume (x10⁹)
siNC
siACSM1
siACSM3
Phase
Volumetric
F
LNCaP-NC
LNCaP-ACSM1
LNCaP-ACSM3
ACSM1
ACSM3
GAPDH
G
Growth assay
Live cells (x10⁵)
Days
LNCaP-NC
LNCaP-ACSM1
LNCaP-ACSM3
Colony assay
Colony number
H
LNCaP
MR49F
Cell proportion (%)
Dead
Apoptotic
Live
siNC
siACSM1
siACSM3
I
Orthotopic xenografts
Luminescence (x10⁵)
LNCaP-NC
LNCaP-shACSM3
Dox treatment commenced
Days

Figure 3. ACSM1 and ACSM3 are pro-growth and pro-survival factors in prostate cancer. (A) Western blotting of AR, ACSM1 and ACSM3 protein expression in PCa cell lines. GAPDH was used as a loading control. **(B)** Efficacy of siRNAs targeting ACSM1 and ACSM3. 10 nM of two distinct siRNAs per gene (siACSM1-1, siACSM1-2, siACSM3-1 and siACSM3-2) were transfected into LNCaP cells for 72 h, after which ACSM1 and ACSM3 protein levels were evaluated by Western blotting. GAPDH was used as a loading control. **(C)** Loss of ACSM1 and ACSM3 inhibits prostate cancer growth, as evaluated by Trypan blue assays. LNCaP, 22Rv1, VCaP, MR49F and PC3 cells were transfected with 2 distinct siRNAs per gene and Trypan blue growth assays were performed. Error bars represent SEM. **(D)** Loss of ACSM1 and ACSM3 inhibits LNCaP colony formation. Colonies with more than 50 cells were counted manually. Data shown is representative of 3 independent experiments. Unpaired t tests were used to compare colony formation of siACSM1/siACSM3 relative to siNC (***, $p < 0.001$). **(E)** Loss of ACSM1 and ACSM3 inhibits growth of prostate cancer spheroids. Spheroid volumes (n=11) were determined using the ReViSP software. Data shown on left is representative of 3 independent experiments. Representative image of spheres and volumetric analyses are shown in right. Unpaired t tests were used to compare spheroid volume of siACSM1/siACSM3 relative to siNC (****, $p < 0.0001$). **(F)** Western blotting showing over-expression of ACSM1 and ACSM3 in stably transduced LNCaP cells. GAPDH was used as a loading control. **(G)** Over-expression of ACSM1 and ACSM3 promotes growth of LNCaP cells, as evaluated by trypan blue growth assays (left) and colony formation assays (right). Unpaired t tests (at day 7 for trypan blue assays) were used to compare siACSM1/siACSM3 relative to siNC (*, $p < 0.05$; **, $p < 0.01$; ****, $p < 0.0001$). **(H)** ACSM1 and ACSm3

knockdown causes apoptosis of LNCaP cells, as determined using flow cytometry-based Annexin V/7-AAD assays. Data represents the mean ± SEM of triplicate samples and are representative of 3 independent experiments. Dead cell proportions were compared to vehicle using ANOVA and Dunnett's multiple comparison tests (*, $p < 0.05$; **, $p < 0.01$; ***, $p < 0.001$; ****, $p < 0.0001$). **(I)** Knockdown of ACSM3 inhibits growth of LNCaP intra-prostatic xenografts. The graph represents luciferase intensity as assessed by whole-animal bioluminescent imaging over time in mice injected with shNC (control) cells (n = 8) or shACSM3 cells (n = 10), as assessed by non-invasive bio-luminescent imaging. Data are presented as mean ± SEM. The shACSM3 and shNC groups were compared at indicated time-points using unpaired t tests (*, $p < 0.05$; **, $p < 0.01$; ***, $p < 0.001$; ****, $p < 0.0001$).

ACSM1 and ACSM3 are potent regulators of prostate cancer metabolism

Members of the ACSM family catalyze the activation of medium chain fatty acids to produce acyl-CoA, a reaction that is indispensable in fatty acid utilization (Fujino et al., 1996). Given their integral role in cellular metabolism, we undertook a series of experiments to interrogate bioenergetic metabolic alterations in response to ACSM1 or ACSM3 loss. ATP assays demonstrated that energy production was decreased in response to knockdown of both factors (Figure 4A). Mass-spectrometry-based lipidomics revealed a dramatic alteration to the cellular fatty acid profile following loss of ACSM1/3 (Figures 4B-C). More specifically, we observed a general accumulation of many fatty acid species across multiple lipid classes and chain lengths (Figures 4D-E) that was most striking in response to loss of ACSM1. Inspection of saturation profiles revealed an increase in saturated and mono-unsaturated fatty acids (MUFAs) in response to knockdown of each of the factors. Inhibition of ACSM1 also caused a striking increase in poly-unsaturated fatty acids (PUFAs) across multiple classes; ACSM3 had a more modest effect on PUFAs, only increasing the levels of the less abundant SM and CER classes (Figure 4E). These data suggested that utilisation of fatty acids as an energy source or for other purposes was impaired by loss of ACSM1/3.

Parallel metabolomic profiling revealed accumulation of the end-product of glycolysis, lactate, as well as glycolytic intermediates such as glucose-6-phosphate and fructose-1,6-bisphosphate (Figure 4B). This observation implied that PCa cells were undergoing a switch from oxidative phosphorylation (OXPHOS) to glycolysis in response to targeting of ACSM1/ACSM3, consistent with a reduced ability of acyl CoA to utilise fatty acid oxidation for energy production (Nassar et al., 2020;

Schlaepfer et al., 2015). Extracellular flux analysis supported this hypothesis, revealing that loss of ACSM1 and ACSM3 dramatically increases extracellular acidification rate (ECAR), a proxy for glycolysis (Figure 4G). Defects in mitochondrial function and OXPHOS in response to targeting of ACSM1/ACSM3 were further supported by intracellular accumulation of amino acids (Figure 4H).

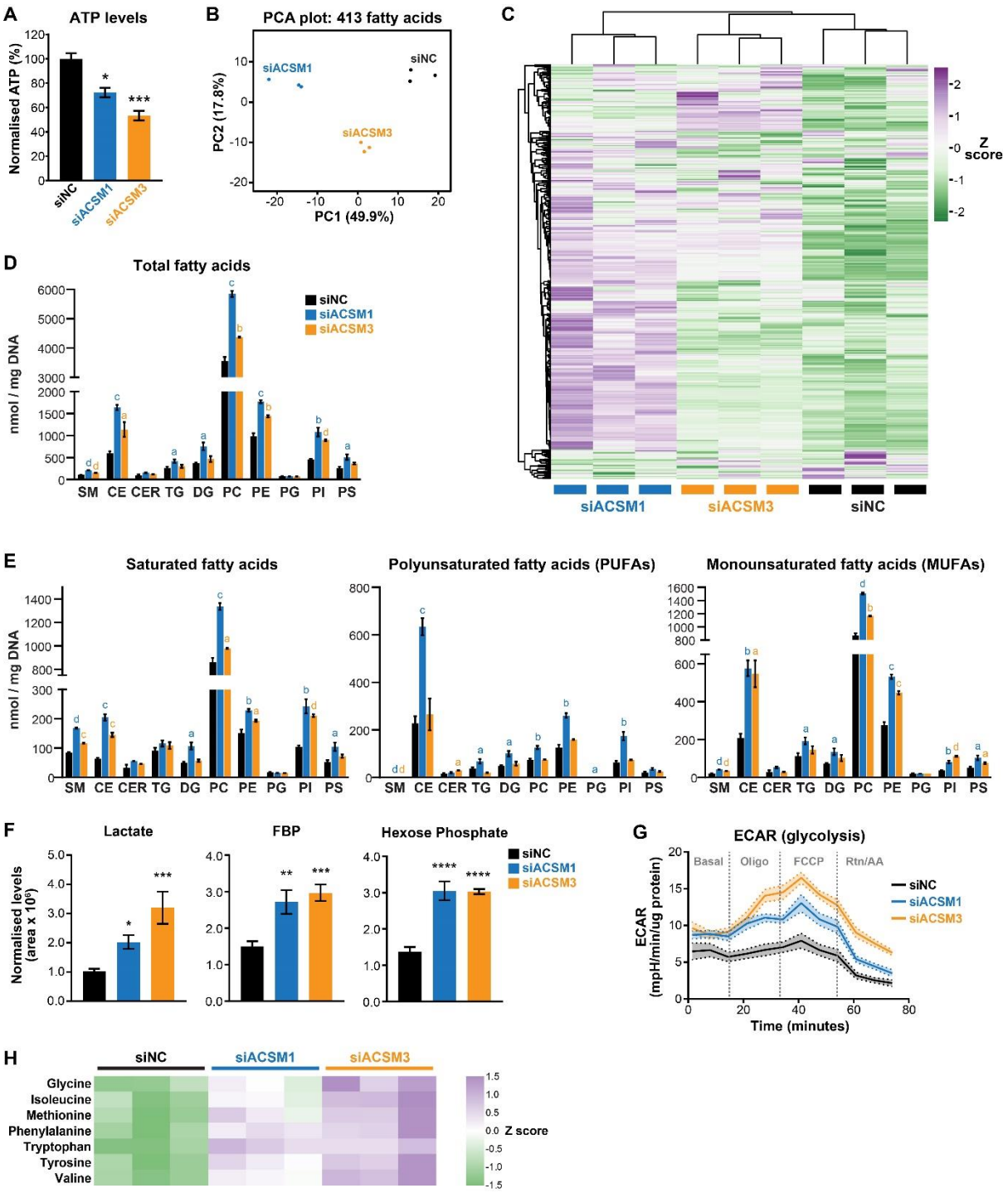

Figure 4. ACSM1 and ACSM3 are key regulators of prostate cancer metabolism.

(A) Loss of ACSM1 and ACSM3 caused a decrease in levels of total ATP. Data was normalised to control (siNC), which was set to 100%. Unpaired t tests were used to compare siACSM1/siACSM3 relative to siNC (*, $p < 0.05$; ***, $p < 0.001$). **(B)** Unsupervised separation of siNC, siACSM1 and siACSM3 samples based on the levels

of 413 fatty acids using using a principal component analysis (PCA). The plot was generated using Clustvis (Metsalu and Vilo, 2015). Unit variance scaling was applied to rows; singular value decomposition with imputation was used to calculate principal components. **(C)** Loss of ACSM1 and ACSM3 causes dysregulation of the prostate cancer lipidome. Heatmaps were generated using Clustvis. Both rows and columns were clustered using correlation distance and average linkage; unit variance scaling is applied to rows. **(D-E)** Abundance of lipid species in response to knockdown of ACSM1 and ACSM3. (D) shows total lipids in each class. (E) shows saturated (left), polyunsaturated (middle) and monounsaturated (right) fatty acids of each class. Data in bar graphs are mean ± SEM. Unpaired t tests were used to compare siACSM1/siACSM3 relative to siNC (a, $p < 0.05$; b, $p < 0.01$; c, $p < 0.001$; d, $p < 0.0001$). SM, sphingomyelins; CE, cholesterol esters; CER, ceramides; TG: triacylglycerides; DG: diacylglycerides; PC: phosphotidylcholines; PE: phosphotidylethanolamines; PG, phosphatidylglycerols; PI: phosphatidylinositols; PS: phosphotidylserines. **(F)** Loss of ACSM1 and ACSM3 in LNCaP cells causes accumulation of lactate and glycolytic intermediates, measured using GC QQQ targeted metabolomics. Data in bar graphs are mean ± SEM. Unpaired t tests were used to compare siACSM1/siACSM3 relative to siNC (*, $p < 0.05$; **, $p < 0.01$; ***, $p < 0.001$; ****, $p < 0.0001$). FBP, fructose bis-phosphate. **(G)** Loss of ACSM1 and ACSM3 alters extracellular acidification rate (ECAR) in LNCaP cells. Each data point represents an ECAR measurement. LNCaP cells were transfected with siACSM1, siACSM3 or siNC for 72 hr, then starved in substrate limited medium for 24 hr; the assay was run in fatty acid oxidation assay medium supplemented with palmitate. **(H)** Loss of ACSM1 and ACSM3 results in accumulation of amino acids, measured using GC QQQ targeted metabolomics. Z scores were derived from metabolomic data; 3 replicates of each treatment (siNC, siACSM1 and siACSM3) are shown.

Targeting of ACSM1 and ACSM3 induces lipid peroxidation and ferroptosis

Our metabolic and lipidomic analyses indicated that targeting ACSM1 and ACSM3 causes mitochondrial dysfunction and dysregulation of the PCa cell lipidome, both of which are likely to increase oxidative stress. In support of this concept, loss of ACSM1/ACSM3 activity dramatically increased the levels of reactive oxygen species (ROS), as determined by a flow cytometry-based assay, in multiple models of PCa (Figure 5A-B). Mitochondrial superoxide was a significant component of the increased cellular ROS, as revealed by MitoSOX assays (Figure 5C). Loss of redox homeostasis in response to targeting ACSM1/3 was consistent with our metabolomic data, which revealed a dramatic decrease in the antioxidant glutathione (γ-L-glutamyl-L-cysteinylglycine, GSH) (Figure 5D) and an increased NAD+:NADH ratio (Figure 5E). Interestingly, the loss of glutathione could not be explained by the availability of its constituent amino acids (cysteine, glutamate and glycine; Figures 4E and 5F). Collectively, these data provide additional evidence for mitochondrial dysfunction in response to knockdown of ACSM1/ACSM3 and reveal that a key role of these factors is to regulate cellular redox homeostasis.

The combination of increased ROS and accumulation of lipids and fatty acids, in particular PUFAs, is likely to result in increased cellular lipid peroxidation. To test this concept, we measured a marker of lipid peroxidation, malondialdehyde (Gawel et al., 2004), and found that it was robustly elevated by knockdown of ACSM1 and ACSM3 (Figure 5G-H). This observation was confirmed by staining cells with BODIPY-C11, which demonstrated accumulation of phospholipid hydroperoxides at cell membranes (Figure 5I). Lipid peroxidation is a hallmark of ferroptosis, an iron-dependent, non-apoptotic form of cell death (Dixon et al., 2012). Treatment of

cells with two inhibitors of ferroptosis, ferrostatin and N-acetylcysteine (NAC), abolished the effect of ACSM1/3 knockdown on ROS production in 3 PCa models (Figure 5J). These orthogonal and complementary approaches jointly demonstrate that cell death occurring in response to loss of these enzymes is largely mediated by ferroptosis. Importantly, over-expression of ACSM1/3 partially reversed the effects of ferroptosis-inducing compounds Erastin and ML210 (Cao and Dixon, 2016), providing direct evidence for their involvement in protection against this form of cell death (Figure 5K).

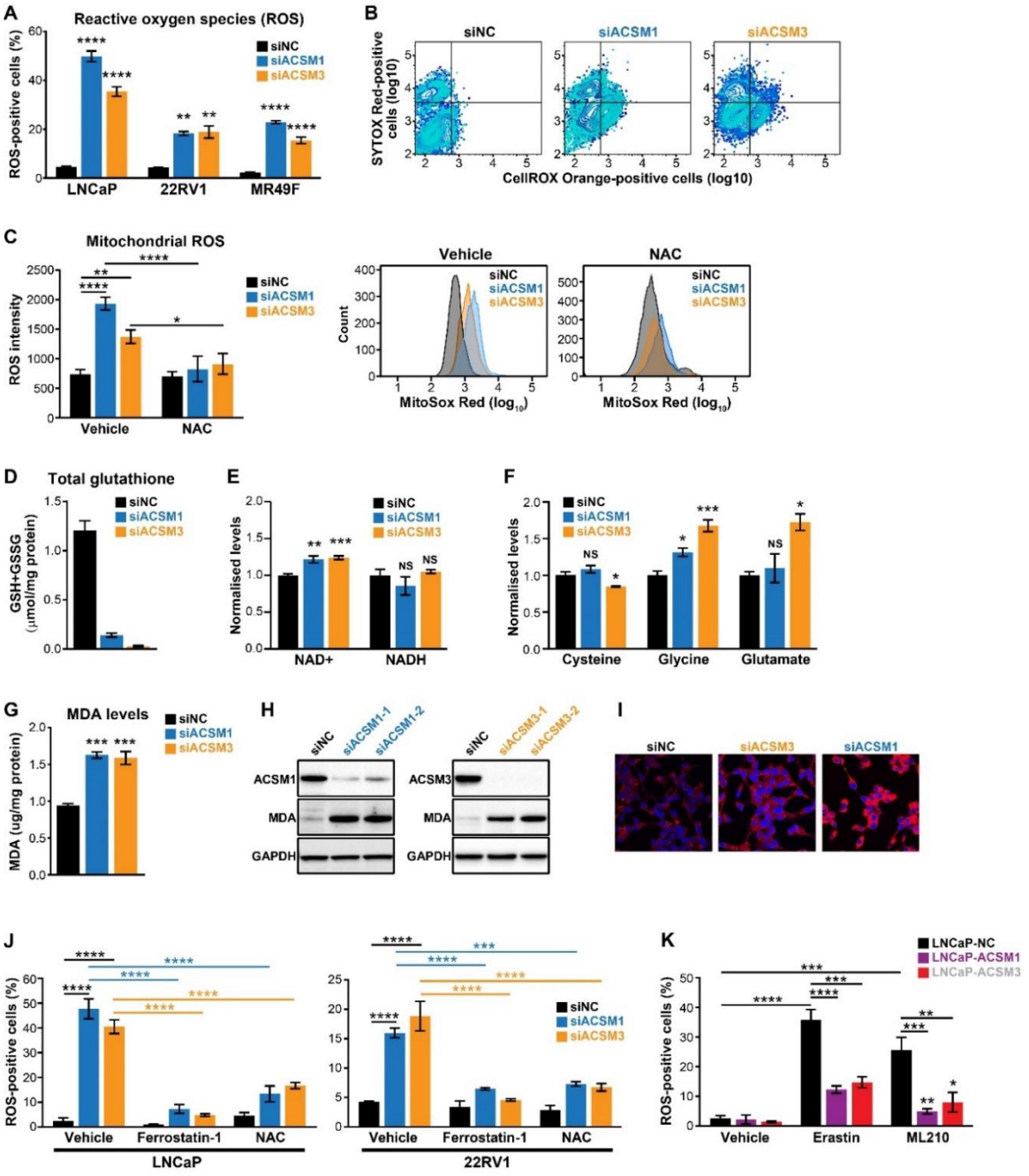

Figure 5. ACSM1 and ACSM3 play a critical role in maintaining redox homeostasis and protecting prostate cancer cells from ferroptosis. (A-B) Loss of ACSM1 and ACSM3 causes accumulation of ROS (A), as determined by a flow cytometric assay. Representative flow cytometry data for LNCaP cells are shown in (B). Data shown in (A) are mean ± SEM. Unpaired t tests were used to compare siACSM1/siACSM3 relative to siNC (**, $p < 0.01$; ****, $p < 0.0001$). **(C)** Loss of ACSM1 and ACSM3 causes accumulation of mitochondrial ROS (left), evaluated

using a MitoSOX assay to measure mitochondrial superoxide levels. Representative flow cytometry data are shown on left. One way ANOVA and Tukey's multiple comparisons test were used to compare groups (*, $p < 0.05$; **, $p < 0.01$; ****, $p < 0.0001$). **(D)** Loss of ACSM1 and ACSM3 causes a reduction in total glutathione (reduced glutathione (GSH) + oxidized glutathione (GSSG). Data are mean ± SEM. Unpaired t tests were used to compare siACSM1/siACSM3 relative to siNC (****, $p < 0.0001$). **(E)** Loss of ACSM1 and ACSM3 alters levels of NAD+, measured using GC QQQ targeted metabolomics. Data are mean ± SEM. Unpaired t tests were used to compare siACSM1/siACSM3 relative to siNC (**, $p < 0.01$; ***, $p < 0.001$). **(F)** Levels of amino acid constituents of glutathione, measured using GC QQQ targeted metabolomics. Data are mean ± SEM. Unpaired t tests were used to compare siACSM1/siACSM3 relative to siNC (*, $p < 0.05$; ***, $p < 0.001$). **(G-H)** Loss of ACSM1 and ACSM3 causes accumulation of malondialdehyde (MDA), as measured using a colourimetric assay (G) and Western blotting (H). For (G), data are mean ± SEM and unpaired t tests were used to compare siACSM1/siACSM3 relative to siNC (***, $p < 0.001$). For (H), GAPDH was used as a loading control. **(I)** Loss of ACSM1 and ACSM3 causes accumulation of membrane phospholipid hydroperoxides, as evaluated using BODIPY-C11 immunofluorescence in LNCaP cells. **(J)** Ferrostatin-1 and NAC rescue ROS induction mediated by loss of ACSM1 and ACSM3. Data are mean ± SEM. One way ANOVA and Tukey's multiple comparisons test were used to compare groups (*, $p < 0.05$; **, $p < 0.01$; ****, $p < 0.0001$). **(K)** Over-expression of ACSM1 and ACSM3 block the effects of ferroptosis-inducing compounds Erastin and ML210. Data are mean ± SEM. One way ANOVA and Tukey's multiple comparisons test were used to compare groups (*, $p < 0.05$; **, $p < 0.01$; ****, $p < 0.0001$).

4.6 DISCUSSION

The AR signalling axis is a major regulator of lipid metabolic processes in prostate cancer, but the molecular mechanisms underlying this regulation and relevance to disease progression remain poorly understood. Exploiting transcriptomic and cistromic data, we formulated an unbiased approach to isolate novel AR-regulated lipid metabolic genes. This approach identified *ACSM1* and *ACSM3*, which encode acyl-coenzyme A (acyl-CoA) synthetases (used interchangeably with acyl-CoA ligases) reported to catalyze the activation of medium chain FAs by CoA to produce an acyl-CoA, an essential step for the utilisation of FAs in further metabolic processes (i.e. storage, signalling, production of energy) (Watkins, 1997).

The functions of ACSM1 and ACSM3 in normal physiology are poorly understood. Indeed, the ACSM family as a whole is highly understudied compared to most other metabolic enzymes (van der Sluis, 2018). The *ACSM1* and *ACSM3* genes share a high degree of homology and structural similarity and are co-located on on chromosome 16p13.1, suggesting that they arose from a common ancestor by gene duplication (Fujino et al., 2001). Upon their discovery, it was demonstrated that human ACSM1 prefers hexanoate (6 carbons) as a substrate (Vessey et al., 1999), whereas the mouse orthologues of ACSM1 and ACSM3 prefer octanoate (8 carbons) and isobutyrate (4 carbons) as substrates, respectively (Fujino et al., 2001). However, these early biochemical studies and subsequent work revealed substantial flexibility in substrate utilisation by ACSMs; indeed, there is significant overlap in the chain length specificity of ACSMs and ACSLs (Ellis et al., 2015; van der Sluis and Erasmus, 2016). This is consistent with our findings: although our mass spectrometry approach to profile lipids was unable to detect medium chain

FAs or their activated forms, we found that loss of ACSM1/3 activity resulted in accumulation of many longer chain FA species. Based on this data, we believe that these enzymes directly catalyze activation of both medium and long chain FAs in PCa cells, although this remains to be definitively proven.

In terms of pathophysiological functions, the majority of research effort has been in establishing and understanding the association between *ACSM1* and *ACSM3* gene polymorphisms and metabolic syndrome (i.e. hypertension, hypertriglyceridemia, hypercholesterolemia and obesity) (Benjafield et al., 2003; Haketa et al., 2004; Iwai et al., 2002; Narita et al., 2002). Although the mechanism(s) underlying the function of ACSMs in metabolic syndrome is unknown, one hypothesis is that dysregulation of ACSM activity could result in increased *de novo* synthesis of long chain FAs in the liver and subsequently impact on obesity and hypertension. Very little is known about the relevance of ACSMs in cancer. ACSM1 was reported to be a marker of both PCa (Alinezhad et al., 2016) and apocrine breast cancer (Celis et al., 2008), whereas ACSM3 has been implicated as a tumour suppressor in hepatocellular carcinoma based on its down-regulation in this disease context (Gopal et al., 2017; Ruan et al., 2017). However, ours is the first study to undertake integrative functional characterisation of ACSM1 and ACSM3 in any cancer type. We found that PCa cells are highly dependent on ACSM1 and ACSM3 activity for optimal growth, which we postulate is largely a consequence of the key role of these enzymes in energy production. Indeed, loss of ACSM1/3 was associated with decreased levels of cellular ATP and mitochondrial dysfunction, both of which could indicate defective utilisation of fatty acids as an energy source. PCa cells would be especially sensitive to such a defect since they exhibit substantially increased rates

of fatty acid oxidation compared to non-malignant prostate cells (Balaban et al., 2019; Schlaepfer et al., 2014). We also observed a shift from oxidative phosphorylation to glycolysis in response to ACSM1/3 inhibition, which is a reported consequence of FA oxidation or impaired mitochondrial activity in PCa (Nassar et al., 2020; Schlaepfer et al., 2015). The high dependence of PCa cells on FA as an energy source has prompted evaluation of FA oxidation inhibitors such as a novel therapeutic strategy, with a focus on carnitine palmitoyltransferase-1 (CPT-1) inhibitors such as etomoxir, perhexiline and ranolazine (Flaig et al., 2017; Itkonen et al., 2017; Nassar et al., 2020). However, the clinical development of etomoxir was terminated due to severe hepatotoxicity associated with treatment (Holubarsch et al., 2007). ACSM1/3 represent alternative targets to suppress FA oxidation and hence inhibit PCa growth; indeed, the tissue specificity of ACSM1 (this study) and its marked enrichment in the malignant state could lend increased selectivity to targeting strategies. Although selective inhibitors of ACSMs are unavailable, their development would be facilitated by the crystal structure of ACSM2A (Kochan et al., 2009), which is 54.0 and 53.5% identical at the amino acid level to ACSM1 and ACSM3, respectively.

Our study revealed that ACSM1/3 are not only growth enhancers but also key survival factors in PCa. ROS are important for proliferation, adaptation to hypoxia and plasticity in cancer (Aggarwal et al., 2019), but excess ROS can cause death and hence tumour cells evolve strategies to counter oxidative stress. We propose that the pro-survival functions of ACSM1/3 largely reflect their ability to regulate levels of mitochondrial ROS. Although the precise mechanism(s) remains to be determined unclear, we envision multiple explanations for maintenance of redox

homeostasis by ACSM1/3. First, ACSM1/3 appear to play a critical role in preserving normal levels of glutathione, which cancer cells require for coping with inherently higher levels of oxidative stress. Second, high ACSM1/3 activity would favour OXPHOS and production of pyruvate, which can serve as a potent antioxidant, whereas low ACSM1/3 activity would result in a switch to glycolysis and lactate production, which is known to increase oxidative stress (El Sayed et al., 2013). Finally, certain carboxylate-containing xenobiotics, including benzoate and salicylate, are known substrates of ACSM2B (and to a lesser extent ACSM1) (van der Sluis, 2018; van der Sluis and Erasmus, 2016). Salicylate can generate hydrogen peroxide via interactions with the mitochondrial respiratory chain (Battaglia et al., 2005). Thus, xenobiotic detoxification is a mechanism by which ACSM1/3 could suppress generation of mitochondrial ROS, a hypothesis we plan to investigate in more detail. It is important to note that none of these mechanisms are mutually exclusive, and it is likely that all would play a role in mitigating cellular ROS by ACSM1/3.

In recent years, ferroptosis has emerged as an important non-apoptotic, iron-dependent mode of cell death (Stockwell and Jiang, 2020). A hallmark of ferroptosis is accumulation of lipid ROS, and in particular the oxidation of PUFA phospholipids in cell membranes (Stockwell and Jiang, 2020). Using both loss and gain of function experiments in combination with ferroptosis-activating compounds, our study conclusively revealed that ACSM1/3 are powerful suppressors of ferroptotic cell death in PCa. This is not surprising given that both factors are important regulators of the cellular lipid profile as well as potent inhibitors of ROS generation. Loss of ACSM1 led to an accumulation of PUFAs and a range of saturated FAs and MUFAs,

whereas loss of ACSM3 was not associated with increased levels of PUFAs. Since saturated FAs and MUFAs are much less susceptible to ROS- or enzyme-mediated oxidation than PUFAs (Stockwell and Jiang, 2020), we propose that the primary mechanism by which ACSM3 inhibits ferroptosis is via its ability to maintain redox homeostasis. The close association between lipid remodelling and ferroptotic death sensitivity is an emerging feature of PCa cells (Tousignant et al., 2020). It is not surprising, therefore, that PCa cells have acquired fatty acid metabolic features that can mitigate this vulnerability. As an example, recent reports demonstrated that another factor required for fatty acid oxidation, DECR1, serves to protect PCa cells from ferroptosis (Blomme et al., 2020; Nassar et al., 2020). In contrast to ACSM1/3, DECR1 is an AR-repressed factor, although (paralleling ACSM1/3) it is upregulated during PCa development and progression and serves to process PUFAs for catabolism. Considering these studies alongside our work, we postulate that therapeutic approaches to elicit ferroptosis are a promising strategy in PCa. Importantly, such a strategy may be more effective in the therapy resistant state, which exhibits increased sensitivity to ferroptosis due to altered fatty acid membrane composition in multiple cancer types and in response to diverse therapies (Hangauer et al., 2017; Tousignant et al., 2020; Viswanathan et al., 2017).

We cannot rule out additional enzymatic functions of ACSM1/3 in PCa beyond activation of fatty acids. For example, recent reports have shown that ACSM1 regulates lipoylation (i.e. addition of a lipoic acid moiety) of pyruvate dehydrogenase (PDH) and α-ketoglutarate dehydrogenase (αKGDH) (Paredes et al., 2018). This post-translational modification enhances the activity of PDH and αKGDH, which in turn promotes the tricarboxylic acid (TCA) cycle and oxidative respiration (McKenna

& Rae, 2015), a process reported to enhance metabolic plasticity under hypoxia and in cancer cells (Paredes et al., 2018). Indeed, we were able to validate the lipoic acid-activating activity of ACSM1 in PCa cells (Supplementary Figure S3). However, since ACSM3 apparently lacks this enzymatic activity (Supplementary Figure S3) but is also required for normal mitochondrial function in PCa cells, we propose that lipoylation only represents a minor contributor to ACSM1-mediated regulation of PCa metabolism.

In summary, our study defines a new link between the AR signalling axis and fatty acid activation. Importantly, the dual roles of ACSM1 and ACSM3 in energy production via FAO and as guardians against oxidative stress and ferroptotic death position them as major players in PCa growth and progression, warranting additional research into their potential as therapeutic targets.

4.7 MATERIALS AND METHODS

Cell lines and cell culture

The human prostate cancer cells lines LNCaP, 22Rv1, VCaP and PC3 were obtained from the American Type Culture Collection (ATCC). V16D and MR49F cells (Bishop et al., 2017) were kindly provided by A. Zoubeidi. LNCaP, 22Rv1, V16D and MR49F cells were maintained in RPMI-1640 containing 10% FBS; MR49F (castration-resistant, enzalutamide-resistant) cell media was additionally supplemented with 10μM enzalutamide. PC3 cells were maintained in RPMI-1640 containing 5% FBS. VCaP cells were maintained in Dulbecco's Modified Eagles's medium (DMEM) containing 10% FBS, % sodium pyruvate, 1% MEM non–essential amino acids, and 0.1nM 5α-dihydrotestosterone (DHT). For serum starvation experiments, cells were grown in phenol red-free RPMI-1640 containing 10% dextran-coated charcoal (DCC) stripped serum. Cell Bank Australia performed verification of all cells lines (2016-2019) via short-tandem repeat profiling. All cell lines were subjected to regular mycoplasma testing.

Cell line transfection

Transfection of cell lines with 10 nM small interfering RNAs (siRNAs) was performed using RNAiMAX Transfection Reagent (Life Technologies) according to the manufacturer's instructions. SiRNAs used in this study were ACSM1 and ACSM3 Silencer Select (Ambion; siACSM1-1 (s41984), siACSM1-2 (s41985), siACSM3 (s12459) and siACSM3 (s12460)) and control siRNA (Qiazen 1027281). For double knockdown, siACSM1-2 (s41985) and siACSM3 (s12460) were co-transfected into cells.

Quantitative Real-Time PCR (qRT-PCR)

Total RNA from cell lines was extracted using TRI Reagent (Sigma), as described previously (Das et al., 2017). Total RNA was treated with Turbo DNA-free kit (Invitrogen), and reverse transcribed using iScript Reverse Transcriptase Supermix kit (Bio-Rad). qRT-PCR was performed in triplicate as described previously (Moore et al., 2012). GAPDH levels were used for normalization of qRT-PCR data. Relative gene expression was calculated using the comparative Ct method. Primer sequences are shown in Table 1.

Table 1. Primers used in this study.

Primer	Sequence	Use
AR_exon1_2_F	CCACTTGTGTCAAAAGCGAAAT	qRT-PCR
AR_exon1_2_R	ATAGTCAATGGGCAAAACATGG	qRT-PCR
ACSM1_mRNA_F	CTGCTCTACGAGAACTATGGGC	qRT-PCR
ACSM1_mRNA_R	CTGTGTTAGGTGGCAGGATGCT	qRT-PCR
ACSM2A_mRNA_F	CAGAAGGAGACATTGGCATCAGG	qRT-PCR
ACSM2A_mRNA_R	AGTCTCCTCGAATGTTGGCTGC	qRT-PCR
ACSM2B_mRNA_F	CAGAAGGAGACATTGGCATCAGG	qRT-PCR
ACSM2B_mRNA_R	AGTCTCCTCGAATGTTGGCTGC	qRT-PCR
ACSM3_mRNA_F	CTGGGCAAAGTCTGCATGGAGT	qRT-PCR
ACSM3_mRNA_R	AGTTGGTGCTGAACAGAAGACTG	qRT-PCR
ACSM4_mRNA_F	GTTCACCCTCTGCGGAAGGTAT	qRT-PCR
ACSM4_mRNA_R	GCCAGGAAGAAAACACACTGCC	qRT-PCR
ACSM5_mRNA_F	CCATCTTTCGGCTGCTTGTGCA	qRT-PCR
ACSM5_mRNA_R	CAGTCTGGTGTTTCCACTTCTCC	qRT-PCR
FASN_mRNA_F	TCTCCGACTCTGGCAGCTT	qRT-PCR
FASN_mRNA_R	GCTCCAGCCTCGCTCTC	qRT-PCR
GADPH_R	GGCATGGACTGTGGTCATGAG	qRT-PCR

GAPDH_F	TGCACCACCAACTGCTTAGC	qRT-PCR
KLK3_F	CAGAGGAGTTCTTGACCCCAA	qRT-PCR
KLK3_R	ACAGCATGAACTTGGTCACCTT	qRT-PCR
ACSM1/3_Peak_1_ChIP_F	TGGTAGAGCAACTCGCCTTT	ChIP PCR
ACSM1/3_Peak_1_ChIP_R	TATGATTGGCCCAGCTTAGG	ChIP PCR
ACSM1/3_Peak_2_ChIP_F	AACAACACGGGCTCAAATTC	ChIP PCR
ACSM1/3_Peak_2_ChIP_R	TACTTGTCCGTGCTGAATGC	ChIP PCR
ACSM1/3_Peak_4_ChIP_F	CAGCCTCACGAAAGCCAGAAA	ChIP PCR
ACSM1/3_Peak_4_ChIP_R	TTAGCCCTGGGAAGAACTTGTG	ChIP PCR
ACSM1/3_Peak_5_ChIP_F	AGGCTCACCAACTGTGGACT	ChIP PCR
ACSM1/3_Peak_5_ChIP_R	AACTGGTTTTGGCAGGTTTG	ChIP PCR
KLK3_ChIP(Prom)_F	GCCTGGATCTGAGAGAGATATCATC	ChIP PCR
KLK3_ChIP(Prom)_R	ACACCTTTTTTTTTCTGGATTGTTG	ChIP PCR
NC2_F	GTGAGTGCCCAGTTAGAGCATCTA	ChIP PCR
NC2_R	GGAACCAGTGGGTCTTGAAGTG	ChIP PCR

Chromatin Immunoprecipitation (ChIP)

LNCaP cells were seeded at 4 x 10^6 cells/plate in 15cm plates in RPMI-1640 medium containing 10% DCC-FBS for 3 days, then treated for 4 hours with 10nM DHT or Vehicle (ethanol). AR ChIP using antibody ER179 (Ab108341, Abcam) was performed as described previously (Paltoglou et al., 2017).

Immunoblotting

Protein extraction from cells using RIPA buffer and western blotting was done as described previously (Moore et al., 2012). The following primary antibodies were used: AR (N20, SC-816, Santa Cruz Biotechnology); β-actin (AC-15, Ab6376, Abcam); ACSM1 (SAB1301678, Sigma-Aldrich); ACSM3 (sc-377173 (G8), Santa Cruz Biotechnology); DLAT (12362S, Cell Signalling Tech) DLST (11954S, Cell

Signalling Tech) Lipoic acid (ab58724, Abcam) α-tubulin (05-829, Millipore); GAPDH (MAB374, Millipore); MDA (ab6463, Abcam); and GPX4 (ab41787, Abcam). Secondary antibodies were anti-mouse (DAKO, E0433, 1:2000) and anti-rabbit (DAKO, E0432, 1:1000).

Analysis of published RNA-seq data

Clinical transcriptomic data was downloaded from GEO (GSE7868, (Wang et al., 2007); GSE22606 (Heemers et al., 2011); and GSE51005 (Rajan et al., 2014), cBioportal (MSKCC (Taylor et al., 2010); TCGA (Abeshouse et al., 2015); SU2C (Abida et al., 2019)). CPGEA data (Li et al., 2020) was obtained from http://bigd.big.ac.cn/gsa-human/.

Analysis of published ChIP-seq data

AR ChIP-seq data from GSE56288 (clinical specimens: 7 normal prostate and 13 primary tumours) (Pomerantz et al., 2015) and GSE55064 (VCaP cells) (Asangani et al., 2014) were obtained from GEO and visualized using the Integrated Genome Browser (IGV) (Thorvaldsdóttir et al., 2013).

Immunohistochemistry (IHC)

IHC was performed essentially as described previously (Hickey et al., 2015). Tissue sections were incubated with primary antibodies ACSM1 (1:100, SAB1301678, Sigma-Aldrich) and ACSM3 (1:50, sc-377173 (G8), Santa Cruz Biotechnology) overnight at 4°C. Biotinylated secondary antibodies (E0432 and E0433, Dako) were added to slides at a 1:400 dilution in blocking solution for 1h at RT followed by HRP-streptavidin at 1:500 for 1 hr at RT. Slides were scanned using a Nanozoomer digital

slide scanner (Hamamatsu). Images were viewed with NDP view software and quantified using ALLRED score (Choudhury et al., 2010).

Proliferation assays

Proliferation of cells transfected with siACSM1 and siACSM3 was measured using Trypan blue exclusion assays. Cells were seeded at 6×10^4 (LNCaP, LNCaP-MR49F, 22RV1), 1×10^5 (VCaP) and 1×10^4 (PC3) in 12-well plates. Live cells were quantified in haemocytometer using Trypan blue.

Apoptosis assays

Apoptosis was measured by collecting cells in FACS binding buffer (47 ml of HANKS buffered saline, 500 µL of Herpes solution and 2.5 mL of 100 mM CaCl2), staining with Annexin V PE (BD PharmagenTM , BD Biosciences, CA, US and 1 mM 7-Aminoactiomycin D (Thermo Fisher Scientific) and analysis by Flow Cytometry using a LSRFortessa X20 (BD Biosciences). RAJ: ADD A REFERENCE AS THE REVIEWER ASKS

Colony and spheroid formation assays

For colony formation assays, cells were washed with PBS, trypsinized, collected, counted and single-cell suspension was prepared. 500 cells were plated in 6-well plates and incubated for 2 weeks at 37°C, with media replenishment every 3-7 days. Cells were then washed with PBS, fixed with 4% paraformaldehyde and stained with 1% crystal violet for 30 minutes. Colonies were counted manually after washing excess stain with water.

For spheroid assays, cells were collected and prepared at a concentration of 7.5 x 10^4 cells/ml. Cell suspensions (1500 cells in 20µl) were pipetted onto 96 well Spheroid ULA/CS plates with 100µL of media and incubated at 37°C for 5 days. Photos of the formed spheres were captured and sphere volume was determined using ReViSP software (Piccinini et al., 2015).

Reactive oxygen species (ROS) assays

Cellular ROS levels were measured using CellROXTM Orange Flow Cytometry Assay Kits (Life Technologies). Briefly, 24 hours post-seeding (5 x 10^5 cells per 6-well plate), the cells were treated with or without antioxidant (0.5 mM Trolox) and incubated for the indicated times. Cells were stained with CellROX Orange and SYTOX Red Stain and analysed by Flow Cytometry (10-30,000 cells/sample) using a LSRFortessa X20.

Total ATP assay

LNCaP cells were transfected with siACSM1 and siACSM3 for 72 hours in 96 well plate format. Total cellular ATP levels measurement were made according to manufacturer's instructions (Luminescent ATP Detection Assay Kit, ab113849) and normalized to the total cellular DNA content / cell number in each well determined by CyQUANT™ Cell Proliferation Assay kit (ThermoFisher Scientific).

Lipid peroxidation analysis

LNCaP cells were transfected with siACSM1 and siACSM3 for 96 h and then plated at 5 x 10^3 cells/well in an 8-well chamber slide. Cells were stained with 5µM BODIPY-581/591 C11 (Thermo Fisher Scientific). Cells were washed and fixed with

4% paraformaldehyde (PFA), and mounted with Prolong Gold anti-fade solution with DAPI (Thermo Fisher Scientific). Cells were imaged at 60 X magnification using a Olympus FV3000 Confocal Microscope as described previously (Nassar et al., 2020). Quantification of BODIPY-C11 stain was performed using ImageJ analysis software.

Seahorse extracellular flux analysis

Cells were plated in XF96 well cell culture microplates (Agilent) at equal densities in substrate-limited medium (DMEM with 0.5mM glucose, 1.0mM glutamine, 0.5mM carnitine and 1% FBS) and incubated overnight. One hour before the beginning OCR measurements, the cells were changed into FAO Assay Medium (111mM NaCl, 4.7mM KCl, 2.0mM $MgSO_4$, 1.2mM Na_2HPO_4, 2.5mM glucose, 0.5mM carnitine and 5mM HEPES). After baseline OCR was stabilized in FAO Assay Medium, 200µM of linoleic-acid (LA) or palmitic acid (PA) were added before initializing measurements. Extracellular flux analysis was performed using the Seahorse XF Cell Mitochondrial Stress Test kit (Seahorse Bioscience) according to the manufacturer's protocol. Extracellular flux experiments were performed on a Seahorse XF96 Analyzer and results were analysed using Seahorse Wave software for XF analyzers. The OCR values were normalized to cell numbers in each well.

Lipidomics

LNCaP cells were transfected with siACSM1/3 for 4 and 6 days, after which culture plates were placed on ice. Media was removed and cells were washed 3 times with cold PBS, after which they were scraped and collected in 1.5 ml tubes by

centrifugation at 20,000g for 5 min. The supernatant was removed and cell pellets were frozen and stored at -80°C. To extract lipids, 700 µl of sample (4 µl of plasma diluted in water, or 700 µl of homogenized cells) was mixed with 800 µl 1 N HCl:CH3OH 1:8 (v/v), 900 µl CHCl3 and 200 µg/ml of the antioxidant 2,6-di-tert-butyl-4-methylphenol (BHT; Sigma Aldrich). 3 µl of SPLASH LIPIDOMIX Mass Spec Standard (#330707, Avanti Polar Lipids) was spiked into the extract mix. The organic fraction was evaporated using a Savant Speedvac spd111v (Thermo Fisher Scientific) at room temperature and the remaining lipid pellet was stored at - 20°C under argon.

Lipid pellets were reconstituted in 100% ethanol. Lipid species were analyzed by liquid chromatography electrospray ionization tandem mass spectrometry (LC-ESI/MS/MS) on a Nexera X2 UHPLC system (Shimadzu) coupled with hybrid triple quadrupole/linear ion trap mass spectrometer (6500+ QTRAP system; AB SCIEX). Chromatographic separation was performed on a XBridge amide column (150 mm ×4.6 mm, 3.5 µm; Waters) maintained at 35°C using mobile phase A [1 mM ammonium acetate in water-acetonitrile 5:95 (v/v)] and mobile phase B [1 mM ammonium acetate in water-acetonitrile 50:50 (v/v)] in the following gradient: (0–6 min: 0% B → 6% B; 6–10 min: 6% B → 25% B; 10–11 min: 25% B → 98% B; 11–13 min: 98% B → 100% B; 13–19 min: 100% B; 19–24 min: 0% B) at a flow rate of 0.7 mL/min which was increased to 1.5 mL/min from 13 min onwards. SM, CE, CER, DCER, HCER, LCER were measured in positive ion mode with a precursor scan of 184.1, 369.4, 264.4, 266.4, 264.4 and 264.4 respectively. TAG, DAG and MAG were measured in positive ion mode with a neutral loss scan for one of the fatty acyl moieties. PC, LPC, PE, LPE, PG, LPG, PI, LPI, PS and LPS were measured in

negative ion mode by fatty acyl fragment ions. Lipid quantification was performed by scheduled multiple reactions monitoring (MRM), the transitions being based on the neutral losses or the typical product ions as described above. The instrument parameters were as follows: Curtain Gas = 35 psi; Collision Gas = 8 a.u. (medium); IonSpray Voltage = 5500 V and −4,500 V; Temperature = 550°C; Ion Source Gas 1 = 50 psi; Ion Source Gas 2 = 60 psi; Declustering Potential = 60 V and −80 V; Entrance Potential = 10 V and −10 V; Collision Cell Exit Potential = 15 V and −15 V. The following fatty acyl moieties were taken into account for the lipidomic analysis: 14:0, 14:1, 16:0, 16:1, 16:2, 18:0, 18:1, 18:2, 18:3, 20:0, 20:1, 20:2, 20:3, 20:4, 20:5, 22:0, 22:1, 22:2, 22:4, 22:5 and 22:6 except for TGs which considered: 16:0, 16:1, 18:0, 18:1, 18:2, 18:3, 20:3, 20:4, 20:5, 22:2, 22:3, 22:4, 22:5, 22:6.

Peak integration was performed with the MultiQuant software version 3.0.3. Lipid species signals were corrected for isotopic contributions (calculated with Python Molmass 2019.1.1) and were normalized to internal standard signals. Unpaired T-test p-values and FDR corrected p-values (using the Benjamini/Hochberg procedure) were calculated in Python StatsModels version 0.10.1.

Metabolomics

LNCaP cells (5.0 x 10^6) were transfected with siRNA for 48 hours in RPMI (phenol red free) with 10% FBS supplemented with 2.0 mM glucose in 6-well plates. Cells were placed on ice and washed twice with 5 ml cold NaCl saline, after which 300µl of ice cold methanol:chloroform (MeOH:CHCl3) extraction solvent containing the internal standards (0.5µl/samples) was added onto each well. Cells were scraped and collected in 15ml tubes, after which an additional 300 µL MeOH:CHCl3 was

added to wells in order to collect remaining cells. 1.5 ml of chloroform was added to each tube followed by vortexing and incubation on ice for 5 mins. Tubes were centrifuged at 4°C for 5 minutes at 2,700g and the top aqueous layer was then transferred into a fresh 1.5ml Eppendorf tube and allowed to dry in a Speedvac. Dried samples were derivatised with 20µl methoxyamine (30mg/ml in pyridine, Sigma Aldrich) and 20µl N,O-Bis(trimethylsilyl)trifluoroacetamide (BSTFA) + 1% Trimethylchlorosilane (TMCS). The derivatised samples were analysed using GC QQQ targeted metabolomics as described (Best et al., 2018).

Lentiviral transduction of cells

SMARTvector Inducible Lentiviral shRNA vectors for ACSM1, ACSM3 and Non-targeting shRNA Control (glycerol stock *E. coli*) were obtained from Dharmacon (catalogue numbers V3SH11252-225482707 and V3SH11252-224860261). For over-expression of ACSM1 and ACSM3 in PCa cells, linear dsDNA fragments containing codon-optmised ACSM1 and ACSM3 cDNA sequences were cloned into Gateway entry vector (pDONR221) and then transferred into pJS64 destination vector. The sequence of the inserts was verified by Sanger sequencing at AGRF. Viral supernatants were prepared by transfection of HEK293T cells with the vector plasmids and packaging plasmids (psPAX2 Addgene 12259 and pMD2.G Addgene 12260). The transfection was performed with polethylenimine (PEI MAX Transfection Grade Linear Polyethylenimine Hydrochloride, 24765-1, Polysciences) as described previously (Das et al., 2017). After 48 hours, supernatants were filtered through 0.45 µm and 0.22 µm syringe filters and then concentrated ~100-fold using Vivaspin 100 kDa cut-off columns by centrifugation at 3000 g at 10°C for 6 hours. Concentrated virus was stored at -80° C. For

transduction, luciferase-tagged LNCaP cells (for shRNA viruses) and untagged LNCaP cells (for over-expression vectors) were seeded at 1.25 x 10^5 cells in 6 well plates and the following day were transduced with concentrated lentivirus for a period of 3 days. Puromycin (1.0 µg per mL) was added to select for transduced cells for an additional 3 days. Cells transduced with shRNA constructs were grown in 2ug µg per ml of doxycycline to induce expression of shRNAs.

Animal experiments

All animal procedures were were approved by the University of Adelaide Animal Ethics Committee (approval number M-2019–037) and carried out in accordance with the guidelines of the National Health and Medical Research Council of Australia. LNCaP-NC and LNCaP-shACSM3 cell suspensions (1 × 10^6 cells in 10 µl PBS) were injected intraprostatically in 8-week old NOD/SCID male mice. Whole-body imaging to monitor luciferase-expressing LNCaP cells was performed at day 3 of the injection and once weekly thereafter using an IVIS Spectrum *in vivo* Imaging System (PerkinElmer). D-luciferin (potassium salt, PerkinElmer) was dissolved in sterile deionized water (0.03 g/ml) and injected subcutaneously (3 mg/20 g of mouse body weight) before imaging. Bioluminescence was reported as the sum of detected photons per second from a constant region of interest.

Statistical analyses

All experiments were performed at least three times. Statistical analysis was performed using GraphPad Prism 7.02 software. Statistical methods are included in figure legends.

ACKNOWLEDGEMENTS

This work was supported by the National Health and Medical Research Council of Australia (1121057 to WDT and LAS). LAS and LMB are supported by Principal Cancer Research Fellowships, awarded by Cancer Council's Beat Cancer project on behalf of its donors, the state Government through the Department of Health and the Australian Government through the Medical Research Future Fund. The research programs of LMB, WDT and LAS are supported by the Movember Foundation and the Prostate Cancer Foundation of Australia through a Movember Revolutionary Team Awards. The authors thank: Jonas Dehairs and Ge Liu for assistance with lipidomics and metabolomics, respectively; and Geraldine Laven-Law, Zoya Kikhtyak, Joanna Gillis, Natalie Ryan, Madi Helm, and Rayzel Candida Fernandes for expert technical assistance. The results published here are in part based on data generated by The Cancer Genome Atlas, established by the National Cancer Institute and the National Human Genome Research Institute, and we are grateful to the specimen donors and relevant research groups.

AUTHOR CONTRIBUTIONS

RS, LMB and LAS conceived the project. RS, LMB and LAS designed experiments. RS, ZDN, CYM, LEQ and MP performed experiments and acquired data. ST, ARH, RI, CYM, MG, MP provided technical assistance. RS, WDT, LMB and LAS interpreted and analysed all data. RS, LEQ, AJH, WDT, JS, LMB and LAS contributed to interpreting the data. RS and LAS wrote the manuscript. All of the authors have read, edited, and approved the paper.

4.8 DECLARATION OF INTERESTS

The authors have no conflicts of interest to disclose.

4.9 SUPPLEMENTARY FIGURES

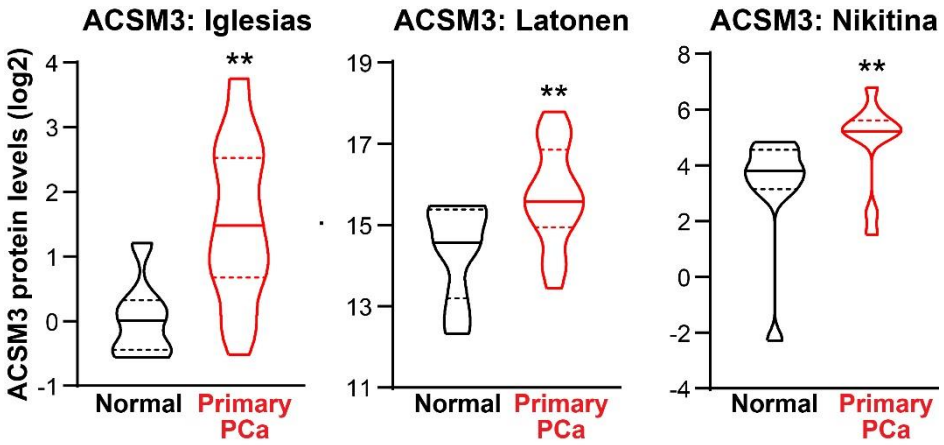

Supplementary Figure S1 (Iglesias-Gato et al., 2018; Latonen et al., 2018; Nikitina et al., 2017)**.** ACSM3 protein levels are elevated in primary prostate cancer (PCa) compared to normal prostate tissues. Violin plots show minimum and maximum (bottom and top lines, respectively) and mean (line within the boxes) values. Unpaired t tests were used to compare expression in normal and cancer tissues (**, $p < 0.01$).

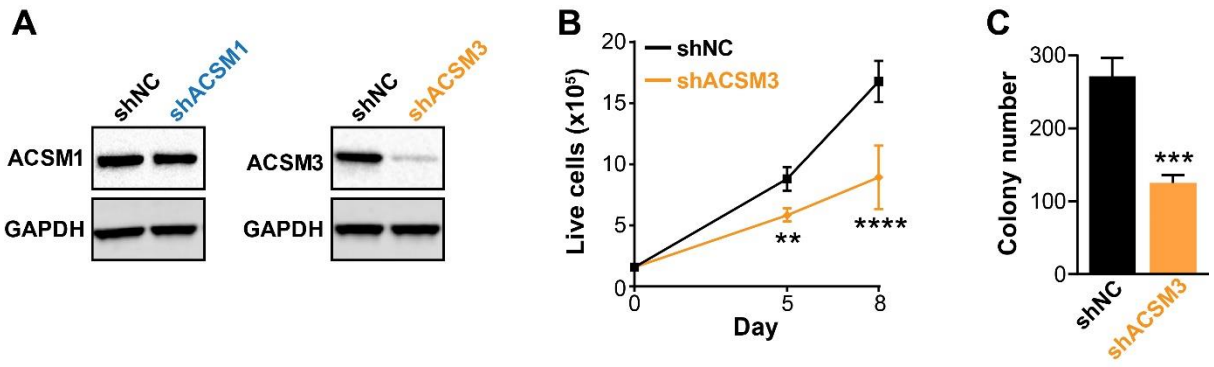

Supplementary Figure S2. (A) ACSM1 and ACSM3 protein levels in LNCaP derivatives stably transduced with shACSM1 and shACSM3. Cells were cultured in doxycycline (2 µg/mL) containing normal growth media for 5 days after which ACSM1 and ACSM3 proteins were evaluated by immunoblotting. GAPDH was used as a loading control. **(B)** Trypan blue assay showing growth of shNC and shACSM3 cells grown in the presence of doxycycline (2 µg/mL). Unpaired t tests were used to compare growth at the indicated time-points (**, $p < 0.01$; ****, $p < 0.0001$). **(C)** Clonogenic cell survival of LNCaP-shACSM3 cells was assessed using a colony formation assay. Cells were cultured for 2 weeks in doxycycline (2 µg/mL) containing normal growth media, washed with PBS, fixed with paraformaldehyde and stained with 1% crystal violet for 30 min. Colonies with were counted manually; data shown is representative of n = 3 independent experiments. An unpaired t test was used to compare shNC and shACSM3 (***, $p < 0.001$).

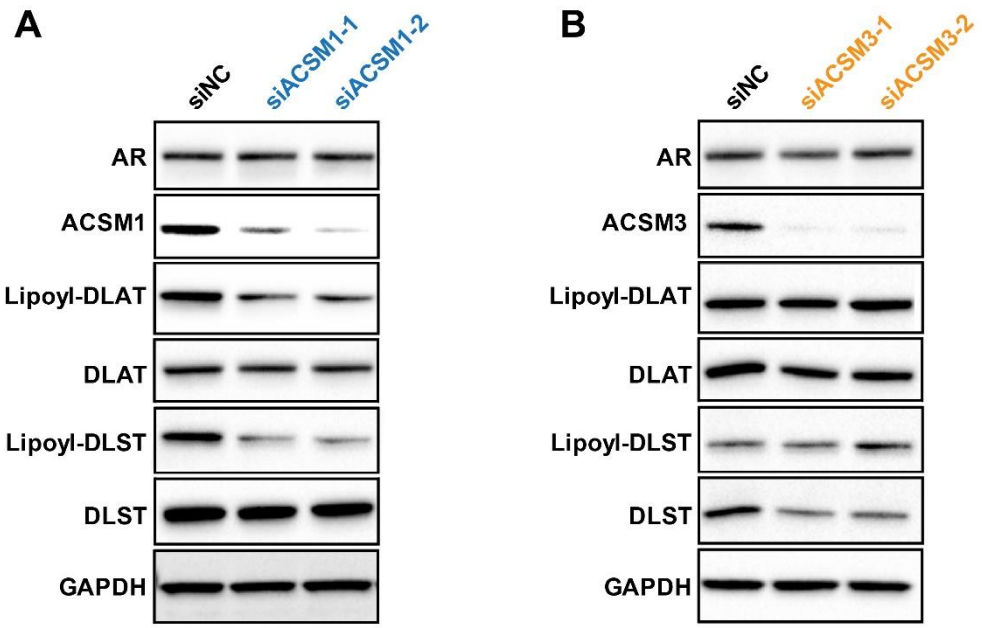

Supplementary Figure S3. Loss of ACSM1 affects protein lipoylation. Lipoylation of the dihydrolipoamide S-acetyltransferase (DLAT) subunit of pyruvate dehydrogenase and the dihydrolipoamide S-succinyltransferase (DLST) subunit of α-ketoglutarate dehydrogenase was assessed by Western blotting in cells treated with siRNAs targeting ACSM1 (A) or ACSM3 (B).

4.10 REFERENCE LIST

Abeshouse, A., Ahn, J., Akbani, R., Ally, A., Amin, S., Andry, C. D., Annala, M., Aprikian, A., Armenia, J., and Arora, A. (2015). The molecular taxonomy of primary prostate cancer. Cell *163*, 1011-1025.

Abida, W., Cyrta, J., Heller, G., Prandi, D., Armenia, J., Coleman, I., Cieslik, M., Benelli, M., Robinson, D., Van Allen, E. M.*, et al.* (2019). Genomic correlates of clinical outcome in advanced prostate cancer. Proc Natl Acad Sci U S A *116*, 11428-11436.

Aggarwal, V., Tuli, H. S., Varol, A., Thakral, F., Yerer, M. B., Sak, K., Varol, M., Jain, A., Khan, M. A., and Sethi, G. (2019). Role of Reactive Oxygen Species in Cancer Progression: Molecular Mechanisms and Recent Advancements. Biomolecules *9*.

Alinezhad, S., Vaananen, R. M., Mattsson, J., Li, Y., Tallgren, T., Tong Ochoa, N., Bjartell, A., Akerfelt, M., Taimen, P., Bostrom, P. J.*, et al.* (2016). Validation of Novel Biomarkers for Prostate Cancer Progression by the Combination of Bioinformatics, Clinical and Functional Studies. PLoS One *11*, e0155901.

Asangani, I. A., Dommeti, V. L., Wang, X., Malik, R., Cieslik, M., Yang, R., Escara-Wilke, J., Wilder-Romans, K., Dhanireddy, S., Engelke, C.*, et al.* (2014). Therapeutic targeting of BET bromodomain proteins in castration-resistant prostate cancer. Nature *510*, 278-282.

Balaban, S., Nassar, Z. D., Zhang, A. Y., Hosseini-Beheshti, E., Centenera, M. M., Schreuder, M., Lin, H. M., Aishah, A., Varney, B., Liu-Fu, F.*, et al.* (2019). Extracellular Fatty Acids Are the Major Contributor to Lipid Synthesis in Prostate Cancer. Mol Cancer Res *17*, 949-962.

Battaglia, V., Salvi, M., and Toninello, A. (2005). Oxidative stress is responsible for mitochondrial permeability transition induction by salicylate in liver mitochondria. J Biol Chem *280*, 33864-33872.

Benjafield, A. V., Iwai, N., Ishikawa, K., Wang, W. Y., and Morris, B. J. (2003). Overweight, but not hypertension, is associated with SAH polymorphisms in Caucasians with essential hypertension. Hypertens Res *26*, 591-595.

Best, S. A., De Souza, D. P., Kersbergen, A., Policheni, A. N., Dayalan, S., Tull, D., Rathi, V., Gray, D. H., Ritchie, M. E., McConville, M. J., and Sutherland, K. D. (2018). Synergy between the KEAP1/NRF2 and PI3K Pathways Drives Non-Small-Cell Lung Cancer with an Altered Immune Microenvironment. Cell Metab *27*, 935-943 e934.

Bishop, J. L., Thaper, D., Vahid, S., Davies, A., Ketola, K., Kuruma, H., Jama, R., Nip, K. M., Angeles, A., Johnson, F.*, et al.* (2017). The Master Neural Transcription Factor BRN2 Is an Androgen Receptor-Suppressed Driver of Neuroendocrine Differentiation in Prostate Cancer. Cancer Discov *7*, 54-71.

Blomme, A., Ford, C. A., Mui, E., Patel, R., Ntala, C., Jamieson, L. E., Planque, M., McGregor, G. H., Peixoto, P., Hervouet, E.*, et al.* (2020). 2,4-dienoyl-CoA reductase regulates lipid homeostasis in treatment-resistant prostate cancer. Nat Commun *11*, 2508.

Butler, L. M., Centenera, M. M., and Swinnen, J. V. (2016). Androgen control of lipid metabolism in prostate cancer: novel insights and future applications. Endocr Relat Cancer *23*, R219-227.

Butler, L. M., Perone, Y., Dehairs, J., Lupien, L. E., de Laat, V., Talebi, A., . . . Swinnen, J. V. (2020). Lipids and cancer: Emerging roles in pathogenesis,

diagnosis and therapeutic intervention. Advanced Drug Delivery Reviews, 159, 245-293.

Cancer Genome Atlas Research, N. (2015). The Molecular Taxonomy of Primary Prostate Cancer. Cell *163*, 1011-1025.

Cao, J. Y., and Dixon, S. J. (2016). Mechanisms of ferroptosis. Cell Mol Life Sci *73*, 2195-2209.

Celis, J. E., Gromov, P., Cabezon, T., Moreira, J. M., Friis, E., Jirstrom, K., Llombart-Bosch, A., Timmermans-Wielenga, V., Rank, F., and Gromova, I. (2008). 15-prostaglandin dehydrogenase expression alone or in combination with ACSM1 defines a subgroup of the apocrine molecular subtype of breast carcinoma. Mol Cell Proteomics *7*, 1795-1809.

Chan, S. C., Selth, L. A., Li, Y., Nyquist, M. D., Miao, L., Bradner, J. E., Raj, G. V., Tilley, W. D., and Dehm, S. M. (2015). Targeting chromatin binding regulation of constitutively active AR variants to overcome prostate cancer resistance to endocrine-based therapies. Nucleic Acids Res *43*, 5880-5897.

Choudhury, K. R., Yagle, K. J., Swanson, P. E., Krohn, K. A., and Rajendran, J. G. (2010). A robust automated measure of average antibody staining in immunohistochemistry images. J Histochem Cytochem *58*, 95-107.

Coleman, R. A., Lewin, T. M., Van Horn, C. G., and Gonzalez-Baro, M. R. (2002). Do long-chain acyl-CoA synthetases regulate fatty acid entry into synthetic versus degradative pathways? J Nutr *132*, 2123-2126.

Coutinho, I., Day, T. K., Tilley, W. D., and Selth, L. A. (2016). Androgen receptor signaling in castration-resistant prostate cancer: a lesson in persistence. Endocr Relat Cancer *23*, T179-T197.

Das, R., Gregory, P. A., Fernandes, R. C., Denis, I., Wang, Q., Townley, S. L., Zhao, S. G., Hanson, A. R., Pickering, M. A., Armstrong, H. K.*, et al.* (2017). MicroRNA-194 Promotes Prostate Cancer Metastasis by Inhibiting SOCS2. Cancer Res *77*, 1021-1034.

Dixon, S. J., Lemberg, K. M., Lamprecht, M. R., Skouta, R., Zaitsev, E. M., Gleason, C. E., Patel, D. N., Bauer, A. J., Cantley, A. M., Yang, W. S.*, et al.* (2012). Ferroptosis: an iron-dependent form of nonapoptotic cell death. Cell *149*, 1060-1072.

El Sayed, S. M., Mahmoud, A. A., El Sawy, S. A., Abdelaal, E. A., Fouad, A. M., Yousif, R. S., Hashim, M. S., Hemdan, S. B., Kadry, Z. M., Abdelmoaty, M. A.*, et al.* (2013). Warburg effect increases steady-state ROS condition in cancer cells through decreasing their antioxidant capacities (anticancer effects of 3-bromopyruvate through antagonizing Warburg effect). Med Hypotheses *81*, 866-870.

Ellis, J. M., Bowman, C. E., and Wolfgang, M. J. (2015). Metabolic and tissue-specific regulation of acyl-CoA metabolism. PLoS One *10*, e0116587.

Flaig, T. W., Salzmann-Sullivan, M., Su, L. J., Zhang, Z., Joshi, M., Gijon, M. A., Kim, J., Arcaroli, J. J., Van Bokhoven, A., Lucia, M. S.*, et al.* (2017). Lipid catabolism inhibition sensitizes prostate cancer cells to antiandrogen blockade. Oncotarget *8*, 56051-56065.

Fujino, T., Kang, M. J., Suzuki, H., Iijima, H., and Yamamoto, T. (1996). Molecular characterization and expression of rat acyl-CoA synthetase 3. J Biol Chem *271*, 16748-16752.

Fujino, T., Takei, Y. A., Sone, H., Ioka, R. X., Kamataki, A., Magoori, K., Takahashi, S., Sakai, J., and Yamamoto, T. T. (2001). Molecular identification and characterization of two medium-chain acyl-CoA synthetases, MACS1 and the Sa gene product. J Biol Chem *276*, 35961-35966.

Gawel, S., Wardas, M., Niedworok, E., and Wardas, P. (2004). [Malondialdehyde (MDA) as a lipid peroxidation marker]. Wiad Lek *57*, 453-455.

Gopal, R., Selvarasu, K., Pandian, P. P., and Ganesan, K. (2017). Integrative transcriptome analysis of liver cancer profiles identifies upstream regulators and clinical significance of ACSM3 gene expression. Cell Oncol (Dordr) *40*, 219-233.

Haketa, A., Soma, M., Nakayama, T., Sato, M., Kosuge, K., Aoi, N., and Matsumoto, K. (2004). Two medium-chain acyl-coenzyme A synthetase genes, SAH and MACS1, are associated with plasma high-density lipoprotein cholesterol levels, but they are not associated with essential hypertension. J Hypertens *22*, 1903-1907.

Hangauer, M. J., Viswanathan, V. S., Ryan, M. J., Bole, D., Eaton, J. K., Matov, A., Galeas, J., Dhruv, H. D., Berens, M. E., Schreiber, S. L.*, et al.* (2017). Drug-tolerant persister cancer cells are vulnerable to GPX4 inhibition. Nature *551*, 247-250.

Heemers, H. V., Schmidt, L. J., Sun, Z., Regan, K. M., Anderson, S. K., Duncan, K., Wang, D., Liu, S., Ballman, K. V., and Tindall, D. J. (2011). Identification of a clinically relevant androgen-dependent gene signature in prostate cancer. Cancer Res *71*, 1978-1988.

Hickey, T. E., Irvine, C. M., Dvinge, H., Tarulli, G. A., Hanson, A. R., Ryan, N. K., Pickering, M. A., Birrell, S. N., Hu, D. G., Mackenzie, P. I.*, et al.* (2015). Expression of androgen receptor splice variants in clinical breast cancers. Oncotarget *6*, 44728-44744.

Holubarsch, C. J., Rohrbach, M., Karrasch, M., Boehm, E., Polonski, L., Ponikowski, P., and Rhein, S. (2007). A double-blind randomized multicentre clinical trial to evaluate the efficacy and safety of two doses of etomoxir in comparison with placebo in patients with moderate congestive heart failure: the ERGO (etomoxir for the recovery of glucose oxidation) study. Clin Sci (Lond) *113*, 205-212.

Iglesias-Gato, D., Thysell, E., Tyanova, S., Crnalic, S., Santos, A., Lima, T. S., . . . Wikström, P. (2018). The Proteome of Prostate Cancer Bone Metastasis Reveals Heterogeneity with Prognostic Implications. *Clin Cancer Res, 24*(21), 5433-5444. doi:10.1158/1078-0432.Ccr-18-1229

Itkonen, H. M., Brown, M., Urbanucci, A., Tredwell, G., Ho Lau, C., Barfeld, S., Hart, C., Guldvik, I. J., Takhar, M., Heemers, H. V.*, et al.* (2017). Lipid degradation promotes prostate cancer cell survival. Oncotarget *8*, 38264-38275.

Iwai, N., Katsuya, T., Mannami, T., Higaki, J., Ogihara, T., Kokame, K., Ogata, J., and Baba, S. (2002). Association between SAH, an acyl-CoA synthetase gene, and hypertriglyceridemia, obesity, and hypertension. Circulation *105*, 41-47.

Kloditz, K., and Fadeel, B. (2019). Three cell deaths and a funeral: macrophage clearance of cells undergoing distinct modes of cell death. Cell Death Discov *5*, 65.

Kochan, G., Pilka, E. S., von Delft, F., Oppermann, U., and Yue, W. W. (2009). Structural snapshots for the conformation-dependent catalysis by human medium-chain acyl-coenzyme A synthetase ACSM2A. J Mol Biol *388*, 997-1008.

Latonen, L., Afyounian, E., Jylhä, A., Nättinen, J., Aapola, U., Annala, M., . . . Visakorpi, T. (2018). Integrative proteomics in prostate cancer uncovers robustness

against genomic and transcriptomic aberrations during disease progression. *Nature Communications, 9*(1), 1176. doi:10.1038/s41467-018-03573-6

Laurent, V., Guerard, A., Mazerolles, C., Le Gonidec, S., Toulet, A., Nieto, L., . . . Muller, C. (2016). Periprostatic adipocytes act as a driving force for prostate cancer progression in obesity. *Nat Commun, 7*, 10230. doi:10.1038/ncomms10230

Li, J., Xu, C., Lee, H. J., Ren, S., Zi, X., Zhang, Z., . . . Sun, Y. (2020). A genomic and epigenomic atlas of prostate cancer in Asian populations. *Nature, 580*(7801), 93-99. doi:10.1038/s41586-020-2135-x

Li, J., Xu, C., Lee, H. J., Ren, S., Zi, X., Zhang, Z., Wang, H., Yu, Y., Yang, C., Gao, X.*, et al.* (2020). A genomic and epigenomic atlas of prostate cancer in Asian populations. Nature *580*, 93-99.

Massie, C. E., Lynch, A., Ramos-Montoya, A., Boren, J., Stark, R., Fazli, L., Warren, A., Scott, H., Madhu, B., Sharma, N.*, et al.* (2011). The androgen receptor fuels prostate cancer by regulating central metabolism and biosynthesis. EMBO J *30*, 2719-2733.

Metsalu, T., and Vilo, J. (2015). ClustVis: a web tool for visualizing clustering of multivariate data using Principal Component Analysis and heatmap. Nucleic Acids Res *43*, W566-570.

Moore, N. L., Buchanan, G., Harris, J. M., Selth, L. A., Bianco-Miotto, T., Hanson, A. R., Birrell, S. N., Butler, L. M., Hickey, T. E., and Tilley, W. D. (2012). An androgen receptor mutation in the MDA-MB-453 cell line model of molecular apocrine breast cancer compromises receptor activity. Endocrine related cancer *19*, 599.

Narita, I., Saito, N., Goto, S., Shirasaki, A., Morioka, Y., Jin, S., Omori, K., Sakatsume, M., Arakawa, M., and Gejyo, F. (2002). Role of genetic polymorphism in the SA gene on the blood pressure and prognosis of renal function in patients with immunoglobulin A nephropathy. Hypertens Res *25*, 831-836.

Nassar, Z. D., Mah, C. Y., Dehairs, J., Burvenich, I. J., Irani, S., Centenera, M. M., Helm, M., Shrestha, R. K., Moldovan, M., Don, A. S.*, et al.* (2020). Human DECR1 is an androgen-repressed survival factor that regulates PUFA oxidation to protect prostate tumor cells from ferroptosis. Elife *9*.

Nelson, P. S., Clegg, N., Arnold, H., Ferguson, C., Bonham, M., White, J., Hood, L., and Lin, B. (2002). The program of androgen-responsive genes in neoplastic prostate epithelium. Proc Natl Acad Sci U S A *99*, 11890-11895.

Nikitina, A. S., Sharova, E. I., Danilenko, S. A., Butusova, T. B., Vasiliev, A. O., Govorov, A. V., . . . Kostryukova, E. S. (2017). Novel RNA biomarkers of prostate cancer revealed by RNA-seq analysis of formalin-fixed samples obtained from Russian patients. *Oncotarget, 8*(20), 32990-33001. doi:10.18632/oncotarget.16518

Paltoglou, S., Das, R., Townley, S. L., Hickey, T. E., Tarulli, G. A., Coutinho, I., Fernandes, R., Hanson, A. R., Denis, I., Carroll, J. S.*, et al.* (2017). Novel Androgen Receptor Coregulator GRHL2 Exerts Both Oncogenic and Antimetastatic Functions in Prostate Cancer. Cancer Res *77*, 3417-3430.

Paredes, F., Sheldon, K., Lassegue, B., Williams, H. C., Faidley, E. A., Benavides, G. A., Torres, G., Sanhueza-Olivares, F., Yeligar, S. M., Griendling, K. K.*, et al.* (2018). Poldip2 is an oxygen-sensitive protein that controls PDH and alphaKGDH lipoylation and activation to support metabolic adaptation in hypoxia and cancer. Proc Natl Acad Sci U S A *115*, 1789-1794.

Peck, B., and Schulze, A. (2019). Lipid Metabolism at the Nexus of Diet and Tumor Microenvironment. Trends Cancer *5*, 693-703.

Piccinini, F., Tesei, A., Arienti, C., and Bevilacqua, A. (2015). Cancer multicellular spheroids: Volume assessment from a single 2D projection. Computer Methods and Programs in Biomedicine *118*, 95-106.

Pomerantz, M. M., Li, F., Takeda, D. Y., Lenci, R., Chonkar, A., Chabot, M., Cejas, P., Vazquez, F., Cook, J., Shivdasani, R. A.*, et al.* (2015). The androgen receptor cistrome is extensively reprogrammed in human prostate tumorigenesis. Nat Genet *47*, 1346-1351.

Rajan, P., Sudbery, I. M., Villasevil, M. E., Mui, E., Fleming, J., Davis, M., Ahmad, I., Edwards, J., Sansom, O. J., Sims, D.*, et al.* (2014). Next-generation sequencing of advanced prostate cancer treated with androgen-deprivation therapy. Eur Urol *66*, 32-39.

Ruan, H. Y., Yang, C., Tao, X. M., He, J., Wang, T., Wang, H., Wang, C., Jin, G. Z., Jin, H. J., and Qin, W. X. (2017). Downregulation of ACSM3 promotes metastasis and predicts poor prognosis in hepatocellular carcinoma. Am J Cancer Res *7*, 543-553.

Schlaepfer, I. R., Glode, L. M., Hitz, C. A., Pac, C. T., Boyle, K. E., Maroni, P., Deep, G., Agarwal, R., Lucia, S. M., Cramer, S. D.*, et al.* (2015). Inhibition of Lipid Oxidation Increases Glucose Metabolism and Enhances 2-Deoxy-2-[(18)F]Fluoro-D-Glucose Uptake in Prostate Cancer Mouse Xenografts. Mol Imaging Biol *17*, 529-538.

Schlaepfer, I. R., Rider, L., Rodrigues, L. U., Gijon, M. A., Pac, C. T., Romero, L., Cimic, A., Sirintrapun, S. J., Glode, L. M., Eckel, R. H., and Cramer, S. D. (2014).

Lipid catabolism via CPT1 as a therapeutic target for prostate cancer. Mol Cancer Ther *13*, 2361-2371.

Soupene, E., and Kuypers, F. A. (2008). Mammalian long-chain acyl-CoA synthetases. Exp Biol Med (Maywood) *233*, 507-521.

Stockwell, B. R., and Jiang, X. (2020). The Chemistry and Biology of Ferroptosis. Cell Chem Biol *27*, 365-375.

Swinnen, J. V., Esquenet, M., Goossens, K., Heyns, W., and Verhoeven, G. (1997). Androgens stimulate fatty acid synthase in the human prostate cancer cell line LNCaP. Cancer Res *57*, 1086-1090.

Taylor, B. S., Schultz, N., Hieronymus, H., Gopalan, A., Xiao, Y., Carver, B. S., Arora, V. K., Kaushik, P., Cerami, E., Reva, B.*, et al.* (2010). Integrative genomic profiling of human prostate cancer. Cancer Cell *18*, 11-22.

Thorvaldsdóttir, H., Robinson, J. T., and Mesirov, J. P. (2013). Integrative Genomics Viewer (IGV): high-performance genomics data visualization and exploration. Briefings in bioinformatics *14*, 178-192.

Tousignant, K. D., Rockstroh, A., Poad, B. L. J., Talebi, A., Young, R. S. E., Taherian Fard, A., Gupta, R., Zang, T., Wang, C., Lehman, M. L.*, et al.* (2020). Therapy-induced lipid uptake and remodeling underpin ferroptosis hypersensitivity in prostate cancer. Cancer Metab *8*, 11.

van der Sluis, R. (2018). Analyses of the genetic diversity and protein expression variation of the acyl: CoA medium-chain ligases, ACSM2A and ACSM2B. Mol Genet Genomics *293*, 1279-1292.

van der Sluis, R., and Erasmus, E. (2016). Xenobiotic/medium chain fatty acid: CoA ligase - a critical review on its role in fatty acid metabolism and the detoxification of benzoic acid and aspirin. Expert Opin Drug Metab Toxicol *12*, 1169-1179.

Vessey, D. A., Kelley, M., and Warren, R. S. (1999). Characterization of the CoA ligases of human liver mitochondria catalyzing the activation of short- and medium-chain fatty acids and xenobiotic carboxylic acids. Biochim Biophys Acta *1428*, 455-462.

Viswanathan, V. S., Ryan, M. J., Dhruv, H. D., Gill, S., Eichhoff, O. M., Seashore-Ludlow, B., Kaffenberger, S. D., Eaton, J. K., Shimada, K., Aguirre, A. J.*, et al.* (2017). Dependency of a therapy-resistant state of cancer cells on a lipid peroxidase pathway. Nature *547*, 453-457.

Wang, Q., Armenia, J., Zhang, C., Penson, A. V., Reznik, E., Zhang, L., Minet, T., Ochoa, A., Gross, B. E., Iacobuzio-Donahue, C. A.*, et al.* (2018). Unifying cancer and normal RNA sequencing data from different sources. Sci Data *5*, 180061.

Wang, Q., Li, W., Liu, X. S., Carroll, J. S., Janne, O. A., Keeton, E. K., Chinnaiyan, A. M., Pienta, K. J., and Brown, M. (2007). A hierarchical network of transcription factors governs androgen receptor-dependent prostate cancer growth. Mol Cell *27*, 380-392.

Watkins, P. A. (1997). Fatty acid activation. Prog Lipid Res *36*, 55-83.

Watt, M. J., Clark, A. K., Selth, L. A., Haynes, V. R., Lister, N., Rebello, R., Porter, L. H., Niranjan, B., Whitby, S. T., Lo, J.*, et al.* (2019). Suppressing fatty acid uptake has therapeutic effects in preclinical models of prostate cancer. Sci Transl Med *11*.

Zadra, G., and Loda, M. (2018). Metabolic Vulnerabilities of Prostate Cancer: Diagnostic and Therapeutic Opportunities. Cold Spring Harb Perspect Med *8*.

Zadra, G., Ribeiro, C. F., Chetta, P., Ho, Y., Cacciatore, S., Gao, X., Syamala, S., Bango, C., Photopoulos, C., Huang, Y*., et al.* (2019). Inhibition of de novo lipogenesis targets androgen receptor signaling in castration-resistant prostate cancer. Proc Natl Acad Sci U S A *116*, 631-640.

CHAPTER 5: INTERPLAY BETWEEN AR AND SREBP-1 TO REGULATE LIPIDOME IN PROSTATE CANCER

5 Interplay between AR and SREBP-1 to regulate lipidome in prostate cancer

5.1 Introduction

Sterol regulatory element binding proteins (SREBPs) are a family of membrane-bound transcription factors that play a critical role in the regulation of cellular lipid homeostasis (Bertolio et al., 2019; M. S. Brown & Goldstein, 1997; Butler et al., 2016; Horton, Goldstein, & Brown, 2002; J. V. Swinnen et al., 1997). SREBPs were discovered in the 1990s during investigations of the upstream regulators of 3-hydroxy-3-methylglutaryl coenzyme A reductase (HMGCR) and low-density lipoprotein receptor (LDLR) (Michael R Briggs, Yokoyama, Wang, Brown, & Goldstein, 1993; X Hua et al., 1993; X. Wang, Sato, Brown, Hua, & Goldstein, 1994; Yokoyama et al., 1993). HMGCR is the rate limiting enzyme in cholesterol synthesis (Goldstein & Brown, 1990) while LDLR regulates uptake of cholesterol via receptor mediated endocytosis in the cells (Go & Mani, 2012). Both of these genes are transcriptionally regulated by SREBPs (M. S. Brown & Goldstein, 1997; Goldstein, DeBose-Boyd, & Brown, 2006). Since those early seminal studies, SREBPs have been shown to directly activate the expression of more than 30 genes involved in the synthesis and uptake of lipids (fatty acids, cholesterol, triglycerides, and phospholipids), as well as the cofactors required to synthesize these molecules (Bertolio et al., 2019; Butler et al., 2016; Edwards, Tabor, Kast, & Venkateswaran, 2000; Horton et al., 2002; Morton & Shimomura, 1999; Sakakura et al., 2001).

5.1.1 SREBP gene and protein structure

SREBPs are members of the basic helix–loop–helix–leucine zipper (bHLH-Zip) transcription factor family, which are produced as inactive precursors anchored to the endoplasmic reticulum (ER) (M. S. Brown & Goldstein, 1997; Michael S. Brown & Goldstein, 1998). SREBPs share a similar protein structure composed of four domains with two membrane–spanning regions (Figure 5.1): 1) an amino terminal transactivation domain of ~480 amino acids, rich in serine and proline, and the bHLH-Zip region for DNA binding and dimerization; 2) a middle hydrophobic region of ~80 amino acids containing two hydrophobic transmembrane helices separated by a short loop of approximately 30 amino acids that projects into the lumen of the endoplasmic reticulum (ER) and nuclear envelope; and 3) a COOH-terminal regulatory domain of ~590 amino acids plays a role in sterol-mediated regulation of SREBP cleavage. Both amino- and carboxy-terminal portions of the proteins project into the cytoplasm (X. Hua, Sakai, Brown, & Goldstein, 1996; Xianxin Hua, Sakai, Y. K., Goldstein, & Brown, 1995).

SREBP-1a has 24 amino acids longer amino terminus that SREBP-1c (Eberlé, Hegarty, Bossard, Ferré, & Foufelle, 2004). SREBP-2 is encoded by S*REBF-2* located on human chromosome 22q13 (Amemiya-Kudo et al., 2002; X Hua et al., 1993; Miserez, Cao, Probst, & Hobbs, 1997). *In vivo* studies using knockout and transgenic mice suggest that SREBP-1c is mainly involved in fatty acid synthesis and insulin-induced glucose metabolism, whereas SREBP-2 is more specific to cholesterol synthesis (Eberlé et al., 2004). SREBP-1c is the predominant isoform in all the tissues and mainly regulates the fatty acid synthesis while SREBP-1a is able to regulated cholesterol and fatty acid synthesis and cholesterol uptake and expressed in specific tissues and cells like heart, macrophage, bone marrow

and intestinal epithelial (Eberlé et al., 2004). However, due to the high structural resemblance between the N-terminal domains of three SREBP isoforms, all the isoforms can activate each of their target genes but with different efficacies.

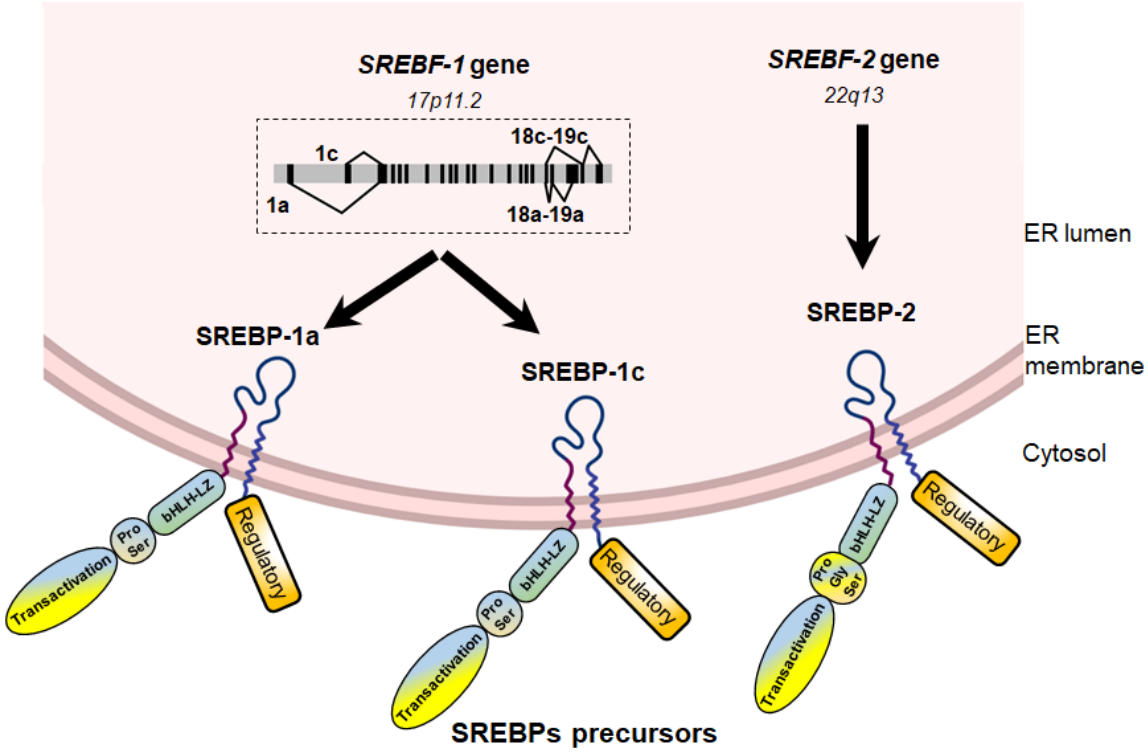

Figure 5.1: SREBP genes and structure. Adopted from(Eberlé et al., 2004)

5.1.2 A proteolytic cascade for the activation of SREBPs

SREBPs are synthesized as inactive precursors of about 1150 amino acids in length, anchored in the endoplasmic reticular membrane, and are activated following cleavage by a sterol-dependent proteolytic process (Michael S. Brown, Ye, Rawson, & Goldstein, 2000). In conditions of high levels of sterol, the C-terminal domain of SREBP binds to SCAP in the ER membrane. This complex is stabilized by INSIG insulin-induced gene-1 protein (INSIG1) and INSIG2. In response to low levels of sterol, INSIGs are post transcriptionally modified (ubiquitylated) by E3 ligases and degraded rapidly, resulting in the loss of interaction between SCAP and

INSIG. This dissociation results in the translocation of the SCAP–SREBP complex from ER to the Golgi (L. P. Sun, Li, Goldstein, & Brown, 2005), where it undergoes sequential cleavage (Edwards et al., 2000; X. Hua et al., 1996; Sakai et al., 1996; X. Wang et al., 1994) by two membrane-bound proteases, site1 proteases (S1P) and site 2 proteases (S2P). Following cleavage, the mature transcriptionally active water soluble N-terminal domain of SREBP is released (Edwards et al., 2000; Ye, Davé, Grishin, Goldstein, & Brown, 2000) and translocated to the nucleus mediated through importin-β (Lee et al., 2003), where it binds to specific DNA sequences called sterol-response elements (SREs) to regulate the transcription of enzymes dedicated to *de novo* lipogenesis (Y. Li et al., 2011).

Brown & Goldstein revealed that the activation and translocation of SREBP-SCAP is regulated by sterol mediated negative feedback loop (Figure 5.2) (M. S. Brown & Goldstein, 1997; X. Cheng, Li, & Guo, 2018). Cholesterol or oxysterol (e.g. 25-hydroxycholesterol) can bind to SCAP or INSIGs to strengthen their association, thereby retaining SREBPs in the ER (L. P. Sun et al., 2005). Low sterol levels promote dissociation of SCAP from INSIGs, leading to proteolytic cleavage and activation of SREBPs. This activation of SREBPs promotes the expression of lipogenic genes and INSIGs, which restores cholesterol and INSIG1 protein and results in stabilization of SREBP/SCAP/INSG and hence retention of SREBPs in the ER (Soyal, Nofziger, Dossena, Paulmichl, & Patsch, 2015).

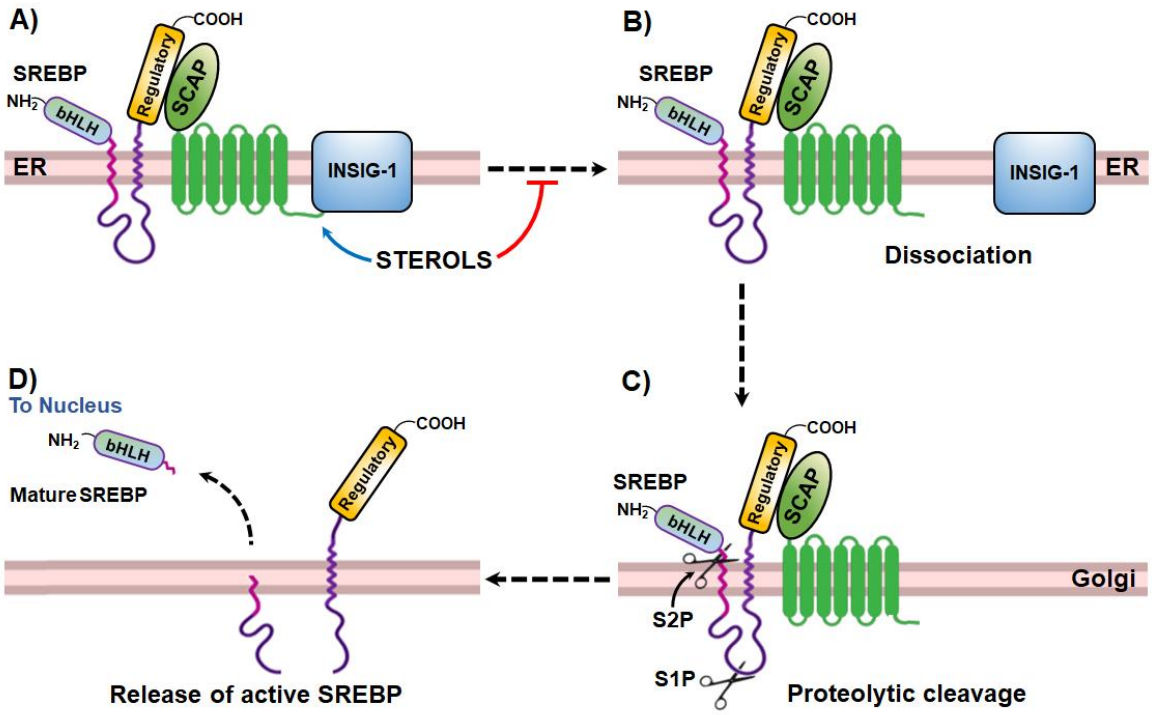

Figure 5.2: Schematic of activation of SREBP. A) SREBPs are synthesized as inactive precursors anchored to the endoplasmic reticulum (ER). SREBP-SCAP complex is stabilized by INSIG complex and retain them in ER in sterol overloaded condition B) in low sterol condition, INSIG-1 dissociates from SREBP-SCAP complex and SCAP facilitates translocation of SREBP to the Golgi body, C) SREBP is activated via a two-step proteolytic mechanism with S1P and S2P. D) Releases NH_2 terminal region of SREBPs (mature/active SREBP) which are transported to the nucleus and activates transcription of the target genes.

Abbreviations: bHLH, basic-helix-loop-helix-leucine zipper domain of SREBP; ER, Endoplasmic reticulum; INSIG, insulin induced gene; S1P, site-1 protease; S2P, site-2 protease

5.1.3 DNA binding sites of SREBPs

Nuclear SREBPs activate their target genes by binding to a key regulatory element in the promoter region known as a sterol-response element (SRE). An SRE is typically defined as a 10bp element in the gene promoter represented by 5'-nTCACnCCA Cn-3' (Edwards et al., 2000). The original canonical SRE in the LDLR promoter is 5′-ATCACCCCAC-3′ (X Hua et al., 1993). Beside these sequences, SREBP-1a and -1c also bind to E-boxes (CAXXTG sequence) (Figure 5.3) (J. B. Kim et al., 1995) (Shimano, 2001). The SRE motif is highly variable and recent studies suggest that this is because SREBP acts co-ordinately with other transcription factors to regulate its target genes (Weber, Boll, & Stampfl, 2004). cAMP response element binding protein (CREB), Sp1 and nuclear factor (NF)-Y are some of the transcription factors known to co-activate SREs (Dooley, Bennett, & Osborne, 1999; Dooley, Millinder, & Osborne, 1998; Jackson, Ericsson, & Edwards, 1997; Magaña, Koo, Towle, & Osborne, 2000; Sanchez, Yieh, & Osborne, 1995) whereas vitamin D receptor interacting protein (DRIC) or TATA box-binding protein (TBP)-associated factors (Näär et al., 1999), activated recruited cofactor (ARC)(Näär et al., 1999) CREB binding protein (Ericsson & Edwards, 1998; Oliner, Andresen, Hansen, Zhou, & Tjian, 1996) are some of the cofactors required for the initiation of transcription.

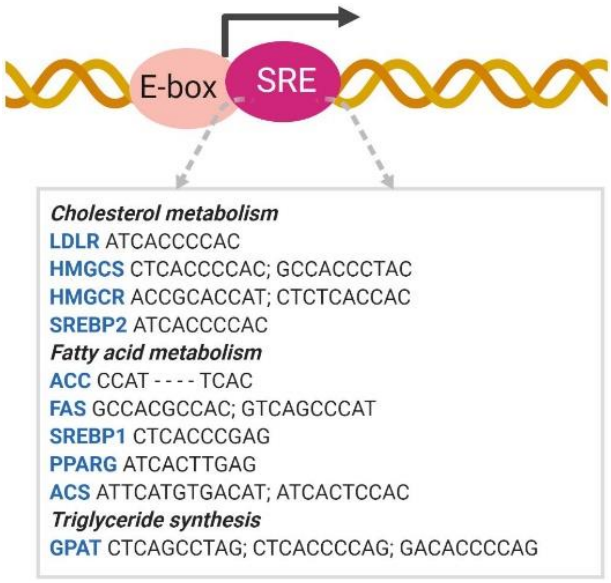

Figure 5.3: SREBP binds to the SRE promoter. SREBP binding to the SRE promoter activates the transcription of target genes involved in lipid metabolism. Adopted from (Dorotea, Koya, & Ha, 2020, Shimano, 2001) (Dorotea et al., 2020; Shimano, 2001)

Abbreviation: ACC, acetyl-CoA carboxylase; ACS, acetyl-CoA synthetase; PPAR, peroxisome proliferator-activated receptor; GPAT, glycerol-3-phosphate acyltransferase ; HMGCS, HMG-CoA synthase

5.2 Targeting SREBPs in cancer

Lipids are critical structural components of all membranes and extensively distributed in cellular organelles (Holthuis & Menon, 2014; Maxfield, 2002; Mukherjee & Maxfield, 2004; Pomorski, Hrafnsdóttir, Devaux, & van Meer, 2001; van Meer, 2010; van Meer, Voelker, & Feigenson, 2008). Rapidly proliferating cancer cells require large amounts of energy and macromolecules (lipids) as building blocks for new membrane synthesis and active signalling in the developing tumour cells. To satisfy the increasing demands, transcription of lipid metabolic

genes and their products (i.e. enzymes, transporters) are upregulated in human cancers (Ray & Roy, 2018). Multiple studies support dysregulated lipid metabolism, including elevated *de novo* lipid biosynthesis and uptake, as a key contributor to tumour progression (C. Cheng, Geng, Cheng, & Guo, 2018). SREBP-1 appears to be a key player in this malignant process, with roles in progression of PCa (Ettinger et al., 2004), breast cancer (Bao et al., 2016; Zhu et al., 2016), glioblastoma (D. Guo et al., 2011; Wen & Reardon, 2016), endometrial tumour (W. Li et al., 2012), hepatocellular carcinoma (C. Li et al., 2014), ovarian carcinoma (Nie et al., 2013) and pancreatic cancer (Y. Sun et al., 2015).

The relevance of SREBPs in cancer has led to the development of strategies to target these factors as a novel therapy. Genetic and pharmacological inhibition of SREBP have demonstrated significant suppression of tumour growth and induction cell death in different types of human cancer (Geng et al., 2016; Gholkar et al., 2016; D. Guo et al., 2009; Hawkins et al., 2008; W. Jiang et al., 2015; Kamisuki et al., 2009; Król, Kiełbus, Rivero-Müller, & Stepulak, 2015; N. Li et al., 2017; X. Li, Chen, Hu, & Huang, 2014; X. Li, Wu, Chung, & Huang, 2015; Miyata, Inoue, Shimizu, & Sato, 2015; Monteiro et al., 2008; Shao, Machamer, & Espenshade, 2016; Soica et al., 2012; von Roemeling et al., 2013; Williams et al., 2013). Like many transcription factors, directly inhibiting SREBPs with small molecules is challenging. As an alternative approach, the field has developed drugs that inhibit its translocation from the ER to the Golgi, such as fatostatin, botulin/betulin and PF-429242 (Hawkins et al., 2008; Król et al., 2015; Shao et al., 2016; Soica et al., 2012). These small molecules interfere with the maturation of SREBPs. Fatostatin is a diarylthiazole compounds that directly binds SCAP and its

blocks Golgi-specific glycosylation, which inhibits ER-to-Golgi transport of SCAP and subsequent SREBP activation (Choi, Kawazoe, Murakami, Misawa, & Uesugi, 2003; Kamisuki et al., 2009). Similarly, the small molecules botulin and betulin also inhibit maturation of SREBP-1 by inducing interaction of SCAP and INSIGs to suppress SCAP/SREBP translocation (Petersen et al., 2002) (Tang et al., 2011), whereas PF-429242 is a reversible competitive aminopyrrolidineamide inhibitor of S1P that also inhibits SREBP processing (Hawkins et al., 2008). Many inhibitors of SREBP-1 have been shown to have anticancer effects. In PCa cells, the inhibitors block cell proliferation, invasion and migration as well as inducing apoptotic cell death (Forestier-Román et al., 2019; X. Li et al., 2014; Nambiar, Deep, Singh, Agarwal, & Agarwal, 2014), and this is linked to decreased cholesterol and fatty acid synthesis (X. Li et al., 2014; Nambiar et al., 2014).

5.3 Interplay between AR and SREBP-1 to regulate lipid metabolism in PCa

There appears to be a positive feedback loop between AR and SREBPs. Androgen directly upregulates SCAP, which results in accumulation of mature SREBPs in the nucleus (H. Heemers et al., 2001). In line with this result, androgen deprivation markedly decreases mature SREBP1 (nSREBP1) in the mouse prostate whereas readministration of testosterone completely restored nSREBP1 protein levels (H. Heemers et al., 2003). Conversely, the expression of AR is itself directly regulated by SREBP1 via its binding at the 5' flanking promotor region of the *AR* gene (Huang, Zhau, & Chung, 2010). This reveals a positive feedback loop for expression of AR and SREBP-1 and hence lipogenic enzymes.

While it is clear that AR and SREBP-1 regulate each other, their ability to cooperate in the transcription of lipid metabolic genes is poorly understood. We hypothesise that this interplay is critical to PCa progression and thus requires further investigation.

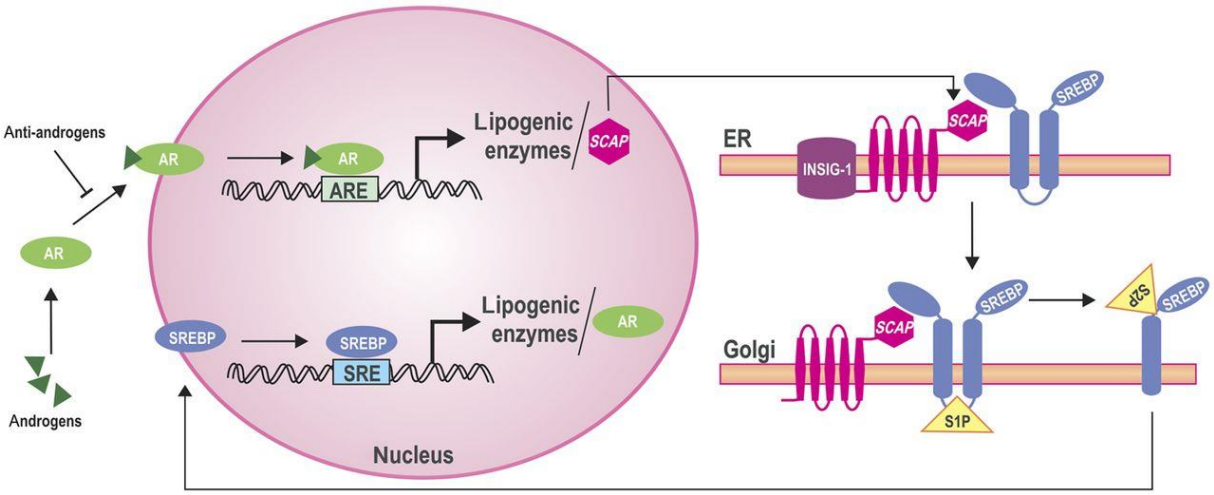

Figure 5.4: Feedback loop between AR and SREBP to regulate lipid metabolism (Butler et al., 2016)

The specific aim of this chapter is to determine whether and how the transcription factor SREBP-1 cooperates with AR to regulate genes involved in lipid metabolism**.**

5.4 METHODS

5.4.1 Western blotting:

Protein extraction and western blotting was done as described in Chapter 2. Antibodies used in this study were AR (Abcam, Ab108341, 1:1000), GAPDH (Millipore, MAB374, 1:1000), α-Tubulin (Millipore, 05-829, 1:2000), SREBP-1 (Santa Cruz, H160, sc8984, 1:1000), SREBP-1 (Santa Cruz, 2A4, sc13551, 1:1000), SREBP-1 (Santa Cruz, E4, sc17755, 1:1000), Secondary antibodies biotinylated: anti-mouse (DAKO, E0433, 1:2000) and anti-rabbit (DAKO, E0432, 1:1000). The imaged protein band on a BioRad Chemidoc MP imaging system were processed using Image Lab Software. Densitometry analysis of the protein expression was normalized with loading control and compared.

5.4.2 Prostate cancer cellular fractionation

LNCaP cells were plated in 15 cm plates with the initial seeding density of $4x10^6$ cells per plate in cell-line in the RPMI medium containing 10% charcoal stripping of foetal calf serum (CSS) for 72 hrs. On the day of androgen treatment, fresh media was prepared and DHT (or vehicle (ethanol)) was added to a final concentration of 10nM. Cells were washed with PBS and collected using trypsin and an equal number of cells was collected from each sample. One half of the cells was resuspended in 100 µL lysis buffer 1 (LB1: 50 mM Hepes-KOH pH7.5,140 mM NaCl, 1 mM EDTA, 10% Glycerol, 0.5% NP-40. 0.25% TX-100) containing protease inhibitor cocktail (Sigma) and kept for whole cell lysate. The other half of each sample was processed through a series of lysis/centrifugation steps to separate cytoplasmic and nuclear fractions. First, cells were resuspended in 100 µL of LB1 containing protease inhibitor cocktail (Sigma) and centrifuged at 9300 rcf for 10sec. The supernatant from this step was kept as the cytoplasmic fraction. Remaining

pellets were washed in 1 mL of LB2 (10 mM Tris-HCl pH 8.0, 200 mM NaCl, 1 mM EDTA, 0.5 mM EGTA) containing protease inhibitor cocktail (Sigma), centrifuged and resulting supernatant was discarded. The nuclear pellets were resuspended in 100 µL LB3 (10mM Tris-HCl pH8.0, 100mM NaCl, 1mM EDTA, 0.5mM EGTA, 0.1% Na-Deoxycholate, 0.5% N-lauroylsarcosine) containing protease inhibitor cocktail (Sigma Aldrich). Both nuclear and whole cell fractions were sonicated on high (Diagenode Life Research Bioruptor Millenium 3 XD10) 10 times for 30 s with 1 minute rest on ice between sets to extract nuclear proteins. Samples were centrifuged at 15700 rcf for 10 minutes and protein supernatant was collected then frozen for later analysis by 4-15% criterion gel and Western blotting.

Total protein concentration of cell lysates was determined using Pierce BCA Protein Assay, Thermo Fisher Scientific, Inc. and equal amount of cytoplasmic and nuclear fragment were subjected to SDS-PAGE (4-12%), followed by transfer into cellulose acetate paper.

5.4.3 Quantitative polymerase chain reaction (RT-qPCR)

RNA extraction and RT-qPCR was done as described in Chapter 2.

Table 5.2. mRNA primers used this chapter

Primer	Sequence	Use
AR_exon1_2_F	CCACTTGTGTCAAAAGCGAAAT	qRT-PCR
AR_exon1_2_R	ATAGTCAATGGGCAAAACATGG	qRT-PCR
FASN_mRNA_F	TCTCCGACTCTGGCAGCTT	qRT-PCR
FASN_mRNA_R	GCTCCAGCCTCGCTCTC	qRT-PCR
GADPH_R	GGCATGGACTGTGGTCATGAG	qRT-PCR
GAPDH_F	TGCACCACCAACTGCTTAGC	qRT-PCR
HMGCR_mRNA_F	GACGTGAACCTATGCTGGTCAG	qRT-PCR
HMGCR_mRNA_R	GGTATCTGTTTCAGCCACTAAGG	qRT-PCR
HMGCS1_mRNA_F	AAGTCACACAAGATGCTACACCG	qRT-PCR
HMGCS1_mRNA_R	TCAGCGAAGACATCTGGTGCCA	qRT-PCR
KLK3_F	CAGAGGAGTTCTTGACCCCAA	qRT-PCR
KLK3_R	ACAGCATGAACTTGGTCACCTT	qRT-PCR
LDLR_mRNA_F	GAATCTACTGGTCTGACCTGTCC	qRT-PCR
LDLR_mRNA_R	GGTCCAGTAGATGTTGCTGTGG	qRT-PCR
SCD_mRNA_F	CCTGGTTTCACTTGGAGCTGTG	qRT-PCR
SCD_mRNA_R	TGTGGTGAAGTTGATGTGCCAGC	qRT-PCR
SREBF-1_mRNA_F	GAGCTCAAGGATCTGGTGGT	qRT-PCR
SREBF-1_mRNA_R	AGTGCGCAGACTTAGGTTCT	qRT-PCR

Table 5.3. ChIP Primers used in this chapter

Primer	Sequence	Use
HMGCR_ChIP_F	CTCTCCCGCGCTAGTAACTG	ChIP PCR
HMGCR_ChIP_R	ACTAGGGCCTGCCTATTGGT	ChIP PCR
HMGCS1_ChIP_F	TAGTCAAGGACACCGCCTCT	ChIP PCR
HMGCS1_ChIP_R	TATAAAGCTGGTGGCGAAGG	ChIP PCR
HMGCS1_ChIP_F(1)	AGAGGCGGGGACAAAGTCT	ChIP PCR
HMGCS1_ChIP_R (1)	CCCGCATCTCCTCTCACTTA	ChIP PCR
KLK3_ChIP(Prom)_F	GCCTGGATCTGAGAGAGATATCATC	ChIP PCR
KLK3_ChIP(Prom)_R	ACACCTTTTTTTTTCTGGATTGTTG	ChIP PCR
LDLR_P1_ChIP_F	ATGCGTTTCCAATTTTGAGG	ChIP PCR
LDLR_P1_ChIP_R	ACCTCACTGCAAGAGGAGGA	ChIP PCR
LDLR_P2_ChIP_F	CCGGGACCCTCTCTTCTAAC	ChIP PCR
LDLR_P2_ChIP_R	GACTGCACCCAACTCAGGAT	ChIP PCR
LDLR_PCa_ChIP_F	CGATGTCACATCGGCCGTTCG	ChIP PCR
LDLR_PCa_ChIP_R	CACGACCTGCTGTGTCCTAGCT	ChIP PCR
NC2_F	GTGAGTGCCCAGTTAGAGCATCTA	ChIP PCR
NC2_R	GGAACCAGTGGGTCTTGAAGTG	ChIP PCR
SCD_ChIP_F	TGGAAGAGAAGCTGAGAAGG	ChIP PCR
SCD_ChIP_R	TTCTGTAAACTCCGGCTCGT	ChIP PCR

5.4.4 Proximity-ligation assay– Fluorescence Detection

Proximity-Ligation Assay (PLA) was performed following the manufacturer`s instructions (Olink Bioscience). In brief, LNCaP cells (~200,000) were seeded in sterile coverslips placed in 6 well plates with 2 mL of media. After 48 hrs, cells were treated with DHT for 16 hrs. Cells were then fixed with paraformaldehyde and permeabilized using 0.1% TritonX at room temperature. The cells were stained with anti-AR (Abcam, ER179, 1:400) and anti-SREBP-1 (Santa Cruz Biotechnology, sc2A4, 1:400). PLA was performed using Duolink® In Situ PLA Probe Anti-Mouse PLUS and Duolink® In Situ PLA® Probe Anti-Rabbit MINUS following the manufacturer`s instructions (Sigma, 92001 and 92005). Imaging was performed using an Olympus FV3000 Confocal Microscope (FLUOVIEW FV3000 series) and analyzed by ImageJ software. Signal from 300 cells were analyzed per experiment.

5.4.5 Computational analyses

5.4.5.1 Gene set enrichment Analysis (GSEA)

GSEA was performed using GSEA preranked module on GenePattern (https://cloud.genepattern.org/gp/pages/index.jsf). Ranked lists were generated from RNA-Seq counts using the signal-to noise metric. Genesets were obtained from MSigDB or from specific published studies.

5.4.5.2 Single Sample Gene Set Enrichment Analysis (ssGSEA)

ssGSEA was performed using ssGSEA Projection module on GenePattern (https://cloud.genepattern.org/gp/pages/index.jsf). GCT files were generated from

relevant microarray or RNA-seq data. Genesets were obtained from (Sowalsky et al., 2018) (AR gene signature) and Chen et al., 2018 (SREBP-1 gene signature).

5.4.5.3 Cistrome analysis:

GREAT (McLean et al., 2010) (http://great.stanford.edu/public/html/) was used to map AR/SREBP-1 binding sites to nearby genes and perform downstream pathway analysis.

5.5 RESULTS

5.5.1 SREBP-1 expression is variable in PCa cell lines

To identify appropriate model systems to investigate SREBP-1 function in PCa, we evaluated the expression of both precursor/full length and mature/nuclear SREBP-1 in a panel of prostate cancer cell lines by Western blotting (Figure 5.5). Full-length SREBP-1 expression was highest in LNCaP cells and its derivative cell lines (C4-2B, MR42D, MR49F, and V16D) and lowest in AR negative cell lines (PC3 and DU145). Most studies in the past have used a polyclonal anti-rabbit antibody sc-8986 (H160) to detect SREBP-1, but this was no longer available. Therefore, we tested available monoclonal anti-mouse antibodies for the detection of SREBP-1 protein. Monoclonal mouse antibodies were less specific for detection of nuclear/mature SREBP-1 compared to alternative polyclonal rabbit antibodies [sc-17755 (E4) and sc-13551 (2A4)]. All 3 antibodies showed a similar result for detection of full-length SREBP-1. The ratio of mature:full-length SREBP-1 levels (detected by H160 antibody) was relatively similar in all cell lines except for the CWR1-AD1 and CWR1-D567 models, which had much higher levels of mature protein (Figure 5.5B).

A feedback loop between AR and SREBP-1 has already been reported in LNCaP and this model is the most widely used for studying androgen-regulated PCa metabolism. For feasibility, we therefore proceeded with this model for a series of further experiments. Immunofluorescence staining was used to determine the subcellular localization of SREBP-1, demonstrating that it localises to both the cytoplasm and nucleus (Figure 5.6).

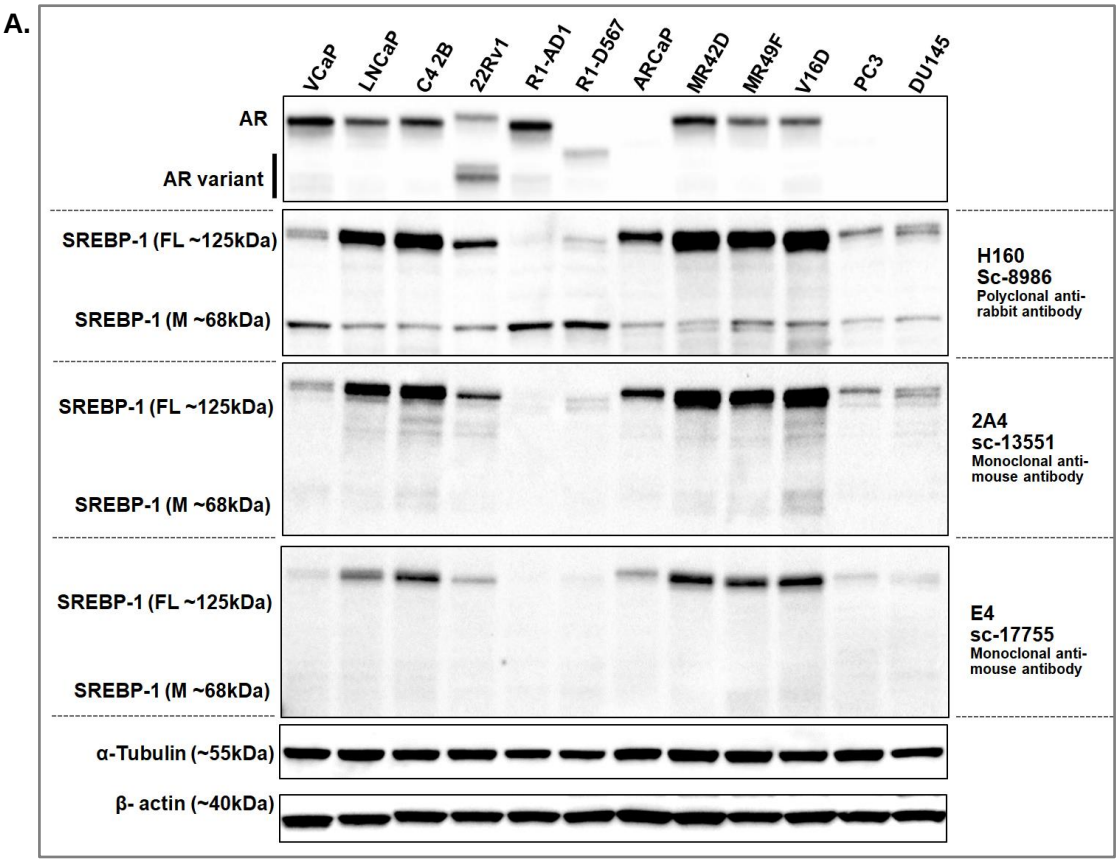
A.
VCaP
LNCaP
C4-2B
22Rv1
R1-AD1
R1-D567
ARCaP
MR42D
MR49F
V16D
PC3
DU145
AR
AR variant
SREBP-1 (FL ~125kDa)
SREBP-1 (M ~68kDa)
H160
Sc-8986
Polyclonal anti-rabbit antibody
SREBP-1 (FL ~125kDa)
SREBP-1 (M ~68kDa)
2A4
sc-13551
Monoclonal anti-mouse antibody
SREBP-1 (FL ~125kDa)
SREBP-1 (M ~68kDa)
E4
sc-17755
Monoclonal anti-mouse antibody
α-Tubulin (~55kDa)
β- actin (~40kDa)

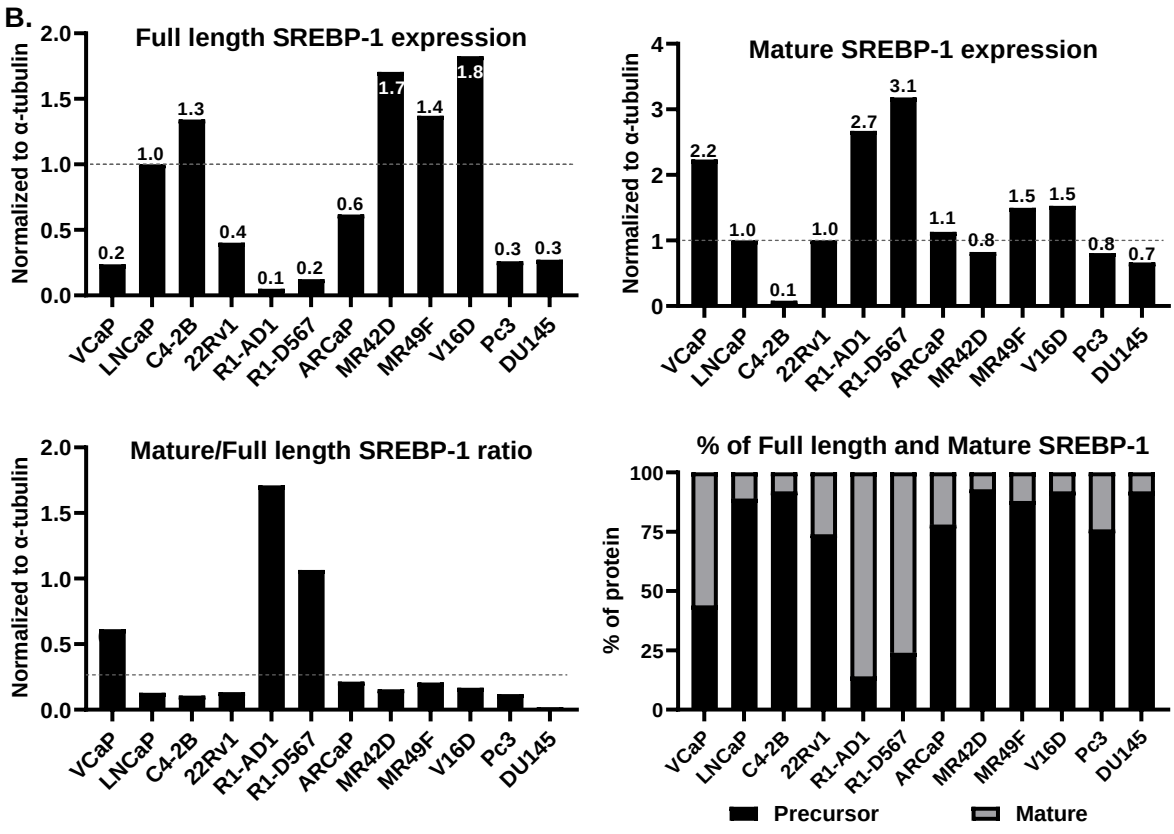
B.
Full length SREBP-1 expression
Normalized to α-tubulin
2.0
1.5
1.0
0.5
0.0
0.2
1.0
1.3
0.4
0.1
0.2
0.6
1.7
1.4
1.8
0.3
0.3
VCaP
LNCaP
C4-2B
22Rv1
R1-AD1
R1-D567
ARCaP
MR42D
MR49F
V16D
Pc3
DU145
Mature SREBP-1 expression
Normalized to α-tubulin
4
3
2
1
0
2.2
1.0
0.1
1.0
2.7
3.1
1.1
0.8
1.5
1.5
0.8
0.7
VCaP
LNCaP
C4-2B
22Rv1
R1-AD1
R1-D567
ARCaP
MR42D
MR49F
V16D
Pc3
DU145
Mature/Full length SREBP-1 ratio
Normalized to α-tubulin
2.0
1.5
1.0
0.5
0.0
VCaP
LNCaP
C4-2B
22Rv1
R1-AD1
R1-D567
ARCaP
MR42D
MR49F
V16D
Pc3
DU145
% of Full length and Mature SREBP-1
% of protein
100
75
50
25
0
VCaP
LNCaP
C4-2B
22Rv1
R1-AD1
R1-D567
ARCaP
MR42D
MR49F
V16D
Pc3
DU145
Precursor
Mature

Figure 5.5: SREBP expression in prostate cancer cell panel; Western blot showing the expression of SREBP-1 protein level in different PCa cell types using monoclonal anti-mouse and polyclonal anti-rabbit antibodies. The polyclonal Rabbit antibody detected both full length (precursor ~125kDa) and nuclear (mature ~68kDa) SREBP-1, while the mouse monoclonal antibody seems more specific for full length SREBP-1. GAPDH and α-Tubulin were used as loading controls. B) Quantification of full length, mature and total SREBP-1 expression in PCa cell panel normalized to loading control α-tubulin.

Abbreviation: FL, Full length; M, Mature.

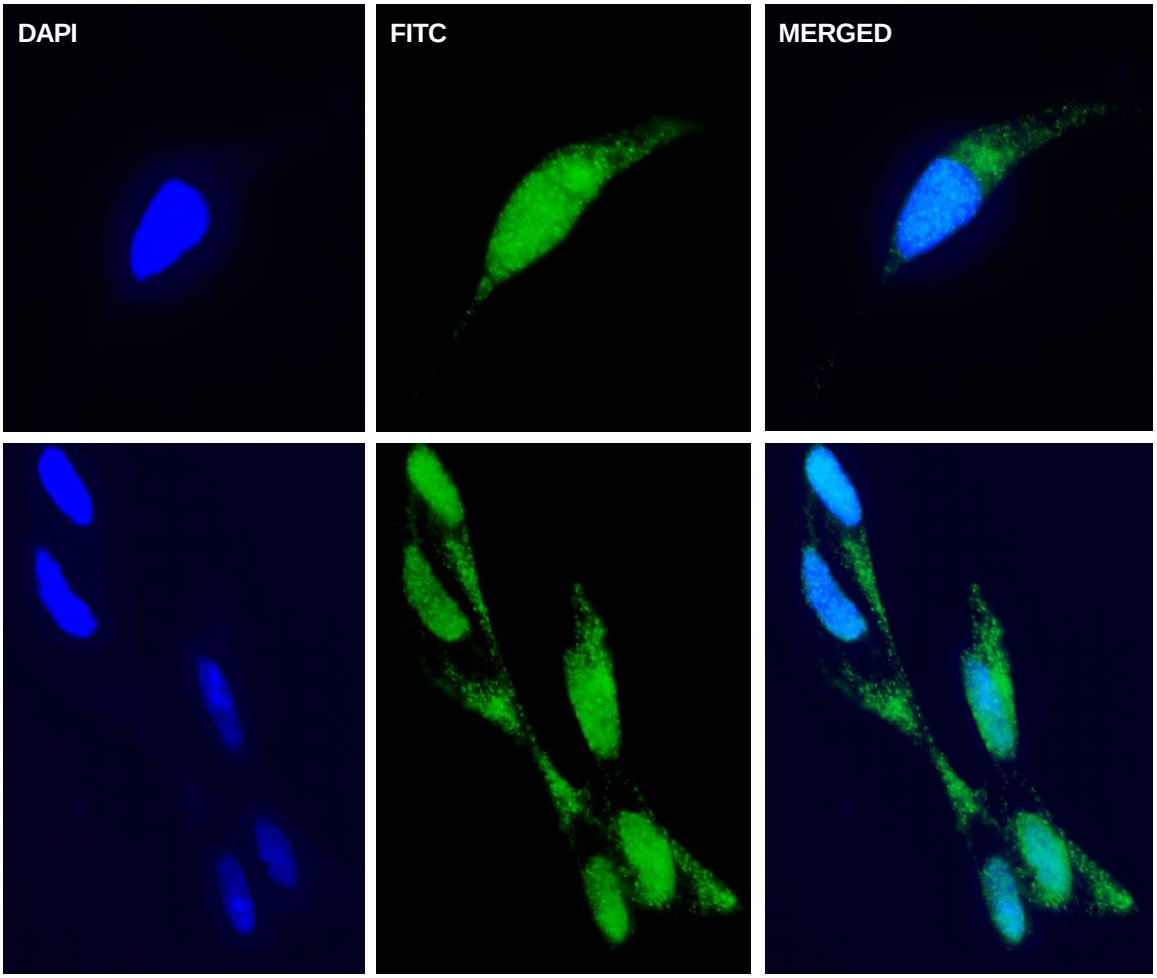

Figure 5.6: SREBP-1 are localized in cytoplasm and nucleus in LNCaP cells. Immunofluorescence staining of LNCaP cells to determine the localization of SREBP-1. Nuclei were labelled using DAPI; Santa Cruz Biotechnology, sc2A4, 1:400 (primary antibody) and Alexa Fluor 488 (secondary antibody) were used to detect SREBP-1 localization.

5.5.2 DHT treatment induces SREBP-1 expression and activation.

It has been reported that AR can promote activation of SREBP-1 (H. V. Heemers et al., 2006). We assessed whether this was the case in LNCaP cells. AR activation with DHT (10nM) treatment in LNCaP cells increased the expression of full-length SREBP-1 as well as its proteolytic cleavage/activation (H. V. Heemers et al., 2006). More specifically, we observed 1.9- and 2.2-fold increase in full-length SREBP-1 after 24 and 48 hrs, respectively, and a 5-fold increase in mature/nuclear SREBP-1 expression after 24 hrs of hormone treatment [Figure 5.7 (A)]. Similarly, Enzalutamide (Enz, 10 μM) treatment and siRNA mediated knockdown of AR in LNCaP cells decreased the expression of full length SREBP-1 [Figure 5.7 (B)]. We evaluated the kinetics of nuclear translocation of SREBP-1 after DHT treatment in LNCaP cells. Fractionation of cellular compartments of LNCaP cells demonstrated maximum nuclear/mature SREBP-1 protein translocation at 12 hrs of hormone treatment (Figure 5.8).

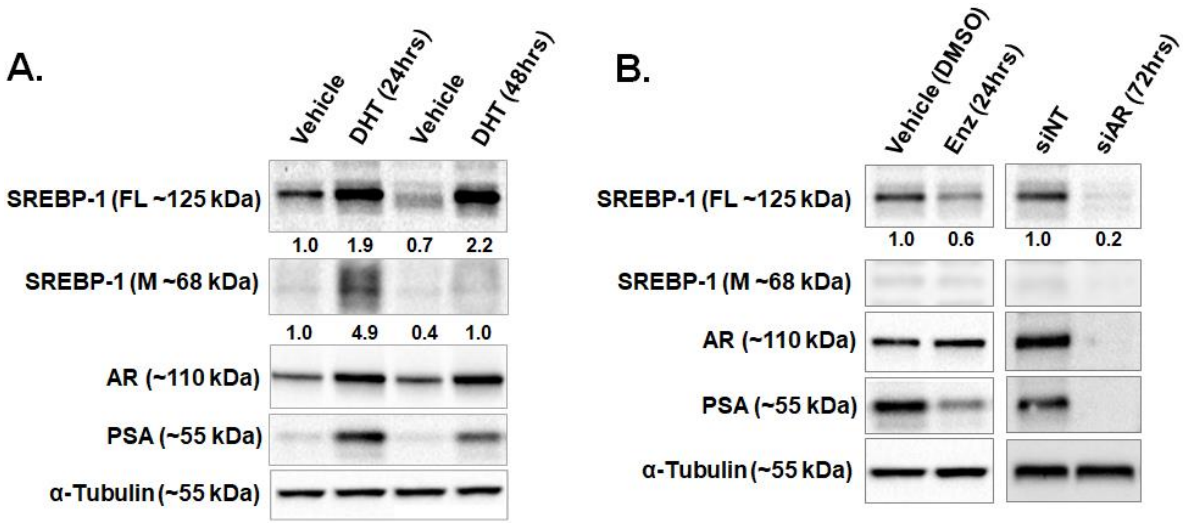

Figure 5.7: AR activation with DHT increases SREBP-1 protein expression and activation and targeting AR by anti-androgen (Enzalutamide) treatment or siRNA mediated knockdown in LNCaP cells decreases its expression as assessed by Western blotting; SREBP-1 expression was detected using Santa Cruz, sc8984 (H160) primary antibody, and normalized to loading control α-tubulin and PSA was used as positive control for DHT treatment. The cells were grown in stripped serum media for 72 hrs before DHT (10 nM) treatment whereas cells Enz (10 µM) treatment and siRNA was transfected to knockdown AR was done in full media.

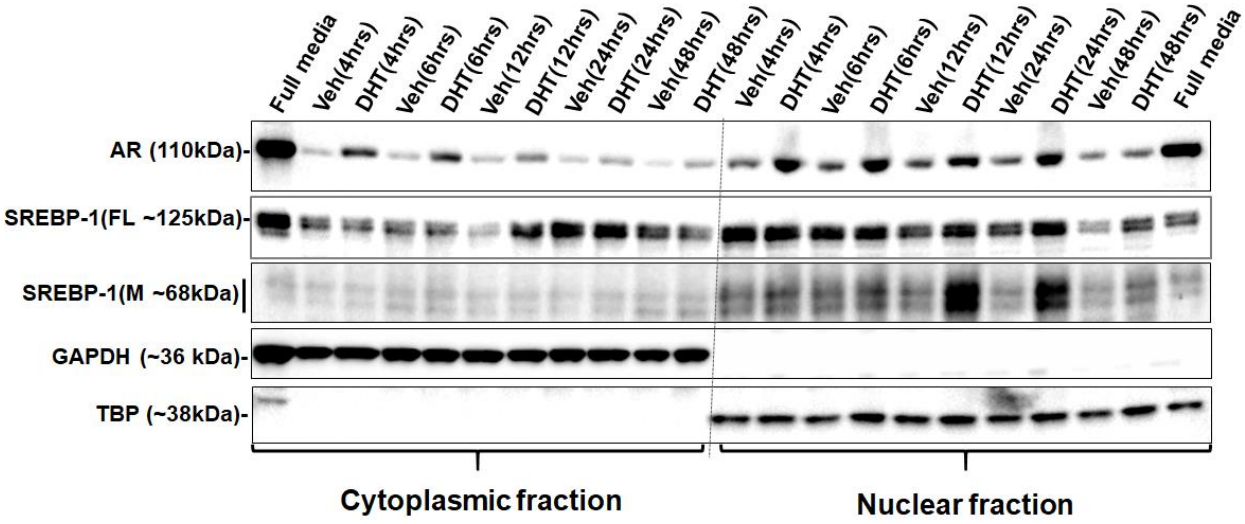

Figure 5.8: DHT treatment increases activation and translocation of SREBP-1 in LNCaP cells in first 12 hrs of treatment assesses by nuclear and cytoplasmic fractionation if LNCaP as assessed by Western blotting. The cells were grown in stripped serum for 72 hrs before DHT (10nM) treatment. Santa Cruz, sc8984 (H160) primary antibody was used to detect SREBP-1 protein. GAPDH and TATA box binding protein (TBP) are loading control for cytoplasmic and nuclear fraction respectively.

5.5.3 Evaluating the role of SREBP-1 in regulating AR and lipid metabolic genes in prostate cancer

Next, we inhibited SREBP-1 using Fatostatin (10 μM) in LNCaP cells to evaluate its effects on SREBP-1 canonical targets as well as AR transcription. As expected, qRT-PCR result demonstrated significant down regulation of canonical SREBP-1 target genes *(HMGCR, HMGCS1, LDLR, SCD)* as early at 6 hrs, with a stronger effect observed at 48 hrs. Downregulation of *AR* expression was observed at 48 hrs but not at the earlier time points (6 and 24 hrs) (Figure 5.9).

We also tested whether AR regulates the expression of these lipid metabolic genes and SREBP-1 in PCa cells. DHT treatment in LNCaP cells significantly increased the expression of *SREBF-1* and its canonical lipid metabolic targets *(HMGCR, HMGCS1, LDLR, SCD)* (Figure 5.10). To test whether SREBP-1 acts downstream of AR to regulate the lipid metabolic genes expression, we treated LNCaP cells with DHT (10 nM) and Fatostatin (10 μM) in combination. This revealed that Fatostatin largely reverses the effect of DHT on lipid metabolic genes (Figure 5.10). Collectively these results are indicative of a positive feedback loop between AR and SREBPs to regulate the lipid metabolic genes in prostate cancer cells.

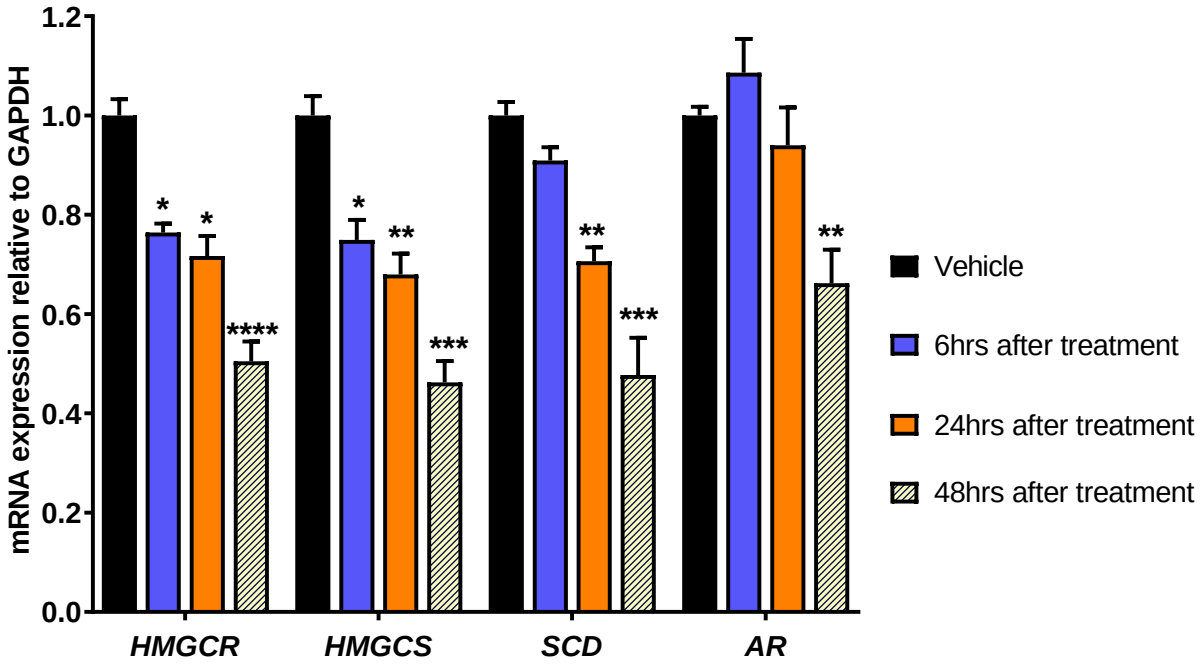

Figure 5.9: SREBP-1 inhibition downregulates the expression of canonical SREBP-1 targets; Gene expression represents the mean ± standard error (SE) of three biological replicates and was normalised to GAPDH; Differential expression was evaluated using unpaired t tests (*, $p < 0.01$; **, $p < 0.001$; ***, $p < 0.0001$). The inhibition of SREBP-1 suppressed the transcription of major SREBP-1 target genes (having SRE in their promoters) involved in cholesterol homeostasis and lipogenesis, including *AR*.

Abbreviation: *AR, Androgen receptor; HMGCR, 3-Hydroxy-3-Methylglutaryl-CoA Reductase; HMGCS, 3-Hydroxy-3-Methylglutaryl Coenzyme A Synthase; SCD, Stearoyl-CoA desaturase; ACSM1, Acyl-CoA Synthetase Medium Chain Family Member 1; ACSM3, Acyl-CoA Synthetase Medium Chain Family Member 3.*

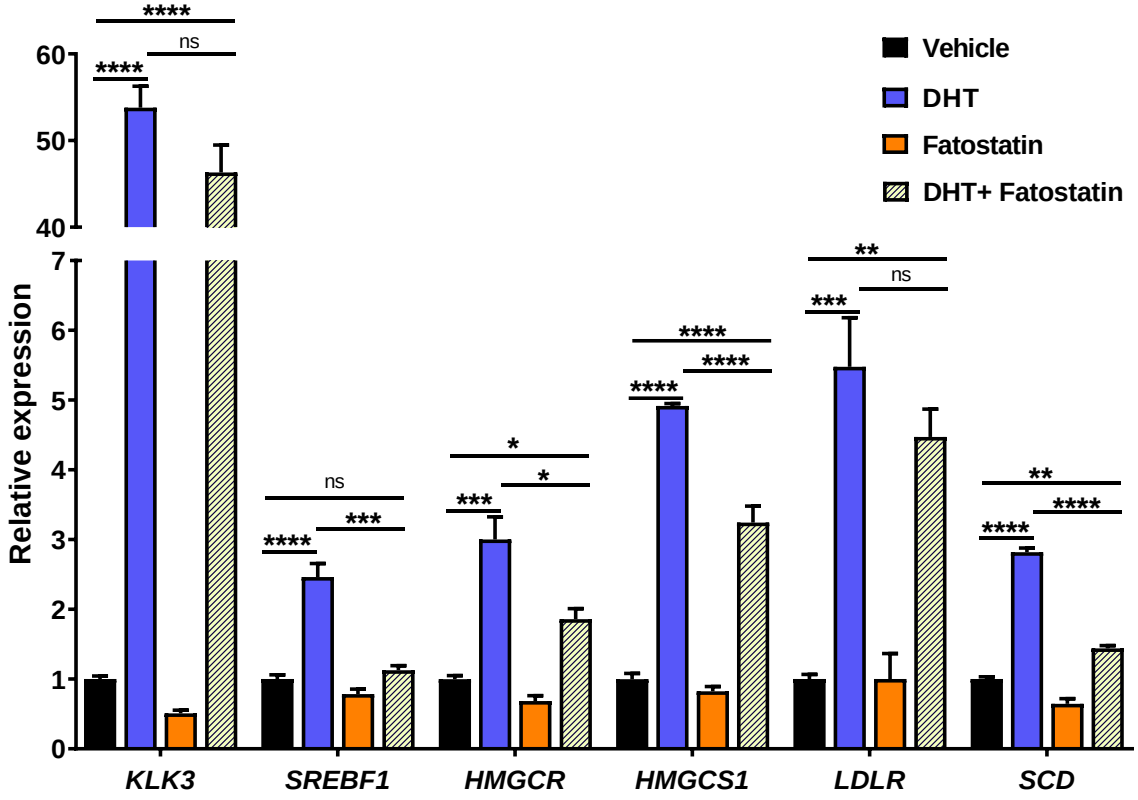

Figure 5.10: DHT treatment and Fatostatin treatment in LNCaP cells; the RT-qPCR of SREBF-1 expression and its canonical targets in response to DHT (10 nM), Fatostatin (10 μM) and combination in LNCaP cells. Cells were serum starved in charcoal-stripped FBS media for 72 h before treatment with Veh or DHT(10 nM) +/- Fatostatin (10 μM) for another 24 h. Gene expression was normalised to GUSB and L19 and represents the mean ± standard error (SE) of three biological replicates. Differential expression was evaluated by t tests (*, $p < 0.05$; **, $p < 0.01$). *KLK3*, a canonical *AR* target was used as positive control.

5.5.4 Evidence for cooperation between AR and SREBP1 in clinical prostate cancer

Based on published work described earlier and our findings above, we hypothesised that AR and SREBP1 activity would be associated in prostate tumours. Therefore, we determine AR and SREBP activities using ssGSEA (Barbie et al., 2009) in different PCa cohorts. To evaluate AR and SREBP1 activity, we used gene sets reported to be regulated by each factor (Ming Chen et al., 2018; C. S. Grasso et al., 2012). As expected, we found a strong direct relationship between AR activity and SREBP-1 activity in three different PCa cohorts (TCGA ("The Molecular Taxonomy of Primary Prostate Cancer," 2015), MSKCC (B. S. Taylor et al., 2010) and SU2C (D. Robinson, E. M. Van Allen, et al., 2015a)) (Figure 5.11).

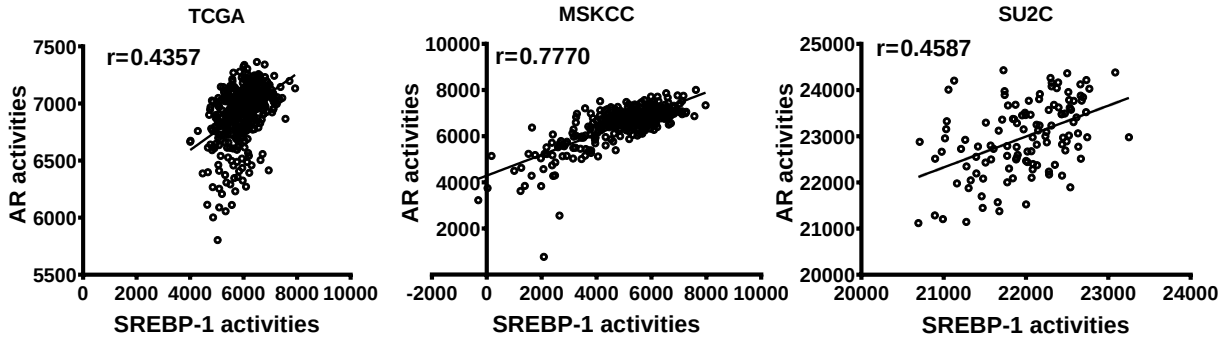

Figure 5.11: AR activities correlates with SREBP activities in prostate cancer; Correlation between AR-regulated gene signatures and SREBP-1 regulated gene signature in primary prostate cancer (left, TCGA cohort), primary and metastatic (middle, MSKCC cohort) and metastatic CRPC (right, SU2C cohort). P and r values were determined using Pearson's correlation tests.

5.5.5 SREBP-1 and AR share binding sites proximal to the TSS of lipid metabolic gene and possibly regulates their transcription

Our data indicate that there is a complex relationship between AR and SREBP-1 activity in PCa cells, but could not demonstrate whether they simultaneously co-regulate lipid metabolism genes. Unfortunately, SREBP-1 ChIP-seq data from PCa cells is not available. In light of this, we turned to SREBP-1 ChIP-seq data from the breast cancer cell line MCF7, which shares many features with LNCaP cells in terms of hormonal regulation of growth and differentiation (Risbridger, Davis, Birrell, & Tilley, 2010). We compared the MCF7 data with prostate tissue AR ChIP-seq data from Pomerantz *et al* dataset, described in Chapter 3 (Pomerantz et al., 2015). The breast cancer SREBP-1 cistrome was smaller than the prostate tumour AR cistrome from two (2) tumour tissue data (Figure 5.12A). Interestingly, 1103 (15.4%) of SREBP-1 binding sites directly overlapped with AR binding sites (Figure 5.12A). The majority (50%) of the overlapping AR/SREBP1 binding sites were present at the promotors of genes (Figure 5.12B), which is distinct from the entire AR cistrome, which is primarily located distal from genes (Figure 5.13). Visualization of the ChIP-seq data using Integrative Genomics Viewer (IGV)-Board institute online (Robinson et al., 2011) clearly demonstrated common binding sites proximal to the TSS of genes (e.g. *GREB1 (Growth Regulating Estrogen Receptor Binding 1*; Figure 5.12C).

Next, we evaluated the functions of genes proximal to shared AR/SREBP-1 binding sites. The GREAT tool" (McLean et al., 2010) identified enrichment of genes in various pathways including cholesterol metabolic, cell cycle and signalling (BCR and mTOR) pathway (Figure 5.12B).

To validate these findings in a PCa model, we attempted to do SREBP-1 ChIP-seq and AR-ChIP-seq in LNCaP cells after 4 and 16 hrs of DHT at treatment. We performed AR and SREBP-1 ChIP and conducted PCR to evaluate known binding sites. AR showed significant enrichment at the *KLK3* gene, a classic AR target (Figure 5.14). For SREBP-1, we designed primers based on binding sites within the promoters of *LDLR* and *HMGCR* genes with reference to “ENCODE” (Dunham et al., 2012) SREBP-1 ChIP-Seq data generated from 4 different cancer cell lines: MCF-7(breast), K562 (leukemia), A549 (lung), HepG2 (Liver) (Figure S5.1). However, ChIP-qPCR revealed no enrichment of these sequences, suggesting failure of the SREBP-1 ChIP Figure 5.14C). Since we could not be confident about the SREBP-1 ChIP, we did not proceed to high-throughput sequencing of the DNA.

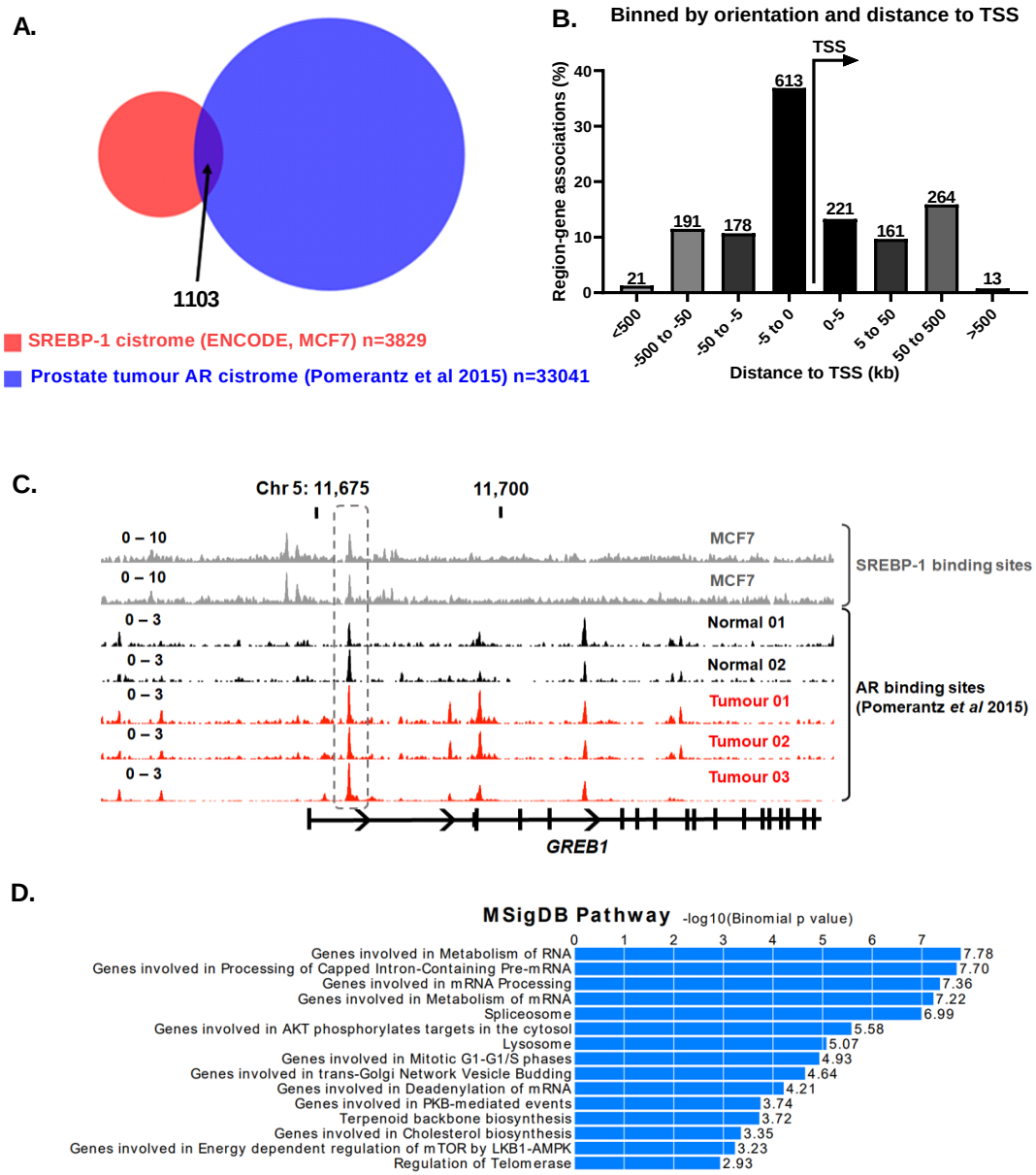

Figure 5.12: AR and SREBP-1 regulates common lipid metabolic pathway; A) Overlap of consensus prostate tumour AR cistrome and breast cancer cells (MCF7) SREBP-1 cistrome. B) Distribution of consensus binding sites from the TSS. C) AR and SREBP-1 chromatin binding events at the *GREB1* gene promoter in MCF7 (SREBP-1 cistrome) and prostate tumour (AR cistrome). D) Pathway analysis of consensus binding sites. The pathway analysis was done using online computational tool “GREAT” (McLean et al., 2010).

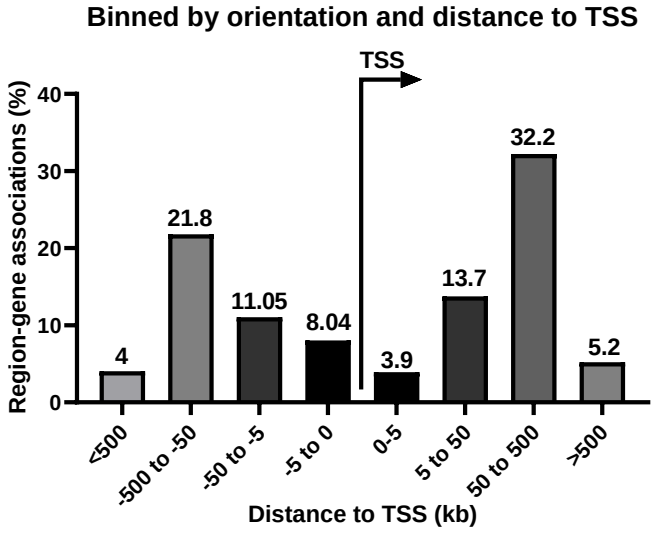

Figure 5.13: Distribution of AR binding events in prostate tumour tissue.

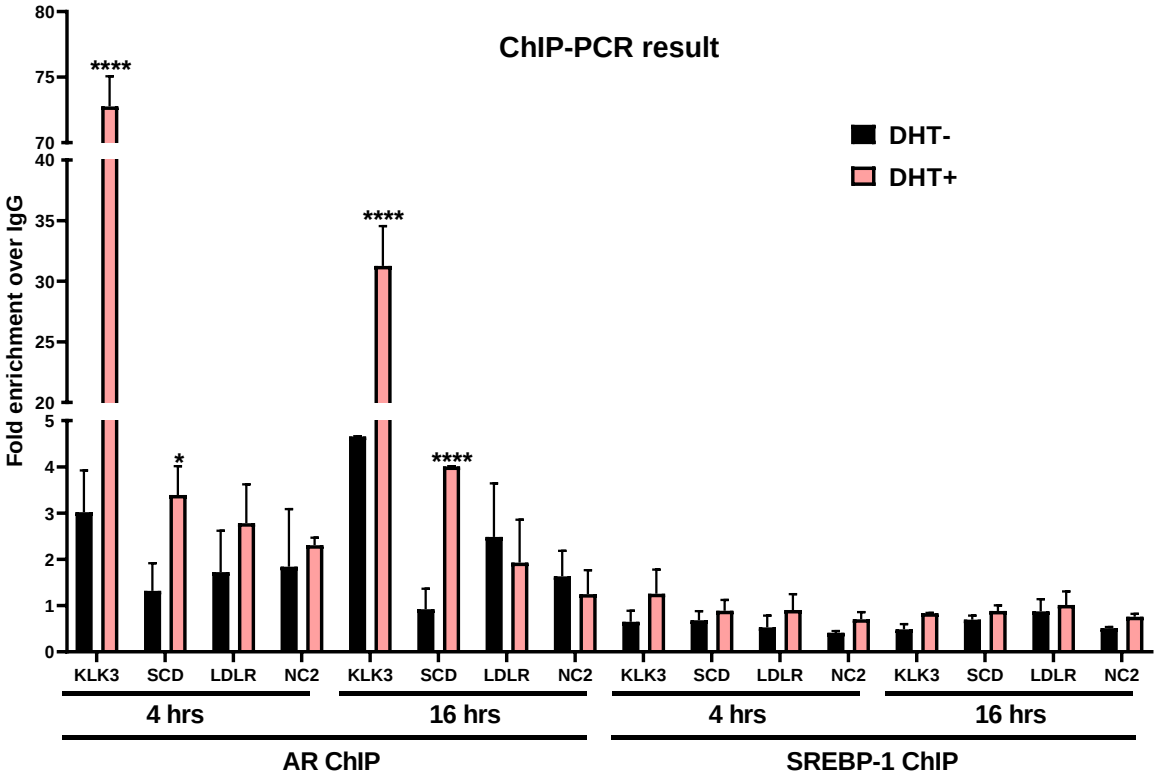

Figure 5.14: AR ChIP-PCR and SREBP-1 ChIP-PCR result; Validation of AR binding sites and SREBP-1 binding sites by AR ChIP-PCR and SREBP-1 ChIP-PCR respectively in LNCaP cells after DHT treatment for 4 and 16 hrs DHT treatment in LNCaP cells. Error bars represent ± SEM from 3 biological replicates.

5.5.6 Co-localisation of AR and SREBP-1

Given that we could not evaluate co-localisation of AR and SRBEP on chromatin using ChIP, we turned to an alternative method to assess their physical interaction in PCa cells. Proximity Ligation Assay (PLA) assays are a powerful tool to investigate protein-protein interactions with high specificity and sensitivity. High content imaging of LNCaP cells showed significant increase in nuclear and total PLA signal after hormone treatment in LNCaP cells (16 hrs), demonstrating interaction of AR and SREBP-1 in the nucleus (Figure 5.15).

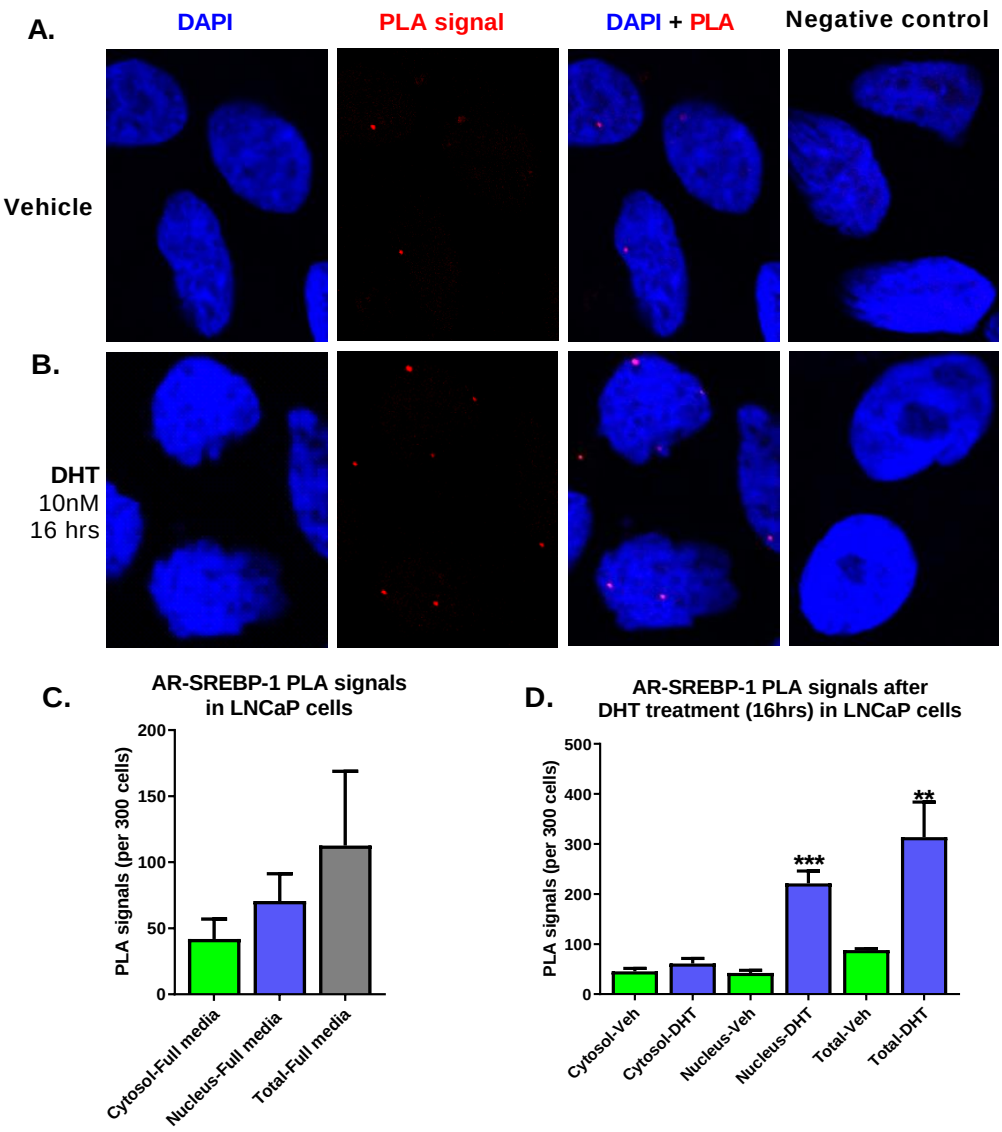

Figure 5.15. DHT treatment increases interaction between AR and SREBP;

A-B) PLA assay for AR interaction with SREBP-1 in LNCaP cells after DHT treatment for 16 hrs. Red fluorescent signal is indicative of protein interaction events. Cells were serum starved in charcoal-stripped FBS media for 72 h before treatment. Imaging was performed using an Olympus FV3000 Confocal Microscope (FLUOVIEW FV3000 series) and the images were analyzed by ImageJ software. B) The number of interactions between AR, and SREBP-1 in LNCaP cells plotted as graph (per 300 LNCaP cells). The data are presented as means ± SEM from three independent experiments. * $p<0.05$; ** $p<0.01$; *** $p<0.001$.

5.6 Discussion:

My results provide new insights into AR/SREBP-1 interplay, and how this might regulate lipid metabolism in PCa. I found that AR activation subsequently increases the expression and proteolytic cleavage/activation of SREBP-1 whereas anti-androgen or AR siRNA decreased expression, irrespective of sterol concentration. Time–course nuclear fractionation of LNCaP cells showed maximum SREBP-1 nuclear translocation to the nucleus between 12-24 hrs of DHT treatment, subsequently leading to a physical interaction with AR itself. Although, previous studies have reported SREBP-1 regulation by androgen through increased SCAP expression (H. V. Heemers et al., 2006), our results are novel because they demonstrate a physical interaction between AR and SREBP-1 inside the nucleus of PCa cells. Although, this remains to be proven, our evaluation of ChIP-seq data would suggest that this interaction occurs at the chromatin level, and we speculate that this would lead to cooperative effects in the regulation of lipid metabolic genes (Figure 5.16).

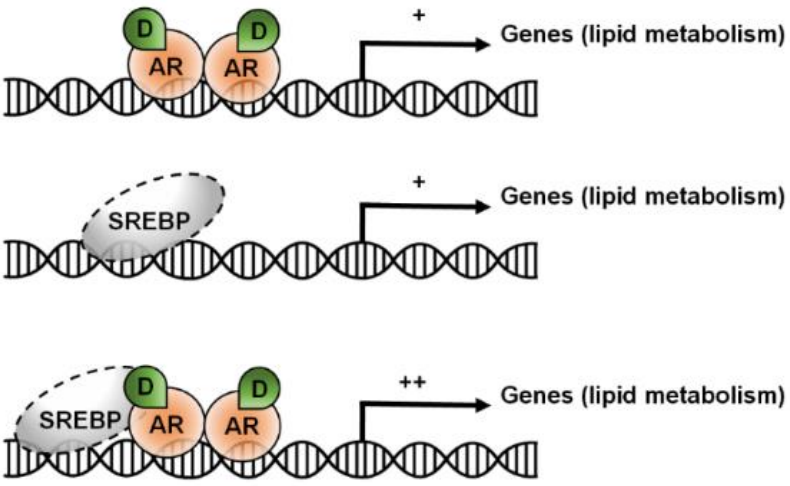

Figure 5.16. Schematic showing the proposed crosstalk between AR and SREBP-1 to regulate the lipid metabolic genes in PCa. SREBP-1 independently regulates the expression of the lipid metabolic genes and there are evidence that AR also directly regulates the transcription of lipid metabolic genes in PCa cells (see Chapter 3 and 4). SREBP-1 and AR could act co-ordinately in PCa and have an additive effect on the transcription of lipid metabolic genes.

SREBP-1 is highly expressed in a variety of human cancers and accumulating evidence suggests it plays a major role in cancer progression (Currie, Schulze, Zechner, Walther, & Farese, 2013; Deliang Guo, Bell, Mischel, & Chakravarti, 2014; Peck et al., 2016; Zaytseva et al., 2014; Zaytseva et al., 2015). It is also well known that the lipid metabolic genes (e.g. *FASN, ACACA, LDLR, HMGCR, HMGCS1 and SCD*) harbour SREBP-1 binding sites in their promoter regions and are tightly regulated by SREBP-1 in many cancer types (Figure S5.1). In addition, AR signalling have been reported to regulate the expression of genes involved in lipid metabolic processes (e.g. *FASN, ACACA, SCD, CD36* and *CPT1*) in PCa (Butler et al., 2016; Mah et al., 2019). One interesting finding that came out

of our analysis of ChIP-seq datasets was the potential for AR/SRBEP-1 interaction at many of these promoters. Generally, AR binds to enhancer regions of genes (Pomerantz et al., 2015; D. Wu et al., 2011) to regulate their expression. This suggests that SREBP-1 may be able to direct AR binding more efficiently to promoters. Due to unavailability of the SREBP-1 ChIP-seq data in PCa cell lines, we used SREBP-1 ChIP-seq and AR ChIP-seq data are from two (2) different cell lines. We chose breast cancer cell line (MCF7), which shares many features with PCa (LNCaP) cells in terms of epithelial phenotype and hormonal regulation of growth and differentiation (Risbridger et al., 2010). Although, these 2 cell lines possess similar cancer-related phenotypes, the integration of data from a PCa and breast cancer cell line is clearly a major limitation of this work. Therefore, one obvious extension of would be to perform SREBP-1 ChIP-seq in PCa cell lines with and without AR activation and to evaluate AR DNA binding at a genome-wide level after activation or inhibition of SREBP-1 in the same models. In the absence of a ChIP-grade antibody for SREBP-1, one option would be to generate PCa cell lines stably expressing tagged SREBP-1.

One of the major limitations of this study was our inability to ChIP SREBP-1. Unfortunately, the antibody used in previous ChIP studies (Santa Cruz, H160, sc8984) has been discontinued. Thus, the aim of evaluating chromatin co-localization of AR and SREBP-1 at a loci-specific level chromatin could not be achieved. To overcome this limitation, we demonstrated protein-protein interaction of AR and SREBP-1 inside nucleus after androgen treatment in PCa cells using an alternative technique, the PLA assay, which confirmed interaction of AR and SREBP-1 in nucleus. While this is a novel finding, it does not demonstrate co-localization of the 2 transcription factors on chromatin at their target genes. Future

work should focus on developing a detailed map of SREBP-1 cistrome and transcriptome in diverse PCa models. Integrative analysis of AR and SREBP-1 would elucidate the molecular mechanism of lipid metabolic pathway regulation by those factors and could identify commonly regulated factors, some of which may be drug targets.

In the future, evaluating the status of active SREBPs and co-staining of SREBP-1 and AR in clinical PCa tissue specimens is crucial to better understand the cooperative roles of these factors. We propose that using novels such as PCa explant culture (Margaret M. Centenera et al., 2018; M. M. Centenera, Raj, Knudsen, Tilley, & Butler, 2013) which can be manipulated with drug treatment (e.g. Fatostatin- a specific inhibitor of SCAP required for SREBP activation), to evaluate SREBP-1 function using transcriptomics, cistromics, lipidomics and metabolomics would be a major step forward in understanding the function of this key transcription factor.

Supplementary figures

A) *LDLR*

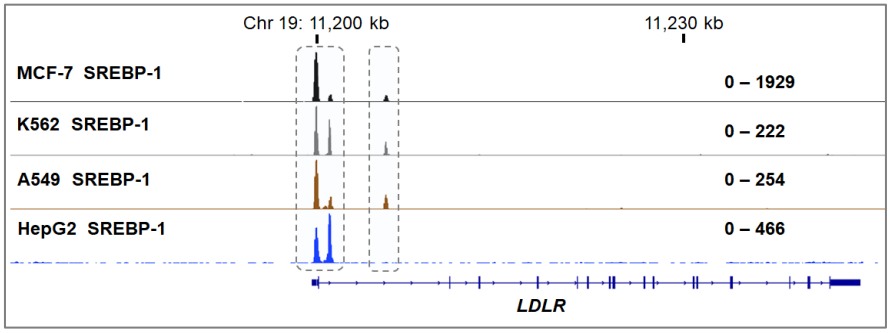

B) *HMGCR*

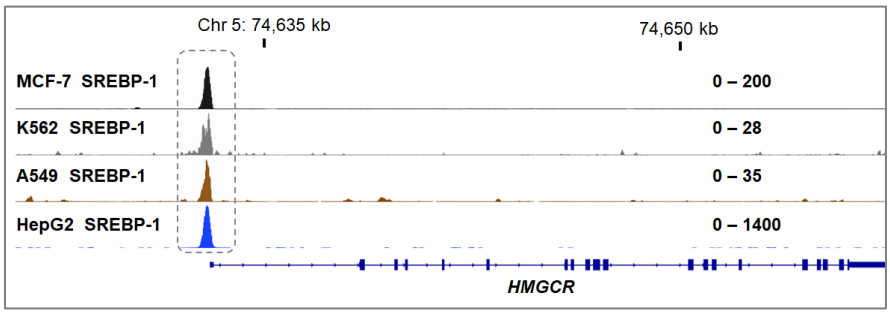

C) *HMGCS1*

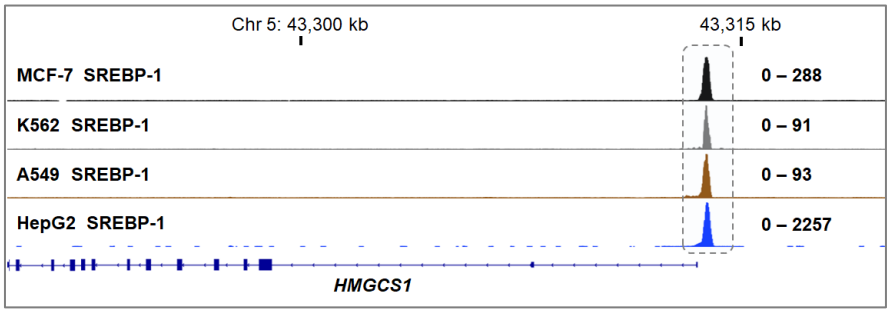

D) *FASN*

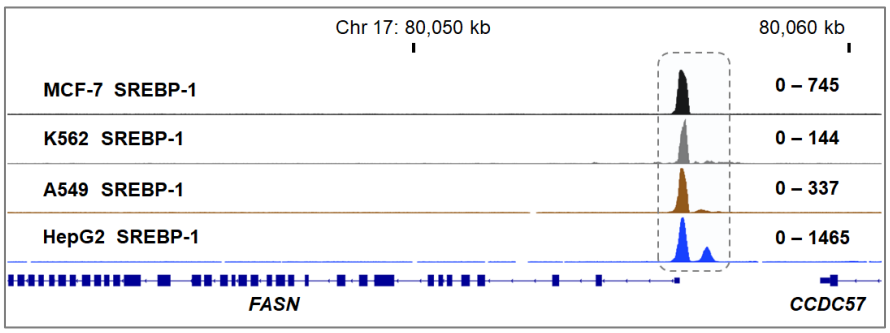

E) *SCD*

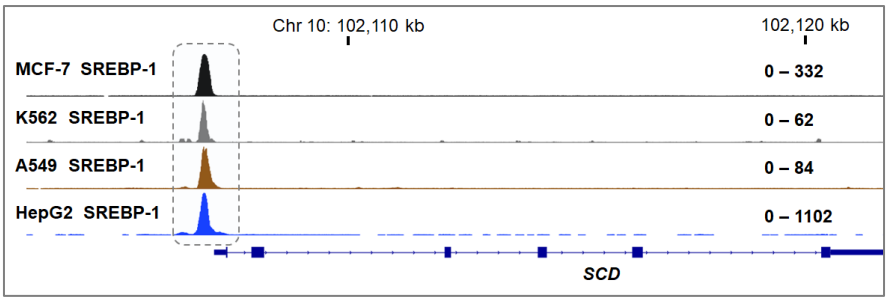

F) *ACACA*

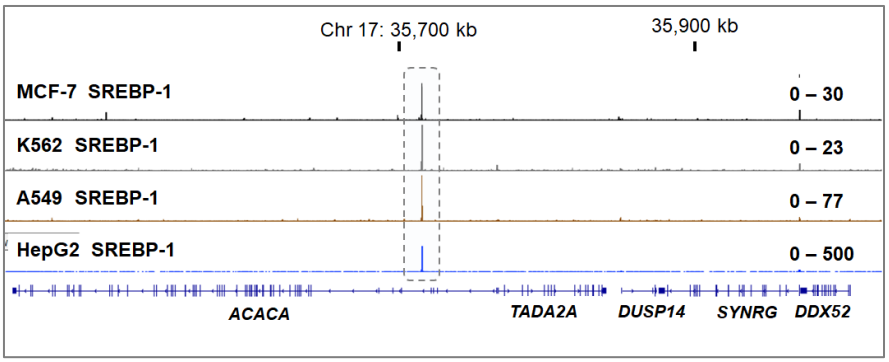

G) *SREBF-1*

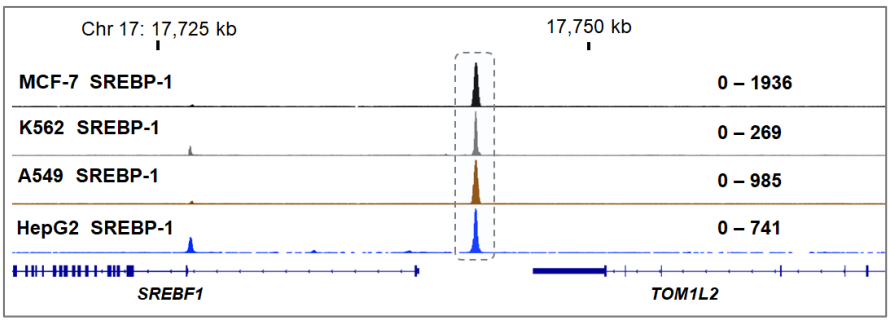

H) *SREBF-2*

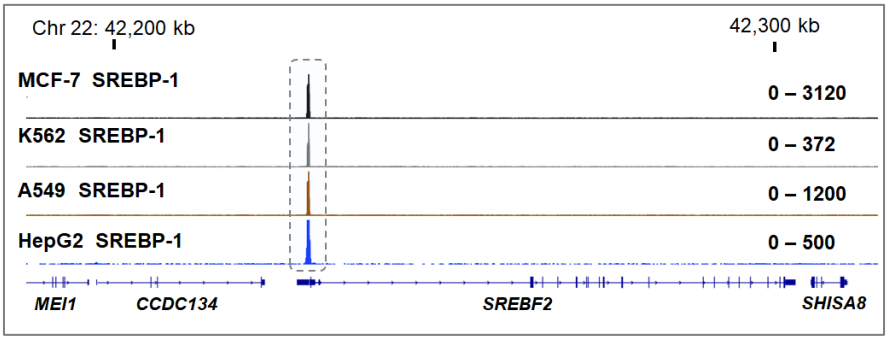

Figure S5.1: SREBP-1 ChIP-Seq data showing SREBP-1 binding peaks in the promoters of SREBP-1 target genes involved in cholesterol uptake and biosynthesis (*LDLR, HMGCR, HMGCS1, FASN, SCD,* and *ACACA*). SREBP-1 ChIP-seq data of MCF7, K562, A549 and HepG2 cell lines. [MCF7: ENCFF050MLH (black track); K562: ENCFF111BSU (grey track); A549: ENCFF572NZX (brown

track); and HepG2: ENCFF000XXR (blue track). The data is from project ENCODE (Dunham et al., 2012) E which were visualized in Integrative Genomics Viewer - Broad Institute (IGV)-Board institute online (Robinson et al., 2011). Interestingly, SREBP-1 binds to its own promoter as well as SREBP-2 promoter. Abbreviation: MCF-7: Breast cancer cell line, K562: leukemia cell line, A549: lung cancer cell line, HepG2: Liver cancer cell line.

CHAPTER 6: DISCUSSION

6 Discussion

Prostate tumours are highly reliant on lipids for growth and survival. An emerging theme in PCa biology is that AR directly regulates lipid metabolic processes, however the molecular mechanisms underlying this remain unclear. A better understanding of AR-regulated lipid metabolism process could identify new biomarkers that can distinguish indolent versus lethal aggressive disease as well as novel therapeutic targets, both of which would improve outcomes associated with this common disease. Therefore, my project aimed to characterise AR regulation of lipid metabolic genes and how this relates to PCa growth and progression.

6.1 Novel AR-regulated genes involved in lipid metabolism

In Chapter 3, using an integrative genomics approach that exploited publicly available cistromic and transcriptomic datasets, we identified 17 genes as putative novel AR-regulated lipid metabolic genes in PCa. We identified multiple genes that had not been reported as AR targets nor implicated in PCa, including *ACSM1*, *ACSM3, ACOT2*, *MMAA, HACL1, MORC2, PCTP, PRKAB2,* are *PTGR2.* We focused our attentions on ACSM1 and ACSM3, but unfortunately could not conduct any functional analysis of the remaining genes due to the scope of this PhD. An obvious next step will be to examine the function of these genes, particularly those that have not been reported in relation to PCa previously, using similar approaches to those described in Chapter 4.

6.2 *ACSM1* and *ACSM3* are key regulators of lipid metabolism and ferroptosis in PCa

My work provided many new insights into the functions of ACSMs in PCa (Figure 6.1). The metabolic dysregulation induced by knockdown of ACSM1 and ACSM3 caused ATP depletion, mitochondrial oxidative stress and subsequent lipid peroxidation, eventually resulting in cell death. Accumulation of mitochondrial reactive oxygen species was abrogated by ferrostatin-1 (an iron chelator), suggesting that cell death was due to an iron-dependent form of apoptosis termed ferroptosis. Supporting this concept, over-expression of ACSM1 and ACSM3 elicited resistance to the ferroptosis inducers Erastin and ML210. Mechanistically, our results suggests an important role of ACSM1 and ACSM3 in protecting PCa cells against iron-dependent free radical damage-ferroptosis in addition to energy production through fatty acid metabolism.

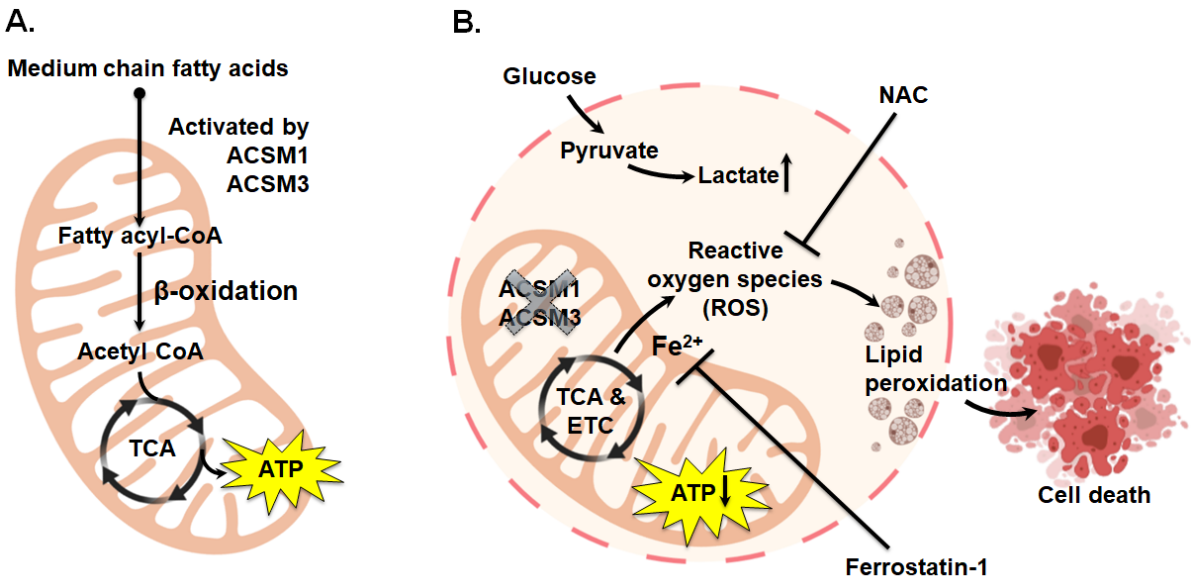

Figure 6.1. ACSM1 and ACSM3 activates medium chain fatty acids for its metabolism and protect PCa cells against ferroptosis. A) Schematic depicting the proposed function of ACSM1 and ACSM3 in human cells for ATP production from fatty acid metabolism; B) Consequences of ACSM1/ACSM3 knockdown in

PCa cells. Cells experience ATP depletion and undergo an adoptive response via substrate switching to glucose. Concomitantly, ROS accumulates in the cells leading to subsequent lipid peroxidation and cell death by ferroptosis.

Despite the extensive functional characterisation that was carried out (Chapter 4), questions remain about the roles of ACSM1 and ACSM3 in PCa. Various studies using both *in vivo* and *in vitro* approaches have revealed substantial flexibility in terms of substrate utilisation by ACSMs (J. M. Ellis, Bowman, & Wolfgang, 2015; Fujino et al., 2001; Vessey, Kelley, & Warren, 1999). A major limitation of our study was an inability to accurately define the substrates of ACSM1 and ACSM3 in PCa cells. Our mass spectrometry (LC-ESI/MS/MS) approach detected a wide range of fatty acids, but unfortunately medium chain fatty acids and their activated forms were not detectable with this approach. Nevertheless, our lipidomics data showed accumulation of fatty acids (over 14C chain length / saturated/unsaturated) in various lipid species including (TAG, DAG, PC, PE, PI, PG and PS) as a result of loss of ACSM1 and ACSM3 function in PCa cells. Based on this observation, we believe that ACSMs directly activates both medium and long chain fatty acids in PCa cells, although this remains to be proven. We expect that advances in mass spectrometry-based detection of lipids (Avela & Sirén, 2020) will enable this question to be answered in the near future. Another strategy to identify the major substrates of ACSM1 and ACSM3 could be to feed different MCFAs and LCFAs to PCa cells. This is not straightforward, however, since exogenous supplementation of fatty acids to PCa cells induces apoptosis and cell death (Balaban et al., 2019), which could be due to accumulation of fatty acids rather than its metabolism in the cells. One possibility is that using PCa cells over-expressing ACSM1 and ACSM3, which I generated in this study, could overcome this issue.

We believe that PCa cells over-expressing ACSM1 and ACSM3 should be able to utilize exogenous supplementation of fatty acids, especially MCFAs, for the fulfilment of their metabolic need. Finally, we also propose that isotope-labelled metabolomics studies would help to clarify the fate of medium/long chain fatty acids in the over-expressing ACSM1 and ACSM3 PCa cells (Jang, Chen, & Rabinowitz, 2018; Llufrio, Cho, & Patti, 2019). In these studies, the path of carbon production and consumption can be tracked to accurately evaluate the utilisation of fatty acids.

Like MCFAs, our metabolomic and lipidomic appraoches did not measure xenobiotic compounds in PCa cell extracts and media. Carboxylate-containing xenobiotics such as benzoates are another proposed substrate for ACSMs (Kochan, Pilka, von Delft, Oppermann, & Yue, 2009; Vessey et al., 1999). Xenobiotic metabolism frequently comes with generation of ROS, which in turn modulates the signal transduction process required for cancer progression (Aggarwal et al., 2019) but overproduction of ROS is harmful to the cells. Most of the xenobiotic compounds get introduced in human body via diet, air, exposure to chemicals, and drug administration (Patterson, Gonzalez, & Idle, 2010). One possibility is that over-expression of ACSM1/3 in PCa could be an adaptive mechanism to protect against these xenobiotics, although very little is known about the levels that prostate tissues would be exposed to. In our experiments, foetal calf serum contains xenobiotics (González, Chen, & Deng, 2017), therefore the results we observed could be explained by accumulation of these compounds. However, this remains to be proven. Similarly to identifying the lipid substrates of ACSM1/3, we could identify whether xenobiotic are important substrates in PCa cells by exploiting our ACSM1/3-over-expression cells, feeding PCa cells various xenobiotic, or using targeted isotope labelling.

One of the drawbacks of research into ACSMs is the lack of specific inhibitors. Salicyclic acid and its different forms (4-methylsalicyclic acid, 4-methylsalicylic acid, 2-hydroxynaphthoic acid, and 2-hydroxyoctanoic acid) have been reported as competitive inhibitors for ACSMs purified from fresh bovine liver (Kasuya, Igarashi, & Fukui, 1996). We obtained 4-Methylsalicylic acid and (±)-2-Hydroxyoctanoic acid and tested their effects on LNCaP cells. Although, high dose of ACSM inhibitors suppressed LNCaP cells growth (Figure 6.2) they did not cause the same effect as ACSM1/3 knockdown in terms of causing cell death (Figure 6.3). Based on these observations, we assumed that these inhibitors have non-specific activities, which precluded their utility for our studies. However, it is worth noting that various derivatives of salicyclic acid are being used for multiple inflammatory diseases with minimal side effects (Bartzatt, Cirillo, & Cirillo, 2007). Therefore, derivatives of salicyclic acid that are highly specific inhibitors of ACSM1 and ACSM3 could potentially be useful therapeutics in the future. In this respect, crystal structures of both enzymes would facilitate drug development, based on salicylic acid or otherwise.

6.3 Interplay between AR and SREBP-1 in PCa

In addition to our focussed research on AR-regualted lipid metabolism, we endeavoured to provide new insights into AR/SREBP-1 cooperative interplay that might regulate lipid metabolism in PCa. Althuogh the feedback loop between AR and SREBP-1 that we observed has already been established in PCa cells, a new finding in this thesis was that AR and SEBP-1 physicallhy interact inside the nucleus of PCa cells after androgen treatment. Whether AR and SREBP1 coordinately regulate the genes identified in Chapter 3 is unknown, but we could address this

possibility by demonstrating co-localization of both transcription factors on chromatin at genes identified in chapter 3. Furthermore, developing a detailed map of the SREBP-1 cistrome and transcriptome in diverse PCa models with variable AR status could identify novel AR targets in lipid metabolism.

6.4 Conclusion:

Collectively, the research in this thesis has identified novel AR-regulated lipid metabolic genes in PCa. It provides key new insights into the role of of lipid activating enzymes ACSM1 and ACSM3 in PCa. We propose that these findings could lead to new therapies targeting PCa metabolism in the future.

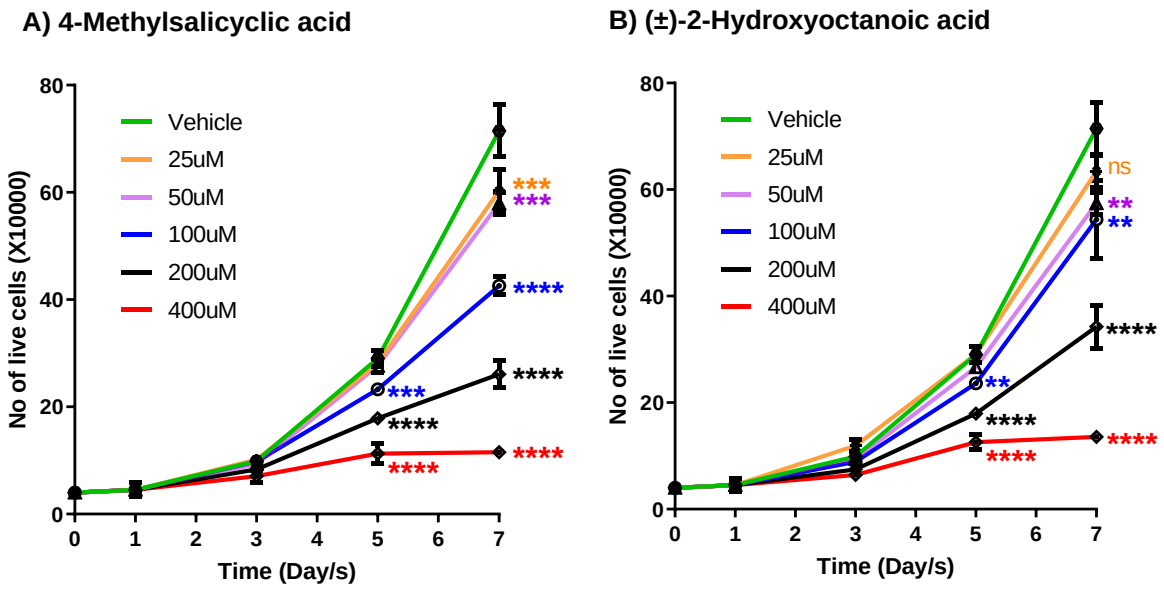

Figure 6.2: Competitive inhibition of ACSM1 and ACSM3 inhibits prostate cancer growth, as evaluated by Trypan blue assays. LNCaP cells were grown in full media with different concentration of inhibitors ((±)-2-Hydroxyoctanoic acid and 4-Methylsalicyclic acid). The graph represents numbers of cells counted by coulter counter (n = 3). Data are presented as mean ± SEM. The adjacent vehicle and different treatment groups were compared at indicated time-points using unpaired t tests (*, $p < 0.05$; **, $p < 0.01$; ***, $p < 0.001$; ****, $p < 0.0001$).

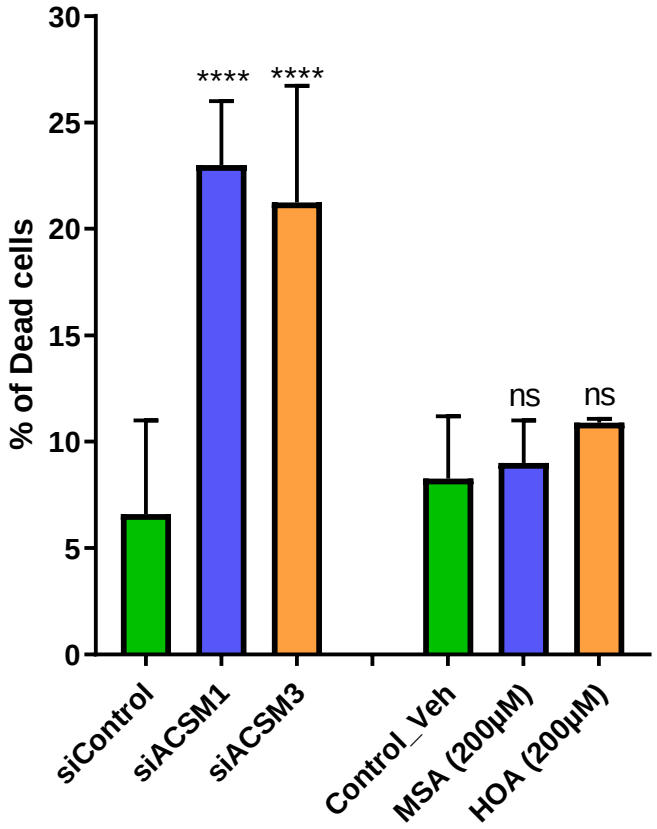

Figure 6.3*:* siRNA mediated ACSM1/3 knockdown and chemical inhibitor mediated inhibition of ACSMs do no show same phenotype (cell death). Cell death determined on Day 6 by a flow cytometric assay using SYTOX™ Red Dead Cell Stain. Data shown are mean ± SEM. The adjacent vehicle and different treatment groups were compared at indicated time-points using unpaired t tests (*, $p < 0.05$; **, $p < 0.01$; ***, $p < 0.001$; ****, $p < 0.0001$).

APPENDICES

7 Appendices

7.1 Human DECR1 is an androgen-repressed survival factor that regulates PUFA oxidation to protect prostate tumor cells from ferroptosis

This section includes the published paper in eLife journal on July 2020 (doi:10.7554/eLife.54166). I contributed to this paper in terms of data curation, formal analysis, investigation, visualization and methodology. Specifically, I conducted the ChIP experiments, analysed ChIP-seq data, and evaluated AR regulation of DECR1.

RESEARCH ARTICLE

Human DECR1 is an androgen-repressed survival factor that regulates PUFA oxidation to protect prostate tumor cells from ferroptosis

Zeyad D Nassar[1,2†], Chui Yan Mah[1,2†], Jonas Dehairs[3], Ingrid JG Burvenich[4], Swati Irani[1,2], Margaret M Centenera[1,2], Madison Helm[1,2], Raj K Shrestha[5], Max Moldovan[2], Anthony S Don[6], Jeff Holst[7], Andrew M Scott[4], Lisa G Horvath[8], David J Lynn[2,9], Luke A Selth[1,5,9], Andrew J Hoy[10], Johannes V Swinnen[3], Lisa M Butler[1,2*]

[1]University of Adelaide Medical School and Freemasons Foundation Centre for Men's Health, University of Adelaide, Adelaide, Australia; [2]South Australian Health and Medical Research Institute, Adelaide, Australia; [3]KU Leuven- University of Leuven, LKI- Leuven Cancer Institute, Department of Oncology, Laboratory of Lipid Metabolism and Cancer, Leuven, Belgium; [4]Tumour Targeting Laboratory, Olivia Newton-John Cancer Research Institute, and School of Cancer Medicine, La Trobe University, Melbourne, Australia; [5]Dame Roma Mitchell Cancer Research Laboratories, University of Adelaide, Adelaide, Australia; [6]NHMRC Clinical Trials Centre, and Centenary Institute, The University of Sydney, Camperdown, Australia; [7]Translational Cancer Metabolism Laboratory, School of Medical Sciences and Prince of Wales Clinical School, UNSW Sydney, Sydney, Australia; [8]Garvan Institute of Medical Research, NSW 2010; University of Sydney, NSW 2006; and University of New South Wales, Darlinghurst, Australia; [9]College of Medicine and Public Health, Flinders University, Bedford Park, Australia; [10]Discipline of Physiology, School of Medical Sciences, Charles Perkins Centre, Faculty of Medicine and Health, The University of Sydney, Camperdown, Australia

***For correspondence:** lisa.butler@adelaide.edu.au

[†]These authors contributed equally to this work

Competing interests: The authors declare that no competing interests exist.

Funding: See page 20

Received: 04 December 2019
Accepted: 16 July 2020
Published: 20 July 2020

Reviewing editor: Nima Sharifi, Cleveland Clinic, United States

Abstract Fatty acid β-oxidation (FAO) is the main bioenergetic pathway in human prostate cancer (PCa) and a promising novel therapeutic vulnerability. Here we demonstrate therapeutic efficacy of targeting FAO in clinical prostate tumors cultured ex vivo, and identify *DECR1*, encoding the rate-limiting enzyme for oxidation of polyunsaturated fatty acids (PUFAs), as robustly overexpressed in PCa tissues and associated with shorter relapse-free survival. *DECR1* is a negatively-regulated androgen receptor (AR) target gene and, therefore, may promote PCa cell survival and resistance to AR targeting therapeutics. DECR1 knockdown selectively inhibited β-oxidation of PUFAs, inhibited proliferation and migration of PCa cells, including treatment resistant lines, and suppressed tumor cell proliferation and metastasis in mouse xenograft models. Mechanistically, targeting of DECR1 caused cellular accumulation of PUFAs, enhanced mitochondrial oxidative stress and lipid peroxidation, and induced ferroptosis. These findings implicate PUFA oxidation via DECR1 as an unexplored facet of FAO that promotes survival of PCa cells.

Introduction

Prostate cancer (PCa) is the most prevalent male cancer and the second leading cause of cancer deaths in men in Western societies (*Bray et al., 2018*). For patients with locally-recurrent and/or metastatic disease, androgen deprivation therapy (ADT) has remained the frontline strategy for clinical management since the 1940s (*Huggins and Hodges, 1941*), due to the dependence of PCa cells on androgens for growth and survival. Although ADT is initially effective in most patients, ultimately all will relapse with castration resistant prostate cancer (CRPC), which remains incurable. The failure of ADT is attributed to the emergence of adaptive survival pathways that reprogram androgen signaling and/or activate alternative tumor survival pathways. Consequently, the development and FDA approval of agents that more effectively target androgen signaling, including enzalutamide (ENZ, Xtandi; an AR antagonist) (*Tran et al., 2009*; *Cai and Balk, 2011*; *Rodrigues et al., 2014*), has expanded the therapeutic options for CRPC. Nevertheless, even these approaches cannot durably control tumor growth and there is considerable variability in the nature and duration of responses between different patients (*Tran et al., 2009*; *Scher et al., 2012*; *Davis et al., 2019*). Thus, alternative therapeutic strategies that enhance response to ADT, and thereby prevent or delay PCa progression to CRPC, are essential.

Increasingly, targeting cancer cell metabolism is a focus of research efforts (*Hanahan and Weinberg, 2011*). While fundamental differences in cellular metabolism pathways between normal and malignant cells were detected by Warburg in the 1920s (*Warburg et al., 1927*), clinical targeting of cancer metabolism has not kept pace with the research advances in understanding metabolic features of cancer cells. PCa is mainly dependent on lipid metabolism for energy production (*Liu, 2006*). The overexpression of genes involved in lipid metabolism is characteristic of PCa at both early and advanced stages (*Wu et al., 2014*; *Chen et al., 2018*; *Swinnen et al., 2002*; *Zadra et al., 2013*; *Zadra and Loda, 2018*; *Ettinger et al., 2004*; *Nomura et al., 2011*), while recent proteomic analyses of primary PCa and bone metastases have shown clear associations between levels of lipid metabolic enzymes, PCa initiation and progression (*Iglesias-Gato et al., 2016*; *Iglesias-Gato et al., 2018*). These observations suggest that PCa may be particularly amenable to metabolic targeting strategies. Despite this, the role and complexity of lipid/fatty acid (FA) metabolism in PCa and its potential as a target for therapy remains underexplored, particularly in the context of a more complex tumor microenvironment.

Until recently, most attention has focused on the therapeutic targeting of de novo FA synthesis and, most recently, uptake of FAs in PCa to limit their availability as a source of energy and cell membrane phospholipids (*Zadra et al., 2013*; *Zadra and Loda, 2018*; *Watt et al., 2019*). However, it has become evident in work from our group and others that β-oxidation of FAs, as the ultimate fate of FAs in the energy production cycle, is upregulated in PCa cells, stimulated by a lipid-rich extracellular environment and critical for viability (*Liu, 2006*; *Schlaepfer et al., 2014*; *Balaban et al., 2019*). In this study, we evaluated the targeting of FA β-oxidation (FAO) in patient-derived prostate tumor explants (PDE) to provide the first clinically-relevant evidence that targeting this pathway is efficacious. We subsequently identify DECR1, a rate-limiting enzyme in an auxiliary pathway for polyunsaturated fatty acid (PUFA) β-oxidation, as a promising novel therapeutic vulnerability for PCa. Importantly, we show that DECR1 is an androgen-repressed gene induced in PCa cells in response to ADT and/or AR-targeted therapies, implicating PUFA oxidation as an adaptive survival response that may contribute to emergence of CRPC and treatment resistance.

Results

Targeting FA oxidation is efficacious in patient-derived PCa explants

In addition to our recent report of enhanced FAO in PCa cells (*Balaban et al., 2019*), an accumulating body of evidence supports the efficacy of targeting key enzymes involved in FAO using in vitro and in vivo models of PCa (*Itkonen et al., 2017*; *Schlaepfer et al., 2014*; *Flaig et al., 2017*). However, to date there is limited evidence that targeting this pathway would be clinically efficacious, which prompted us to target this pathway in clinical tumors. Using our well-defined patient derived explant (PDE) model that recapitulates the complexity of the clinical tissue microenvironment (*Centenera et al., 2012*), we targeted the rate-limiting enzyme in mitochondrial FAO, carnitine palmitoyltransferase-1 (CPT-1), in cultured PDEs using the chemical inhibitor etomoxir. Consistent with

literature reports, etomoxir had weak activity against the LNCaP PCa cell line in vitro, with an IC50 of 170 µM (***Figure 1—figure supplement 1A***), but was considerably potent in the PDEs, in which a dose of 100 µM inhibited cell proliferation by an average of 48.4 ± 16.6% (n = 13 patients; $p<0.05$) (***Figure 1A***). Etomoxir effectively inhibited FAO in the tissues, evidenced by a significant decrease in multiple acylcarnitines in the conditioned medium (***Figure 1B***).

In order to prioritize key functional genes involved in PCa progression, we conducted a meta-analysis of the expression of 735 genes involved in lipid metabolism (as identified from REACTOME) in four clinical datasets with malignant and matched normal RNA sequencing data (***Nikitina et al., 2017***; ***Ren et al., 2012***; ***Ding et al., 2016***). Genes were rank-ordered on the basis of their *meta effect size* scores in PCa malignant versus matched normal tissues (***Figure 1—figure supplement 1B***). The meta-analysis revealed a strikingly consistent deregulation of lipid metabolism genes, including genes involved in FAO (***Figure 1C***), despite the predicted high inter-individual heterogeneity of patient PCa tissues. We conducted disease-relapse survival analysis using TCGA data for each of the top 20 genes from the meta-analysis. This identified *DECR1*, a rate-limiting enzyme in the mitochondrial β-oxidation of polyunsaturated fatty acids, as a robustly overexpressed gene in PCa tissues that is associated with shorter relapse-free survival rates.

DECR1 is upregulated in clinical prostate tumors

Consistently, *DECR1* mRNA expression was significantly higher in malignant compared to benign prostate tissues in ten independent expression datasets of PCa tissues versus non-malignant tissues (***Figure 1D***, ***Figure 1—figure supplement 1C***). Further analysis of the TCGA data revealed increased *DECR1* expression with increased Gleason score or in with advanced disease stage (***Figure 1E***). Consistent with our observation of increased DECR1 mRNA expression in PCa, *DECR1* gene copy gain was evident in several clinical datasets accessed via cBioPortal (***Cerami et al., 2012***; ***Figure 1F***). Interestingly, the top three cancer types exhibiting increased *DECR1* copy gain were hormone-dependent tumors (uterine, breast and prostate), suggestive of a relationship between DECR1 expression and hormone signaling (***Figure 1G***). *DECR1* mRNA expression was associated with shorter relapse-free survival rates and overall survival rates (***Figure 1H***), and in the TCGA dataset, *DECR1* amplification was significantly associated with shorter recurrence-free survival rates (***Figure 1I***).

We confirmed overexpression of DECR1 protein in clinical PCa using two independent proteomic datasets (***Figure 2A***). We observed overexpression of DECR1 in PCa tissues (n = 8) compared with benign tissues (n = 3) (***Figure 2B***), and increased expression was evident in high grade versus low grade cancer tissue. Quantitative IHC staining analysis revealed a significant increase of DECR1 expression in malignant *vs* benign tissues. Furthermore, intra-tissue analysis exposed a significant increase of DECR1 expression in malignant regions *vs* benign ones within the same core (***Figure 2C***). DECR1 expression was markedly increased in a panel of hormone-dependent and -independent cancer cell lines compared with non-malignant PNT1 and PNT2 prostate cell lines (***Figure 2D***). Consistent with its function, DECR1 localises to the mitochondria, confirmed using immunocytochemistry and Western blot of nuclear, cytoplasmic and mitochondrial cell fractions (***Figure 2E***). Together, the mRNA and protein findings suggest that expression of DECR1 is closely linked to PCa progression and patient outcomes, and therefore might represent an unexplored therapeutic target.

DECR1 is a directly androgen-repressed gene in PCa

The relationship between androgen receptor (AR) signaling and lipid metabolic genes is well established. Many studies have reported a marked stimulatory effect of AR on key lipid metabolism pathways either directly or indirectly through activation of a family of transcription factors called sterol regulatory element-binding proteins (SREBPs) (***Butler et al., 2016***). We therefore investigated the relationship between AR and DECR1 using a panel of in vitro, ex vivo and in vivo models. DECR1 expression is notably more abundant in AR-negative cells (PC3) than in AR-expressing cells (***Figure 2D***), consistent with negative regulation of DECR1 expression by AR. We confirmed that androgen (5α-dihydrotestosterone) significantly decreased DECR1 expression in androgen-dependent LNCaP and VCaP cell lines at both mRNA and protein levels (***Figure 3A***). Data mining of publicly available microarray datasets also revealed downregulation of DECR1 in LNCaP cells after treatment with DHT or the synthetic androgen R1881 (***Figure 3—figure supplement 1A***); GSE7868,

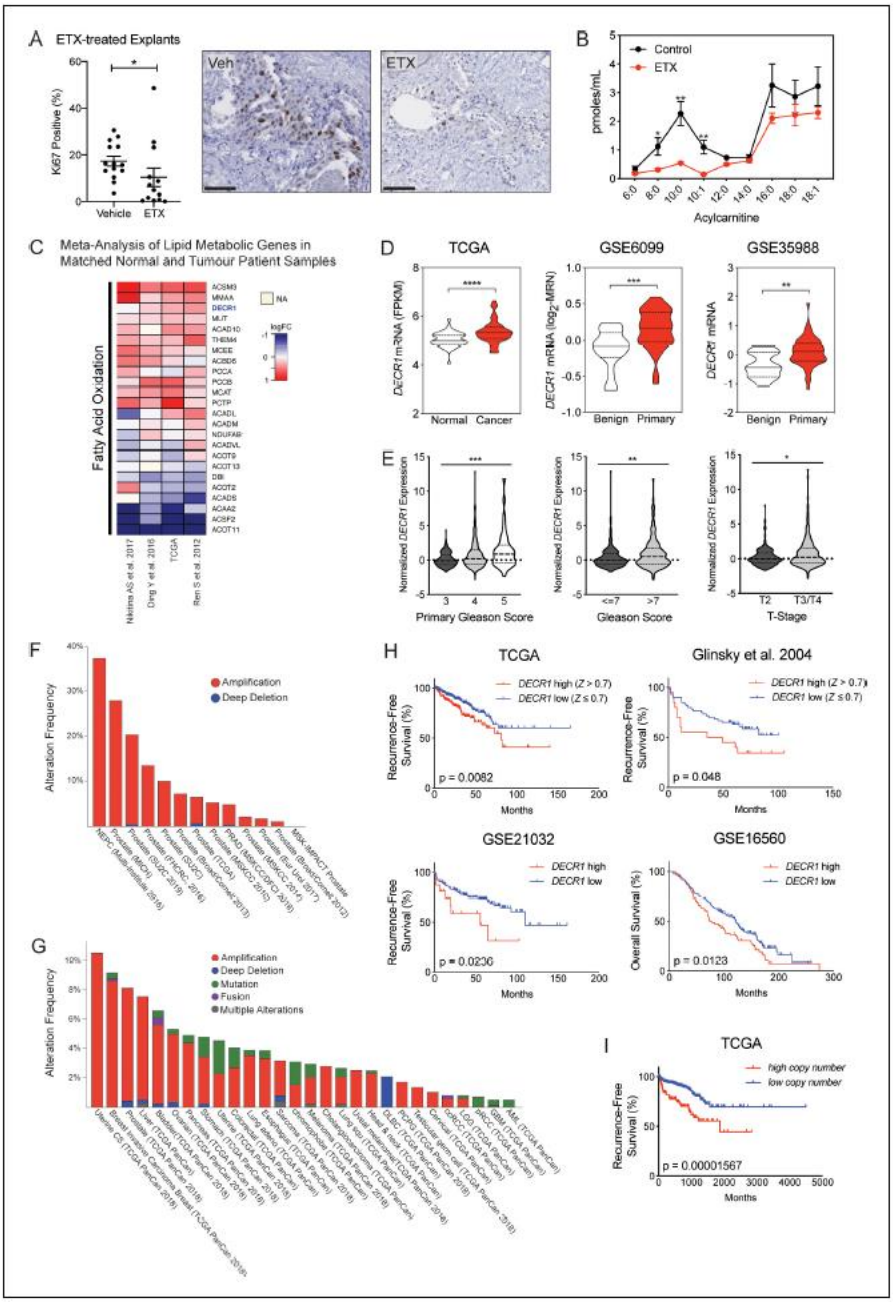

Figure 1. Fatty acid β-oxidation genes are overexpressed in prostate cancer and targeting this process is effective in patient-derived human prostatic ex vivo tumor explants. (**A**) Etomoxir reduced cell proliferation in patient-derived human prostatic ex vivo tumor explants. Tissues were treated with 100 µM etomoxir for 72 hr, sections were fixed in formalin, paraffin embedded and stained against the proliferative marker Ki67 (n = 13) (scale bar = 50 µm). (**B**) Etomoxir (100 µM) decreased acylcarnitine species, the products of CPT1 activity. Acylcarnitines secreted to the conditioned medium were

Figure 1 continued on next page

Figure 1 continued

measured after 72 hr treatment of PDEs (n = 9). (**C**) A meta-analysis of fatty acid oxidation genes using four clinical datasets with malignant and matched normal RNA-sequencing data (n = 122). Genes were rank-ordered on the basis of their *meta effect size* scores in PCa malignant tissues versus matched normal tissues. (**D**) Violin plots demonstrate DECR1 mRNA overexpression in PCa primary/malignant tissues compared to normal/benign tissues in three independent datasets. (**E**) DECR1 mRNA expression is associated with PCa primary Gleason score, total Gleason score (>7) and diseases stage (T-stage). Data were extracted from TCGA PCa dataset. (**F**) Histogram displaying DECR1 mutation and copy-number amplification frequency across 13 PCa genomic datasets, and (**G**) across 28 tumor types. Histograms were obtained from CbioPortal platform. (**H**) DECR1 mRNA expression is associated with shorter relapse-free survival in TCGA PCa, ***Glinsky et al., 2005*** and GSE21032 datasets, and shorter overall survival rates in GSE16560 dataset. (**I**) DECR1 copy number amplification frequency is associated with shorter relapse-free survival in TCGA PCa dataset. Data in (**A**) are represented as as the mean ± s.e.m and were statistically analysed using a Wilcoxon matched-pairs signed rank test. Data in (**B**) are represented as the mean ± s.e.m and were statistically analysed using two-tailed Student's *t*-test. Data in (**D**) and (**E**) are represented as violin plots in GraphPad prism: the horizontal line within the violin represents the median, and were statistically analysed using a Mann-Whitney two-tailed t-test. Data in (**H**) and (**I**) were statistically analysed using a two-sided log-rank test. *p<0.05, **p<0.01, ***p<0.001 and ****p<0.0001.

The online version of this article includes the following figure supplement(s) for figure 1:

Figure supplement 1. Fatty acid metabolism is consistently altered in clinical prostate tumors.

GSE22606). In contrast to the effect of androgens, AR-targeted therapies increase DECR1 expression. LNCaP and VCaP cell treatment with the androgen antagonist enzalutamide (ENZ) significantly increased DECR1 expression at both mRNA and protein levels (***Figure 3B***). In vivo, LNCaP tumors exhibited increased DECR1 expression in mice treated with ENZ (10 mg/kg) or castration, which was enhanced further in mice treated with both ENZ and castration (***Figure 3C***). Our observations were supported by published microarray datasets which showed that treatment of LNCaP or VCaP cells with ENZ increases *DECR1* mRNA expression (***Figure 3—figure supplement 1B***; GSE69249). In vivo, castration of mice increased DECR1 expression in prostate (***Figure 3—figure supplement 1C***; GSE5901), while in LNCaP/AR xenografts treatment with the AR antagonist ARN-509 (apalutamide) for 4 days significantly increased DECR1 expression (***Figure 3—figure supplement 1D***; GSE52169). To confirm androgenic regulation of DECR1 in a clinical context, we validated these data using PDEs. ENZ treatment of PDEs significantly increased DECR1 expression whereas, as expected, mRNA levels of the well-characterized AR target genes *KLK3* and *KLK2* were decreased (***Figure 3D, E***). To determine whether AR directly represses *DECR1*, we interrogated published chromatin immunoprecipitation (ChIP) sequencing data. In VCaP cells, AR bound strongly to the *DECR1* promoter in response to DHT treatment, but not when co-treated with AR antagonists (***Figure 3F***; GSE55064). Moreover, AR binding was enriched at the *DECR1* promoter in benign and malignant prostate tissues (***Figure 3—figure supplement 1E***; GSE56288). A site-specific ChIP-qPCR assay revealed DHT-stimulated AR occupancy at this region in LNCaP cells (***Figure 3G***). Collectively, these data reveal *DECR1* as a novel AR-repressed gene.

Targeting DECR1 disrupts PUFA oxidation in PCa cells

FAs are metabolized mainly in mitochondria through the β-oxidation process to generate acetyl-CoA, which enters the tricarboxylic acid cycle (TCA) and produces ATP and NADH as energy for the cell. Unlike saturated FAs, all unsaturated FAs with double bonds originating at even-numbered positions, and some unsaturated FAs with double bonds originating at odd-numbered positions, require three auxiliary enzymes to generate intermediates that are harmonious with the standard β-oxidation pathway (***Hiltunen and Qin, 2000***; ***Shoukry and Schulz, 1998***): Enoyl CoA isomerase (ECI1), 2,4 Dienoyl-CoA reductase (DECR1) and Dienoyl CoA isomerase (ECH1) (***Figure 4A***). DECR1 catalyses the rate limiting step in this pathway (***Alphey et al., 2005***). Given the critical role of DECR1 in PUFA metabolism, we studied the consequences of DECR1 downregulation on β-oxidation of PUFAs in PCa cells. DECR1 knockdown was achieved successfully (>80% downregulation) using two different siRNAs (***Figure 4B***). DECR1 knockdown resulted in an increase in linoleic acid (***Figure 4C***) as well as an accumulation of 2-trans,4-cis-decadienoylcarnitine (acylcarnitine 10:2; ***Figure 4D***), an intermediate of linoleic acid metabolism, indicating incomplete PUFA β-oxidation. Mitochondrial β-oxidation provides reducing equivalents that drive ATP production. LNCaP cells increased ATP levels in response to exogenous linoleic acid supplementation when cultured in glucose-free media containing the lipase inhibitor diethylumbelliferyl phosphate (DEUP), to prevent the cells from using intracellular FAs (***Figure 4E***). However, cells transfected with DECR1-targeting

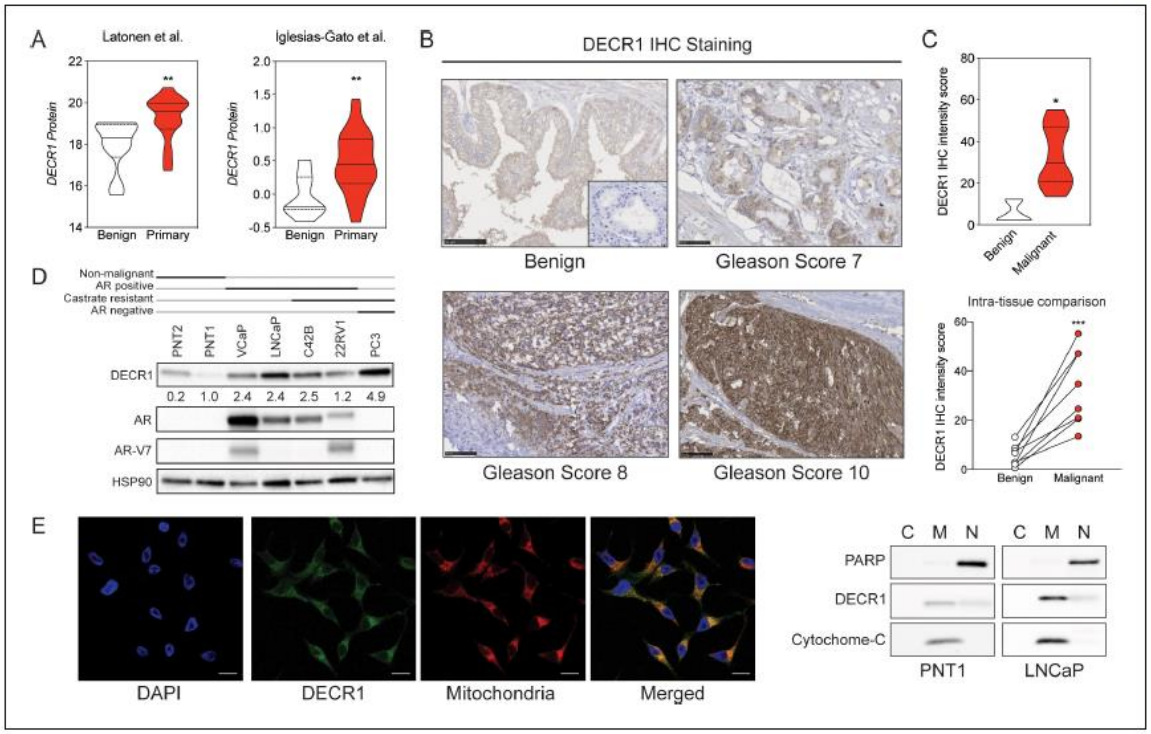

Figure 2. DECR1 protein in overexpressed in malignant prostate cells/tissues. (**A**) Violin plots of DECR1 protein overexpression in primary PCa tissues compared to benign prostate tissues in two independent datasets. (**B**) Representative DECR1 IHC staining of benign prostate tissues and PCa tissues (negative control stain included in bottom right box). Scale bar, 50 µm. (**C**) Violin plot of DECR1 protein expression in a validation cohort consisting of benign prostate tissues (n = 3) and PCa tissues (n = 8) (*top panel*). Intra-tissue IHC analysis of DECR1 expression in PCa tissues (n = 8) (*bottom panel*). (**D**) DECR1 protein expression in non-malignant prostate cell lines (PNT1 and PNT2) and PCa cell lines (LNCaP, VCaP, 22RV1, C42B and PC3). (**E**) Immunocytochemistry staining of LNCaP cells to determine the subcellular localization of DECR1: nuclei were labelled using DAPI; mitochondria were labelled using MitoTracker Red; and DECR1 proteins were labelled using Alexa Fluor 488 secondary antibody, (Scale bar = 10 µm). Immunoblot of PNT1 and LNCaP cells separated into cytosolic, mitochondrial and nuclear fractions and incubated with poly (ADP-ribose) polymerase (PARP) and cytochrome-C antibodies to mark nuclear and mitochondrial fractions. Data are represented as violin plots in GraphPad prism: the horizontal line within the violin represents the median. Statistical analysis was performed using a Mann-Whitney two-tailed t-test (A and C *top panel*), or two-tailed paired t-test (C *bottom panel*): *p<0.05, **p<0.01 and ***p<0.001.

siRNAs failed to increase ATP levels with linoleic acid supplementation (***Figure 4E***), indicating impaired capacity to metabolize PUFAs.

Next, we employed extracellular flux analysis to determine the intrinsic rate and capacity of PCa cells to oxidise PUFAs in conditions where other exogenous substrates were limiting. Exogenous linoleic acid stimulated basal oxygen consumption rates (OCR), as a measure of mitochondrial oxidative phosphorylation, and maximal respiration, ATP production, and mitochondrial spare capacity (***Figure 4F***, ***Figure 4—figure supplement 1A***) as determined by consecutive cell exposure to respiration chain inhibitors and uncouplers. This supports the observed increased in total ATP levels in response to linoleic acid supplementation (***Figure 4E***). Importantly, DECR1 knockdown prevented the exogenous linoleic acid induction of basal and maximal respiration, ATP production, and mitochondrial spare capacity (***Figure 4F***, ***Figure 4—figure supplement 1A***). In contrast, DECR1 knockdown has no impact on mitochondrial metabolism of the saturated FA, palmitate (***Figure 4G***). Further, DECR1 knockdown increased glycolysis, as determined by ECAR (***Figure 4H***, ***Figure 4—figure supplement 1B***), as well as decreased glucose and fructose concentrations (***Figure 4I***), to sustain

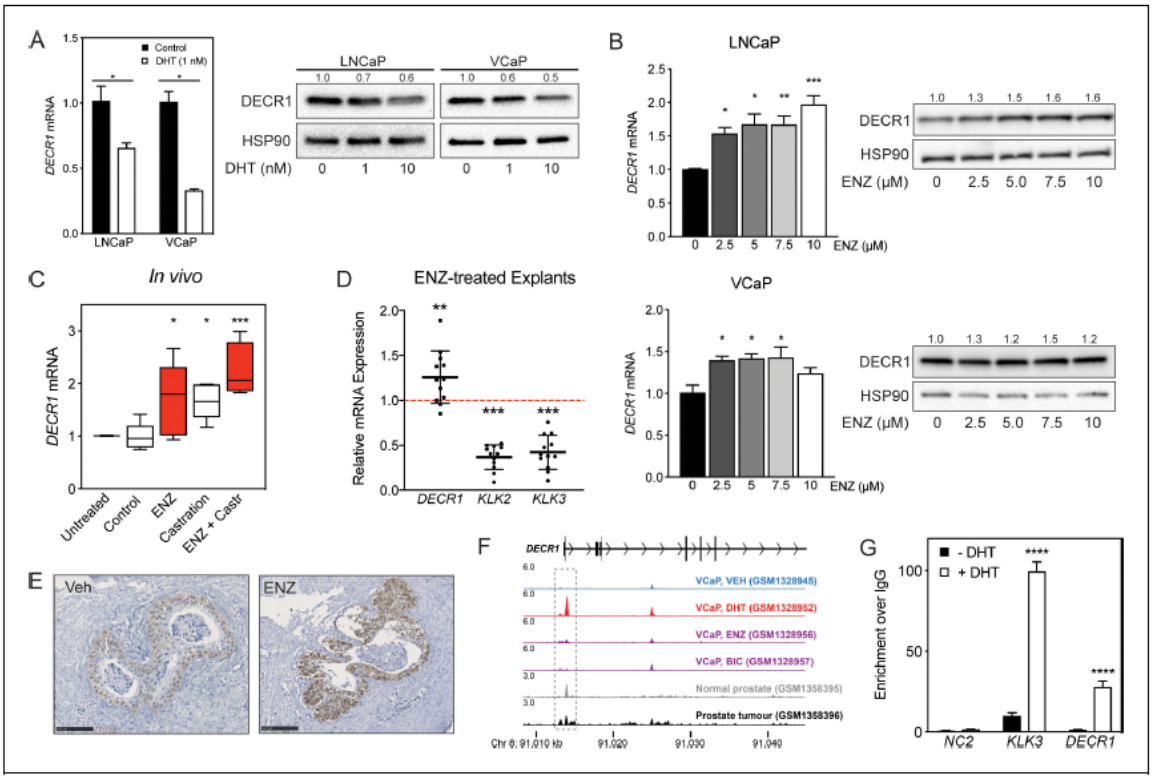

Figure 3. DECR1 is an androgen-repressed gene. (**A**) DECR1 mRNA and protein was measured by qRT-PCR and western blot analysis after PCa cell treatment with dihydrotestosterone (DHT), or (**B**) enzalutamide (ENZ). Relative mRNA expression of *DECR1* was calculated using comparative CT method, where the cells treated with vehicle (control) were set to one and normalised to the geometric mean CT value of *GUSB* and *L19* (housekeeping genes). Densitometry quantification of relative DECR1 protein expression was normalized to the HSP90 internal control. $n = 3$ independent experiments. (**C**) qRT-PCR analysis of *DECR1* mRNA expression in LNCaP-derived tumors treated with enzalutamide (ENZ) and/or castration (Castr). (**D**) qRT-PCR analysis of *DECR1* and androgen regulated genes *KLK2* and *KLK3* mRNA expression in a cohort of 10 patient-derived human prostatic ex vivo tumor explants treated with enzalutamide (ENZ, 10 μM). Relative mRNA expression was calculated using comparative CT method, where the matched untreated tissue from the same patient was set to one and normalized to the geometric mean CT value of *TUBA1B*, *PPIA* and *GAPDH*. (**E**) Representative DECR1 IHC staining of patient-derived human prostatic ex vivo tumor explants treated with enzalutamide (ENZ, 10 μM). Scale bar, 100 μm. (**F**) AR ChIP-sequencing data from VCaP cells (top panel), normal human prostate and primary human prostate tumor specimens (bottom panel). Data from GSE55064 and GSE56288. (G) ChIP-qPCR analysis demonstrates AR binding at *DECR1* locus in LNCaP cells after treatment with DHT. Data in bar graphs (A, B and G) are represented as the mean ± s.e.m. Data in (**C**) are represented as box plots using the Tukey method in GraphPad prism. Statistical analysis was performed using two-tailed Student's *t*-test (A, C, D and G) or one-way ANOVA, followed by Dunnett's multiple comparisons test (**B**): *p<0.05, **p<0.01, ***p<0.001 and ****p<0.0001.

The online version of this article includes the following figure supplement(s) for figure 3:

Figure supplement 1. Androgenic regulation of DECR1 expression.

TCA cycle intermediate levels (***Figure 4J***) as a consequence of disruption of PUFA β-oxidation. While DECR1 exhibited selectivity in inhibition of PUFA metabolism, as expected, etomoxir inhibited both PUFA and saturated fatty acids (***Figure 4—figure supplement 1C***). There was no effect of ETX treatment on DECR1 expression (***Figure 4—figure supplement 1D***). Collectively, these results demonstrate that DECR1 is critical for PUFA metabolism in LNCaP PCa cells.

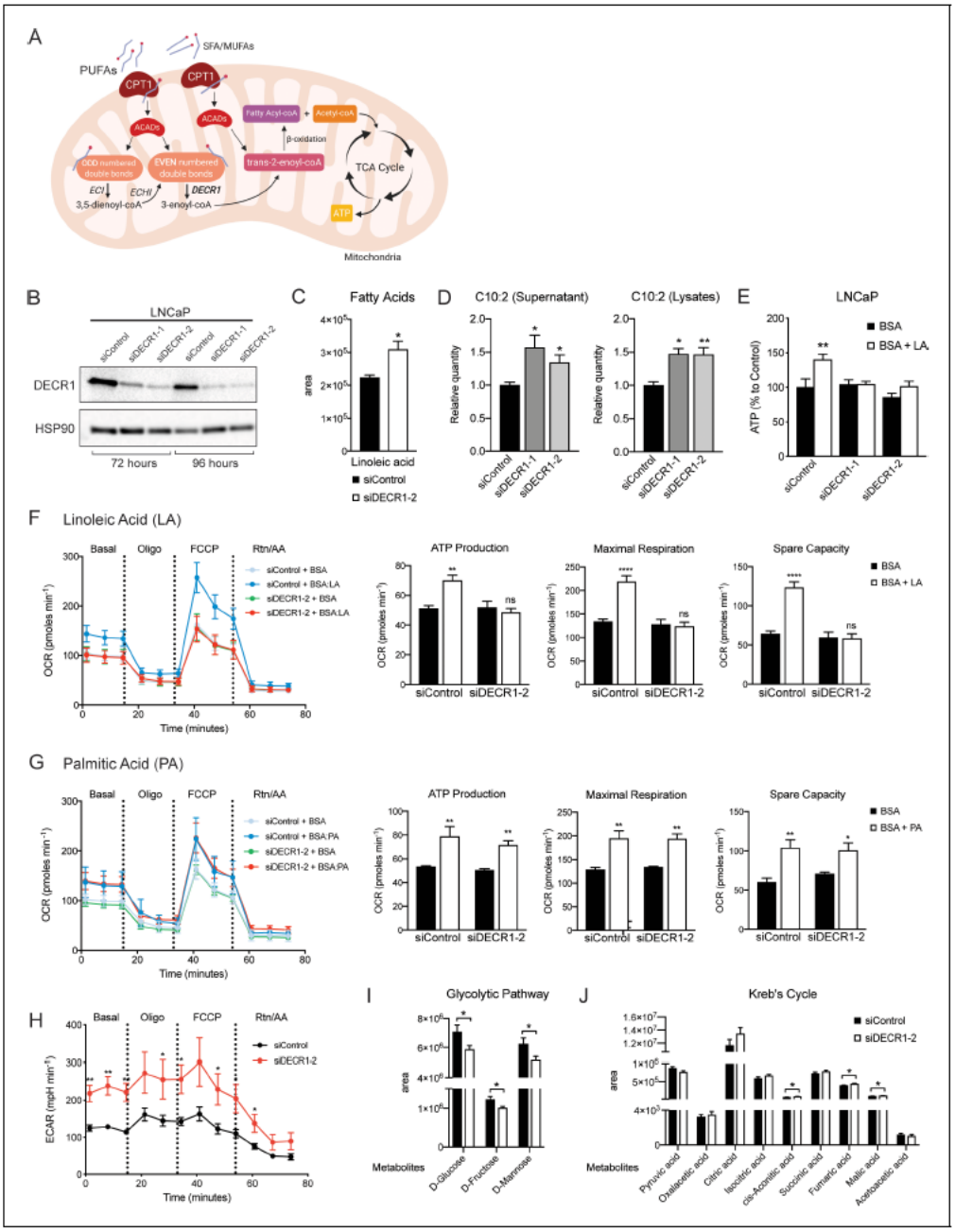

Figure 4. DECR1 knockdown interrupts PUFA β-oxidation in PCa cells. (**A**) Schematic of DECR1 function in fatty acid (FA) β-oxidation. In order to translocate FAs into the mitochondria, CPT1 converts long-chain acyl-CoA species to their corresponding long-chain acylcarnitine species. This is followed by a dehydrogenation step mediated by acyl CoA dehydrogenase (ACAD) to generate trans-2-enoyl-CoA, the only intermediate that can be processed by downstream enzymes in the β-oxidation process. Many FAs have unsaturated bonds either on an odd-numbered carbon or in the cis-

Figure 4 continued on next page

Figure 4 continued

configuration, resulting in the generation of enoyl-CoA intermediates that cannot be directly processed via the downstream β-oxidation enzymes. These FAs require the activity of 3 auxiliary enzymes, ECI1, ECH1 and DECR1 in order to form trans-2-enoyl-CoA before undergoing β-oxidation. DECR1 catalyzes the conversion of either 2-trans,4-cis-dienoyl or 2-trans,4-trans-dienoyl-CoA to 3-trans-enoyl-CoA. A complete cycle of β-oxidation results in the release of the first two carbon units as acetyl-CoA, and a fatty-acyl-CoA minus two carbons. The acetyl-CoA enters the TCA cycle to produce energy (ATP). The shortened fatty-acyl-CoA is processed again starting with the ACADs to form trans-2-enoyl-CoA either directly or with the aid of the auxiliary enzymes depending on the presence of double bonds. This process continues until all carbons in the fatty acid chain are turned into acetyl-CoA. (**B**) DECR1 protein expression after 72 hr or 96 hr siRNA transfection. Densitometry quantification of relative DECR1 protein expression was normalized to the HSP90 internal control. (**C**) Linoleic acid level in LNCaP cells quantified in following 96 hr DECR1 knockdown using GC QQQ targeted metabolomics. (**D**) Relative quantities of the C10:2 acylcarnitine species in LNCaP cell conditioned medium (left) or cell lysates (right) (n = 3). (**E**) Quantification of ATP levels in LNCaP cell lysates. LNCaP cells were transfected with DECR1 siRNAs for 48 hr and then starved in no-glucose medium and treated with the lipolysis inhibitor DEUP (100 μM) in the presence (BSA-LA) or absence (BSA) of the PUFA linoleic acid for 48 hr before measuring ATP levels. (**F**) Oxygen consumption rate (OCR) was assessed in LNCaP cells supplemented with the PUFA linoleic acid (LA) or (**G**) the saturated fatty acid palmitic acid (PA). Each data point represents an OCR measurement. ATP production, maximal mitochondrial respiration and mitochondrial spare capacity were assessed. (**H**) Extracellular acidification rate (ECAR) was assessed in LNCaP cells. Each data point represents an ECAR measurement. For experiments (**F-H**) LNCaP cells were transfected with DECR1 siRNAs for 72 hr, then starved in substrate limited medium for 24 hr; the assay was run in FAO assay medium. (**I and J**) Metabolites were quantified in LNCaP cells following 96 hr DECR1 knockdown using GC QQQ targeted metabolomics. Data in bar graphs are represented as the mean ± s.e.m (n = 3). Statistical analysis was performed using two-tailed Student's *t*-test: *p<0.05, **p<0.01 and ****p<0.0001.

The online version of this article includes the following figure supplement(s) for figure 4:

Figure supplement 1. Effects of DECR1 on prostate cancer cellular metabolism.

Targeting DECR1 suppresses PCa oncogenesis

The consistently increased expression of DECR1 in PCa tissue and its association with shorter-relapse times and survival rates (***Figure 1*** and ***2***), taken together with its impact on PUFA metabolism (***Figure 4***), suggested that it may contribute to PCa cell viability and invasive behaviour. We evaluated the impact of DECR1 downregulation or overexpression on various oncogenic properties of PCa cells using a series of in vitro and in vivo experiments. While there was no effect of DECR1 downregulation on the non-malignant prostate cell line PNT1, a significant attenuation of PCa proliferation and induction of cell death was observed in a panel of PCa lines (***Figure 5A***), comprising androgen-dependent (VCaP and LNCaP), CRPC (22RV1 and V16D) and acquired ENZ-resistant cells (MR49F). Notably, this effect on PCa cell viability was lost when cells were cultured in lipid-depleted media (***Figure 5—figure supplement 1***), suggesting that the observed effect is due to interference with FA metabolism. Likewise, stable DECR1 knockdown using a short hairpin vector attenuated LNCaP cell line viability and induced cell death (***Figure 5B***) In contrast, stable DECR1 overexpression significantly enhanced LNCaP cell viability (***Figure 5C***) and colony formation ability (***Figure 5D***), while stable DECR1 knockdown markedly decreased colony formation (***Figure 5E***). DECR1 knockdown also decreased LNCaP growth in 3D spheroids (***Figure 5F***), which better mimic in vivo conditions than 2-dimensional cell culture (***Duval et al., 2017***). In addition, DECR1 knockdown reduced LNCaP, 22RV1 and MR49F cell migration by ~50% (***Figure 5G***) and 22RV1 invasion by ~65% (***Figure 5H***). In vivo, LNCaP cells stably depleted of DECR1 showed highly variable growth rates in a subcutaneous model (***Figure 5—figure supplement 2A***), but inspection of the resultant tumors revealed significantly reduced cellular proliferation compared to control cells, concomitant with reduced DECR1 expression (***Figure 5I***, ***Figure 5—figure supplement 2B***). To study the effect of DECR1 downregulation on PCa in the prostate microenvironment, we undertook a second study using LNCaP orthotopic xenografts. DECR1 knockdown significantly retarded tumor growth (***Figure 5K***, (***Figure 5—figure supplement 2C,D,E***), and significantly inhibited lung metastasis in the orthotopic tumor model (***Figure 5L***).

DECR1 targeting induces lipid peroxidation and cellular ferroptosis

DECR1 knockdown resulted in inhibition of PUFA β-oxidation and led to accumulation of PUFAs in phospholipids (***Figure 6A***). Inspection of the phospholipid profile revealed accumulation of PUFAs in the PC, PI and PS classes (***Figure 6B***) with no impact on total saturated or MUFA phospholipids (***Figure 6—figure supplement 1A***). PUFA are highly susceptible to peroxidation, so we next assessed the effect of DECR1 knockdown on lipid peroxidation. DECR1 knockdown increased levels of

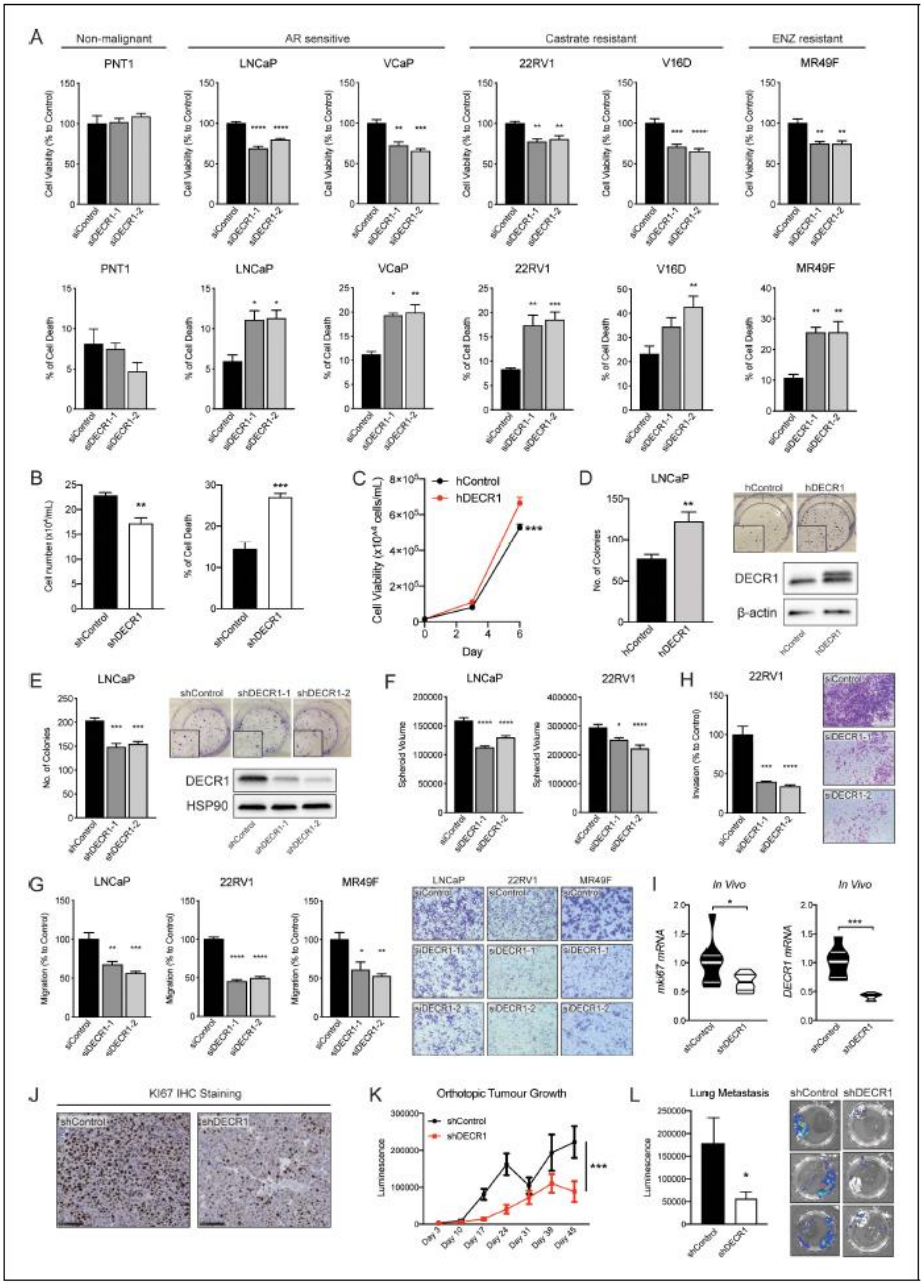

Figure 5. DECR1 knockdown suppresses oncogenic phenotypes of PCa cells. (**A**) Cell viability after DECR1 knockdown in non-malignant PNT1 prostate cells; hormone-responsive PCa cell lines (LNCaP and VCaP); castrate-resistant V16D and 22RV1 cell lines and enzalutamide-resistant MR94F cells cultured in full serum media. (**B**) Cell viability and cell death of stable DECR1 knockdown LNCaP cells cultured in full serum media. (**C**) Cell viability of stable DECR1-overexpressed LNCaP cells cultured in full serum media. Cell viability and cell death were measured using trypan blue exclusion

Figure 5 continued on next page

Figure 5 continued

following 96 hr DECR1 knockdown. Percentages are represented relative to the control siRNA; *n* = 3 independent experiments per cell line. (**D**) Clonogenic cell survival of LNCaP cells was assessed using colony formation assay. Stable DECR1-overexpressed cells or (**E**) stable DECR1 knockdown was achieved using two different short hairpin (sh) vectors and DECR1 expression was confirmed using western blot. Cells were cultured for 2 weeks, washed with PBS, fixed with paraformaldehyde and stained with 1% crystal violet for 30 min. Colonies with more than 50 cells were counted manually; data shown is representative of *n* = 2 independent experiments. (**F**) LNCaP and 22RV1 cell growth in 3D spheres. Spheroids were prepared using the hang drop assay following 48 hr DECR1 knockdown. Spheroid volumes were determined after five days of culturing the cells in 20 µl drops; at least 25 spheres per cell line were assessed using the ReViSP software, *n* = 3 independent experiments per cell line. (**G**) LNCaP, 22RV1 and MR49F cell migration and (**H**) 22RV1 cell invasion were assessed using a transwell migration/invasion assay. Cells were transfected with DECR1 siRNA or control siRNA for 48 hr prior to the assay; data shown is representative of *n* = 3 independent experiments. (**I**) Violin plots of mKi67 and DECR1 mRNA expression in subcutaneous LNCaP tumors (n = 5 mice, shControl; n = 4 mice, shDECR1). (**J**) Representative Ki67 IHC staining of subcutaneous LNCaP tumors. Scale bar, 100 µm. Data in bar graphs are represented as the mean ± s.e.m. Statistical analysis was performed using one-way ANOVA, followed by Dunnett's multiple comparisons test: *p<0.05, **p<0.01, ***p<0.001 and ****p<0.0001. (**K**) Tumor growth of intraprostatically injected LNCaP cells (shControl and shDECR1). (J) Lung luminescence readings following DECR1 knockdown in mice. Data are presented as mean ± s.e.m. Statistical analysis was performed using two-way ANOVA or two-tailed student's t-test: *p<0.05 and ***p<0.001.

The online version of this article includes the following figure supplement(s) for figure 5:

Figure supplement 1. Depletion of extracellular lipids prevents antiproliferative effects of DECR1 in prostate cancer cells.

Figure supplement 2. DECR1 suppresses growth of prostate tumor xenografts in mice.

Figure supplement 3. The sequence of the DECR1 shRNA and hDECR1 vectors.

malondialdehyde, a marker of lipid peroxidation (***Gaweł et al., 2004***; ***Figure 6C***). In contrast, DECR1 overexpression markedly decreased cellular malondialdehyde levels (***Figure 6C***). We observed enhanced mitochondrial oxidative stress measured using MitoSOX, a mitochondrial superoxide indicator (***Figure 6D***), in response to DECR1 knockdown. Moreover, DECR1 knockdown resulted in significant accumulation of phospholipid hydroperoxides, a hallmark of ferroptosis (***Figure 6E***). In contrast, DECR1 overexpression significantly decreased mitochondrial oxidative stress under basal (***Figure 6F***) and linoleic acid-induced conditions (***Figure 6G***). Lipid peroxidation is a major driver of ferroptosis, an iron-dependent non-apoptotic form of cell death (***Dixon et al., 2012***). Cell treatment with the ferroptosis inhibitors, deferoxamine or ferrostatin, abolished the effect of DECR1 knockdown on PCa cell death (***Figure 6H–I***), while cell treatment with the ferroptosis inducers, erastin, FIN56 or ML210, enhanced the cytotoxic action of DECR1 downregulation (***Figure 6J–K***, ***Figure 6—figure supplement 1B***). Supporting ferroptosis as the cell death mechanism, DECR1 knockdown did not induce apoptosis (***Figure 6—figure supplement 2A***), and the apoptosis inhibitor ZVAD did not rescue the cells from cell death induced by DECR1 depletion (***Figure 6—figure supplement 2B***). Collectively, these results suggest that DECR1 expression protect cells from oxidative stress and that DECR1 knockdown-induced cell death is primarily mediated by induction of ferroptosis.

Discussion

Metabolic rewiring is both a hallmark feature of cancer cells and a promising therapeutic vulnerability. Several anabolic and catabolic metabolism pathways have been explored, however, few agents have been investigated clinically. This can at least partly be explained by the relatively recent appreciation of cancer metabolism as a target, the high toxicity, particularly hepatotoxicity, expected to be associated with targeting certain metabolic pathways, the predictable metabolic heterogeneity within and between patients and the lack of intermediate pre-clinical models that can predict clinically efficacious outcomes. Previous research has largely focused on studying and targeting FA synthetic pathways in PCa. Major lipogenic enzymes such as ATP citrate lyase (ACLY), acetyl-CoA carboxylase (ACC) and fatty acid synthase (FASN) are all overexpressed in PCa compared to benign tissue (***Wu et al., 2014***; ***Rossi et al., 2003***; ***Shurbaji et al., 1996***). While many first-generation FA synthesis inhibitors (e.g. FASN inhibitors) showed promising preclinical efficacy against PCa, unfavorable drug solubility and pharmacokinetics profiles, off-target effects and side effects including weight loss have hindered clinical development of this agent class (***Zadra et al., 2013***). In addition to de novo synthesis of FAs, PCa cells depend on lipid uptake from the circulation, and from stromal adipocytes (***Watt et al., 2019***; ***Kuemmerle et al., 2011***; ***Gazi et al., 2007***). We showed previously that extracellular FAs are the major contributor to lipid synthesis in PCa (***Balaban et al., 2019***).

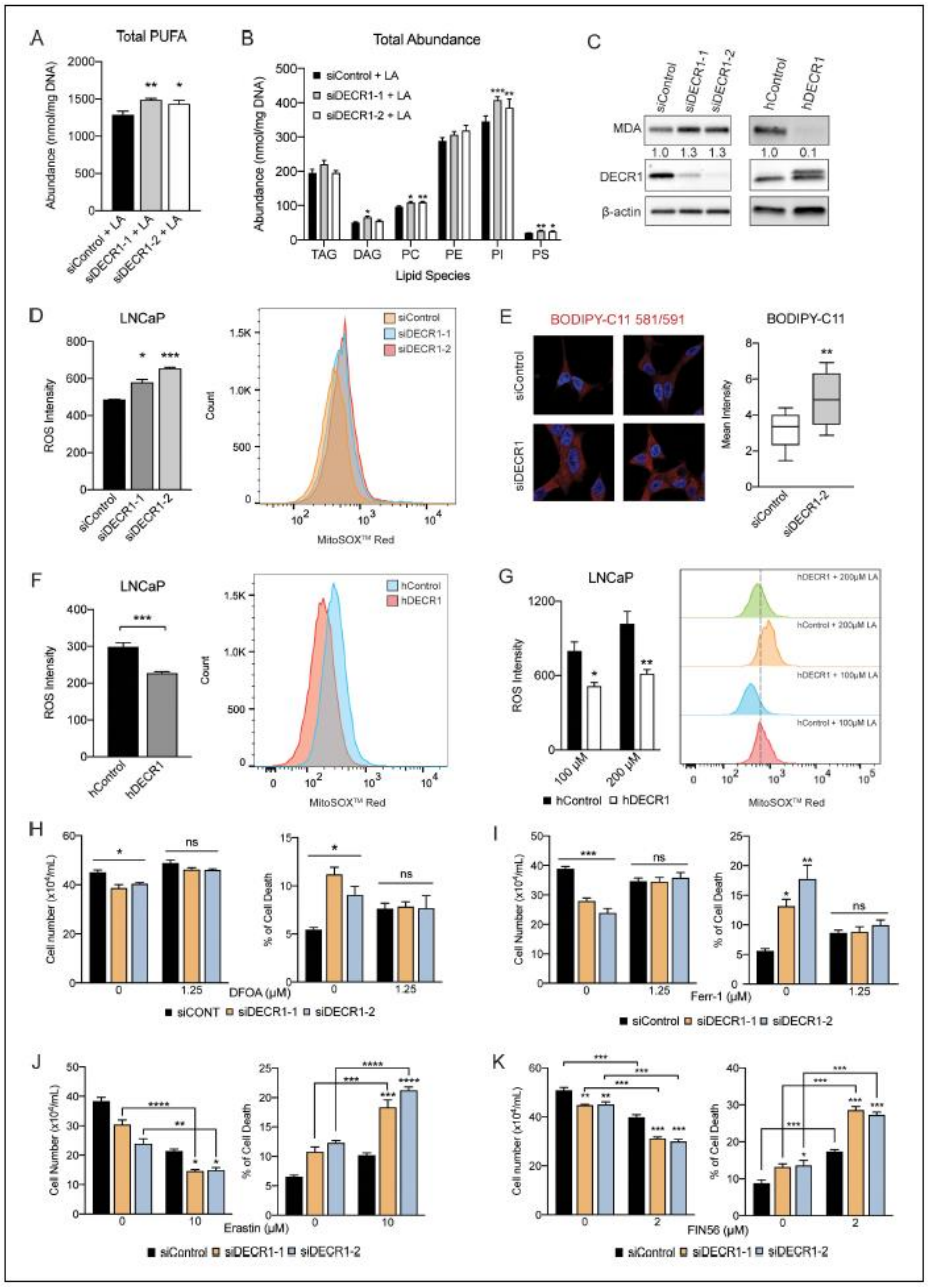

Figure 6. DECR1 knockdown induces PUFA accumulation, lipid peroxidation and ferroptosis. (**A**) Abundance of total PUFAs and (**B**) total abundance of lipid species in phospholipids from control and DECR1 knockdown cells supplemented with linoleic acid (LA). (**C**) Malondialdehyde (MDA), an oxidative stress marker, was measured by western blot in LNCaP cells transfected with DECR1 siRNAs and in DECR1-overexpressed LNCaP cells. (**D**) Mitochondrial superoxide levels were quantified following 96 hr DECR1 knockdown using MitoSOX red stain. Fluorescent intensity was quantified using

Figure 6 continued on next page

Figure 6 continued

flow cytometry and ROS levels presented as mean fluorescent intensity. (**E**) Fluorescent images of BODIPY-C11 stained LNCaP cells following DECR1 knockdown (left). Fluorescent intensity was quantified using ImageJ and presented as mean fluorescent intensity (right). (F) Mitochondrial superoxide levels were quantified in stable DECR1-overexpressing LNCaP cells using MitoSOX red stain under basal or (**G**) linoleic acid (100 µM or 200 µM) conditions. Fluorescence intensity was quantified using flow cytometry and ROS levels were presented as mean fluorescent intensity. Cell viability of LNCaP cells after 48 hr DECR1 knockdown, treated with (**H**) deferoxamine (DFOA, 1.25 µM), (I) ferrostatin (Ferr-1, 1.25 µM), (J) erastin (10 µM), or (**K**) FIN56 (2 µM). Data in bar graphs are represented as the mean ± s.e.m. Statistical analysis was performed using two-tailed Student's *t*-test (**A-G**) or one-way ANOVA, followed by Holm-Sidak's multiple comparisons test (**H-K**): ns, not significant, *p<0.05, **p<0.01, ***p<0.001 and ****p<0.0001. TAG: triacylglycerol; DAG: diacylglycerol; PC: phosphotidylcholine; PE: phosphotidylethanolamine; PI: phosphatidylinositol; PS: phosphotidylserine.
The online version of this article includes the following figure supplement(s) for figure 6:

Figure supplement 1. Depletion of DECR1 sensitizes prostate cancer cells to ferroptosis inducing agents.
Figure supplement 2. Targeting DECR1 does not induce apoptosis of prostate cancer cells.

Moreover, targeting FA uptake using an antibody against CD36, a major transporter for exogenous FAs into the cells, reduced cancer severity in patient-derived xenografts, and *CD36* deletion slowed cancer progression in prostate-specific *PTEN*$^{-/-}$ mice. However, it is increasingly evident that PCa exhibits plasticity in attaining FAs and that crosstalk between de novo synthesis and FA uptake requires dual targeting of the two pathways to achieve maximal efficacy (***Watt et al., 2019***), an approach that would likely be associated with greater toxicity. In this study, we focused on another understudied aspect of FA metabolism in PCa, β-oxidation, to evaluate its therapeutic potential.

We showed previously (***Balaban et al., 2019***), as have others (***Schlaepfer et al., 2014***; ***Schlaepfer et al., 2015***), that PCa cells exhibit increased FAO compared to prostate epithelial PNT-1 cells, or benign epithelial cells BPH-1 and WPMY-1. This metabolic phenotype is a vulnerability for PCa cells (***Schlaepfer et al., 2014***; ***Itkonen et al., 2017***; ***Flaig et al., 2017***). FAO inhibitors such as etomoxir, perhexiline or ranolazin inhibited tumor growth in vitro and in vivo (***Schlaepfer et al., 2014***; ***Itkonen et al., 2017***; ***Flaig et al., 2017***) and sensitized cells to ENZ treatment (***Itkonen et al., 2017***; ***Flaig et al., 2017***). However, all of these studies were undertaken using immortalized cell line models of PCa, and as cancer metabolism is markedly influenced by the tumor microenvironment (***Martinez-Outschoorn et al., 2012***; ***Nieman et al., 2011***; ***Nassar et al., 2018***), employing preclinical models and primary tissues that retain the complexity of this microenvironment as a stepping stone to clinical trials may accelerate clinical translation and avoid futile targeting strategies or agents. In this study, we evaluated the efficacy of the FAO inhibitor, etomoxir, using our established PDE model. Remarkably, etomoxir inhibited effectively cell proliferation in PDEs (***Figure 1A***), strengthening the case that targeting FA oxidation may be a promising clinical strategy. Interestingly, etomoxir was more potent in inhibition of cell proliferation in PDEs than in vitro 2-dimensional growth of LNCaP cells, emphasizing that in vitro models based on 2D cultured cells alone are suboptimal when evaluating anti-metabolism agents. This problem is compounded by the fact that standard growth media is rich in sugar and proteins, but contains low levels of lipids. As the clinical development of etomoxir was terminated due to severe hepatotoxicity associated with treatment (***Holubarsch et al., 2007***), we sought to identify new β-oxidation targets in PCa. As DECR1 is a directly androgen-repressed gene, its expression increases after castration or treatment with anti-androgens and is hypothesized to maintain tumor cell survival under castration conditions. Androgen-repressed genes are markedly understudied compared with androgen-induced genes, despite the fact that they possibly mediate adaptive survival pathways when androgen signalling is perturbed, and have already yielded novel therapeutic targets (***Kregel et al., 2013***; ***Tse et al., 2017***).

Surprisingly, very little is known about the biological role of DECR1 in cancer. Human DECR1 deficiency is lethal, with patients exhibiting hypocarnitinemia, decreased cellular oxygen consumption, increased lactic acidosis, and unusual accumulation of FA intermediates in urine and blood due to incomplete β-oxidation (***Roe et al., 1990***; ***Houten et al., 2014***). DECR1-null mice exhibit impaired lipid metabolism, hypoglycemia and activation of ketogenesis, and cold intolerance (***Miinalainen et al., 2009***; ***Mäkelä et al., 2019***). These phenotypes highlight the critical role of DECR1 in lipid metabolism. We confirmed the metabolic activities of DECR1 in PCa cells using a panel of metabolomic and lipidomic analyses. DECR1 knockdown increased levels of certain acylcarnitine species, indicating inhibition of β-oxidation. These results are consistent with previous studies reporting acylcarnitine accumulation in *Decr1*$^{-/-}$ mice and *DECR1*-deficient patients (***Roe et al.,***

1990; Miinalainen et al., 2009). We showed that DECR1 knockdown selectively inhibited PUFA catabolism, accompanied by an increase in glycolysis rate, which is also consistent with previous reports of FAO inhibition or impaired mitochondrial function leading to enhanced glucose uptake and glycolysis (Schlaepfer et al., 2015; Houten et al., 2014). Lipidomic analysis showed that DECR1 knockdown increased the abundance of PUFAs and certain lipids, particularly PE and PI phospholipid species, accompanied by increased levels of mitochondrial oxidative stress and particularly lipid peroxidation. In contrast to MUFAs, PUFAs are highly susceptible to peroxidation, thereby enhancing free radical generation and accumulation of toxic lipid peroxides (Das, 2011; Magtanong et al., 2019). Consistent with a role for PUFA oxidation in DECR1 function, ectopic DECR1 overexpression decreased mitochondrial oxidative stress. An important cellular protective response to excess intracellular lipid peroxides is the induction of ferroptosis, an iron-dependent form of cell death that is triggered by lipid peroxidation. Here, we show that the ferroptosis inhibitors ferrostatin and deferoxamine or the ferroptosis inducers erastin, FIN56 and ML210 abolished and augmented the effect of DECR1 on PCa cell death, respectively. These findings are consistent with a mechanism by which DECR1 knockdown-induced cell death is a ferroptosis-mediated process caused by PUFA accumulation, a conclusion that was independently validated in human prostate cancer during revision of this article (Blomme et al., 2020). It is therefore possible that PCa cells commonly select for DECR1 overexpression, not only to enhance ATP production to fulfil energy requirements, but also to protect cells from the tumoricidal effects of excess PUFAs.

PUFAs are essential FAs that cannot be synthesized in mammals and are only obtained from the diet. Dietary fat not only promotes obesity, but also PCa progression and disease aggressiveness. Several preclinical PCa studies have compared high-fat (or Western-style diets) versus low fat diet and reported that the former promotes AKT and ERK activity, tumor growth, tumor incidence in genetically engineered/transgenic mouse models, tumor progression to CRPC and metastasis (reviewed in Narita et al., 2019). Clinical case-control studies indicated saturated fat is associated with an increased risk of advanced PCa (Bairati et al., 1998; Stéfani et al., 2000; Slattery et al., 1990; Whittemore et al., 1995). Several underlying mechanisms were proposed to explain the association between dietary fat and PCa development and progression, including growth factor signalling (such as IGF-1), inflammation, and endocrine modulation (Narita et al., 2019). While the evidence supporting the negative impacts of saturated dietary FAs are more consistent, the effect of dietary PUFAs on PCa aggressiveness remains inconclusive and differences between omega-3 and omega-6 have been reported (Bairati et al., 1998; Stéfani et al., 2000; Park et al., 2009; Fu et al., 2015). In contrast to omega-3 PUFAs, which are reported to inhibit PCa progression (Wang et al., 2012), omega-6 PUFAs (Khankari et al., 2016; Brown et al., 2010), and higher omega-6/omega-3 PUFA ratio, increase PCa risk (Williams et al., 2011; Apte et al., 2013). Dietary intervention by decreasing total fat intake and increasing omega-3 PUFAs was found to improve PCa survivorship (Epstein et al., 2012; Colli and Colli, 2005; Davies et al., 2011; Ornish et al., 2005). It is unclear whether there is a preference for n-6 or n-3 PUFA β-oxidation in PCa cells, however both require DECR1 for complete β-oxidation.

Although FAO is a complex process that requires the activity of several enzymes, to date the entire focus of drug development strategies has been inhibitors against CPT1, the rate-limiting step of FA β-oxidation. CPT1 is responsible for synthesizing fatty acyl-carnitines from fatty acyl-CoAs which are then transported from the cytoplasm into the mitochondria by carnitine acylcarnitine translocase for subsequent processing then entry into the β-oxidation pathway. Even though targeting CPT1 is efficient in inhibiting FA β-oxidation, the clinical use of CPT1 inhibitors is challenging. Based on our current findings, we propose that DECR1 is an attractive alternative target to CPT1. CPT1 inhibition would suppress β-oxidation of all long FA species (saturated FA, MUFA and PUFA), whilst in contrast DECR1 is specific for PUFA. Homozygous *CPT1* deficiency, of either the liver or muscle isoform, is lethal in mice (Nyman et al., 2005; Ji et al., 2008; Haynie et al., 2014), but *Decr1*$^{-/-}$ mice are viable, and clinical symptoms arose only after metabolic stress (Miinalainen et al., 2009; Mäkelä et al., 2019). The marked overexpression of DECR1 in prostate tumors across multiple clinical cohorts, potentially coupled to PUFA-related dietary interventions, may lend further selectivity to targeting strategies. Of note, the crystal structure of DECR1 active site has been solved (Alphey et al., 2005), and thus developing DECR1 inhibitors is feasible.

In summary, herein we strengthen the evidence base for the critical importance of FAO and, specifically, PUFA oxidation in PCa, thereby identifying a promising new therapeutic candidate, DECR1.

Materials and methods

Meta-Analysis of lipid metabolism genes

Individual RNA-sequencing (RNA-seq) datasets composed of matched normal versus tumor prostate cancer patient tissue samples were acquired and are listed as follows: (**Bray et al., 2018**) The Cancer Genome Atlas (TCGA, n = 53); (**Huggins and Hodges, 1941**) Nikitina AS et al. (GSE89223, n = 10) (**Nikitina et al., 2017**; **Tran et al., 2009**) Ren S et al. (n = 14) (**Ren et al., 2012**; and (**Cai and Balk, 2011**) Ding Y et al. (GSE89194, n = 45) (**Ding et al., 2016**). Before the meta-analysis, RNA-seq data was quality controlled and analysed using the R limma voom-*eBayes pipeline* (**Law et al., 2016**). Effect sizes (log-fold changes) and corresponding variances were collected from the differential expression analysis under the matched-pairs design. Meta-analysis was performed by applying a restricted maximum-likelihood estimator (REML) within a random-effects model using the *rma* function from the R *metafor* package. At most one missing observation out of four was allowed per gene. Next, the retained genes were intersected with the list of pre-selected 735 genes involved in lipid metabolism as identified from REACTOME. Finally, the remaining genes were rank-ordered on the basis of their *meta effect size* scores across all four RNA-seq datasets. Top 20 candidate genes were selected for further disease-free survival association analyses from well-characterized clinical cohorts.

Clinical datasets

Transcriptomic data was downloaded from The Cancer Genome Atlas (TCGA) data portal, cBioPortal (**Cerami et al., 2012**), and GEO; GSE21032 **Taylor et al., 2010**; GSE35988 **Grasso et al., 2012**; GSE6099 **Tomlins et al., 2007**; GSE16560 (**Sboner et al., 2010**). Proteomics data was extracted from **Iglesias-Gato et al., 2018**.

Cell lines and tissue culture

The human normal prostate epithelial cell lines PNT1 and PNT2 were obtained from the European Collection of Authenticated Cell Cultures (ECACC), and prostate carcinoma cells LNCaP, VCaP, and 22RV1 were obtained from the American Type Culture Collection (ATCC; Rockville, MD, USA). Castrate resistant V16D and enzalutamide resistant MR49F cells were derived through serial xenograft passage of LNCaP cells (**Toren et al., 2016**) were a kind gift from Prof. Amina Zoubeidi laboratory. Cell lines were verified in 2018 via short tandem repeat profiling (Cell Bank Australia). Cell lines were maintained in RPMI-1640 medium containing 10% fetal bovine serum (FBS; Sigma-Aldrich, NSW, Australia) in 5% CO_2 in a humidified atmosphere at 37˚C. Prior to androgen treatment, cells were seeded in medium supplemented with 5% dextran charcoal coated FBS (DCC-FBS) and after 24 hr, 1 nM or 10 nM of dihydrotestosterone (DHT) was added. For anti-androgen treatment, cells were cultured in growth medium supplemented with 2.5 µM, 5 µM, 7.5 µM or 10 µM Enzalutamide (dissolved in dimethyl sulfoxide, DMSO; Sigma Aldrich). The sources and experimental conditions for primary antibodies used in this study are listed in the Key Resources Table. Primers were obtained from Sigma-Aldrich and their sequences are detailed in the Key Resources Table.

Ex vivo culture of human prostate tumors

Patient derived-explant culture was carried out according to techniques established in our laboratory and as described previously (**Armstrong et al., 2016**; **Centenera et al., 2018**; **Centenera et al., 2013**). 6 mm/8 mm biopsy cores were collected from men undergoing robotic radical prostatectomy at St. Andrew's Hospital (Adelaide, South Australia) with written informed consent through the Australian Prostate Cancer BioResource. The tissue was dissected into smaller 1 mm^3 pieces and cultured on Gelfoam sponges (80 × 125 mm Pfizer 1205147) in 24-well plates pre-soaked in 500 µl RPMI-1640 with 10% FBS, antibiotic/antimycotic solution. Etomoxir (100 µM) or Enzalutamide (10 µM) was added into each well and the tissues were cultured in 5% CO_2 in a humidified atmosphere at 37˚C for 48 hr, then snap frozen in liquid nitrogen and stored at −80˚C, or formalin-fixed and paraffin-embedded.

Immunohistochemistry (IHC)

Paraffin-embedded tissue sections (2–4 µm) were deparaffinized in xylene, rehydrated through graded ethanol, and blocked for endogenous peroxidase before being subjected to heat-induced epitope retrieval (**Armstrong et al., 2016**). IHC staining was performed using DECR1 (HPA023238, Sigma Aldrich, diluted 1:500) antibody and the 3,3′-Diaminobenzidine (DAB) Enhanced Liquid Substrate System tetrahydrochloride (Sigma Aldrich) as described previously (**Armstrong et al., 2016**). Intensity of DECR1 immunostaining was measured by video image analysis (**Armstrong et al., 2016**).

Western blotting

Protein lysates were collected in RIPA lysis buffer (10 mM Tris, 150 mM NaCl, 1 mM EDTA, 1% Triton X-100, 10% protease inhibitor). Western blotting on whole cell protein lysates were performed as previously described (**Armstrong et al., 2016**). *Cell Fractionation*. Protein lysates from each subcellular fraction (cytoplasm, mitochondria, and nucleus) were obtained from PNT1 and LNCaP cells using the cell fractionation kit (Abcam, VIC, Australia) according to the manufacturer's protocol.

Quantitative Real-Time PCR (qPCR)

RNA was extracted from cells using the RNeasy RNA extraction kit (Qiagen), followed by the iScript cDNA Synthesis kit (Bio-Rad, NSW, Australia). qPCR was performed with a 1:10 dilution of cDNA using SYBR Green (Bio-Rad) on a CFX384 Real-Time System (Bio-Rad). Relative gene expression was calculated using the comparative Ct method and normalized to the internal control genes *GUSB* and *L19* for prostate cancer cells and LNCaP-derived tumors, or *TUBA1B, PPIA* and *GAPDH* for PDEs.

Analysis of published ChIP-seq data

AR ChIP-seq data from published external datasets, GSE56288 (clinical specimens; seven normal prostate and 13 primary tumors) (**Pomerantz et al., 2015**) and GSE55064 (VCaP cell line; Veh, DHT treated, MDV3100 treated and Bicalutamide treated) (**Asangani et al., 2014**) were obtained from GEO and visualized using the Integrated Genome Browser (IGV).

Chromatin immunoprecipitation (ChIP)

LNCaP cells were seeded at 3×10^6 cells/plate in 15 cm plates in RPMI-1640 medium containing 10% DCC-FBS for 3 days, then treated for 4 hr with 10 nM DHT or Vehicle (ethanol). AR ChIP was performed as described previously (**Paltoglou et al., 2017**).

Transient RNA interference

The human DECR1 ON-TARGET plus small interfering RNAs (siRNAs) and control siRNA (D-001810-01-20 ON-TARGET plus Non-targeting siRNA #1) were purchased from Millennium Science (VIC, Australia). Four siRNA were tested and the two most effective were selected for our experimentation: siDECR1-1 (J-009642-05-0002) and siDECR1-2 (J-009642-06-0002). The siRNAs at a concentration of 5 nM were reverse transfected using Lipofectamine RNAiMAX transfection reagent (Invitrogen, VIC, Australia) according to the manufacturer's protocol. DECR1 downregulation (>80%) was confirmed on mRNA and protein levels.

Generation of stable shDECR1 and hDECR1 LNCaP cells

Short hairpin lentiviral expression vector

LNCaP cells were transduced with the universal negative control shRNA lentiviral particles (shControl), DECR1 shRNA lentiviral particles (shDECR1) or hDECR1 (GFP-Puro) designed by GenTarget Inc (San Diego, CA, USA) according to the manufacturer's protocol (**Figure 5—figure supplement 3**).

Functional assays

Cell viability

Cells were seeded in triplicates in 24-well plates at a density of 3.0×10^4–6.0×10^4 cells/well and reverse transfected with siRNA overnight. Cells were manually counted using a hemocytometer 96

hr post-siRNA knockdown and viability was assessed by Trypan Blue exclusion as described previously (*Armstrong et al., 2016*).

Cell migration

Transwell migration assays were performed using 24-well polycarbonate Transwell inserts (3422, Sigma Aldrich). LNCaP, 22RV1 and MR49F cells transfected overnight with siRNA were seeded into the upper chamber of the Transwell at a density of 8×10^4–2.5×10^5 cells/well in serum-free medium. 650 µl of medium containing 5% FBS was added to the bottom chamber. Cells were incubated at 37˚C for 48 hr. Non-migrated cells were gently removed using a cotton-tipped swab. The inserts were fixed in 4% paraformaldehyde for 20 min and stained with 1% crystal violet for 30 min. The images of migrated cells were captured using the Axio Scope A1 Fluorescent Microscope (Zeiss) at 40X magnification. The number of migrated cells were counted manually and presented as percentages relative to control cells ± SEM.

Cell invasion

Cell invasion were assessed using 24-well-plate BD Biocoat Matrigel Invasion Chambers (In Vitro Technologies, NSW, Australia) according to the supplier instructions. After 48 hr of siRNA transfection, 650 µl of medium containing 10% FBS was added to the bottom chamber, and equal number of cells within 1% FBS-contained medium were transferred to the upper chamber. After incubation at 37˚C, 5% CO_2 for 48 hr, non-invading cells as well as the Matrigel from the interior of the inserts were gently removed using a cotton-tipped swab. The inserts were fixed in 4% paraformaldehyde for 20 min and stained with 1% crystal violet for 30 min. The images of invaded cells were captured using the Axio Scope A1 Fluorescent Microscope (Zeiss) at 40X magnification. The number of invaded cells were counted manually and presented as percentages relative to control cells ± SEM.

Colony formation assay

DECR1 stable knockdown cells (shDECR1) or negative control cells (shControl) were prepared in a single-cell suspension before being plated in 6-well plates (500 cells/well). Cells were incubated for 2 weeks at 37˚C and medium was replenished every 3–7 days. After 3 weeks, cells were washed with PBS, fixed with 4% paraformaldehyde and stained with 1% crystal violet for 30 min. Colonies were counted manually, and results were reported as number of colonies ± SEM.

3D Spheroid growth assay

LNCaP and 22RV1 cells were transfected with siRNA in 6-well plates for 48 hr. Cells were collected and prepared at a concentration of 7.5×10^4 cells/ml. Cell suspensions (1500 cells in 20 µl) were pipetted onto the inside of a petri dish lid, and 15 ml of PBS was added to the dish to prevent the drops from drying. The petri dishes were reassembled and incubated at 37˚C for 5 days. Photos of the formed spheres were captured, and the sphere volume was determined using ReViSP software (*Piccinini et al., 2015*).

Seahorse extracellular flux analysis

Cells were plated on XF96 well cell culture microplates (Agilent, VIC, Australia) at equal densities in substrate-limited medium (DMEM with 0.5 mM glucose, 1.0 mM glutamine, 0.5 mM carnitine and 1% FBS) and incubated overnight. One hour before the beginning of OCR measurement, the cells were changed into FAO Assay Medium (111 mM NaCl, 4.7 mM KCl, 2.0 mM $MgSO_4$, 1.2 mM Na_2HPO_4, 2.5 mM glucose, 0.5 mM carnitine and 5 mM HEPES). After baseline OCR is stabilized in FAO Assay Medium, 200 µM of linoleic-acid (LA) or palmitic acid (PA) were added before initializing measurements. Extracellular flux analysis was performed using the Seahorse XF Cell Mitochondrial Stress Test kit (Seahorse Bioscience) according to the manufacturer's protocol. Extracellular flux experiments were performed on a Seahorse XF96 Analyzer and results were analysed using Seahorse Wave software for XF analyzers. The OCR values were normalized to cell numbers in each well.

Metabolomics

LNCaP cells were transfected with siRNA for 96 hr in no glucose medium (containing 10% FBS) supplemented with 2.5 mM glucose in 6-well plates. Cells were washed with 1 ml of 37˚C Milli-Q water

on the shaker for 2 s. The plate was placed in sufficient volumes of liquid nitrogen, enough to cover the surface of the plate and was briefly stored on dry ice. 600 µl of ice cold 90% 9:1 methanol:chloroform (MeOH:$CHCl_3$) extraction solvent containing the internal standards (0.5 µl/samples) was added onto each well and allowed to incubate for 10 min. Cells were collected into 1.5 ml Eppendorf tubes, incubated on ice for 5 min, and centrifuged at 4˚C for 5 min at 16,100 g. The supernatant was then transferred into a fresh 1.5 ml Eppendorf tube and allowed to dry in a Speedvac. Dried samples were derivatised with 20 µl methoxyamine (30 mg/ml in pyridine, Sigma Aldrich) and 20 µl N,O-Bis(trimethylsilyl)trifluoroacetamide (BSTFA) + 1% Trimethylchlorosilane (TMCS). The derivatised samples were analysed using GC QQQ targeted metabolomics as described in ***Best et al., 2018***.

Lipidomics

Lipid extraction

700 µl of sample (4 µl of plasma diluted in water, or 700 µl of homogenized cells) was mixed with 800 µl 1 N HCl:CH3OH 1:8 (v/v), 900 µl CHCl3 and 200 µg/ml of the antioxidant 2,6-di-tert-butyl-4-methylphenol (BHT; Sigma Aldrich). 3 µl of SPLASH LIPIDOMIX Mass Spec Standard (#330707, Avanti Polar Lipids) was spiked into the extract mix. The organic fraction was evaporated using a Savant Speedvac spd111v (Thermo Fisher Scientific) at room temperature and the remaining lipid pellet was stored at - 20˚C under argon.

Mass spectrometry

Lipid pellets were reconstituted in 100% ethanol. Lipid species were analyzed by liquid chromatography electrospray ionization tandem mass spectrometry (LC-ESI/MS/MS) on a Nexera X2 UHPLC system (Shimadzu) coupled with hybrid triple quadrupole/linear ion trap mass spectrometer (6500+ QTRAP system; AB SCIEX). Chromatographic separation was performed on a XBridge amide column (150 mm ×4.6 mm, 3.5 µm; Waters) maintained at 35˚C using mobile phase A [1 mM ammonium acetate in water-acetonitrile 5:95 (v/v)] and mobile phase B [1 mM ammonium acetate in water-acetonitrile 50:50 (v/v)] in the following gradient: (0–6 min: 0% B → 6% B; 6–10 min: 6% B → 25% B; 10–11 min: 25% B → 98% B; 11–13 min: 98% B → 100% B; 13–19 min: 100% B; 19–24 min: 0% B) at a flow rate of 0.7 mL/min which was increased to 1.5 mL/min from 13 min onwards. SM, CE, CER, DCER, HCER, LCER were measured in positive ion mode with a precursor scan of 184.1, 369.4, 264.4, 266.4, 264.4 and 264.4 respectively. TAG, DAG and MAG were measured in positive ion mode with a neutral loss scan for one of the fatty acyl moieties. PC, LPC, PE, LPE, PG, LPG, PI, LPI, PS and LPS were measured in negative ion mode by fatty acyl fragment ions. Lipid quantification was performed by scheduled multiple reactions monitoring (MRM), the transitions being based on the neutral losses or the typical product ions as described above. The instrument parameters were as follows: Curtain Gas = 35 psi; Collision Gas = 8 a.u. (medium); IonSpray Voltage = 5500 V and −4,500 V; Temperature = 550˚C; Ion Source Gas 1 = 50 psi; Ion Source Gas 2 = 60 psi; Declustering Potential = 60 V and −80 V; Entrance Potential = 10 V and −10 V; Collision Cell Exit Potential = 15 V and −15 V. The following fatty acyl moieties were taken into account for the lipidomic analysis: 14:0, 14:1, 16:0, 16:1, 16:2, 18:0, 18:1, 18:2, 18:3, 20:0, 20:1, 20:2, 20:3, 20:4, 20:5, 22:0, 22:1, 22:2, 22:4, 22:5 and 22:6 except for TGs which considered: 16:0, 16:1, 18:0, 18:1, 18:2, 18:3, 20:3, 20:4, 20:5, 22:2, 22:3, 22:4, 22:5, 22:6.

Data analysis

Peak integration was performed with the MultiQuant software version 3.0.3. Lipid species signals were corrected for isotopic contributions (calculated with Python Molmass 2019.1.1) and were normalized to internal standard signals. Unpaired T-test p-values and FDR corrected p-values (using the Benjamini/Hochberg procedure) were calculated in Python StatsModels version 0.10.1.

Mitochondrial ROS measurement

LNCaP cells were transfected with siRNA for 96 hr in 6-well plates. Cells were collected into fluorescence-activated cell sorting (FACS) tubes and stained with 2.5 µM of MitoSOX Red stain (Thermo Fisher Scientific, VIC, Australia) for 30 min in a 37˚C water bath. Cells were centrifuged at 1,500 rpm for 5 min, washed twice with 500 µl of PBS, and resuspended in 500 µl of pre-warmed PBS before the samples are read on a BD FACSymphony flow cytometer.

Acylcarnitine measurement

Total lipids were extracted from cells using two-phase extraction with methyl-tert-butyl-ether (MTBE)/methanol/water (10:3:2.5, v/v/v) (**Matyash et al., 2008**). Cell pellets were frozen in 8:1 methanol/water prior to extraction with the above solvent mixture; for cell culture supernatant samples, the cell culture medium replaced the water component. Deuterated (D3)-palmitoylcarnitine was included as an internal standard (200 pmole/sample for LNCaP samples; 20 pmole/sample for tumor explant samples). Samples were reconstituted in 200 µL of the HPLC starting condition, defined below.

Acylcarnitines were quantified by liquid chromatography-tandem mass spectrometry using a Q-Exactive HF-X mass spectrometer with heated electrospray ionization and a Vantage HPLC system (ThermoFisher Scientific). Extracts were resolved on a 2.1 × 100 mm Waters Acquity C18 UPLC column (1.7 µm pore size), using an 18 min binary gradient at 0.28 mL/min flow rate, as follows: 0 min, 80:20 A/B; 3 min, 80:20 A/B; 6 min, 57:43 A/B; 8 min, 35:65 A/B; 9 min, 0:100 A/B; 14 min, 0:100 A/B; 14.5 min, 80:20 A/B; 18 min, 80:20 A/B. Solvent A: 10 mM ammonium formate, 0.1% formic acid in acetonitrile:water (60:40); Solvent B: 10 mM ammonium formate, 0.1% formic acid in isopropanol: acetonitrile (90:10). Data was acquired in positive ion mode with data-dependent acquisition (full scan resolution 70,000 FWHM, scan range 220–1600 *m/z*). The ten most abundant ions in each cycle were subjected to fragmentation (collision energy 30 eV, resolution 17,500 FWHM). An exclusion list of background ions was used based on a solvent blank. TraceFinder v5.0 (Thermo Fisher Scientific) was used for peak detection and integration, based on exact precursor ion mass (*m/z* tolerance four ppm) and *m/z* 85.0 acylcarnitine product ion. Peak areas were normalised to the D3-palmitoylcarnitine internal standard.

Lipid peroxidation analysis by imaging

For imaging, LNCaP cells following DECR1 knockdown were plated at 5 × 10^3 cells/well in a 8-well chamber slide. Cells were then washed with Hank's balanced salt solution (HBSS) and incubated with 5 µM BODIPY-581/591 C11 stain (Thermo Fisher Scientific). Cells were washed and fixed with 4% paraformaldehyde (PFA), and mounted with Prolong Gold anti-fade solution with DAPI (Thermo Fisher Scientific). Cells were imaged at 60 X magnification using a Olympus FV3000 Confocal Microscope. Quantification of BODIPY-C11 stain was performed using ImageJ analysis software.

In vivo experiments

Castration + ENZ study

LNCaP cells (5 × 10^6 cells in 50 µL 10% FBS/RPMI 1640 medium) were co-injected subcutaneously with 50 µL Matrigel in 6-week-old NOD Scid Gamma male mice (Bioresource Facility, Austin Health, Heidelberg, Australia). When tumors reached ~200 mm^3, mice were randomized in different therapy groups. One group was left untreated (n = 5), one group was treated with vehicle control (10% DMSO/PBS; n = 5), one group was treated with enzalutamide (10 mg/kg MDV3100 in 10% DMSO/PBS) and one group was castrated by surgical castration under isofluorane anesthesia (n = 9). Five of the ten castrated mice were then treated daily with enzalutamide (10 mg/kg MDV3100 in 10% DMSO/PBS) by oral gavage for 7 days. Enzalutamide therapy of castrated mice started five days after surgery.

Subcutaneous tumor growth

DECR1 stable knockdown cells (shDECR1) or negative control cells (shControl) (5 × 10^6 cells in 50 µL 10% FBS/RPMI 1640 medium) were co-injected subcutaneously with 50 µL matrigel in 6-week-old NOD Scid Gamma male mice. Tumors were measured using callipers and their volumes were calculated using the formula length × $width^2/2$.

Orthotopic tumor growth

Ten microliter containing 1 × 10^6 DECR1 stable knockdown cells (shDECR1) or negative control cells (shControl) were -injected intraprostatically in 8 week old NOD/SCID male mice. Whole-body imaging to monitor luciferase-expressing LNCaP cells was performed at day 3 of the injection and once weekly after that using the IVIS Spectrum In Vivo Imaging System (PerkinElmer). D-luciferin (potassium salt, PerkinElmer) was dissolved in sterile deionized water (0.03 g/ml) and injected

subcutaneously (3 mg/20 g of mouse body weight) before imaging. Bioluminescence is reported as the sum of detected photons per second from a constant region of interest. After the animals were sacrificed, lungs and livers were excised for ex vivo imaging using the IVIS system.

After each study, tumors were excised and half was snap frozen for RNA extraction while the other half was formalin fixed and paraffin embedded. All animal procedures were carried out in accordance with the guidelines of the National Health and Medical Research Council of Australia, with subcutaneous xenograft studies approved by the Austin Health Animal Ethics Committee (approval number A2015/05311) and orthotopic xenograft studies approved by the University of Adelaide Animal Ethics Committee (approval number M-2019–037).

Statistical analysis

Results are reported as mean ± S.E.M. Statistical analysis was performed using GraphPad Prism (V7.0 for Windows). Differences between treatment groups were compared by T-test or one-way ANOVA followed by Tukey or Dunnett post hoc test. Significance is expressed as *$p < 0.05$, **$p < 0.01$, ***$p < 0.001$, ****$p < 0.0001$.

Acknowledgements

The results published here are in part based on data generated by The Cancer Genome Atlas, established by the National Cancer Institute and the National Human Genome Research Institute, and we are grateful to the specimen donors and relevant research groups associated with this project. Tissues for the patient-derived explants used in the study were collected with informed consent via the Australian Prostate Cancer BioResource and we thank the doctors, patients and health care professionals involved. We acknowledge expert technical assistance in the study from Natalie Ryan, Joanna Gillis, Kayla Bremert, Samira Khabbazi, Nhi Huynh, and Holly P McEwen. Flow cytometry analysis was performed at the South Australian Health Medical Research Institute (SAHMRI) in the ACRF Cellular Imaging and Cytometry Core Facility. The Facility is generously supported by the Australian Cancer Research Foundation (ACRF), Detmold Hoopman Group and Australian Government through the Zero Childhood Cancer Program. Animal studies were performed at the Bioresource Facilities at Austin Health, Heidelberg, Australia and the South Australian Health and Medical Research Institute. The authors thank Metabolomics Australia, Bio21 Institute, and Adelaide Microscopy (University of Adelaide).

Additional information

Funding

Funder	Grant reference number	Author
National Health and Medical Research Council	1138648	Zeyad D Nassar
National Health and Medical Research Council	1121057	Luke A Selth
National Health and Medical Research Council	1100626	Anthony S Don
National Health and Medical Research Council	1084178	Andrew M Scott
Prostate Cancer Foundation of Australia	YI 1417	Zeyad D Nassar
Cure Cancer Australia Foundation	1164798	Zeyad D Nassar
EMBL Australia	Group Leader Award	David J Lynn
University of Sydney	Robinson Fellowship	Andrew J Hoy
Fonds Wetenschappelijk Onderzoek	Project Grants G.0841.15 and G.0C22.19N	Johannes V Swinnen

KU Leuven	Project Grants C16/15/073 and C32/17/052	Johannes V Swinnen
Australian Research Council	FT130101004	Lisa M Butler
Cancer Council South Australia	PRF1117	Lisa M Butler
Movember Foundation	MRTA3	Lisa M Butler
Freemasons Foundation Centre for Men's Health, University of Adelaide		Lisa M Butler

The funders had no role in study design, data collection and interpretation, or the decision to submit the work for publication.

Author contributions

Zeyad D Nassar, Conceptualization, Data curation, Formal analysis, Supervision, Funding acquisition, Investigation, Methodology, Writing - original draft, Writing - review and editing; Chui Yan Mah, Data curation, Formal analysis, Validation, Investigation, Visualization, Methodology, Writing - original draft, Writing - review and editing; Jonas Dehairs, Data curation, Methodology, Writing - review and editing; Ingrid JG Burvenich, Swati Irani, Anthony S Don, Investigation, Methodology, Writing - review and editing; Margaret M Centenera, Supervision, Methodology, Writing - review and editing; Madison Helm, Investigation, Methodology; Raj K Shrestha, Investigation, Writing - review and editing; Max Moldovan, Formal analysis, Investigation, Writing - review and editing; Jeff Holst, Lisa G Horvath, Methodology, Writing - review and editing; Andrew M Scott, Supervision, Writing - review and editing; David J Lynn, Data curation, Formal analysis, Supervision, Methodology, Writing - review and editing; Luke A Selth, Data curation, Formal analysis, Supervision, Investigation, Visualization, Methodology, Writing - review and editing; Andrew J Hoy, Data curation, Supervision, Investigation, Methodology, Writing - review and editing; Johannes V Swinnen, Conceptualization, Data curation, Supervision, Funding acquisition, Methodology, Writing - review and editing; Lisa M Butler, Conceptualization, Resources, Data curation, Supervision, Funding acquisition, Writing - original draft, Project administration, Writing - review and editing

Author ORCIDs

Zeyad D Nassar http://orcid.org/0000-0002-7779-2697
Chui Yan Mah http://orcid.org/0000-0002-8820-4037
Lisa M Butler https://orcid.org/0000-0003-2698-3220

Ethics

Human subjects: Fresh and archival prostate tissue specimens were collected from men undergoing robotic radical prostatectomy at St Andrew's Hospital (Adelaide, South Australia) with written informed consent through the Australian Prostate Cancer BioResource. Ethical Approval was provided by the Human Research Ethics Committees of the University of Adelaide (H-2012-016) and St Andrew's Hospital.
Animal experimentation: Animal studies were approved by the Austin Health Animal Ethics Committee (approval number A2015/05311), Heidelberg, Australia, and the University of Adelaide Animal Ethics Committee (approval number M-2019-037), and were carried out in accordance with the recommendations of the National Health and Medical Research Council of Australia.

Decision letter and Author response

Decision letter https://doi.org/10.7554/eLife.54166.sa1
Author response https://doi.org/10.7554/eLife.54166.sa2

Additional files

Supplementary files

- Transparent reporting form

Data availability

All data generated or analysed during this study are included in the manuscript and supporting files.

The following previously published datasets were used:

Author(s)	Year	Dataset title	Dataset URL	Database and Identifier
Nikitina AS, Sharova EI, Danilenko SA, Butusova TB, Vasiliev AO, Govorov AV, Prilepskaya EA, Pushkar DY, Kostryukova ES	2017	Novel RNA biomarkers of prostate cancer revealed by RNA-seq analysis of formalin-fixed samples obtained from Russian patients	https://www.ncbi.nlm.nih.gov/geo/query/acc.cgi?acc=GSE89223	NCBI Gene Expression Omnibus, GSE89223
Ding Y, Wu H, Warden C, Steele L, Liu X, Iterson MV, Wu X, Nelson R, Liu Z, Yuan YC, Neuhausen SL	2016	Age-Related Gene Expression Changes in Prostate Cancer Patients	https://www.ncbi.nlm.nih.gov/geo/query/acc.cgi?acc=GSE89194	NCBI Gene Expression Omnibus, GSE89194
Ren S, Peng Z, Mao JH, Yu Y, Yin C, Gao X, Cui Z, Zhang J, Yi K, Xu W, Chen C, Wang F, Guo X, Lu J, Yang J, Wei M, Tian Z, Guan Y, Tang L, Xu C, Wang L, Tian W, Wang J, Yang H, Sun Y	2012	RNA-seq analysis of prostate cancer in the Chinese population identifies recurrent gene fusions, cancer-associated long noncoding RNAs and aberrant alternative splicings	https://www.ncbi.nlm.nih.gov/pubmed/22349460	Pubmed, 22349460
TCGA	2019	The Cancer Genome Atlas Prostate Adenocarcinoma (TCGA-PRAD)	https://portal.gdc.cancer.gov/projects/TCGA-PRAD	National Cancer Institute, TCGA-PRAD
Tomlins SA, Mehra R, Rhodes DR, Cao X, Wang L, Dhanasekaran SM, Kalyana-Sundaram S, Wei JT, Rubin MA, Pienta KJ, Shah RB, Chinnaiyan AM	2006	Integrative Molecular Concepts Modeling of Prostate Cancer Progression	https://www.ncbi.nlm.nih.gov/geo/query/acc.cgi?acc=GSE6099	NCBI Gene Expression Omnibus, GSE6099
Grasso CS, Wu YM, Robinson DR, Cao X, Dhanasekaran SM, Khan AP, Quist MJ, Jing X, Lonigro RJ, Brenner JC, Asangani IA, Ateeq B, Chun SY, Siddiqui J, Sam L, Anstett M, Mehra R, Prensner JR, Palanisamy N, Ryslik GA, Vandin F, Raphael BJ, Kunju LP, Rhodes DR, Pienta KJ, Chinnaiyan AM, Tomlins SA	2012	The Mutational Landscape of Lethal Castrate Resistant Prostate Cancer	https://www.ncbi.nlm.nih.gov/geo/query/acc.cgi?acc=GSE35988	NCBI Gene Expression Omnibus, GSE35988
Taylor BS, Schultz N, Hieronymus H, Gopalan A, Xiao Y, Carver BS, Arora VK, Kaushik P, Cerami E, Reva B, Antipin Y, Mitsiades N, Landers T, Dolgalev I, Major JE, Wilson M, Socci	2010	Integrative genomic profiling of human prostate cancer	https://www.ncbi.nlm.nih.gov/geo/query/acc.cgi?acc=GSE21032	NCBI Gene Expression Omnibus, GSE21032

ND, Lash AE, Heguy A, Eastham JA, Scher HI, Reuter VE, Scardino PT, Sander C, Sawyers CL, Gerald WL				
Sboner A, Demichelis F, Calza S, Pawitan Y, Setlur SR, Hoshida Y, Perner S, Adami HO, Fall K, Mucci LA, Kantoff PW, Stampfer M, Andersson SO, Varenhorst E, Johansson JE, Gerstein MB, Golub TR, Rubin MA, Andrén O	2010	Molecular Sampling of Prostate Cancer: a dilemma for predicting disease progression	https://www.ncbi.nlm.nih.gov/geo/query/acc.cgi?acc=GSE16560	NCBI Gene Expression Omnibus, GSE16560
Wang Q, Li W, Liu XS, Carroll JS, Jänne OA, Keeton EK, Chinnaiyan AM, Pienta KJ, Brown M	2007	A hierarchical network of transcription factors governs androgen receptor-dependent prostate cancer growth	https://www.ncbi.nlm.nih.gov/geo/query/acc.cgi?acc=GSE7868	NCBI Gene Expression Omnibus, GSE7868
Heemers HV, Schmidt LJ, Sun Z, Regan KM, Anderson SK, Duncan K, Wang D, Liu S, Ballman KV, Tindall DJ	2011	Identification of an SRF- and androgen-dependent gene signature in prostate cancer	https://www.ncbi.nlm.nih.gov/geo/query/acc.cgi	NCBI Gene Expression Omnibus, GSE22606
Asangani IA, Dommeti VL, Wang X, Malik R, Cieslik M, Yang R, Escara-Wilke J, Wilder-Romans K, Dhanireddy S, Engelke C, Iyer MK, Jing X, Wu YM, Cao X, Qin ZS, Wang S, Feng FY, Chinnaiyan AM	2014	Therapeutic Targeting of BET Bromodomain Proteins in Castration-Resistant Prostate Cancer	https://www.ncbi.nlm.nih.gov/geo/query/acc.cgi?acc=GSE55064	NCBI Gene Expression Omnibus, GSE55064
Li L, Karanika S, Yang G, Wang J, Park S, Broom BM, Manyam GC, Wu W, Luo Y, Basourakos S, Song JH, Gallick GE, Karantanos T, Korentzelos D, Azad AK, Kim J, Corn PG, Aparicio AM, Logothetis CJ, Troncoso P, Heffernan T, Toniatti C, Lee HS, Lee JS, Zuo X, Chang W, Yin J, Thompson TC	2016	Genome-wide analysis of enzalutamide- and/or olaparib-responsive gene expression in prostate cancer cells	https://www.ncbi.nlm.nih.gov/geo/query/acc.cgi?acc=GSE69249	NCBI Gene Expression Omnibus, GSE69249
Wang X, Wang B, Soriano R, Zha J, Zhang Z, Modrusan Z, Cunha GR, Gao W	2006	Expression profiling of the mouse prostate after castration and hormone replacement	https://www.ncbi.nlm.nih.gov/geo/query/acc.cgi?acc=GSE5901	NCBI Gene Expression Omnibus, GSE5901
Arora VK, Schenkein E, Murali R, Subudhi SK, Wongvipat J, Balbas MD, Shah N, Cai L, Efstathiou E,	2013	Glucocorticoid Receptor Confers Resistance to Anti-Androgens by Bypassing Androgen Receptor Blockade	https://www.ncbi.nlm.nih.gov/geo/query/acc.cgi?acc=GSE52169	NCBI Gene Expression Omnibus, GSE52169

Logothetis C, Zheng D, Sawyers CL				
Pomerantz MM, Li F, Takeda D, Chonkar A, Chabot M, Li Q, Cejas P, Vazquez F, Shivdasani RA, Seo J, Bowden M, Lis R, Hahn WC, Kantoff PW, Brown M, Loda M, Long HW, Freedman ML	2015	Androgen receptor programming in human tissue implicates HOXB13 in prostate pathogenesis [ChIP-Seq]	https://www.ncbi.nlm.nih.gov/geo/query/acc.cgi?acc=GSE56288	NCBI Gene Expression Omnibus, GSE56288
Glinsky GV, Glinskii AB, Stephenson AJ, Hoffman RM, Gerald WL	2004	Gene expression profiling predicts clinical outcome of prostate cancer	https://www.ncbi.nlm.nih.gov/pubmed/15067324	Pubmed, 15067324
Latonen L, Afyounian E, Jylhä A, Nättinen J, Aapola U, Annala M, Kivinummi KK, Tammela TTL, Beuerman RW, Uusitalo H, Nykter M, Visakorpi T	2018	Integrative proteomics in prostate cancer uncovers robustness against genomic and transcriptomic aberrations during disease progression	https://www.nature.com/articles/s41467-018-03573-6#Sec31	Peptide Atlas repository, PASS01126
Iglesias-Gato D, Thysell E, Tyanova S, Crnalic S, Santos A, Lima TS, Geiger T, Cox J, Widmark A, Bergh A, Mann M, Flores-Morales A, Wikström P	2018	The Proteome of Prostate Cancer Bone Metastasis Reveals Heterogeneity with Prognostic Implications	https://clincancerres.aacrjournals.org/content/24/21/5433	ProteomeXchange, PXD009868

References

Alphey MS, Yu W, Byres E, Li D, Hunter WN. 2005. Structure and reactivity of human mitochondrial 2,4-dienoyl-CoA reductase: enzyme-ligand interactions in a distinctive short-chain reductase active site. *The Journal of Biological Chemistry* **280**:3068–3077. DOI: https://doi.org/10.1074/jbc.M411069200, PMID: 15531764

Apte SA, Cavazos DA, Whelan KA, Degraffenried LA. 2013. A low dietary ratio of omega-6 to omega-3 fatty acids may delay progression of prostate Cancer. *Nutrition and Cancer* **65**:556–562. DOI: https://doi.org/10.1080/01635581.2013.775316, PMID: 23659447

Armstrong HK, Koay YC, Irani S, Das R, Nassar ZD, Selth LA, Centenera MM, McAlpine SR, Butler LM, Australian Prostate Cancer BioResource. 2016. A novel class of Hsp90 C-Terminal modulators have Pre-Clinical efficacy in prostate tumor cells without induction of a heat shock response. *The Prostate* **76**:1546–1559. DOI: https://doi.org/10.1002/pros.23239, PMID: 27526951

Asangani IA, Dommeti VL, Wang X, Malik R, Cieslik M, Yang R, Escara-Wilke J, Wilder-Romans K, Dhanireddy S, Engelke C, Iyer MK, Jing X, Wu YM, Cao X, Qin ZS, Wang S, Feng FY, Chinnaiyan AM. 2014. Therapeutic targeting of BET bromodomain proteins in castration-resistant prostate Cancer. *Nature* **510**:278–282. DOI: https://doi.org/10.1038/nature13229, PMID: 24759320

Bairati I, Meyer F, Fradet Y, Moore L. 1998. Dietary fat and advanced prostate Cancer. *Journal of Urology* **159**:1271–1275. DOI: https://doi.org/10.1016/S0022-5347(01)63579-1, PMID: 9507851

Balaban S, Nassar ZD, Zhang AY, Hosseini-Beheshti E, Centenera MM, Schreuder M, Lin HM, Aishah A, Varney B, Liu-Fu F, Lee LS, Nagarajan SR, Shearer RF, Hardie RA, Raftopulos NL, Kakani MS, Saunders DN, Holst J, Horvath LG, Butler LM, et al. 2019. Extracellular fatty acids are the major contributor to lipid synthesis in prostate Cancer. *Molecular Cancer Research* **17**:949–962. DOI: https://doi.org/10.1158/1541-7786.MCR-18-0347, PMID: 30647103

Best SA, De Souza DP, Kersbergen A, Policheni AN, Dayalan S, Tull D, Rathi V, Gray DH, Ritchie ME, McConville MJ, Sutherland KD. 2018. Synergy between the KEAP1/NRF2 and PI3K pathways drives Non-Small-Cell lung Cancer with an altered immune microenvironment. *Cell Metabolism* **27**:935–943. DOI: https://doi.org/10.1016/j.cmet.2018.02.006, PMID: 29526543

Blomme A, Ford CA, Mui E, Patel R, Ntala C, Jamieson LE, Planque M, McGregor GH, Peixoto P, Hervouet E, Nixon C, Salji M, Gaughan L, Markert E, Repiscak P, Sumpton D, Blanco GR, Lilla S, Kamphorst JJ, Graham D, et al. 2020. 2,4-dienoyl-CoA reductase regulates lipid homeostasis in treatment-resistant prostate Cancer. *Nature Communications* **11**:2508. DOI: https://doi.org/10.1038/s41467-020-16126-7, PMID: 32427840

Bray F, Ferlay J, Soerjomataram I, Siegel RL, Torre LA, Jemal A, statistics G. 2018. GLOBOCAN estimates of incidence and mortality worldwide for 36 cancers in 185 countries. *CA: A Cancer Journal for Clinicians* **68**:394–424. DOI: https://doi.org/10.3322/caac.21492

Brown MD, Hart C, Gazi E, Gardner P, Lockyer N, Clarke N. 2010. Influence of omega-6 PUFA arachidonic acid and bone marrow adipocytes on metastatic spread from prostate Cancer. *British Journal of Cancer* **102**:403–413. DOI: https://doi.org/10.1038/sj.bjc.6605481, PMID: 19997104

Butler LM, Centenera MM, Swinnen JV. 2016. Androgen control of lipid metabolism in prostate Cancer: novel insights and future applications. *Endocrine-Related Cancer* **23**:R219–R227. DOI: https://doi.org/10.1530/ERC-15-0556, PMID: 27130044

Cai C, Balk SP. 2011. Intratumoral androgen biosynthesis in prostate Cancer pathogenesis and response to therapy. *Endocrine-Related Cancer* **18**:R175–R182. DOI: https://doi.org/10.1530/ERC-10-0339, PMID: 21712345

Centenera MM, Gillis JL, Hanson AR, Jindal S, Taylor RA, Risbridger GP, Sutherland PD, Scher HI, Raj GV, Knudsen KE, Yeadon T, Tilley WD, Butler LM, Australian Prostate Cancer BioResource. 2012. Evidence for efficacy of new Hsp90 inhibitors revealed by ex vivo culture of human prostate tumors. *Clinical Cancer Research* **18**:3562–3570. DOI: https://doi.org/10.1158/1078-0432.CCR-12-0782, PMID: 22573351

Centenera MM, Raj GV, Knudsen KE, Tilley WD, Butler LM. 2013. Ex vivo culture of human prostate tissue and drug development. *Nature Reviews Urology* **10**:483–487. DOI: https://doi.org/10.1038/nrurol.2013.126, PMID: 23752995

Centenera MM, Hickey TE, Jindal S, Ryan NK, Ravindranathan P, Mohammed H, Robinson JL, Schiewer MJ, Ma S, Kapur P, Sutherland PD, Hoffmann CE, Roehrborn CG, Gomella LG, Carroll JS, Birrell SN, Knudsen KE, Raj GV, Butler LM, Tilley WD. 2018. A patient-derived explant (PDE) model of hormone-dependent Cancer. *Molecular Oncology* **12**:1608–1622. DOI: https://doi.org/10.1002/1878-0261.12354, PMID: 30117261

Cerami E, Gao J, Dogrusoz U, Gross BE, Sumer SO, Aksoy BA, Jacobsen A, Byrne CJ, Heuer ML, Larsson E, Antipin Y, Reva B, Goldberg AP, Sander C, Schultz N. 2012. The cBio Cancer genomics portal: an open platform for exploring multidimensional Cancer genomics data. *Cancer Discovery* **2**:401–404. DOI: https://doi.org/10.1158/2159-8290.CD-12-0095, PMID: 22588877

Chen M, Zhang J, Sampieri K, Clohessy JG, Mendez L, Gonzalez-Billalabeitia E, Liu XS, Lee YR, Fung J, Katon JM, Menon AV, Webster KA, Ng C, Palumbieri MD, Diolombi MS, Breitkopf SB, Teruya-Feldstein J, Signoretti S, Bronson RT, Asara JM, et al. 2018. An aberrant SREBP-dependent lipogenic program promotes metastatic prostate Cancer. *Nature Genetics* **50**:206–218. DOI: https://doi.org/10.1038/s41588-017-0027-2, PMID: 29335545

Colli JL, Colli A. 2005. Comparisons of prostate Cancer mortality rates with dietary practices in the united states. *Urologic Oncology: Seminars and Original Investigations* **23**:390–398. DOI: https://doi.org/10.1016/j.urolonc.2005.03.020, PMID: 16301115

Das UN. 2011. Essential fatty acids enhance free radical generation and lipid peroxidation to induce apoptosis of tumor cells. *Clinical Lipidology* **6**:463–489. DOI: https://doi.org/10.2217/clp.11.34

Davies NJ, Batehup L, Thomas R. 2011. The role of diet and physical activity in breast, colorectal, and prostate Cancer survivorship: a review of the literature. *British Journal of Cancer* **105 Suppl 1**:S52–S73. DOI: https://doi.org/10.1038/bjc.2011.423, PMID: 22048034

Davis ID, Martin AJ, Stockler MR, Begbie S, Chi KN, Chowdhury S, Coskinas X, Frydenberg M, Hague WE, Horvath LG, Joshua AM, Lawrence NJ, Marx G, McCaffrey J, McDermott R, McJannett M, North SA, Parnis F, Parulekar W, Pook DW, et al. 2019. Enzalutamide with standard First-Line therapy in metastatic prostate Cancer. *New England Journal of Medicine* **381**:121–131. DOI: https://doi.org/10.1056/NEJMoa1903835, PMID: 31157964

Ding Y, Wu H, Warden C, Steele L, Liu X, Iterson MV, Wu X, Nelson R, Liu Z, Yuan YC, Neuhausen SL. 2016. Gene expression differences in prostate cancers between young and old men. *PLOS Genetics* **12**:e1006477. DOI: https://doi.org/10.1371/journal.pgen.1006477, PMID: 28027300

Dixon SJ, Lemberg KM, Lamprecht MR, Skouta R, Zaitsev EM, Gleason CE, Patel DN, Bauer AJ, Cantley AM, Yang WS, Morrison B, Stockwell BR. 2012. Ferroptosis: an iron-dependent form of nonapoptotic cell death. *Cell* **149**:1060–1072. DOI: https://doi.org/10.1016/j.cell.2012.03.042, PMID: 22632970

Duval K, Grover H, Han LH, Mou Y, Pegoraro AF, Fredberg J, Chen Z. 2017. Modeling physiological events in 2D vs. 3D cell culture. *Physiology* **32**:266–277. DOI: https://doi.org/10.1152/physiol.00036.2016, PMID: 28615311

Epstein MM, Kasperzyk JL, Mucci LA, Giovannucci E, Price A, Wolk A, Håkansson N, Fall K, Andersson SO, Andrén O. 2012. Dietary fatty acid intake and prostate Cancer survival in Orebro county, Sweden. *American Journal of Epidemiology* **176**:240–252. DOI: https://doi.org/10.1093/aje/kwr520, PMID: 22781428

Ettinger SL, Sobel R, Whitmore TG, Akbari M, Bradley DR, Gleave ME, Nelson CC. 2004. Dysregulation of sterol response element-binding proteins and downstream effectors in prostate Cancer during progression to androgen independence. *Cancer Research* **64**:2212–2221. DOI: https://doi.org/10.1158/0008-5472.CAN-2148-2, PMID: 15026365

Flaig TW, Salzmann-Sullivan M, Su LJ, Zhang Z, Joshi M, Gijón MA, Kim J, Arcaroli JJ, Van Bokhoven A, Lucia MS, La Rosa FG, Schlaepfer IR. 2017. Lipid catabolism inhibition sensitizes prostate Cancer cells to antiandrogen blockade. *Oncotarget* **8**:56051–56065. DOI: https://doi.org/10.18632/oncotarget.17359, PMID: 28915573

Fu YQ, Zheng JS, Yang B, Li D. 2015. Effect of individual omega-3 fatty acids on the risk of prostate Cancer: a systematic review and dose-response meta-analysis of prospective cohort studies. *Journal of Epidemiology* **25**:261–274. DOI: https://doi.org/10.2188/jea.JE20140120, PMID: 25787237

Gaweł S, Wardas M, Niedworok E, Wardas P. 2004. [Malondialdehyde (MDA) as a lipid peroxidation marker]. *Wiadomosci Lekarskie* **57**:453–455. PMID: 15765761

Gazi E, Gardner P, Lockyer NP, Hart CA, Brown MD, Clarke NW. 2007. Direct evidence of lipid translocation between adipocytes and prostate Cancer cells with imaging FTIR microspectroscopy. *Journal of Lipid Research* **48**:1846–1856. DOI: https://doi.org/10.1194/jlr.M700131-JLR200, PMID: 17496269

Glinsky GV, Berezovska O, Glinskii AB. 2005. Microarray analysis identifies a death-from-cancer signature predicting therapy failure in patients with multiple types of Cancer. *Journal of Clinical Investigation* **115**:1503–1521. DOI: https://doi.org/10.1172/JCI23412, PMID: 15931389

Grasso CS, Wu YM, Robinson DR, Cao X, Dhanasekaran SM, Khan AP, Quist MJ, Jing X, Lonigro RJ, Brenner JC, Asangani IA, Ateeq B, Chun SY, Siddiqui J, Sam L, Anstett M, Mehra R, Prensner JR, Palanisamy N, Ryslik GA, et al. 2012. The mutational landscape of lethal castration-resistant prostate Cancer. *Nature* **487**:239–243. DOI: https://doi.org/10.1038/nature11125, PMID: 22722839

Hanahan D, Weinberg RA. 2011. Hallmarks of Cancer: the next generation. *Cell* **144**:646–674. DOI: https://doi.org/10.1016/j.cell.2011.02.013, PMID: 21376230

Haynie KR, Vandanmagsar B, Wicks SE, Zhang J, Mynatt RL. 2014. Inhibition of carnitine palymitoyltransferase1b induces cardiac hypertrophy and mortality in mice. *Diabetes, Obesity and Metabolism* **16**:757–760. DOI: https://doi.org/10.1111/dom.12248, PMID: 24330405

Hiltunen JK, Qin Y. 2000. beta-oxidation - strategies for the metabolism of a wide variety of acyl-CoA esters. *Biochimica Et Biophysica Acta (BBA) - Molecular and Cell Biology of Lipids* **1484**:117–128. DOI: https://doi.org/10.1016/S1388-1981(00)00013-5, PMID: 10760462

Holubarsch CJ, Rohrbach M, Karrasch M, Boehm E, Polonski L, Ponikowski P, Rhein S. 2007. A double-blind randomized multicentre clinical trial to evaluate the efficacy and safety of two doses of etomoxir in comparison with placebo in patients with moderate congestive heart failure: the ERGO (etomoxir for the recovery of glucose oxidation) study. *Clinical Science* **113**:205–212. DOI: https://doi.org/10.1042/CS20060307, PMID: 17319797

Houten SM, Denis S, Te Brinke H, Jongejan A, van Kampen AH, Bradley EJ, Baas F, Hennekam RC, Millington DS, Young SP, Frazier DM, Gucsavas-Calikoglu M, Wanders RJ. 2014. Mitochondrial NADP(H) deficiency due to a mutation in NADK2 causes dienoyl-CoA reductase deficiency with hyperlysinemia. *Human Molecular Genetics* **23**:5009–5016. DOI: https://doi.org/10.1093/hmg/ddu218, PMID: 24847004

Huggins C, Hodges CV. 1941. Studies on prostatic Cancer. I. the effect of castration, of estrogen and of androgen injection on serum phosphatases in metastatic carcinoma of the prostate. *Cancer Research* **1**:293–297. DOI: https://doi.org/10.3322/canjclin.22.4.232

Iglesias-Gato D, Wikström P, Tyanova S, Lavallee C, Thysell E, Carlsson J, Hägglöf C, Cox J, Andrén O, Stattin P, Egevad L, Widmark A, Bjartell A, Collins CC, Bergh A, Geiger T, Mann M, Flores-Morales A. 2016. The proteome of primary prostate Cancer. *European Urology* **69**:942–952. DOI: https://doi.org/10.1016/j.eururo.2015.10.053, PMID: 26651926

Iglesias-Gato D, Thysell E, Tyanova S, Crnalic S, Santos A, Lima TS, Geiger T, Cox J, Widmark A, Bergh A, Mann M, Flores-Morales A, Wikström P. 2018. The proteome of prostate Cancer bone metastasis reveals heterogeneity with prognostic implications. *Clinical Cancer Research* **24**:5433–5444. DOI: https://doi.org/10.1158/1078-0432.CCR-18-1229, PMID: 30042207

Itkonen HM, Brown M, Urbanucci A, Tredwell G, Ho Lau C, Barfeld S, Hart C, Guldvik IJ, Takhar M, Heemers HV, Erho N, Bloch K, Davicioni E, Derua R, Waelkens E, Mohler JL, Clarke N, Swinnen JV, Keun HC, Rekvig OP, et al. 2017. Lipid degradation promotes prostate Cancer cell survival. *Oncotarget* **8**:38264–38275. DOI: https://doi.org/10.18632/oncotarget.16123, PMID: 28415728

Ji S, You Y, Kerner J, Hoppel CL, Schoeb TR, Chick WS, Hamm DA, Sharer JD, Wood PA. 2008. Homozygous carnitine palmitoyltransferase 1b (muscle isoform) deficiency is lethal in the mouse. *Molecular Genetics and Metabolism* **93**:314–322. DOI: https://doi.org/10.1016/j.ymgme.2007.10.006, PMID: 18023382

Khankari NK, Murff HJ, Zeng C, Wen W, Eeles RA, Easton DF, Kote-Jarai Z, Al Olama AA, Benlloch S, Muir K, Giles GG, Wiklund F, Gronberg H, Haiman CA, Schleutker J, Nordestgaard BG, Travis RC, Donovan JL, Pashayan N, Khaw KT, et al. 2016. Polyunsaturated fatty acids and prostate Cancer risk: a mendelian randomisation analysis from the PRACTICAL consortium. *British Journal of Cancer* **115**:624–631. DOI: https://doi.org/10.1038/bjc.2016.228, PMID: 27490808

Kregel S, Kiriluk KJ, Rosen AM, Cai Y, Reyes EE, Otto KB, Tom W, Paner GP, Szmulewitz RZ, Vander Griend DJ. 2013. Sox2 is an androgen receptor-repressed gene that promotes castration-resistant prostate Cancer. *PLOS ONE* **8**:e53701. DOI: https://doi.org/10.1371/journal.pone.0053701, PMID: 23326489

Kuemmerle NB, Rysman E, Lombardo PS, Flanagan AJ, Lipe BC, Wells WA, Pettus JR, Froehlich HM, Memoli VA, Morganelli PM, Swinnen JV, Timmerman LA, Chaychi L, Fricano CJ, Eisenberg BL, Coleman WB, Kinlaw WB. 2011. Lipoprotein lipase links dietary fat to solid tumor cell proliferation. *Molecular Cancer Therapeutics* **10**:427–436. DOI: https://doi.org/10.1158/1535-7163.MCT-10-0802, PMID: 21282354

Law CW, Alhamdoosh M, Su S, Smyth GK, Ritchie ME. 2016. RNA-seq analysis is easy as 1-2-3 with limma, glimma and edgeR. *F1000Research* **5**:1408. DOI: https://doi.org/10.12688/f1000research.9005.1

Liu Y. 2006. Fatty acid oxidation is a dominant bioenergetic pathway in prostate Cancer. *Prostate Cancer and Prostatic Diseases* **9**:230–234. DOI: https://doi.org/10.1038/sj.pcan.4500879, PMID: 16683009

Magtanong L, Ko PJ, To M, Cao JY, Forcina GC, Tarangelo A, Ward CC, Cho K, Patti GJ, Nomura DK, Olzmann JA, Dixon SJ. 2019. Exogenous monounsaturated fatty acids promote a Ferroptosis-Resistant cell state. *Cell Chemical Biology* **26**:420–432. DOI: https://doi.org/10.1016/j.chembiol.2018.11.016, PMID: 30686757

Mäkelä AM, Hohtola E, Miinalainen IJ, Autio JA, Schmitz W, Niemi KJ, Hiltunen JK, Autio KJ. 2019. Mitochondrial 2,4-dienoyl-CoA reductase (Decr) deficiency and impairment of thermogenesis in mouse Brown adipose tissue. *Scientific Reports* **9**:12038. DOI: https://doi.org/10.1038/s41598-019-48562-x, PMID: 31427678

Martinez-Outschoorn UE, Lin Z, Whitaker-Menezes D, Howell A, Lisanti MP, Sotgia F. 2012. Ketone bodies and two-compartment tumor metabolism: stromal ketone production fuels mitochondrial biogenesis in epithelial Cancer cells. *Cell Cycle* **11**:3956–3963. DOI: https://doi.org/10.4161/cc.22136, PMID: 23082721

Matyash V, Liebisch G, Kurzchalia TV, Shevchenko A, Schwudke D. 2008. Lipid extraction by methyl-tert-butyl ether for high-throughput lipidomics. *Journal of Lipid Research* **49**:1137–1146. DOI: https://doi.org/10.1194/jlr.D700041-JLR200, PMID: 18281723

Miinalainen IJ, Schmitz W, Huotari A, Autio KJ, Soininen R, Ver Loren van Themaat E, Baes M, Herzig KH, Conzelmann E, Hiltunen JK. 2009. Mitochondrial 2,4-dienoyl-CoA reductase deficiency in mice results in severe hypoglycemia with stress intolerance and unimpaired ketogenesis. *PLOS Genetics* **5**:e1000543. DOI: https://doi.org/10.1371/journal.pgen.1000543, PMID: 19578400

Narita S, Nara T, Sato H, Koizumi A, Huang M, Inoue T, Habuchi T. 2019. Research evidence on High-Fat Diet-Induced prostate Cancer development and progression. *Journal of Clinical Medicine* **8**:597. DOI: https://doi.org/10.3390/jcm8050597

Nassar ZD, Aref AT, Miladinovic D, Mah CY, Raj GV, Hoy AJ, Butler LM. 2018. Peri-prostatic adipose tissue: the metabolic microenvironment of prostate Cancer. *BJU International* **121**:9–21. DOI: https://doi.org/10.1111/bju.14173

Nieman KM, Kenny HA, Penicka CV, Ladanyi A, Buell-Gutbrod R, Zillhardt MR, Romero IL, Carey MS, Mills GB, Hotamisligil GS, Yamada SD, Peter ME, Gwin K, Lengyel E. 2011. Adipocytes promote ovarian Cancer metastasis and provide energy for rapid tumor growth. *Nature Medicine* **17**:1498–1503. DOI: https://doi.org/10.1038/nm.2492, PMID: 22037646

Nikitina AS, Sharova EI, Danilenko SA, Butusova TB, Vasiliev AO, Govorov AV, Prilepskaya EA, Pushkar DY, Kostryukova ES. 2017. Novel RNA biomarkers of prostate Cancer revealed by RNA-seq analysis of formalin-fixed samples obtained from russian patients. *Oncotarget* **8**:32990–33001. DOI: https://doi.org/10.18632/oncotarget.16518, PMID: 28380430

Nomura DK, Lombardi DP, Chang JW, Niessen S, Ward AM, Long JZ, Hoover HH, Cravatt BF. 2011. Monoacylglycerol lipase exerts dual control over endocannabinoid and fatty acid pathways to support prostate Cancer. *Chemistry & Biology* **18**:846–856. DOI: https://doi.org/10.1016/j.chembiol.2011.05.009, PMID: 21802006

Nyman LR, Cox KB, Hoppel CL, Kerner J, Barnoski BL, Hamm DA, Tian L, Schoeb TR, Wood PA. 2005. Homozygous carnitine palmitoyltransferase 1a (liver isoform) deficiency is lethal in the mouse. *Molecular Genetics and Metabolism* **86**:179–187. DOI: https://doi.org/10.1016/j.ymgme.2005.07.021, PMID: 16169268

Ornish D, Weidner G, Fair WR, Marlin R, Pettengill EB, Raisin CJ, Dunn-Emke S, Crutchfield L, Jacobs FN, Barnard RJ, Aronson WJ, McCormac P, McKnight DJ, Fein JD, Dnistrian AM, Weinstein J, Ngo TH, Mendell NR, Carroll PR. 2005. Intensive lifestyle changes may affect the progression of prostate Cancer. *Journal of Urology* **174**:1065–1070. DOI: https://doi.org/10.1097/01.ju.0000169487.49018.73, PMID: 16094059

Paltoglou S, Das R, Townley SL, Hickey TE, Tarulli GA, Coutinho I, Fernandes R, Hanson AR, Denis I, Carroll JS, Dehm SM, Raj GV, Plymate SR, Tilley WD, Selth LA. 2017. Novel androgen receptor coregulator GRHL2 exerts both oncogenic and antimetastatic functions in prostate Cancer. *Cancer Research* **77**:3417–3430. DOI: https://doi.org/10.1158/0008-5472.CAN-16-1616, PMID: 28473532

Park SY, Wilkens LR, Henning SM, Le Marchand L, Gao K, Goodman MT, Murphy SP, Henderson BE, Kolonel LN. 2009. Circulating fatty acids and prostate Cancer risk in a nested case-control study: the multiethnic cohort. *Cancer Causes & Control* **20**:211–223. DOI: https://doi.org/10.1007/s10552-008-9236-4, PMID: 18821021

Piccinini F, Tesei A, Arienti C, Bevilacqua A. 2015. Cancer multicellular spheroids: volume assessment from a single 2D projection. *Computer Methods and Programs in Biomedicine* **118**:95–106. DOI: https://doi.org/10.1016/j.cmpb.2014.12.003, PMID: 25561413

Pomerantz MM, Li F, Takeda DY, Lenci R, Chonkar A, Chabot M, Cejas P, Vazquez F, Cook J, Shivdasani RA, Bowden M, Lis R, Hahn WC, Kantoff PW, Brown M, Loda M, Long HW, Freedman ML. 2015. The androgen receptor cistrome is extensively reprogrammed in human prostate tumorigenesis. *Nature Genetics* **47**:1346–1351. DOI: https://doi.org/10.1038/ng.3419, PMID: 26457646

R Development Core Team. 2019. R: A language and environment for statistical computing. Vienna, Austria, R Foundation for Statistical Computing. https://www.R-project.org/

Ren S, Peng Z, Mao JH, Yu Y, Yin C, Gao X, Cui Z, Zhang J, Yi K, Xu W, Chen C, Wang F, Guo X, Lu J, Yang J, Wei M, Tian Z, Guan Y, Tang L, Xu C, et al. 2012. RNA-seq analysis of prostate Cancer in the chinese population identifies recurrent gene fusions, cancer-associated long noncoding RNAs and aberrant alternative splicings. *Cell Research* **22**:806–821. DOI: https://doi.org/10.1038/cr.2012.30, PMID: 22349460

Rodrigues DN, Butler LM, Estelles DL, de Bono JS. 2014. Molecular pathology and prostate Cancer therapeutics: from biology to bedside. *The Journal of Pathology* **232**:178–184. DOI: https://doi.org/10.1002/path.4272, PMID: 24108540

Roe CR, Millington DS, Norwood DL, Kodo N, Sprecher H, Mohammed BS, Nada M, Schulz H, McVie R. 1990. 2, 4-Dienoyl-coenzyme A reductase deficiency: a possible new disorder of fatty acid oxidation. *Journal of Clinical Investigation* **85**:1703–1707. DOI: https://doi.org/10.1172/JCI114624, PMID: 2332510

Rossi S, Graner E, Febbo P, Weinstein L, Bhattacharya N, Onody T, Bubley G, Balk S, Loda M. 2003. Fatty acid synthase expression defines distinct molecular signatures in prostate Cancer. *Molecular Cancer Research : MCR* **1**:707–715. PMID: 12939396

Sboner A, Demichelis F, Calza S, Pawitan Y, Setlur SR, Hoshida Y, Perner S, Adami HO, Fall K, Mucci LA, Kantoff PW, Stampfer M, Andersson SO, Varenhorst E, Johansson JE, Gerstein MB, Golub TR, Rubin MA, Andrén O. 2010. Molecular sampling of prostate Cancer: a dilemma for predicting disease progression. *BMC Medical Genomics* **3**:8. DOI: https://doi.org/10.1186/1755-8794-3-8, PMID: 20233430

Scher HI, Fizazi K, Saad F, Taplin ME, Sternberg CN, Miller K, de Wit R, Mulders P, Chi KN, Shore ND, Armstrong AJ, Flaig TW, Fléchon A, Mainwaring P, Fleming M, Hainsworth JD, Hirmand M, Selby B, Seely L, de Bono JS, AFFIRM Investigators. 2012. Increased survival with enzalutamide in prostate Cancer after chemotherapy. *New England Journal of Medicine* **367**:1187–1197. DOI: https://doi.org/10.1056/NEJMoa1207506, PMID: 22894553

Schlaepfer IR, Rider L, Rodrigues LU, Gijón MA, Pac CT, Romero L, Cimic A, Sirintrapun SJ, Glodé LM, Eckel RH, Cramer SD. 2014. Lipid catabolism via CPT1 as a therapeutic target for prostate Cancer. *Molecular Cancer Therapeutics* **13**:2361–2371. DOI: https://doi.org/10.1158/1535-7163.MCT-14-0183, PMID: 25122071

Schlaepfer IR, Glodé LM, Hitz CA, Pac CT, Boyle KE, Maroni P, Deep G, Agarwal R, Lucia SM, Cramer SD, Serkova NJ, Eckel RH. 2015. Inhibition of lipid oxidation increases glucose metabolism and enhances 2-Deoxy-2-[(18)F]Fluoro-D-Glucose uptake in prostate Cancer mouse xenografts. *Molecular Imaging and Biology* **17**:529–538. DOI: https://doi.org/10.1007/s11307-014-0814-4, PMID: 25561013

Shoukry K, Schulz H. 1998. Significance of the reductase-dependent pathway for the beta-oxidation of unsaturated fatty acids with odd-numbered double bonds. Mitochondrial metabolism of 2-trans-5-cis-octadienoyl-CoA. *The Journal of Biological Chemistry* **273**:6892–6899. DOI: https://doi.org/10.1074/jbc.273.12.6892, PMID: 9506993

Shurbaji MS, Kalbfleisch JH, Thurmond TS. 1996. Immunohistochemical detection of a fatty acid synthase (OA-519) as a predictor of progression of prostate Cancer. *Human Pathology* **27**:917–921. DOI: https://doi.org/10.1016/S0046-8177(96)90218-X, PMID: 8816886

Slattery ML, Schumacher MC, West DW, Robison LM, French TK. 1990. Food-consumption trends between adolescent and adult years and subsequent risk of prostate Cancer. *The American Journal of Clinical Nutrition* **52**:752–757. DOI: https://doi.org/10.1093/ajcn/52.4.752, PMID: 2403069

Stéfani ED, Deneo-Pellegrini H, Boffetta P, Ronco A, Mendilaharsu M. 2000. α-Linolenic acid and risk of prostate Cancer: a Case-Control study in Uruguay. *Cancer Epidemiology Biomarkers & Prevention* **9**:335–338. DOI: https://doi.org/10.1007/s11745-004-1315-2

Swinnen JV, Roskams T, Joniau S, Van Poppel H, Oyen R, Baert L, Heyns W, Verhoeven G. 2002. Overexpression of fatty acid synthase is an early and common event in the development of prostate Cancer. *International Journal of Cancer* **98**:19–22. DOI: https://doi.org/10.1002/ijc.10127, PMID: 11857379

Taylor BS, Schultz N, Hieronymus H, Gopalan A, Xiao Y, Carver BS, Arora VK, Kaushik P, Cerami E, Reva B, Antipin Y, Mitsiades N, Landers T, Dolgalev I, Major JE, Wilson M, Socci ND, Lash AE, Heguy A, Eastham JA, et al. 2010. Integrative genomic profiling of human prostate Cancer. *Cancer Cell* **18**:11–22. DOI: https://doi.org/10.1016/j.ccr.2010.05.026, PMID: 20579941

Tomlins SA, Mehra R, Rhodes DR, Cao X, Wang L, Dhanasekaran SM, Kalyana-Sundaram S, Wei JT, Rubin MA, Pienta KJ, Shah RB, Chinnaiyan AM. 2007. Integrative molecular concept modeling of prostate Cancer progression. *Nature Genetics* **39**:41–51. DOI: https://doi.org/10.1038/ng1935, PMID: 17173048

Toren P, Kim S, Johnson F, Zoubeidi A. 2016. Combined AKT and MEK pathway blockade in Pre-Clinical models of Enzalutamide-Resistant prostate Cancer. *PLOS ONE* **11**:e0152861. DOI: https://doi.org/10.1371/journal.pone.0152861, PMID: 27046225

Tran C, Ouk S, Clegg NJ, Chen Y, Watson PA, Arora V, Wongvipat J, Smith-Jones PM, Yoo D, Kwon A, Wasielewska T, Welsbie D, Chen CD, Higano CS, Beer TM, Hung DT, Scher HI, Jung ME, Sawyers CL. 2009. Development of a second-generation antiandrogen for treatment of advanced prostate Cancer. *Science* **324**:787–790. DOI: https://doi.org/10.1126/science.1168175, PMID: 19359544

Tse BWC, Volpert M, Ratther E, Stylianou N, Nouri M, McGowan K, Lehman ML, McPherson SJ, Roshan-Moniri M, Butler MS, Caradec J, Gregory-Evans CY, McGovern J, Das R, Takhar M, Erho N, Alshalafa M, Davicioni E, Schaeffer EM, Jenkins RB, et al. 2017. Neuropilin-1 is upregulated in the adaptive response of prostate tumors to androgen-targeted therapies and is prognostic of metastatic progression and patient mortality. *Oncogene* **36**:3417–3427. DOI: https://doi.org/10.1038/onc.2016.482, PMID: 28092670

Wang S, Wu J, Suburu J, Gu Z, Cai J, Axanova LS, Cramer SD, Thomas MJ, Perry DL, Edwards IJ, Mucci LA, Sinnott JA, Loda MF, Sui G, Berquin IM, Chen YQ. 2012. Effect of dietary polyunsaturated fatty acids on castration-resistant Pten-null prostate Cancer. *Carcinogenesis* **33**:404–412. DOI: https://doi.org/10.1093/carcin/bgr290

Warburg O, Wind F, Negelein E. 1927. The metabolism of tumors in the body. *The Journal of General Physiology* **8**:519–530. DOI: https://doi.org/10.1085/jgp.8.6.519, PMID: 19872213

Watt MJ, Clark AK, Selth LA, Haynes VR, Lister N, Rebello R, Porter LH, Niranjan B, Whitby ST, Lo J, Huang C, Schittenhelm RB, Anderson KE, Furic L, Wijayaratne PR, Matzaris M, Montgomery MK, Papargiris M, Norden S, Febbraio M, et al. 2019. Suppressing fatty acid uptake has therapeutic effects in preclinical models of prostate Cancer. *Science Translational Medicine* **11**:eaau5758. DOI: https://doi.org/10.1126/scitranslmed.aau5758, PMID: 30728288

Whittemore AS, Kolonel LN, Wu AH, John EM, Gallagher RP, Howe GR, Burch JD, Hankin J, Dreon DM, West DW. 1995. Prostate Cancer in relation to diet, physical activity, and body size in blacks, whites, and asians in the united states and Canada. *JNCI Journal of the National Cancer Institute* **87**:652–661. DOI: https://doi.org/10.1093/jnci/87.9.652, PMID: 7752270

Williams CD, Whitley BM, Hoyo C, Grant DJ, Iraggi JD, Newman KA, Gerber L, Taylor LA, McKeever MG, Freedland SJ. 2011. A high ratio of dietary n-6/n-3 polyunsaturated fatty acids is associated with increased risk of prostate Cancer. *Nutrition Research* **31**:1–8. DOI: https://doi.org/10.1016/j.nutres.2011.01.002, PMID: 21310299

Wu X, Daniels G, Lee P, Monaco ME. 2014. Lipid metabolism in prostate Cancer. *American Journal of Clinical and Experimental Urology* **2**:111–120. DOI: https://doi.org/10.3390/ijms20112626, PMID: 25374912

Zadra G, Photopoulos C, Loda M. 2013. The fat side of prostate Cancer. *Biochimica Et Biophysica Acta* **1831**: 1518–1532. DOI: https://doi.org/10.1016/j.bbalip.2013.03.010

Zadra G, Loda M. 2018. Metabolic vulnerabilities of prostate Cancer: diagnostic and therapeutic opportunities. *Cold Spring Harbor Perspectives in Medicine* **8**:a030569. DOI: https://doi.org/10.1101/cshperspect.a030569, PMID: 29229664

Appendix 1

Key Resources Table

Appendix 1—key resources table

Reagent type (species) or resource	Designation	Source or reference	Identifiers	Additional information
Strain, strain background (*M. musculus*, male,)	NOD scid Gamma (*M. musculus*, male,) Mice	The Jackson Laboratory/Interbred at SAHMRI Bioresources	NOD.Cg-Prkdcscid/J RRID:IMSR_JAX:001303	
Cell line (*Homo-sapiens*)	LNCaP	ATCC	ATCC CRL-1740 RRID:CVCL_1379	
Cell line (*Homo-sapiens*)	VCaP	ATCC	ATCC CRL-2876 RRID:CVCL_2235	
Cell line (*Homo-sapiens*)	22RV1	ATCC	ATCC CRL-2505 RRID:CVCL_1045	
Cell line (*Homo-sapiens*)	PNT1A	The European Collection of Authenticated Cell Cultures (ECACC)	Cat# 95012614 RRID:CVCL_2163	
Cell line (*Homo-sapiens*)	PNT2	The European Collection of Authenticated Cell Cultures (ECACC)	Cat# 95012613 RRID:CVCL_2164	
Cell line (*Homo-sapiens*)	V16D	PMID:27046225	Kind gift from Prof. Amina Zoubeidi	
Cell line (*Homo-sapiens*)	MR49F	PMID:27046225	Kind gift from Prof. Amina Zoubeidi	
Transfected construct (*Homo sapiens*)	control siRNA	Dharmacon	D-001810-01-20 ON-TARGET plus Non-targeting siRNA #1	transfected construct (human)
Transfected construct (*Homo sapiens*)	siDECR1-1	Dharmacon	J-009642-05-0002	transfected construct (human)
Transfected construct (*Homo sapiens*)	siDECR1-2	Dharmacon	J-009642-06-0002	transfected construct (human)
Transfected construct (*Homo sapiens*)	DECR1 shRNA lentivector	GenTargrt	LVS-1002	Lentiviral construct to transfect and express the shRNA.

Appendix 1—key resources table continued

Reagent type (species) or resource	Designation	Source or reference	Identifiers	Additional information
Transfected construct (*Homo sapiens*)	hDECR1 Overexpressing Lentivector	GenTargrt	LVS-2002	Lentiviral construct to transfect and over-express DECR1.
Transfected construct (*Homo sapiens*)	Negative control shRNA lentivector	GenTargrt	LVS-1002	Lentiviral construct to transfect and express the shRNA.
Antibody	Anti-human β-Actin (Mouse monoclonal)	Sigma-Aldrich	Cat#: A5441 RRID:AB_476744	(WB 1:2000)
Antibody	Anti-human-HSP90 (Rabbit Polyclonal)	Cell Signalling Technology	Cat#: 48745 RRID:CVCL_E547	(WB 1:1000)
Antibody	Anti-human DECR1 (Rabbit Polyclonal)	Prestige Antibodies (Sigma-Aldrich)	Cat#: HPA023238 RRID:AB_1847587	(WB 1:1000) (IHC: 1:500)
Antibody	Anti-human Malondialdehyde (Rabbit Polyclonal)	Abcam	Cat#: ab6463 RRID:AB_305484	(WB 1:1000)
Antibody	Anti- human Androgen receptor (Rabbit Polyclonal)	Santa Cruz Biotechnology	Cat#: sc-816 RRID:AB_1563391	(WB 1:1000)
Antibody	Anti-human PARP (Rabbit Polyclonal)	Cell Signalling Technology	Cat#: 9542 RRID:AB_592473	(WB 1:1000)
Antibody	Anti-human Cyto-chrome C (Rabbit Polyclonal)	Abcam	Cat#: ab90529 RRID:AB_10673869	(WB 1:2000)
Other	MitoTracker Red CMXRos	Thermo Fisher Scientific	Cat#: M7512	ICC 1:1000
Other	MitoSOX Red Mitochondrial Superoxide Indicator	Thermo Fisher Scientific	Cat#: M36008	Flow Cytometry: 2.5 µM
Other	3,3′-Diaminobenzi-dine (DAB) Enhanced Liquid Substrate System tetrahydrochloride	Sigma Aldrich	Cat#: D3939	
Other	BODIPY-C11	Thermo Fisher Scientific	Cat#: D3861	Imaging: 5 µM
Antibody	Anti-human KI67 (Mouse monoclonal)	DAKO	Cat#: M7240 RRID:AB_2142367	(IHC 1:200)
Antibody	Anti-human AR (Rabbit polyclonal)	Santa Cruz	Cat#: sc-816 RRID:AB_1563391	(WB 1:1000)
Sequence-based reagent	DECR1_F	This paper	PCR primers	CTAAATGGCA-CAGCCTTCGT

Appendix 1—key resources table continued

Reagent type (species) or resource	Designation	Source or reference	Identifiers	Additional information
Sequenced-based reagent	DECR1_R	This paper	PCR primers	AACCTGAACCAG TCTCAGCA
Sequence-based reagent	GAPDH_F	This paper	PCR primers	TGCACCACCAAC TGCTTAGC
Sequenced-based reagent	GAPDH_R	This paper	PCR primers	GGCATGGACTG TGGTCATGAG
Sequence-based reagent	PPIA_F	This paper	PCR primers	GCATACGGGTCC TGGCAT
Sequence-based reagent	PPIA_R	This paper	PCR primers	ACATGCTTGCCA TCCAACC
Sequence-based re-agent	TUBA1B _F	This paper	PCR primers	CCTTCGCCTCC TAATCCCTA
Sequence-based reagent	TUBA1B _R	This paper	PCR primers	CCGTGTTCCAGG-CAGTAGA
Sequence-based reagent	MKI67_F	This paper	PCR primers	GCCTGC TCGACCCTACA-GA
Sequence-based reagent	MIK67_R	This paper	PCR primers	GCTTGTCAAC TGCGGTTGC
Sequence-based reagent	L19_F	This paper	PCR primers	TGCCAG TGGAAAAA TCAGCCA
Sequence-based reagent	L19_R	This paper	PCR primers	CAAAGCAAATC TCGACACCTTG
Sequence-based reagent	GUSB_F	This paper	PCR primers	CGTCCCACCTA-GAATCTGCT
Sequence-based reagent	GUSB_R	This paper	PCR primers	TTGCTCA-CAAAGGTCA-CAGG
Sequence-based reagent	DECR1_F	This paper	ChIP-qPCR	TTCTGGAGCGC TAAGAGAGC
Sequence-based reagent	DECR1_R	This paper	ChIP-qPCR	AGGGCTTCATC TGACAGTGG
Sequence-based reagent	KLK3_F	This paper	ChIP-qPCR	GCCTGGATCTGA-GAGAGATATCA TC
Sequence-based reagent	KLK3_R	This paper	ChIP-qPCR	ACACC TTTTTTTTCTGGA TTGTTG
Sequence-based reagent	NC2_F	This paper	ChIP-qPCR	GTGAGTGCCCAG TTAGAGCATCTA

Appendix 1—key resources table continued

Reagent type (species) or resource	Designation	Source or reference	Identifiers	Additional information
Sequence-based reagent	NC2_R	This paper	ChIP-qPCR	GGAACCAGTGGG TCTTGAAGTG
Chemical compound, drug	Etomoxir	Sigma Aldrich	Cat#: E1905	
Chemical compound, drug	Dihydrotestosterone	Sigma Aldrich	Cas#: 521-18-6	
Chemical compound, drug	Enzalutamide	Sapphire Bioscience	Cat#: S1250	
Chemical compound, drug	Bovine-serum albu-min	Bovostar	Cat#: BSAS-AU	
Chemical compound, drug	Linoleic acid	Sigma Aldrich	Cat#: L1376	
Chemical compound, drug	Palmitic acid	Sigma Aldrich	Cat#: P0500	
Chemical compound, drug	D-Luciferin	PerkinElmer	Cat#: 122799	3 mg/20 g
Chemical compound, drug	Deferoxamine	Sigma Aldrich	Cat#: D9533	
Chemical compound, drug	Ferrostatin	Sigma Aldrich	Cat#: SML0583	
Chemical compound, drug	Erastian	Sigma Aldrich	Cat#: E7781	
Chemical compound, drug	ML210	Tocris Bioscience	Cat#: 6429	
Chemical compound, drug	FIN56	Tocris Bioscience	Cat#: 6280	
Chemical compound, drug	cell fractionation kit	Abcam	Cat#: ab109719	
Chemical compound, drug	RNeasy RNA extrac-tion kit	Qiagen	Cat#: 74136	
Chemical compound, drug	iScript cDNA Synthesis kit	Bio-Rad	Cat#: 1708890	
Chemical compound, drug	Seahorse XF Cell Mito chondrial Stress Test kit	Agilent	Cat#: 103015–100	
Software, algorithm	GraphPad Prism	GraphPad Software, Inc	Prism V7 RRID:SCR_ 002798	

Appendix 1—key resources table continued

Reagent type (species) or resource	Designation	Source or reference	Identifiers	Additional information
Software, algorithm	R	***R Development Core Team, 2019***	R version 3.6.2 RRID:SCR_001905	
Software, algorithm	ReViSP	PMID:25561413	ReViSP	Volume assessment of cancer spheroids
Software, algorithm	IVIS Spectrum In Vivo Imaging System	PerkinElmer	IVIS Spectrum In Vivo Imaging System RRID:SCR_018621	Tumor volume analysis
Other	Lipofectamine RNAiMAX transfection reagent	Thermo Fisher Scientific	13778075	
Software, algorithm	ImageJ analysis software	NIH	ImageJ RRID:SCR_003070	
Software, algorithm	TraceFinder v5.0	Thermo Fisher Scientific	OPTON-30688	

7.2 Map of inducible SMARTvector supplied by Dharmacon

horizon™
INSPIRED CELL SOLUTIONS

PLASMID MAP

Dharmacon™ SMARTvector™ Inducible Lentiviral shRNA

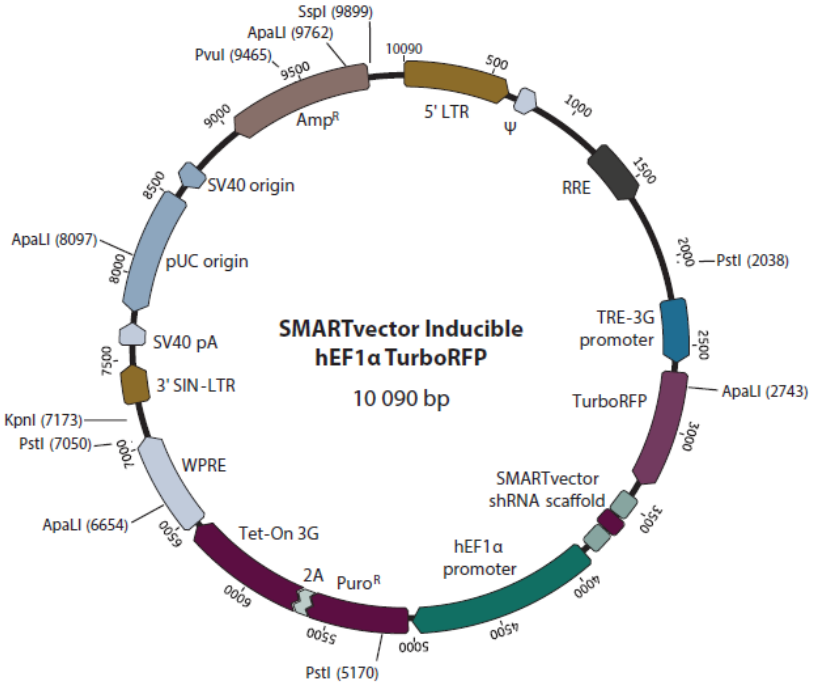

Plasmid features	Position
5' LTR	1–635
ψ	685–822
RRE	1252–1605
TRE-3G promoter	2240–2615
TurboRFP	2668–3363
SMARTvector shRNA scaffold	3458–3864
hEF1α promoter	3885–5002
Puro^R	5021–5623
2A	5624–5683
Tet-On™ 3G	5684–6430
WPRE	6444–7035
3' SIN-LTR	7239–7473
SV40 pA	7582–7712
pUC origin	7783–8508
SV40 origin	8578–8713
Amp^R	9021–9881

Restriction sites	Position
ApaLI	2743, 6654, 8097, 9762
KpnI	7173
PstI	2038, 5170, 7050
PvuI	9465
SspI	9899

If you have any questions, contact

t +44 (0) 1223 976 000 (UK) **or** +1 800 235 9880 (USA); +1 303 604 9499 (USA)
f + 44 (0)1223 655 581
w horizondiscovery.com/contact–us **or** dharmacon.horizondiscovery.com/service-and-support
Horizon Discovery, 8100 Cambridge Research Park, Waterbeach, Cambridge, CB25 9TL, United Kingdom

7.3 Map of plasmid used for preparation ACSM1/3 over expressing vectors

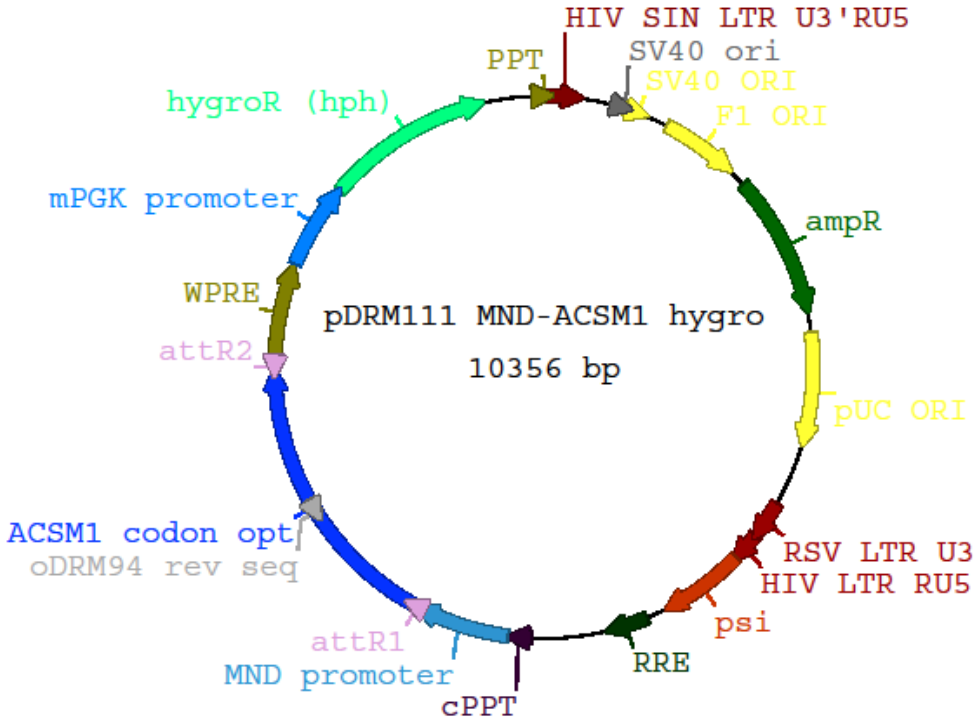

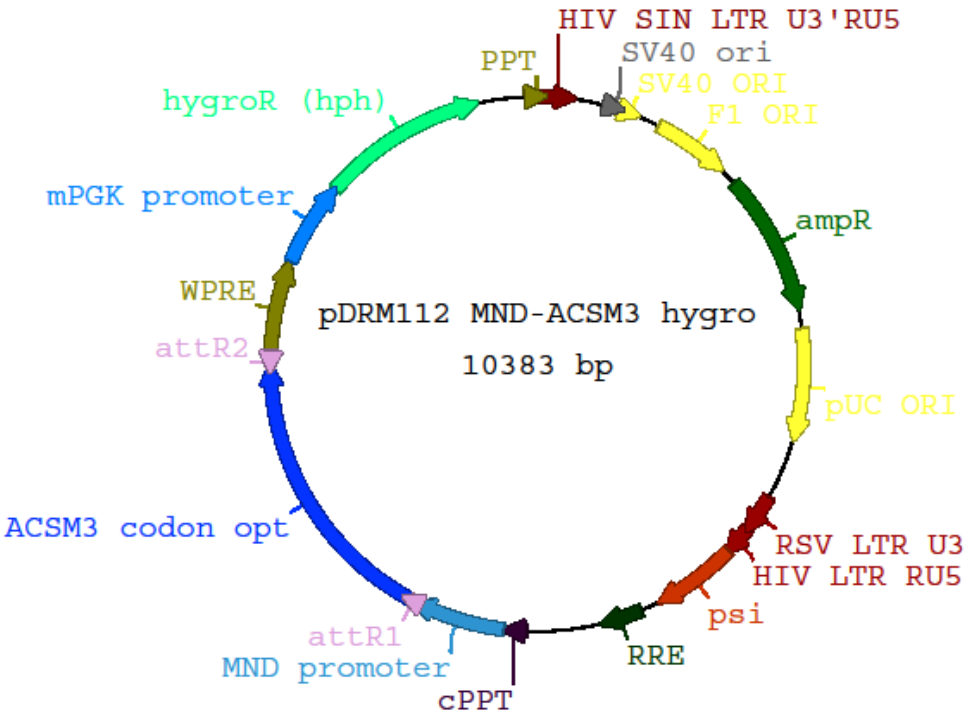

7.4 Sequence of gblock used for the preparation of overexpressing vectors

7.4.1 ACSM1 gBlock sequence (tDRM17)

GGGACAAGTTTGTACAAAAAAGCAGGCTgccaccATGCAGTGGTTGATG
AGATTTAGAACACTCTGGGGCATACACAAAAGCTTTCACAATATTCACCCTGC
CCCGTCCCAGCTGCGCTGCAGAAGTCTTTCCGAATTCGGAGCCCCCCGCTG
GAATGACTATGAGGTTCCGGAAGAATTCAATTTCGCTAGTTATGTGCTGGACT
ACTGGGCTCAAAAGGAAAAGGAAGGCAAAAGGGGTCCTAACCCGGCATTCT
GGTGGGTAAATGGCCAGGGTGATGAAGTCAAATGGAGCTTTAGGGAGATGG
GGGATCTGACTCGAAGAGTGGCAAACGTGTTCACGCAAACGTGCGGGCTTC
AGCAGGGAGACCACCTGGCACTCATGTTGCCAAGAGTGCCCGAATGGTGGC
TCGTGGCTGTTGGGTGCATGAGGACGGGCATTATATTTATTCCCGCGACCAT
TCTCCTGAAAGCCAAAGACATCCTCTATCGGTTGCAGCTGTCCAAGGCTAAG
GGAATCGTCACAATAGATGCGCTCGCCAGCGAAGTTGACTCTATCGCGTCTC
AATGTCCTTCCTTGAAGACAAAGCTCCTGGTATCAGATCACTCTCGCGAGGG
TTGGCTTGACTTCCGGAGCCTTGTCAAGTCCGCGTCTCCGGAGCACACTTGT
GTTAAGAGCAAAACCCTTGACCCAATGGTGATATTCTTTACAAGTGGGACTAC
TGGCTTCCCTAAGATGGCTAAGCATAGCCATGGTCTCGCTCTCCAGCCATCA
TTTCCTGGATCTAGAAAACTTAGAAGTCTTAAGACAAGCGATGTATCCTGGTG
CCTCTCCGATAGTGGGTGGATTGTAGCAACTATCTGGACACTGGTCGAGCCC
TGGACAGCCGGTTGCACTGTGTTCATTCACCACCTTCCACAGTTTGATACCA
AAGTCATCATACAAACCCTTCTCAAGTACCCGATCAACCACTTCTGGGGGGT
TAGCTCTATCTATCGCATGATTCTTCAGCAGGATTTTACTAGCATCAGGTTCC
CCGCTCTCGAACACTGCTATACCGGAGGCGAGGTGGTACTGCCTAAAGATC
AAGAGGAATGGAAACGCAGAACGGGGCTTCTCCTCTATGAAAACTACGGCC
AGTCCGAGACCGGTCTCATATGTGCTACATATTGGGGGATGAAAATAAAGCC
CGGTTTCATGGGAAAAGCTACTCCTCCTTACGATGTTCAGGTAATAGATGAC
AAAGGTTCTATCCTTCCCCCGAACACAGAAGGCAACATAGGTATTCGCATTA
AGCCGGTACGCCCGGTATCTCTCTTTATGTGCTATGAGGGTGATCCGGAAAA
AACCGCAAAGGTAGAGTGCGGCGACTTTTATAACACTGGCGATCGAGGGAA
GATGGATGAGGAAGGTTACATATGCTTTTTGGGAAGGAGTGACGACATAATC
AACGCCTCTGGGTATCGGATTGGTCCTGCGGAGGTGGAGTCTGCGCTCGTC
GAGCATCCTGCGGTCGCTGAGTCAGCTGTTGTAGGGAGTCCTGATCCGATC
CGGGGTGAGGTTGTGAAGGCCTTCATTGTGTTGACGCCCCAGTTTCTGTCTC
ACGACAAGGACCAGTTGACCAAAGAGCTTCAACAGCATGTCAAGTCTGTCAC
GGCCCCGTATAAGTATCCTCGGAAAGTCGAATTTGTCTCTGAGTTGCCTAAG
ACAATCACGGGGAAGATCGAACGCAAGGAGCTGCGAAAAAAAGAGACGGGA
CAGATGTAAacccagctttcttgtacaaagtggtcccc

7.4.2 ACSM3 gBlock sequence (tDRM18)

GGGACAAGTTTGTACAAAAAAGCAGGCTgccaccATGCTTGCTCGAGTG
ACCCGGAAAATGCTGCGCCACGCCAAATGTTTCCAGAGGCTCGCGATTTTCG
GGTCAGTGAGAGCTCTTCATAAGGACAACAGAACGGCTACCCCCCAAAACTT
TAGCAATTACGAATCTATGAAACAAGATTTCAAATTGGGCATACCGGAGTACT
TTAATTTCGCAAAAGATGTGCTTGATCAATGGACTGACAAGGAGAAAGCAGG
TAAAAAGCCGAGCAATCCTGCATTTTGGTGGATAAACAGGAACGGCGAAGAG
ATGCGGTGGTCCTTTGAGGAACTTGGCTCTCTGTCTCGCAAGTTTGCTAACA
TACTTTCCGAGGCGTGTAGCCTTCAGCGCGgtgaCcgcgtCattttAatATTGCCACG
GGTCCCCGAATGGTGGTTGGCCAATGTCGCGTGCCTCCGGACCGGAACAGT
TCTTATACCGGGCACAACGCAACTTACACAAAAGGATATACTTTATAGACTTC
AAAGTAGCAAGGCTAACTGCATTATTACCAACGATGTACTCGCACCCGCCGT
AGATGCAGTCGCCTCCAAGTGCGAAAACTTGCATTCAAAGCTTATCGTTTCT
GAGAACTCCCGGGAAGGATGGGGTAATCTCAAGGAACTGATGAAACATGCC
TCAGACTCTCATACTTGTGTGAAAACCAAACATAATGAGATTATGGCTATATT
CTTTACGTCCGGCACCAGTGGCTATCCCAAAATGACGGCACACACGCATAGC
TCATTCGGTCTTGGACTTAGTGTCAATGGTAGATTTTGGCTTGACCTGACTCC
AAGTGATGTTATGTGGAATACGTCAGACACTGGATGGGCTAAGTCCGCTTGG
AGCAGTGTCTTCAGTCCTTGGATTCAAGGTGCCTGCGTATTTACTCACCATCT
TCCCCGGTTTGAACCTACGAGTATTCTCCAGACATTGAGCAAGTACCCCATC
ACAGTGTTCTGCTCTGCACCAACGGTTTATAGGATGTTGGTTCAAAATGACAT
CACGAGCTATAAATTTAAATCCCTGAAACACTGCGTATCAGCGGGTGAACCT
ATCACACCAGATGTAACGGAAAAATGGCGGAACAAAACAGGACTTGATATCT
ACGAGGGGTATGGACAAACGGAGACGGTCTTGATATGCGGAAATTTCAAGG
GTATGAAGATTAAGCCTGGGTCAATGGGCAAGCCTTCCCCGGCCTTTGATGT
CAAAATCGTTGATGTAAATGGCAATGTCCTGCCCCCAGGTCAGGAAGGCGAT
ATAGGAATTCAGGTTCTTCCGAATAGGCCATTTGGGTTGTTCACGCATTATGT
AGACAACCCCTCCAAAACAGCTAGTACTCTTCGAGGAAATTTTTACATCACAG
GAGATAGGGGCTACATGGATAAAGACGGCTACTTTTGGTTCGTGGCGCGGG
CAGATGACGTTATACTGAGTAGTGGATACCGAATCGGGCCCTTCGAGGTAGA
GAATGCGTTGAATGAACACCCATCCGTGGCCGAGTCAGCAGTAGTCTCCTCC
CCTGATCCGATTCGCGGAGAGGTTGTTAAGGCATTTGTGGTACTCAATCCAG
ACTACAAATCTCACGATCAAGAACAACTTATAAAAGAGATACAAGAGCATGTG
AAAAAGACGACCGCTCCTTACAAATACCCCCGCAAGGTCGAATTTATACAAG
AGTTGCCGAAGACGATAAGCGGGAAGACTAAGAGGAACGAACTCCGGAAAA
AAGAATGGAAGACTATCTAAacccagctttcttgtacaaagtggtcccc

7.5 Amino acid mapping ACSM1 versus ACSM2A

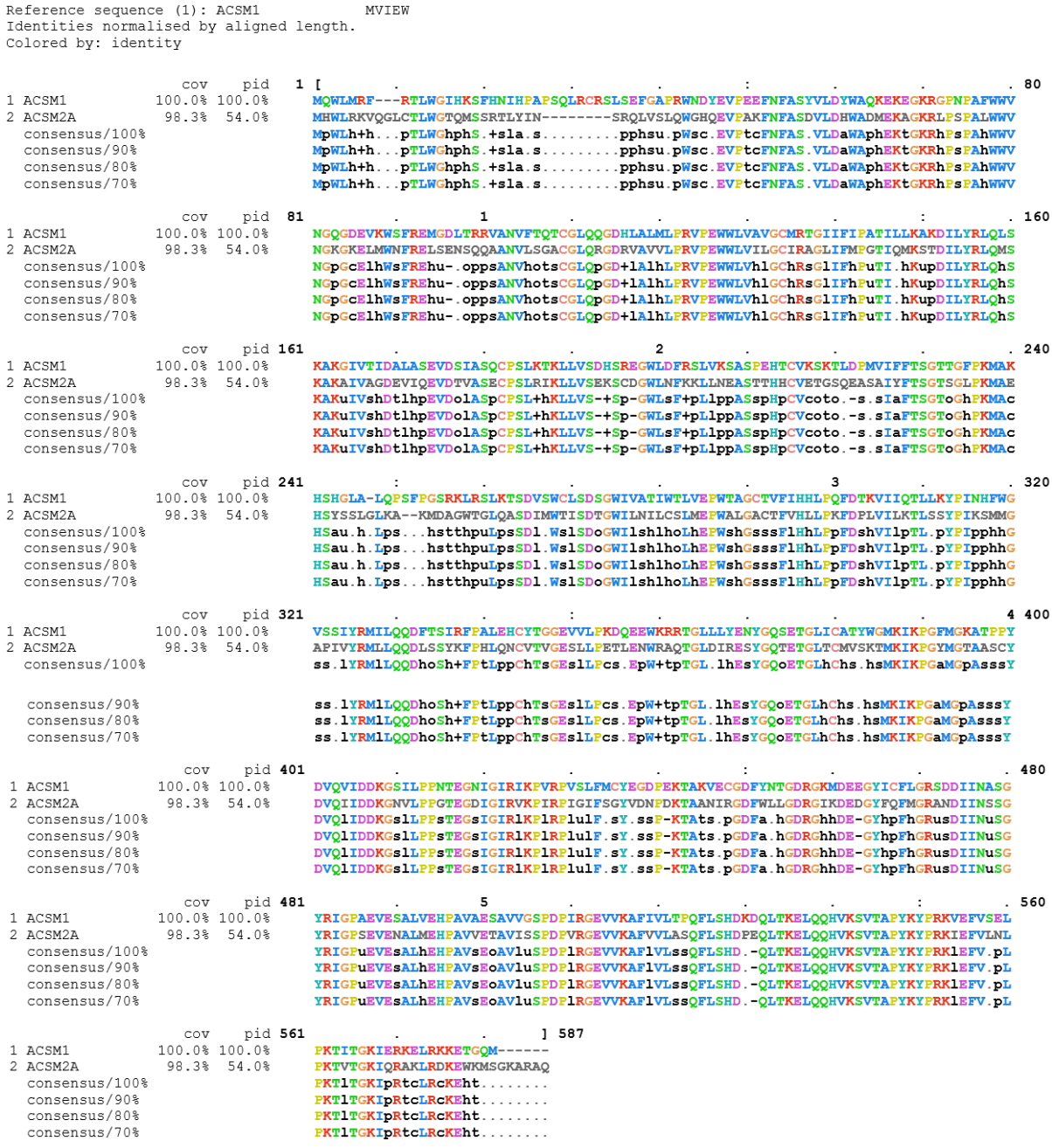

7.6 Amino acid mapping ACSM3 versus ACSM2A

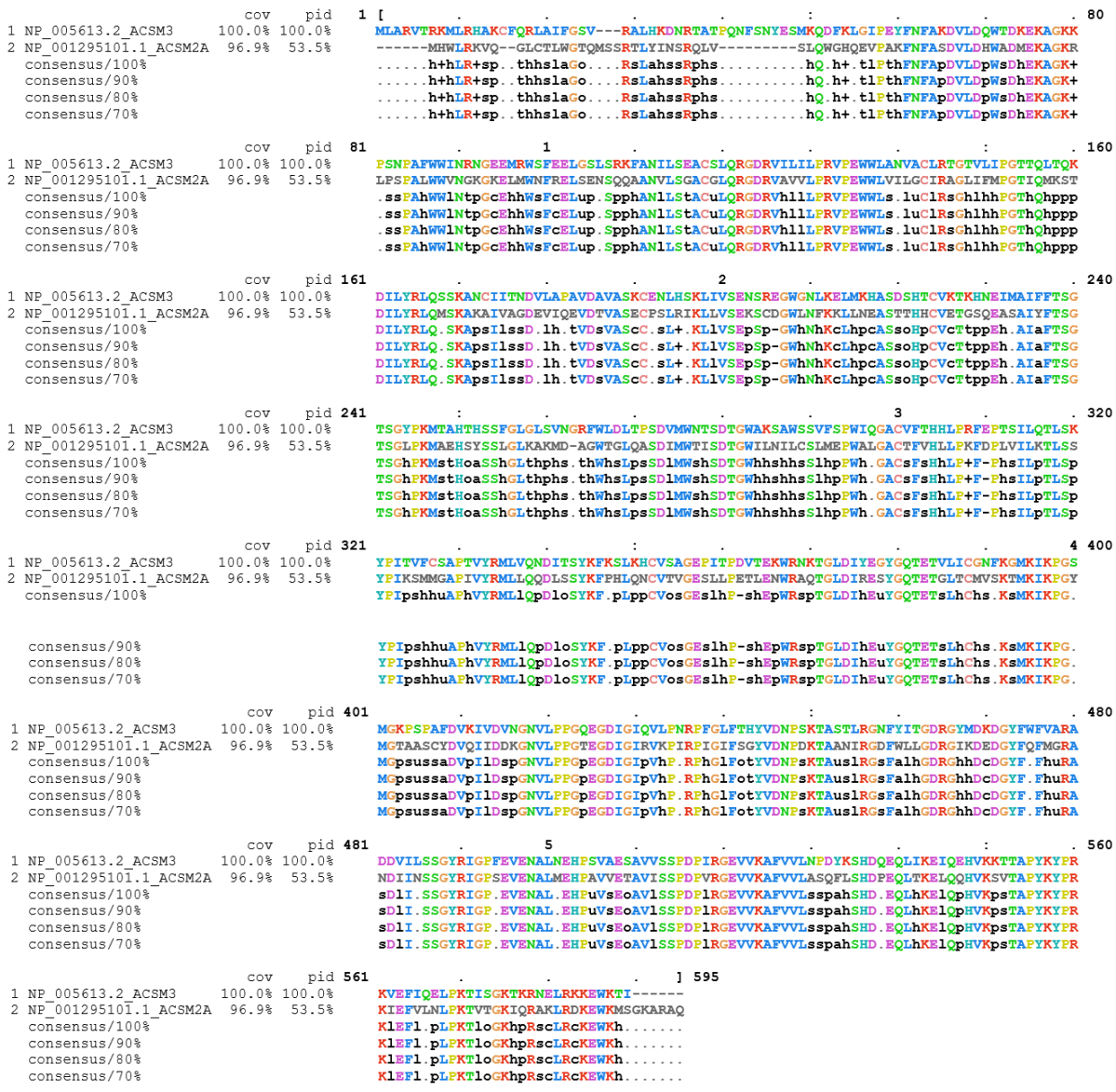

7.7 Function of the candidate genes involved in Lipid metabolic processes.

Fig No.	Gene name	Function of candidate gene/s in lipid metabolism
3.1.1.	***ACACA/ACC*** (Acetyl-CoA carboxylase 1)	ACACA catalyzes the carboxylation of acetyl-CoA to form malonyl-CoA (irreversible reaction), the committed metabolite in FA synthesis; and fatty acid synthase (FASN) then sequentially adds 2-carbon units until a long-chain fatty acid is produced (Padanad et al., 2016). ACACA regulates both biosynthesis and breakdown of long chain fatty acids. Two isozymes, ACC1 and ACC2, mediate distinctive physiological functions within the cell, with ACC1 localized primarily to the cytosol and ACC2 to the mitochondria (Abu-Elheiga et al., 2000).
3.1.2	***ACOT2*** (Acyl-coenzyme A thioesterase 2, mitochondrial)	ACOT2 are a group of enzymes that catalyze the hydrolysis of acyl-CoAs to the free fatty acid and coenzyme A (CoASH), providing the potential to regulate intracellular levels of acyl-CoAs, free fatty acids and CoASH (Hunt, Rautanen, Westin, Svensson, & Alexson, 2006). ACOT2 displays higher activity toward long chain acyl CoAs (C14-C20) ACOT2 is involved in enhancing the hepatic fatty acid oxidation in mitochondria (Hunt et al., 2006; Jones & Gould, 2000).
3.1.3	***ACSL3*** (Long-chain-fatty-acid--CoA ligase 3*)*	The protein encoded by this gene is an isozyme of the long-chain fatty-acid-coenzyme A ligase family. Individual isozyme has substrate specificity subcellular localization, and tissue distribution. All the members of ACSL family convert free long-chain fatty acids into fatty acyl-CoA esters, and thereby play a key role in lipid biosynthesis and fatty acid degradation.

		Thus, ACSL3 also activates long-chain fatty acids for both synthesis of cellular lipids, and degradation via beta-oxidation (Coleman, Lewin, Van Horn, & Gonzalez-Baró, 2002; Nakahara et al., 2012). ACSL3 plays important role for the incorporation of fatty acids into phosphatidylcholine, the major phospholipid located on the surface of VLDL (very low density lipoproteins) (Yao & Ye, 2008). Exogeneous fatty acids and de novo fatty acid synthesis are the source of fatty acid in cells. Once fatty acids are in the cell, ACSLs also promote their retention by converting them into hydrophilic fatty acyl-CoA esters so that cannot exit cells (Kamp & Hamilton, 2006). ACSL enzymes are ubiquitously expressed across different tissues, ACSL3 is mainly expressed in the endoplasmic reticulum (ER) and lipid droplets(Grevengoed, Klett, & Coleman, 2014; Soupene & Kuypers, 2008) ACSL enzymes also been reported to participate in the metabolic reprogramming of cancer cells. E.g., pharmacologic inhibition of ACSLs results in apoptosis in a subset of TP53-deficient cancer cells. ACSL3 play a role in the maintenance of cancers expressing mutant KRAS (Padanad et al., 2016).
3.1.4.	***ACSM1*** (Acyl-coenzyme A synthetase ACSM1, mitochondrial)	The function of ACSM1 and ACSM3 will be discussed in more details in chapter 4.

3.1.5	***ACSM3*** (Acyl-coenzyme A synthetase ACSM3, mitochondrial)	
3.1.6	***ELOVL5*** (Elongation of very long chain fatty acids protein 5)	Elongases of very long-chain fatty acids (ELOVL) catalyze the rate-limiting condensation step in the elongation of fatty acids including long-chain polyunsaturated fatty acids (LC-PUFA) biosynthesis (Jakobsson, Westerberg, & Jacobsson, 2006; Nugteren, 1965). Condensing enzyme that acts specifically toward polyunsaturated acyl-CoA with the higher activity toward C18:3(n-6) acyl-CoA. ELOVL5 has been identified and functionally characterized as crucial enzymes involved in the biosynthetic pathway of LC-PUFA. Importantly, functional studies have shown that ELOVL5 can effectively elongate both C18 and C20 PUFA (Castro, Tocher, & Monroig, 2016). ELOVL7 is the family member of ELOVL which is overexpressed in PCa and play critical role in lipid metabolism (Tamura et al., 2009). ELOVL7 could affect fatty acid composition in phospholipids and neutral lipids including cholesterol ester in prostate cancer cells, possibly contributing to de novo steroidogenesis in prostate cancer cells (Tamura et al., 2009).
3.1.7	***ELOVL7*** (Elongation of very long chain fatty acids protein 7)	
3.1.8	***FASN*** (Fatty acid synthase)	FASN is a multienzyme protein that catalyzes the synthesis of fatty acids (mainly the long-chain saturated fatty acid palmitate) from acetyl-CoA and malonyl-CoA in the presence

		of nicotinamide adenine dinucleotide phosphate reduced form (NADPH)(Javier A. Menendez & Ruth Lupu, 2007). Upregulation of FASN in a common event in multiple cancers and accumulating evidence suggests that it is a metabolic oncogene with an important role in tumor growth and survival, making it an attractive target for cancer therapy (Flavin, Peluso, Nguyen, & Loda, 2010).
3.1.9	***HACL1*** (2-hydroxyacyl-CoA lyase 1)	Peroxisomal 2-OH acyl-CoA lyase involved in the cleavage (C1 removal) reaction in the fatty acid alpha-oxydation in a thiamine pyrophosphate (TPP)-dependent manner (Foulon et al., 1999; Fraccascia, Casteels, De Schryver, & Van Veldhoven, 2011; Kitamura, Seki, & Kihara, 2017). Involved in the degradation of 3-methyl-branched fatty acids like phytanic acid and the shortening of 2-hydroxy long-chain fatty acids manner (Foulon et al., 1999; Fraccascia et al., 2011; Kitamura et al., 2017).
3.1.10	***HSD17B4*** (Peroxisomal multifunctional enzyme type 2)	HSDs play central roles in the biosynthesis and inactivation of steroid hormones, but some of them are also involved in the mechanism of diverse non-steroidal compounds(Hoffmann & Maser, 2007) . HSD17Bs are enzymes that regulate both androgen and estrogen action, via oxidation of the C17 alcohol to an inactive or less active ketone, or via reduction of the ketone to an active steroid (dihydrotestosterone, testosterone, or estradiol). Along with HSD17B2, HSD17B4 is capable of oxidizing Δ5-androstenediol (the precursor of testosterone) to dihydroepiandrosterone (DHEA)(Maltais, Luu-The, & Poirier, 2002) One of the HSD17B4 splice isoforms harbors enzymatic

		activity, which normally inactivates androgens and suppresses AR signaling, and that specific loss of this transcript-encoded enzyme enables the clinical development of CRPC and HSD17B4 highly associated with progression from initiation of ADT to the development of CRPC (Ross et al., 2008). In addition, HSD17B (bifunctional enzyme) catalyzes the formation of 3-ketoacyl-CoA intermediates from straight-chain, 2-methyl-branched-chain fatty acids bile acid intermediates. HSD17B4 is essential for the oxidation of a wide range of peroximal substrates (very long chain acyl CoAs, branched chain acyl CoA) (Lines et al., 2014).
3.1.11	***MAPKAPK2*** (MAP kinase-activated protein kinase 2)	This gene encodes a member of the Ser/Thr protein kinase family. This kinase is regulated through direct phosphorylation by p38 MAP kinase. In conjunction with p38 MAP kinase, this kinase is known to be involved in many cellular processes including stress and inflammatory responses, nuclear export, gene expression regulation and cell proliferation. Heat shock protein HSP27 was shown to be one of the substrates of this kinase in vivo. Two transcript variants encoding two different isoforms have been found for this gene. Source: https://www.ncbi.nlm.nih.gov/gene/9261
3.1.12	***MMAA*** (Methylmalonic aciduria type A protein, mitochondrial)	The MMAA gene provides instructions for making a protein that is involved in the formation of a compound called adenosylcobalamin (AdoCbl). AdoCbl, which is derived from vitamin B12 (also called cobalamin), is necessary for the normal function of an enzyme known as methylmalonyl CoA mutase. This enzyme helps break down certain proteins, fats

		(lipids), and cholesterol Research indicates that the MMAA protein may play a role in one of the last steps in AdoCbl formation, the transport of vitamin B12 into mitochondria (specialized structures inside cells that serve as energy-producing centers). Additional chemical reactions then convert vitamin B12 into AdoCbl. Other studies suggest that the MMAA protein may help stabilize methylmalonyl CoA mutase and protect the enzyme from being turned off (inactivated). Source https://ghr.nlm.nih.gov/gene/MMAA GTPase, binds and hydrolyzes GTP (Froese et al., 2010; Plessl et al., 2017). Involved in intracellular vitamin B12 metabolism, mediates the transport of cobalamin (Cbl) into mitochondria for the final steps of adenosylcobalamin (AdoCbl) synthesis. Functions as a G-protein chaperone that assists AdoCbl cofactor delivery from MMAB to the methylmalonyl-CoA mutase (MMUT) and reactivation of the enzyme during catalysis (Froese et al., 2010; Plessl et al., 2017).
3.1.13	***MORC2*** (ATPase MORC2)	This gene encodes a member of the Microrchidia (MORC) protein superfamily. The encoded protein is known to regulate the condensation of heterochromatin in response to DNA damage and play a role in repressing transcription. The protein has been found to regulate the activity of ATP citrate lyase via specific interaction with this enzyme in the cytosol of lipogenic breast cancer cells. The protein also plays a role in lipogenesis and adipocyte differentiation. Alternative splicing results in multiple transcript variants encoding different isoforms Source: https://ghr.nlm.nih.gov/gene/MORC2

3.1.14	***PCCB*** (Propionyl-CoA carboxylase beta chain, mitochondrial)	The PCCB gene provides instructions for making part of an enzyme called propionyl-CoA carboxylase, specifically, the beta subunit of this enzyme. Six beta subunits come together with six alpha subunits (produced from the PCCA gene) to form a functioning enzyme. Propionyl-CoA carboxylase plays a role in the normal processing of proteins. It carries out a particular step in the breakdown of several protein building blocks (amino acids) called isoleucine, methionine, threonine, and valine. Propionyl-CoA carboxylase also helps break down certain types of lipids (fats) and cholesterol. First, several chemical reactions convert the amino acids, lipids, or cholesterol to a molecule called propionyl-CoA. Using the B vitamin biotin, propionyl-CoA carboxylase then converts propionyl-CoA to a molecule called methylmalonyl-CoA. Additional enzymes break down methylmalonyl-CoA into other molecules that are used for energy. Source: https://ghr.nlm.nih.gov/gene/PCCB This is one of the 2 subunits of the biotin-dependent propionyl-CoA carboxylase (PCC), a mitochondrial enzyme involved in the catabolism of odd chain fatty acids, branched-chain amino acids isoleucine, threonine, methionine, and valine and other metabolites (H. Jiang, Rao, Yee, & Kraus, 2005; Kalousek, Darigo, & Rosenberg, 1980). Propionyl-CoA carboxylase catalyzes the carboxylation of propionyl-CoA/propanoyl-CoA to D-methylmalonyl-CoA/(S)-methylmalonyl-CoA (H. Jiang et al., 2005; Kalousek et al., 1980). Within the holoenzyme, the alpha subunit catalyzes the ATP-dependent carboxylation of the biotin carried by the biotin carboxyl carrier (BCC) domain, while the beta subunit then transfers the carboxyl group from

		carboxylated biotin to propionyl-CoA (By similarity). Propionyl-CoA carboxylase also significantly acts on butyryl-CoA/butanoyl-CoA, which is converted to ethylmalonyl-CoA/(2S)-ethylmalonyl-CoA at a much lower rate (Kalousek et al., 1980). Other alternative minor substrates include (2E)-butenoyl-CoA/crotonoyl-CoA.
3.1.15	***PCTP*** (Phosphatidylcholine transfer protein)	PCTP is a cytosolic Catalyzes the transfer of phosphatidylcholine between membranes (Roderick et al., 2002). PCTP promote the rapid intermembrane exchange of phosphatidylcholines but no other phospholipid class (B. H. Geijtenbeek, Smith, Borst, & Wirtz, 1996; Cohen & Green, 1995; Cohen, Green, Wu, & Beier, 1999; van Helvoort et al., 1999; K. W. Wirtz & Zilversmit, 1968; K. W. A. Wirtz, 1991; M. K. Wu, Boylan, & Cohen, 1999). PCTP, phosphatidylinositol transfer protein (PI-TP) and sterol carrier protein 2 (SCP2) account for most of the phospholipid exchange activity present within the cytosol (Roderick et al., 2002). its highest level of expression in humans is found in the liver, liver, placenta, testis, kidney and heart (Cohen et al., 1999).
3.1.16	***PRKAB2*** (Protein Kinase AMP-Activated Non-Catalytic Subunit Beta 2)	The protein encoded by this gene is a regulatory subunit of the AMP-activated protein kinase (AMPK). AMPK is a heterotrimer consisting of an alpha catalytic subunit, and non-catalytic beta and gamma subunits. AMPK is an important energy-sensing enzyme that monitors cellular energy status. In response to cellular metabolic stresses, AMPK is activated, and thus phosphorylates and inactivates acetyl-CoA carboxylase (ACC) and beta-hydroxy beta-methylglutaryl-CoA reductase

		(HMGCR), key enzymes involved in regulating de novo biosynthesis of fatty acid and cholesterol. This subunit may be a positive regulator of AMPK activity. It is highly expressed in skeletal muscle and thus may have tissue-specific roles. Multiple alternatively spliced transcript variants have been found for this gene. Non-catalytic subunit of AMP-activated protein kinase (AMPK), an energy sensor protein kinase that plays a key role in regulating cellular energy metabolism. In response to reduction of intracellular ATP levels, AMPK activates energy-producing pathways and inhibits energy-consuming processes: inhibits protein, carbohydrate and lipid biosynthesis, as well as cell growth and proliferation. AMPK acts via direct phosphorylation of metabolic enzymes, and by longer-term effects via phosphorylation of transcription regulators. Also acts as a regulator of cellular polarity by remodeling the actin cytoskeleton; probably by indirectly activating myosin. Beta non-catalytic subunit acts as a scaffold on which the AMPK complex assembles, via its C-terminus that bridges alpha (PRKAA1 or PRKAA2) and gamma subunits (PRKAG1, PRKAG2 or PRKAG3). Source: https://ghr.nlm.nih.gov/gene/PRKAB2
3.1.17	***PTGR2*** (Prostaglandin reductase 2)	PTGR2 catalyzes an NADPH-dependent reduction of the conjugated α,β-unsaturated double bond of 15-keto-PGE2, a key step in terminal inactivation of prostaglandins and suppression of PPARγ-mediated adipocyte differentiation (Y. H. Wu et al., 2008).

		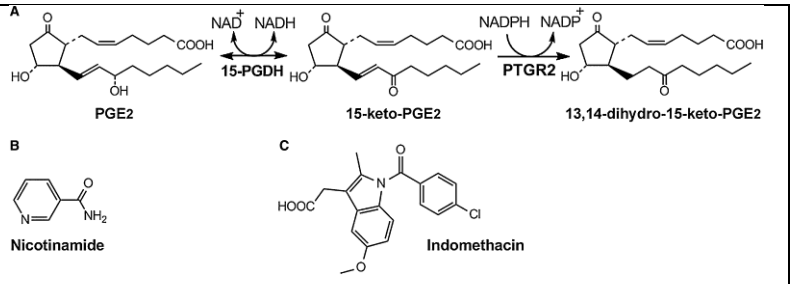 A NAD+ NADH 15-PGDH NADPH NADP+ PTGR2 COOH HO OH O PGE2 15-keto-PGE2 13,14-dihydro-15-keto-PGE2 B N NH2 Nicotinamide C HOOC N Cl O Indomethacin

8 BIBLIOGRAPHY

Abida, W., Cyrta, J., Heller, G., Prandi, D., Armenia, J., Coleman, I., . . . Van Allen, E. M. (2019). Genomic correlates of clinical outcome in advanced prostate cancer. *Proceedings of the National Academy of Sciences, 116*(23), 11428-11436.

Abu-Elheiga, L., Brinkley, W. R., Zhong, L., Chirala, S. S., Woldegiorgis, G., & Wakil, S. J. (2000). The subcellular localization of acetyl-CoA carboxylase 2. *Proc Natl Acad Sci U S A, 97*(4), 1444-1449. doi:10.1073/pnas.97.4.1444

Accioly, M. T., Pacheco, P., Maya-Monteiro, C. M., Carrossini, N., Robbs, B. K., Oliveira, S. S., . . . Viola, J. P. (2008). Lipid bodies are reservoirs of cyclooxygenase-2 and sites of prostaglandin-E2 synthesis in colon cancer cells. *Cancer Res, 68*(6), 1732-1740. doi:10.1158/0008-5472.Can-07-1999

Aggarwal, R., Zhang, T., Small, E. J., & Armstrong, A. J. (2014). Neuroendocrine prostate cancer: subtypes, biology, and clinical outcomes. *Journal of the National Comprehensive Cancer Network, 12*(5), 719-726.

Ahmed, M., & Li, L. C. (2013). Adaptation and clonal selection models of castration-resistant prostate cancer: current perspective. *Int J Urol, 20*(4), 362-371. doi:10.1111/iju.12005

Akamatsu, S., Inoue, T., Ogawa, O., & Gleave, M. E. (2018). Clinical and molecular features of treatment-related neuroendocrine prostate cancer. *International Journal of Urology, 25*(4), 345-351.

Amemiya-Kudo, M., Shimano, H., Hasty, A. H., Yahagi, N., Yoshikawa, T., Matsuzaka, T., . . . Yamada, N. (2002). Transcriptional activities of nuclear SREBP-

1a, -1c, and -2 to different target promoters of lipogenic and cholesterogenic genes. *J Lipid Res, 43*(8), 1220-1235.

Amler, L. C., Agus, D. B., LeDuc, C., Sapinoso, M. L., Fox, W. D., Kern, S., . . . Hampton, G. M. (2000). Dysregulated expression of androgen-responsive and nonresponsive genes in the androgen-independent prostate cancer xenograft model CWR22-R1. *Cancer Res, 60*(21), 6134-6141.

Antonarakis, E. S. (2013). Enzalutamide: the emperor of all anti-androgens. *Translational andrology and urology, 2*(2), 119.

Armandari, I., Hamid, A. R., Verhaegh, G., & Schalken, J. (2014). Intratumoral steroidogenesis in castration-resistant prostate cancer: a target for therapy. *Prostate International, 2*(3), 105-113. doi:http://dx.doi.org/10.12954/PI.14063

Artibani, W., Porcaro, A. B., De Marco, V., Cerruto, M. A., & Siracusano, S. (2018). Management of Biochemical Recurrence after Primary Curative Treatment for Prostate Cancer: A Review. *Urol Int, 100*(3), 251-262. doi:10.1159/000481438

Arunakaran, J., Aruldhas, M. M., & Govindarajulu, P. (1987). Influence of castration and testosterone propionate on prostatic and seminal vesicular lipids in mature monkeys. *Indian J Physiol Pharmacol, 31*(3), 184-189.

Arunakaran, J., Aruldhas, M. M., & Govindarajulu, P. (1990). Effects of prolactin and androgens on the prostatic lipids of castrated mature bonnet monkeys. *Prostate, 17*(3), 247-260. doi:10.1002/pros.2990170309

Arunakaran, J., Balasubramanian, K., Srinivasan, N., Aruldhas, M. M., & Govindarajulu, P. (1992). Interaction of androgens and prolactin on prostatic enzymes of the pyruvate-malate cycle involved in lipogenesis in castrated mature monkey, Macaca radiata. *Cytobios, 70*(280), 33-40.

ARVER, S. (1982). Zinc and zinc ligands in human seminal plasma. *Acta Physiologica Scandinavica, 116*(1), 67-73. doi:10.1111/j.1748-1716.1982.tb10600.x

Asangani, I. A., Dommeti, V. L., Wang, X., Malik, R., Cieslik, M., Yang, R., . . . Chinnaiyan, A. M. (2014). Therapeutic targeting of BET bromodomain proteins in castration-resistant prostate cancer. *Nature, 510*(7504), 278-282. doi:10.1038/nature13229

Ather, M. H., Abbas, F., Faruqui, N., Israr, M., & Pervez, S. (2008). Correlation of three immunohistochemically detected markers of neuroendocrine differentiation with clinical predictors of disease progression in prostate cancer. *BMC Urol, 8*, 21. doi:10.1186/1471-2490-8-21

Audet-Walsh, E., Dufour, C. R., Yee, T., Zouanat, F. Z., Yan, M., Kalloghlian, G., . . . Giguere, V. (2017). Nuclear mTOR acts as a transcriptional integrator of the androgen signaling pathway in prostate cancer. *Genes Dev, 31*(12), 1228-1242. doi:10.1101/gad.299958.117

Audet-Walsh, E., Vernier, M., Yee, T., Laflamme, C., Li, S., Chen, Y., & Giguere, V. (2018). SREBF1 Activity Is Regulated by an AR/mTOR Nuclear Axis in Prostate Cancer. *Mol Cancer Res, 16*(9), 1396-1405. doi:10.1158/1541-7786.Mcr-17-0410

Avela, H. F., & Sirén, H. (2020). Advances in lipidomics. *Clinica Chimica Acta, 510*, 123-141. doi:https://doi.org/10.1016/j.cca.2020.06.049

B. H. Geijtenbeek, T., Smith, A. J., Borst, P., & Wirtz, K. W. A. (1996). cDNA cloning and tissue-specific expression of the phosphatidylcholine transfer protein gene. *Biochemical Journal, 316*(1), 49-55. doi:10.1042/bj3160049

Balaban, S., Lee, L. S., Schreuder, M., & Hoy, A. J. (2015). Obesity and cancer progression: is there a role of fatty acid metabolism? *BioMed research international, 2015*.

Balaban, S., Nassar, Z. D., Zhang, A. Y., Hosseini-Beheshti, E., Centenera, M. M., Schreuder, M., . . . Hoy, A. J. (2019). Extracellular Fatty Acids Are the Major Contributor to Lipid Synthesis in Prostate Cancer. *Molecular Cancer Research, 17*(4), 949-962. doi:10.1158/1541-7786.Mcr-18-0347

Balk, S. P. (2014). Androgen receptor functions in prostate cancer development and progression. *Asian journal of andrology, 16*(4), 561-564. doi:10.4103/1008-682X.126396

Banerjee, P. P., Banerjee, S., Brown, T. R., & Zirkin, B. R. (2018). Androgen action in prostate function and disease. *American journal of clinical and experimental urology, 6*(2), 62-77.

Bao, J., Zhu, L., Zhu, Q., Su, J., Liu, M., & Huang, W. (2016). SREBP-1 is an independent prognostic marker and promotes invasion and migration in breast cancer. *Oncol Lett, 12*(4), 2409-2416. doi:10.3892/ol.2016.4988

Barbie, D. A., Tamayo, P., Boehm, J. S., Kim, S. Y., Moody, S. E., Dunn, I. F., . . . Hahn, W. C. (2009). Systematic RNA interference reveals that oncogenic KRAS-driven cancers require TBK1. *Nature, 462*(7269), 108-112. doi:10.1038/nature08460

Barfeld, S. J., Itkonen, H. M., Urbanucci, A., & Mills, I. G. (2014). Androgen-regulated metabolism and biosynthesis in prostate cancer. *Endocr Relat Cancer, 21*(4), T57-66. doi:10.1530/erc-13-0515

Bartzatt, R., Cirillo, S. L. G., & Cirillo, J. D. (2007). Antibacterial activity of dipeptide constructs of acetylsalicylic acid and nicotinic acid. *Drug Deliv, 14*(2), 105-109. doi:10.1080/10717540600740128

Bassil, N., Alkaade, S., & Morley, J. E. (2009). The benefits and risks of testosterone replacement therapy: a review. *Therapeutics and clinical risk management, 5*(3), 427-448. doi:10.2147/tcrm.s3025

Beckers, A., Organe, S., Timmermans, L., Scheys, K., Peeters, A., Brusselmans, K., . . . Swinnen, J. V. (2007). Chemical inhibition of acetyl-CoA carboxylase induces growth arrest and cytotoxicity selectively in cancer cells. *Cancer Research, 67*(17), 8180-8187.

Beloribi-Djefaflia, S., Vasseur, S., & Guillaumond, F. (2016). Lipid metabolic reprogramming in cancer cells. *Oncogenesis, 5*, e189. doi:10.1038/oncsis.2015.49

Bertolio, R., Napoletano, F., Mano, M., Maurer-Stroh, S., Fantuz, M., Zannini, A., . . . Del Sal, G. (2019). Sterol regulatory element binding protein 1 couples mechanical cues and lipid metabolism. *Nature Communications, 10*(1), 1326. doi:10.1038/s41467-019-09152-7

Best, S. A., De Souza, D. P., Kersbergen, A., Policheni, A. N., Dayalan, S., Tull, D., . . . Sutherland, K. D. (2018). Synergy between the KEAP1/NRF2 and PI3K Pathways Drives Non-Small-Cell Lung Cancer with an Altered Immune Microenvironment. *Cell Metab, 27*(4), 935-943 e934. doi:10.1016/j.cmet.2018.02.006

Bhavsar, A., & Verma, S. (2014). Anatomic imaging of the prostate. *Biomed Res Int, 2014*, 728539. doi:10.1155/2014/728539

Bishop, J. L., Thaper, D., Vahid, S., Davies, A., Ketola, K., Kuruma, H., . . . Johnson, F. (2017). The Master Neural Transcription Factor BRN2 Is an Androgen Receptor–Suppressed Driver of Neuroendocrine Differentiation in Prostate Cancer. *Cancer discovery, 7*(1), 54-71.

Bluemn, E. G., Coleman, I. M., Lucas, J. M., Coleman, R. T., Hernandez-Lopez, S., Tharakan, R., . . . Corella, A. N. (2017). Androgen receptor pathway-independent prostate cancer is sustained through FGF signaling. *Cancer cell, 32*(4), 474-489. e476.

Bluemn, E. G., Coleman, I. M., Lucas, J. M., Coleman, R. T., Hernandez-Lopez, S., Tharakan, R., . . . Nelson, P. S. (2017). Androgen Receptor Pathway-Independent Prostate Cancer Is Sustained through FGF Signaling. *Cancer Cell, 32*(4), 474-489.e476. doi:10.1016/j.ccell.2017.09.003

Bonora, M., Wieckowsk, M. R., Chinopoulos, C., Kepp, O., Kroemer, G., Galluzzi, L., & Pinton, P. (2015). Molecular mechanisms of cell death: central implication of ATP synthase in mitochondrial permeability transition. *Oncogene, 34*(12), 1608. doi:10.1038/onc.2014.462

Briggs, M. R., Kadonaga, J. T., Bell, S. P., & Tjian, R. (1986). Purification and biochemical characterization of the promoter-specific transcription factor, Sp1. *Science, 234*(4772), 47-52. doi:10.1126/science.3529394

Briggs, M. R., Yokoyama, C., Wang, X., Brown, M. S., & Goldstein, J. L. (1993). Nuclear protein that binds sterol regulatory element of low density lipoprotein receptor promoter. I. Identification of the protein and delineation of its target nucleotide sequence. *Journal of Biological Chemistry, 268*(19), 14490-14496.

Brinkmann, A. O., Blok, L. J., de Ruiter, P. E., Doesburg, P., Steketee, K., Berrevoets, C. A., & Trapman, J. (1999). Mechanisms of androgen receptor activation and function. *J Steroid Biochem Mol Biol, 69*(1-6), 307-313.

Brinkmann, A. O., Jenster, G., Kuiper, G. G. J. M., Ris, C., van Laar, J. H., van der Korput, J. A. G. M., . . . Trapman, J. (1992). The human androgen receptor: Structure/function relationship in normal and pathological situations. *The Journal of Steroid Biochemistry and Molecular Biology, 41*(3), 361-368. doi:https://doi.org/10.1016/0960-0760(92)90362-M

Brown, M. S., & Goldstein, J. L. (1997). The SREBP pathway: Regulation of cholesterol metabolism by proteolysis of a membrane-bound transcription factor. *Cell, 89*(3), 331-340. doi:10.1016/S0092-8674(00)80213-5

Brown, M. S., & Goldstein, J. L. (1998). Sterol Regulatory Element Binding Proteins (Srebps): Controllers of Lipid Synthesis and Cellular Uptake. *Nutrition Reviews, 56*(suppl_1), S1-S3. doi:10.1111/j.1753-4887.1998.tb01680.x

Brown, M. S., Ye, J., Rawson, R. B., & Goldstein, J. L. (2000). Regulated Intramembrane Proteolysis: A Control Mechanism Conserved from Bacteria to Humans. *Cell, 100*(4), 391-398. doi:https://doi.org/10.1016/S0092-8674(00)80675-3

Brusselmans, K., De Schrijver, E., Verhoeven, G., & Swinnen, J. V. (2005). RNA Interference–Mediated Silencing of the Acetyl-CoA-Carboxylase-α Gene Induces Growth Inhibition and Apoptosis of Prostate Cancer Cells. *Cancer Research, 65*(15), 6719-6725.

Butler, L. M., Centenera, M. M., & Swinnen, J. V. (2016). Androgen control of lipid metabolism in prostate cancer: novel insights and future applications. *Endocr Relat Cancer, 23*(5), R219-227. doi:10.1530/erc-15-0556

Cancer Genome Atlas Research, N. (2015). The Molecular Taxonomy of Primary Prostate Cancer. *Cell, 163*(4), 1011-1025. doi:10.1016/j.cell.2015.10.025

Castro, L. F., Tocher, D. R., & Monroig, O. (2016). Long-chain polyunsaturated fatty acid biosynthesis in chordates: Insights into the evolution of Fads and Elovl gene repertoire. *Prog Lipid Res, 62*, 25-40. doi:10.1016/j.plipres.2016.01.001

Centenera, M. M., Hickey, T. E., Jindal, S., Ryan, N. K., Ravindranathan, P., Mohammed, H., . . . Tilley, W. D. (2018). A patient-derived explant (PDE) model of hormone-dependent cancer. *Molecular oncology, 12*(9), 1608-1622. doi:10.1002/1878-0261.12354

Centenera, M. M., Raj, G. V., Knudsen, K. E., Tilley, W. D., & Butler, L. M. (2013). Ex vivo culture of human prostate tissue and drug development. *Nat Rev Urol, 10*(8), 483-487. doi:10.1038/nrurol.2013.126

Chandrasekar, T., Yang, J. C., Gao, A. C., & Evans, C. P. (2015). Mechanisms of resistance in castration-resistant prostate cancer (CRPC). *Translational andrology and urology, 4*(3), 365-380. doi:10.3978/j.issn.2223-4683.2015.05.02

Chen, C. D., Welsbie, D. S., Tran, C., Baek, S. H., Chen, R., Vessella, R., . . . Sawyers, C. L. (2004). Molecular determinants of resistance to antiandrogen therapy. *Nat Med, 10*(1), 33-39. doi:10.1038/nm972

Chen, C. D., Welsbie, D. S., Tran, C., Baek, S. H., Chen, R., Vessella, R., . . . Sawyers, C. L. (2004). Molecular determinants of resistance to antiandrogen therapy. *Nature medicine, 10*(1), 33.

Chen, M., Zhang, J., Sampieri, K., Clohessy, J. G., Mendez, L., Gonzalez-Billalabeitia, E., . . . Pandolfi, P. P. (2018). An aberrant SREBP-dependent lipogenic program promotes metastatic prostate cancer. *Nature genetics, 50*(2), 206-218. doi:10.1038/s41588-017-0027-2

Chen, M., Zhang, J., Sampieri, K., Clohessy, J. G., Mendez, L., Gonzalez-Billalabeitia, E., . . . Pandolfi, P. P. (2018). An aberrant SREBP-dependent lipogenic program promotes metastatic prostate cancer. *Nat Genet*. doi:10.1038/s41588-017-0027-2

Chen, Y., Clegg, N. J., & Scher, H. I. (2009). Anti-androgens and androgen-depleting therapies in prostate cancer: new agents for an established target. *The lancet oncology, 10*(10), 981-991.

Cheng, C., Geng, F., Cheng, X., & Guo, D. (2018). Lipid metabolism reprogramming and its potential targets in cancer. *Cancer Communications, 38*(1), 27. doi:10.1186/s40880-018-0301-4

Cheng, L., Montironi, R., Bostwick, D. G., Lopez-Beltran, A., & Berney, D. M. (2012). Staging of prostate cancer. *Histopathology, 60*(1), 87-117. doi:10.1111/j.1365-2559.2011.04025.x

Cheng, X., Li, J., & Guo, D. (2018). SCAP/SREBPs are Central Players in Lipid Metabolism and Novel Metabolic Targets in Cancer Therapy. *Current topics in medicinal chemistry, 18*(6), 484-493. doi:10.2174/1568026618666180523104541

Chodak, G. W., Kranc, D. M., Puy, L. A., Takeda, H., Johnson, K., & Chang, C. (1992). Nuclear Localization of Androgen Receptor In Heterogeneous Samples Of Normal, Hyperplastic And Neoplastic Human Prostate. *Journal of Urology, 147*(3 Part 2), 798-803. doi:doi:10.1016/S0022-5347(17)37389-5

Choi, Y., Kawazoe, Y., Murakami, K., Misawa, H., & Uesugi, M. (2003). Identification of bioactive molecules by adipogenesis profiling of organic compounds. *J Biol Chem, 278*(9), 7320-7324. doi:10.1074/jbc.M210283200

Chong, J. T., Oh, W. K., & Liaw, B. C. (2018). Profile of apalutamide in the treatment of metastatic castration-resistant prostate cancer: evidence to date. *OncoTargets and therapy, 11*, 2141.

Chou, R., Dana, T., Bougatsos, C., Fu, R., Blazina, I., Gleitsmann, K., & Rugge, J. B. (2011). In *Treatments for Localized Prostate Cancer: Systematic Review to Update the 2002 U.S. Preventive Services Task Force Recommendation*. Rockville (MD).

Choudhury, K. R., Yagle, K. J., Swanson, P. E., Krohn, K. A., & Rajendran, J. G. (2010). A robust automated measure of average antibody staining in immunohistochemistry images. *The journal of histochemistry and cytochemistry : official journal of the Histochemistry Society, 58*(2), 95-107. doi:10.1369/jhc.2009.953554

Chughtai, B., Forde, J. C., Thomas, D. D. M., Laor, L., Hossack, T., Woo, H. H., . . . Kaplan, S. A. (2016). Benign prostatic hyperplasia. *Nature Reviews Disease Primers, 2*, 16031. doi:10.1038/nrdp.2016.31

Coakley, F. V., & Hricak, H. (2000). RADIOLOGIC ANATOMY OF THE PROSTATE GLAND: A CLINICAL APPROACH. *Radiologic Clinics of North America, 38*(1), 15-30. doi:https://doi.org/10.1016/S0033-8389(05)70147-0

Cohen, D. E., & Green, R. M. (1995). Cloning and characterization of a cDNA encoding the specific phosphatidylcholine transfer protein from bovine liver. *Gene, 163*(2), 327-328. doi:https://doi.org/10.1016/0378-1119(95)00382-G

Cohen, D. E., Green, R. M., Wu, M. K., & Beier, D. R. (1999). Cloning, tissue-specific expression, gene structure and chromosomal localization of human phosphatidylcholine transfer protein11The nucleotide sequence data in this paper have been submitted to GenBank and have been assigned accession numbers AF114430–AF114437. *Biochimica et Biophysica Acta (BBA) - Gene Structure and Expression, 1447*(2), 265-270. doi:https://doi.org/10.1016/S0167-4781(99)00163-3

Coleman, R. A., Lewin, T. M., Van Horn, C. G., & Gonzalez-Baró, M. R. (2002). Do long-chain acyl-CoA synthetases regulate fatty acid entry into synthetic versus degradative pathways? *J Nutr, 132*(8), 2123-2126. doi:10.1093/jn/132.8.2123

Collins, L. C., Botero, M. L., & Schnitt, S. J. (2005). Bimodal frequency distribution of estrogen receptor immunohistochemical staining results in breast cancer: an analysis of 825 cases. *Am J Clin Pathol, 123*(1), 16-20. doi:10.1309/hcf035n9wk40etj0

Comstock, C. E., & Knudsen, K. E. (2007). The complex role of AR signaling after cytotoxic insult: implications for cell-cycle-based chemotherapeutics. *Cell Cycle, 6*(11), 1307-1313. doi:10.4161/cc.6.11.4353

Costello, L. C., Akuffo, V., & Franklin, R. B. (1988). Testosterone Stimulates Net Citrate Production from Aspartate by Prostate Epithelial Cells. *Horm Metab Res, 20*(04), 252-253. doi:10.1055/s-2007-1010807

Costello, L. C., Feng, P., Milon, B., Tan, M., & Franklin, R. B. (2004). Role of zinc in the pathogenesis and treatment of prostate cancer: critical issues to resolve. *Prostate Cancer and Prostatic Diseases, 7*(2), 111-117. doi:10.1038/sj.pcan.4500712

Costello, L. C., & Franklin, R. B. (1991). Concepts of citrate production and secretion by prostate 1. Metabolic relationships. *Prostate, 18*(1), 25-46. doi:10.1002/pros.2990180104

Costello, L. C., & Franklin, R. B. (1998). Novel role of zinc in the regulation of prostate citrate metabolism and its implications in prostate cancer. *Prostate, 35*(4), 285-296. doi:10.1002/(sici)1097-0045(19980601)35:4<285::Aid-pros8>3.0.Co;2-f

Costello, L. C., & Franklin, R. B. (2000). The Intermediary Metabolism of the Prostate: A Key to Understanding the Pathogenesis and Progression of Prostate Malignancy. *Oncology, 59*(4), 269-282. doi:10.1159/000012183

Costello, L. C., Franklin, R. B., Feng, P., Tan, M., & Bagasra, O. (2005). Zinc and prostate cancer: a critical scientific, medical, and public interest issue (United States). *Cancer Causes Control, 16*(8), 901-915. doi:10.1007/s10552-005-2367-y

Costello, L. C., Liu, Y., & Franklin, R. B. (1995). Testosterone stimulates the biosynthesis of m-aconitase and citrate oxidation in prostate epithelial cells. *Mol Cell Endocrinol, 112*(1), 45-51. doi:https://doi.org/10.1016/0303-7207(95)03582-R

Costello, L. C., Liu, Y., & Franklin, R. B. (1996). Testosterone and prolactin stimulation ofmitochondrial aconitase in pig prostate epithelial cells. *Urology, 48*(4), 654-659. doi:https://doi.org/10.1016/S0090-4295(96)00217-8

Costello, L. C., Liu, Y., Zou, J., & Franklin, R. B. (2000). Mitochondrial aconitase gene expression is regulated by testosterone and prolactin in prostate epithelial cells. *Prostate, 42*(3), 196-202. doi:10.1002/(sici)1097-0045(20000215)42:3<196::Aid-pros5>3.0.Co;2-8

Costello, L. C., Liu, Y., Zou, J., & Franklin, R. B. (2000). The pyruvate dehydrogenase E1 alpha gene is testosterone and prolactin regulated in prostate epithelial cells. *Endocrine Research, 26*(1), 23-39.

Coutinho, I., Day, T. K., Tilley, W. D., & Selth, L. A. (2016). Androgen receptor signaling in castration-resistant prostate cancer: a lesson in persistence. *Endocrine-Related Cancer, 23*(12), T179-T197.

Currie, E., Schulze, A., Zechner, R., Walther, T. C., & Farese, R. V., Jr. (2013). Cellular fatty acid metabolism and cancer. *Cell Metab, 18*(2), 153-161. doi:10.1016/j.cmet.2013.05.017

Dahabreh, I. J., Chung, M., Balk, E. M., Yu, W. W., Mathew, P., Lau, J., & Ip, S. (2012). Active surveillance in men with localized prostate cancer: a systematic review. *Ann Intern Med, 156*(8), 582-590. doi:10.7326/0003-4819-156-8-201204170-00397

Dang, Q., Chen, Y.-A., & Hsieh, J.-T. (2019). The dysfunctional lipids in prostate cancer. *American journal of clinical and experimental urology, 7*(4), 273-280.

Dardenne, E., Beltran, H., Benelli, M., Gayvert, K., Berger, A., Puca, L., . . . MacDonald, T. (2016). N-Myc induces an EZH2-mediated transcriptional program driving neuroendocrine prostate cancer. *Cancer cell, 30*(4), 563-577.

Das, R., Gregory, P. A., Fernandes, R. C., Denis, I., Wang, Q., Townley, S. L., . . . Selth, L. A. (2017). MicroRNA-194 Promotes Prostate Cancer Metastasis by Inhibiting SOCS2. *Cancer Res, 77*(4), 1021-1034. doi:10.1158/0008-5472.Can-16-2529

Davies, A. H., Beltran, H., & Zoubeidi, A. (2018). Cellular plasticity and the neuroendocrine phenotype in prostate cancer. *Nature Reviews Urology*.

DeBerardinis, R. J., Mancuso, A., Daikhin, E., Nissim, I., Yudkoff, M., Wehrli, S., & Thompson, C. B. (2007). Beyond aerobic glycolysis: transformed cells can engage in glutamine metabolism that exceeds the requirement for protein and nucleotide synthesis. *Proc Natl Acad Sci U S A, 104*(49), 19345-19350. doi:10.1073/pnas.0709747104

Decker, K. F., Zheng, D., He, Y., Bowman, T., Edwards, J. R., & Jia, L. (2012). Persistent androgen receptor-mediated transcription in castration-resistant prostate cancer under androgen-deprived conditions. *Nucleic Acids Research, 40*(21), 10765-10779. doi:10.1093/nar/gks888

Deep, G., & Schlaepfer, I. R. (2016). Aberrant Lipid Metabolism Promotes Prostate Cancer: Role in Cell Survival under Hypoxia and Extracellular Vesicles Biogenesis. *Int J Mol Sci, 17*(7). doi:10.3390/ijms17071061

Dehm, S. M., & Tindall, D. J. (2011). Alternatively spliced androgen receptor variants. *Endocrine-Related Cancer, 18*(5), R183-R196. doi:10.1530/ERC-11-0141

DePrimo, S. E., Diehn, M., Nelson, J. B., Reiter, R. E., Matese, J., Fero, M., . . . Brooks, J. D. (2002). Transcriptional programs activated by exposure of human prostate cancer cells to androgen. *Genome Biol, 3*(7), Research0032.

DePrimo, S. E., Diehn, M., Nelson, J. B., Reiter, R. E., Matese, J., Fero, M., . . . Brooks, J. D. (2002). Transcriptional programs activated by exposure of human prostate cancer cells to androgen. *Genome biology, 3*(7), RESEARCH0032-RESEARCH0032. doi:10.1186/gb-2002-3-7-research0032

Desouki, M. M., Geradts, J., Milon, B., Franklin, R. B., & Costello, L. C. (2007). hZip2 and hZip3 zinc transporters are down regulated in human prostate

adenocarcinomatous glands. *Molecular Cancer, 6*(1), 37. doi:10.1186/1476-4598-6-37

Donjacour, A. A., & Cunha, G. R. (1993). Assessment of prostatic protein secretion in tissue recombinants made of urogenital sinus mesenchyme and urothelium from normal or androgen-insensitive mice. *Endocrinology, 132*(6), 2342-2350. doi:10.1210/endo.132.6.7684975

Dooley, K. A., Bennett, M. K., & Osborne, T. F. (1999). A critical role for cAMP response element-binding protein (CREB) as a Co-activator in sterol-regulated transcription of 3-hydroxy-3-methylglutaryl coenzyme A synthase promoter. *J Biol Chem, 274*(9), 5285-5291. doi:10.1074/jbc.274.9.5285

Dooley, K. A., Millinder, S., & Osborne, T. F. (1998). Sterol regulation of 3-hydroxy-3-methylglutaryl-coenzyme A synthase gene through a direct interaction between sterol regulatory element binding protein and the trimeric CCAAT-binding factor/nuclear factor Y. *J Biol Chem, 273*(3), 1349-1356. doi:10.1074/jbc.273.3.1349

Dorotea, D., Koya, D., & Ha, H. (2020). Recent Insights Into SREBP as a Direct Mediator of Kidney Fibrosis via Lipid-Independent Pathways. *Frontiers in Pharmacology, 11*. doi:10.3389/fphar.2020.00265

Drudge-Coates, L. (2010). GnRH blockers: A changing paradigm in the management of prostate cancer. *International Journal of Urological Nursing, 3*, 85-92. doi:10.1111/j.1749-771X.2009.01081.x

Dunham, I., Kundaje, A., Aldred, S. F., Collins, P. J., Davis, C. A., Doyle, F., . . . HudsonAlpha Institute, C. U. C. I. S. g. (2012). An integrated encyclopedia of DNA

elements in the human genome. *Nature, 489*(7414), 57-74. doi:10.1038/nature11247

Eberlé, D., Hegarty, B., Bossard, P., Ferré, P., & Foufelle, F. (2004). SREBP transcription factors: master regulators of lipid homeostasis. *Biochimie, 86*(11), 839-848. doi:https://doi.org/10.1016/j.biochi.2004.09.018

Edwards, P. A., Tabor, D., Kast, H. R., & Venkateswaran, A. (2000). Regulation of gene expression by SREBP and SCAP. *Biochimica et Biophysica Acta (BBA) - Molecular and Cell Biology of Lipids, 1529*(1), 103-113. doi:https://doi.org/10.1016/S1388-1981(00)00140-2

Eisermann, K., Wang, D., Jing, Y., Pascal, L. E., & Wang, Z. (2013). Androgen receptor gene mutation, rearrangement, polymorphism. *Translational andrology and urology, 2*(3), 137.

Ellis, J. M., Bowman, C. E., & Wolfgang, M. J. (2015). Metabolic and tissue-specific regulation of acyl-CoA metabolism. *PLoS One, 10*(3), e0116587-e0116587. doi:10.1371/journal.pone.0116587

Ellis, L., & Loda, M. (2018). LSD1: A single target to combat lineage plasticity in lethal prostate cancer. *Proceedings of the National Academy of Sciences, 115*(18), 4530-4531.

Epstein, J. I., Amin, M. B., Beltran, H., Lotan, T. L., Mosquera, J. M., Reuter, V. E., . . . Rubin, M. A. (2014). Proposed morphologic classification of prostate cancer with neuroendocrine differentiation. *Am J Surg Pathol, 38*(6), 756-767. doi:10.1097/pas.0000000000000208

Ericsson, J., & Edwards, P. A. (1998). CBP is required for sterol-regulated and sterol regulatory element-binding protein-regulated transcription. *J Biol Chem, 273*(28), 17865-17870. doi:10.1074/jbc.273.28.17865

Ettinger, S. L., Sobel, R., Whitmore, T. G., Akbari, M., Bradley, D. R., Gleave, M. E., & Nelson, C. C. (2004). Dysregulation of sterol response element-binding proteins and downstream effectors in prostate cancer during progression to androgen independence. *Cancer Res, 64*(6), 2212-2221. doi:10.1158/0008-5472.can-2148-2

Feldman, B. J., & Feldman, D. (2001). The development of androgen-independent prostate cancer. *Nat Rev Cancer, 1*(1), 34-45. doi:10.1038/35094009

Flaig, T. W., Salzmann-Sullivan, M., Su, L. J., Zhang, Z., Joshi, M., Gijon, M. A., . . . Schlaepfer, I. R. (2017). Lipid catabolism inhibition sensitizes prostate cancer cells to antiandrogen blockade. *Oncotarget*. doi:10.18632/oncotarget.17359

Flavin, R., Peluso, S., Nguyen, P. L., & Loda, M. (2010). Fatty acid synthase as a potential therapeutic target in cancer. *Future oncology (London, England), 6*(4), 551-562. doi:10.2217/fon.10.11

Ford, W. C. L., & Harrison, A. (1984). The role of citrate in determining the activity of calcium ions in human semen. *International Journal of Andrology, 7*(3), 198-202. doi:10.1111/j.1365-2605.1984.tb00777.x

Forestier-Román, I. S., López-Rivas, A., Sánchez-Vázquez, M. M., Rohena-Rivera, K., Nieves-Burgos, G., Ortiz-Zuazaga, H., . . . Martínez-Ferrer, M. (2019). Andrographolide induces DNA damage in prostate cancer cells. *Oncotarget, 10*(10), 1085-1101. doi:10.18632/oncotarget.26628

Foulon, V., Antonenkov, V. D., Croes, K., Waelkens, E., Mannaerts, G. P., Van Veldhoven, P. P., & Casteels, M. (1999). Purification, molecular cloning, and expression of 2-hydroxyphytanoyl-CoA lyase, a peroxisomal thiamine pyrophosphate-dependent enzyme that catalyzes the carbon-carbon bond cleavage during alpha-oxidation of 3-methyl-branched fatty acids. *Proc Natl Acad Sci U S A, 96*(18), 10039-10044. doi:10.1073/pnas.96.18.10039

Fraccascia, P., Casteels, M., De Schryver, E., & Van Veldhoven, P. P. (2011). Role of thiamine pyrophosphate in oligomerisation, functioning and import of peroxisomal 2-hydroxyacyl-CoA lyase. *Biochim Biophys Acta, 1814*(10), 1226-1233. doi:10.1016/j.bbapap.2011.06.007

Franklin, R. B., Brandly, R. L., & Costello, L. C. (1982). Mitochondrial Aspartate Aminotransferase and the Effect of Testosterone on Citrate Production in Rat Ventral Prostate. *Journal of Urology, 127*(4), 798-802. doi:doi:10.1016/S0022-5347(17)54052-5

Franklin, R. B., Feng, P., Milon, B., Desouki, M. M., Singh, K. K., Kajdacsy-Balla, A., . . . Costello, L. C. (2005). hZIP1 zinc uptake transporter down regulation and zinc depletion in prostate cancer. *Molecular Cancer, 4*(1), 32. doi:10.1186/1476-4598-4-32

Froese, D. S., Kochan, G., Muniz, J. R. C., Wu, X., Gileadi, C., Ugochukwu, E., . . . Yue, W. W. (2010). Structures of the human GTPase MMAA and vitamin B12-dependent methylmalonyl-CoA mutase and insight into their complex formation. *J Biol Chem, 285*(49), 38204-38213. doi:10.1074/jbc.m110.177717

Fujino, T., Takei, Y. A., Sone, H., Ioka, R. X., Kamataki, A., Magoori, K., . . . Yamamoto, T. T. (2001). Molecular identification and characterization of two

medium-chain acyl-CoA synthetases, MACS1 and the Sa gene product. *J Biol Chem, 276*(38), 35961-35966. doi:10.1074/jbc.M106651200

Gardini, A. (2017). Global Run-On Sequencing (GRO-Seq). *Methods Mol Biol, 1468*, 111-120. doi:10.1007/978-1-4939-4035-6_9

Geng, F., Cheng, X., Wu, X., Yoo, J. Y., Cheng, C., Guo, J. Y., . . . Guo, D. (2016). Inhibition of SOAT1 Suppresses Glioblastoma Growth via Blocking SREBP-1-Mediated Lipogenesis. *Clin Cancer Res, 22*(21), 5337-5348. doi:10.1158/1078-0432.Ccr-15-2973

Gholkar, A. A., Cheung, K., Williams, K. J., Lo, Y. C., Hamideh, S. A., Nnebe, C., . . . Torres, J. Z. (2016). Fatostatin Inhibits Cancer Cell Proliferation by Affecting Mitotic Microtubule Spindle Assembly and Cell Division. *J Biol Chem, 291*(33), 17001-17008. doi:10.1074/jbc.C116.737346

Gleason, D. F., & Mellinger, G. T. (2017). Prediction of Prognosis for Prostatic Adenocarcinoma by Combined Histological Grading and Clinical Staging. *J Urol, 197*(2s), S134-s139. doi:10.1016/j.juro.2016.10.099

Go, G. W., & Mani, A. (2012). Low-density lipoprotein receptor (LDLR) family orchestrates cholesterol homeostasis. *Yale J Biol Med, 85*(1), 19-28.

Goldstein, J. L., & Brown, M. S. (1990). Regulation of the mevalonate pathway. *Nature, 343*(6257), 425-430. doi:10.1038/343425a0

Goldstein, J. L., DeBose-Boyd, R. A., & Brown, M. S. (2006). Protein sensors for membrane sterols. *Cell, 124*(1), 35-46. doi:10.1016/j.cell.2005.12.022

González, S., Chen, L., & Deng, S. X. (2017). Comparative Study of Xenobiotic-Free Media for the Cultivation of Human Limbal Epithelial Stem/Progenitor Cells.

Tissue Engineering Part C: Methods, 23(4), 219-227. doi:10.1089/ten.tec.2016.0388

Gordon, K., & Hodgen, G. D. (1992). Evolving role of gonadotropin-releasing hormone antagonists. *Trends in Endocrinology & Metabolism, 3*(7), 259-263.

Gottlieb, B., Beitel, L. K., Nadarajah, A., Paliouras, M., & Trifiro, M. (2012). The androgen receptor gene mutations database: 2012 update. *Hum Mutat, 33*(5), 887-894. doi:10.1002/humu.22046

Grasso, C. S., Wu, Y.-M., Robinson, D. R., Cao, X., Dhanasekaran, S. M., Khan, A. P., . . . Brenner, J. C. (2012). The mutational landscape of lethal castration-resistant prostate cancer. *Nature, 487*(7406), 239.

Grasso, C. S., Wu, Y. M., Robinson, D. R., Cao, X., Dhanasekaran, S. M., Khan, A. P., . . . Tomlins, S. A. (2012). The mutational landscape of lethal castration-resistant prostate cancer. *Nature, 487*(7406), 239-243. doi:10.1038/nature11125

Green, S. M., Mostaghel, E. A., & Nelson, P. S. (2012). Androgen action and metabolism in prostate cancer. *Mol Cell Endocrinol, 360*(1-2), 3-13. doi:10.1016/j.mce.2011.09.046

Grevengoed, T. J., Klett, E. L., & Coleman, R. A. (2014). Acyl-CoA metabolism and partitioning. *Annu Rev Nutr, 34*, 1-30. doi:10.1146/annurev-nutr-071813-105541

Grigore, A. D., Ben-Jacob, E., & Farach-Carson, M. C. (2015). Prostate cancer and neuroendocrine differentiation: more neuronal, less endocrine? *Front Oncol, 5*, 37. doi:10.3389/fonc.2015.00037

Grobholz, R., Griebe, M., Sauer, C. G., Michel, M. S., Trojan, L., & Bleyl, U. (2005). Influence of neuroendocrine tumor cells on proliferation in prostatic carcinoma. *Hum Pathol, 36*(5), 562-570. doi:10.1016/j.humpath.2005.02.019

Guo, D., Bell, E. H., Mischel, P., & Chakravarti, A. (2014). Targeting SREBP-1-driven lipid metabolism to treat cancer. *Current pharmaceutical design, 20*(15), 2619-2626. doi:10.2174/13816128113199990486

Guo, D., Prins, R. M., Dang, J., Kuga, D., Iwanami, A., Soto, H., . . . Mischel, P. S. (2009). EGFR signaling through an Akt-SREBP-1-dependent, rapamycin-resistant pathway sensitizes glioblastomas to antilipogenic therapy. *Sci Signal, 2*(101), ra82. doi:10.1126/scisignal.2000446

Guo, D., Reinitz, F., Youssef, M., Hong, C., Nathanson, D., Akhavan, D., . . . Mischel, P. S. (2011). An LXR agonist promotes glioblastoma cell death through inhibition of an EGFR/AKT/SREBP-1/LDLR-dependent pathway. *Cancer Discov, 1*(5), 442-456. doi:10.1158/2159-8290.Cd-11-0102

Gururajan, M., Cavassani, K. A., Sievert, M., Duan, P., Lichterman, J., Huang, J. M., . . . Posadas, E. M. (2015). SRC family kinase FYN promotes the neuroendocrine phenotype and visceral metastasis in advanced prostate cancer. *Oncotarget, 6*(42), 44072-44083. doi:10.18632/oncotarget.6398

Gutierrez-Pajares, J. L., Ben Hassen, C., Chevalier, S., & Frank, P. G. (2016). SR-BI: Linking Cholesterol and Lipoprotein Metabolism with Breast and Prostate Cancer. *Front Pharmacol, 7*, 338. doi:10.3389/fphar.2016.00338

Han, W., Gao, S., Barrett, D., Ahmed, M., Han, D., Macoska, J. A., . . . Cai, C. (2017). Reactivation of androgen receptor-regulated lipid biosynthesis drives the

progression of castration-resistant prostate cancer. *Oncogene*. doi:10.1038/onc.2017.385

Han, W., Gao, S., Barrett, D., Ahmed, M., Han, D., Macoska, J. A., . . . Cai, C. (2018). Reactivation of androgen receptor-regulated lipid biosynthesis drives the progression of castration-resistant prostate cancer. *Oncogene, 37*(6), 710-721. doi:10.1038/onc.2017.385

Hasegan, A. (2014). RADICAL PROSTATECTOMY IN PROSTATE CANCER TREATMENT. *Acta Medica Transilvanica, 19*(3).

Hatzivassiliou, G., Zhao, F., Bauer, D. E., Andreadis, C., Shaw, A. N., Dhanak, D., . . . Thompson, C. B. (2005). ATP citrate lyase inhibition can suppress tumor cell growth. *Cancer Cell, 8*(4), 311-321.

Hawkins, J. L., Robbins, M. D., Warren, L. C., Xia, D., Petras, S. F., Valentine, J. J., . . . Harwood, H. J., Jr. (2008). Pharmacologic inhibition of site 1 protease activity inhibits sterol regulatory element-binding protein processing and reduces lipogenic enzyme gene expression and lipid synthesis in cultured cells and experimental animals. *J Pharmacol Exp Ther, 326*(3), 801-808. doi:10.1124/jpet.108.139626

Heemers, H., Maes, B., Foufelle, F., Heyns, W., Verhoeven, G., & Swinnen, J. V. (2001). Androgens stimulate lipogenic gene expression in prostate cancer cells by activation of the sterol regulatory element-binding protein cleavage activating protein/sterol regulatory element-binding protein pathway. *Mol Endocrinol, 15*(10), 1817-1828. doi:10.1210/mend.15.10.0703

Heemers, H., Vanderhoydonc, F., Roskams, T., Shechter, I., Heyns, W., Verhoeven, G., & Swinnen, J. V. (2003). Androgens stimulate coordinated lipogenic

gene expression in normal target tissues in vivo. *Mol Cell Endocrinol, 205*(1-2), 21-31.

Heemers, H., Verrijdt, G., Organe, S., Claessens, F., Heyns, W., Verhoeven, G., & Swinnen, J. V. (2004). Identification of an androgen response element in intron 8 of the sterol regulatory element-binding protein cleavage-activating protein gene allowing direct regulation by the androgen receptor. *J Biol Chem, 279*(29), 30880-30887. doi:10.1074/jbc.M401615200

Heemers, H. V., Verhoeven, G., & Swinnen, J. V. (2006). Androgen activation of the sterol regulatory element-binding protein pathway: Current insights. *Molecular Endocrinology, 20*(10), 2265-2277.

Heidenreich, A. (2011). EAU guidelines on prostate cancer. Part 1: screening, diagnosis, and treatment of clinically localised disease. *Eur Urol, 59*(1), 61-71. doi:10.1016/j.eururo.2010.10.039

Heidenreich, A., Bellmunt, J., Bolla, M., Joniau, S., Mason, M., Matveev, V., . . . European Association of, U. (2011). EAU guidelines on prostate cancer. Part 1: screening, diagnosis, and treatment of clinically localised disease. *Eur Urol, 59*(1), 61-71. doi:10.1016/j.eururo.2010.10.039

Heinlein, C. A., & Chang, C. (2002). Androgen receptor (AR) coregulators: an overview. *Endocr Rev, 23*(2), 175-200. doi:10.1210/edrv.23.2.0460

Heinlein, C. A., & Chang, C. (2004). Androgen receptor in prostate cancer. *Endocr Rev, 25*(2), 276-308. doi:10.1210/er.2002-0032

Hicks, J. J., Martínez-Manautou, J., Pedron, N., & Rosado, A. (1972). Metabolic changes in human spermatozoa related to capacitation. *Fertil Steril, 23*(3), 172-179.

Hoffmann, F., & Maser, E. (2007). Carbonyl reductases and pluripotent hydroxysteroid dehydrogenases of the short-chain dehydrogenase/reductase superfamily. *Drug metabolism reviews, 39*(1), 87-144. doi:10.1080/03602530600969440

Holthuis, J. C., & Menon, A. K. (2014). Lipid landscapes and pipelines in membrane homeostasis. *Nature, 510*(7503), 48-57. doi:10.1038/nature13474

Holzbeierlein, J., Lal, P., LaTulippe, E., Smith, A., Satagopan, J., Zhang, L., . . . Gerald, W. L. (2004). Gene expression analysis of human prostate carcinoma during hormonal therapy identifies androgen-responsive genes and mechanisms of therapy resistance. *Am J Pathol, 164*(1), 217-227. doi:10.1016/s0002-9440(10)63112-4

Hori, T., Masuda, T., Kobayashi, M., & Kawakami, E. (2017). Role of prostatic fluid in cooled canine epididymal sperm. *Reproduction in Domestic Animals, 52*(4), 655-660. doi:10.1111/rda.12963

Horton, J. D., Goldstein, J. L., & Brown, M. S. (2002). SREBPs: activators of the complete program of cholesterol and fatty acid synthesis in the liver. *J Clin Invest, 109*(9), 1125-1131. doi:10.1172/JCI15593

Hu, R., Denmeade, S. R., & Luo, J. (2010). Molecular processes leading to aberrant androgen receptor signaling and castration resistance in prostate cancer. *Expert Rev Endocrinol Metab, 5*(5), 753-764. doi:10.1586/eem.10.49

Hua, X., Sakai, J., Brown, M. S., & Goldstein, J. L. (1996). Regulated cleavage of sterol regulatory element binding proteins requires sequences on both sides of the endoplasmic reticulum membrane. *J Biol Chem, 271*(17), 10379-10384. doi:10.1074/jbc.271.17.10379

Hua, X., Sakai, J., Y. K., H., Goldstein, J. L., & Brown, M. S. (1995). Hairpin Orientation of Sterol Regulatory Element-binding Protein-2 in Cell Membranes as Determined by Protease Protection. *Journal of Biological Chemistry, 270*(49), 29422-29427. doi:10.1074/jbc.270.49.29422

Hua, X., Yokoyama, C., Wu, J., Briggs, M. R., Brown, M. S., Goldstein, J. L., & Wang, X. (1993). SREBP-2, a second basic-helix-loop-helix-leucine zipper protein that stimulates transcription by binding to a sterol regulatory element. *Proceedings of the National Academy of Sciences, 90*(24), 11603-11607. doi:10.1073/pnas.90.24.11603

Huang, W. C., Zhau, H. E., & Chung, L. W. (2010). Androgen receptor survival signaling is blocked by anti-beta2-microglobulin monoclonal antibody via a MAPK/lipogenic pathway in human prostate cancer cells. *J Biol Chem, 285*(11), 7947-7956. doi:10.1074/jbc.M109.092759

Huggins, C., & Hodges, C. V. (1941). Studies on Prostatic Cancer. I. The Effect of Castration, of Estrogen and of Androgen Injection on Serum Phosphatases in Metastatic Carcinoma of the Prostate. *Cancer Res, 1*(4), 293-297.

Hunt, M. C., Rautanen, A., Westin, M. A., Svensson, L. T., & Alexson, S. E. (2006). Analysis of the mouse and human acyl-CoA thioesterase (ACOT) gene clusters shows that convergent, functional evolution results in a reduced number of human peroxisomal ACOTs. *Faseb j, 20*(11), 1855-1864. doi:10.1096/fj.06-6042com

Jackson, S. M., Ericsson, J., & Edwards, P. A. (1997). Signaling molecules derived from the cholesterol biosynthetic pathway. *Subcell Biochem, 28*, 1-21. doi:10.1007/978-1-4615-5901-6_1

Jakobsson, A., Westerberg, R., & Jacobsson, A. (2006). Fatty acid elongases in mammals: their regulation and roles in metabolism. *Prog Lipid Res, 45*(3), 237-249. doi:10.1016/j.plipres.2006.01.004

Jang, C., Chen, L., & Rabinowitz, J. D. (2018). Metabolomics and Isotope Tracing. *Cell, 173*(4), 822-837. doi:https://doi.org/10.1016/j.cell.2018.03.055

Jang, T. L., Patel, N., Faiena, I., Radadia, K. D., Moore, D. F., Elsamra, S. E., . . . Scardino, P. T. (2018). Comparative effectiveness of radical prostatectomy with adjuvant radiotherapy versus radiotherapy plus androgen deprivation therapy for men with advanced prostate cancer. *Cancer, 124*(20), 4010-4022.

Jenster, G., van der Korput, H. A., van Vroonhoven, C., van der Kwast, T. H., Trapman, J., & Brinkmann, A. O. (1991). Domains of the human androgen receptor involved in steroid binding, transcriptional activation, and subcellular localization. *Mol Endocrinol, 5*(10), 1396-1404. doi:10.1210/mend-5-10-1396

Jernberg, E., Bergh, A., & Wikström, P. (2017). Clinical relevance of androgen receptor alterations in prostate cancer. *Endocrine connections, 6*(8), R146-R161. doi:10.1530/EC-17-0118

Ji, H., Jiang, H., Ma, W., Johnson, D. S., Myers, R. M., & Wong, W. H. (2008). An integrated software system for analyzing ChIP-chip and ChIP-seq data. *Nature biotechnology, 26*(11), 1293-1300. doi:10.1038/nbt.1505

Jiang, H., Rao, K. S., Yee, V. C., & Kraus, J. P. (2005). Characterization of four variant forms of human propionyl-CoA carboxylase expressed in Escherichia coli. *J Biol Chem, 280*(30), 27719-27727. doi:10.1074/jbc.M413281200

Jiang, W., Zhao, S., Xu, L., Lu, Y., Lu, Z., Chen, C., . . . Yang, L. (2015). The inhibitory effects of xanthohumol, a prenylated chalcone derived from hops, on cell

growth and tumorigenesis in human pancreatic cancer. *Biomed Pharmacother, 73*, 40-47. doi:10.1016/j.biopha.2015.05.020

Jin, H. J., Kim, J., & Yu, J. (2013). Androgen receptor genomic regulation. *Translational andrology and urology, 2*(3), 157-177. doi:10.3978/j.issn.2223-4683.2013.09.01

Jones, J. M., & Gould, S. J. (2000). Identification of PTE2, a human peroxisomal long-chain acyl-CoA thioesterase. *Biochem Biophys Res Commun, 275*(1), 233-240. doi:10.1006/bbrc.2000.3285

Juang, H. H., Costello, L. C., & Franklin, R. B. (1995). Androgen modulation of multiple transcription start sites of the mitochondrial aspartate aminotransferase gene in rat prostate. *Journal of Biological Chemistry, 270*(21), 12629-12634. doi:10.1074/jbc.270.21.12629

Kallio, H. M., Hieta, R., Latonen, L., Brofeldt, A., Annala, M., Kivinummi, K., . . . Lilja, H. G. (2018). Constitutively active androgen receptor splice variants AR-V3, AR-V7 and AR-V9 are co-expressed in castration-resistant prostate cancer metastases. *British journal of cancer, 119*(3), 347.

Kalousek, F., Darigo, M. D., & Rosenberg, L. E. (1980). Isolation and characterization of propionyl-CoA carboxylase from normal human liver. Evidence for a protomeric tetramer of nonidentical subunits. *J Biol Chem, 255*(1), 60-65.

Kamisuki, S., Mao, Q., Abu-Elheiga, L., Gu, Z., Kugimiya, A., Kwon, Y., . . . Uesugi, M. (2009). A small molecule that blocks fat synthesis by inhibiting the activation of SREBP. *Chem Biol, 16*(8), 882-892. doi:10.1016/j.chembiol.2009.07.007

Kamp, F., & Hamilton, J. A. (2006). How fatty acids of different chain length enter and leave cells by free diffusion. *Prostaglandins Leukot Essent Fatty Acids, 75*(3), 149-159. doi:10.1016/j.plefa.2006.05.003

Kanehisa, M., Furumichi, M., Tanabe, M., Sato, Y., & Morishima, K. (2017). KEGG: new perspectives on genomes, pathways, diseases and drugs. *Nucleic Acids Research, 45*(D1), D353-D361. doi:10.1093/nar/gkw1092

Kasuya, F., Igarashi, K., & Fukui, M. (1996). Inhibition of a medium chain acyl-CoA synthetase involved in glycine conjugation by carboxylic acids. *Biochem Pharmacol, 52*(10), 1643-1646.

Kavanagh, J. P. (1985). Sodium, potassium, calcium, magnesium, zinc, citrate and chloride content of human prostatic and seminal fluid. *75*(1), 35. doi:10.1530/jrf.0.0750035

Kim, J. B., Spotts, G. D., Halvorsen, Y. D., Shih, H. M., Ellenberger, T., Towle, H. C., & Spiegelman, B. M. (1995). Dual DNA binding specificity of ADD1/SREBP1 controlled by a single amino acid in the basic helix-loop-helix domain. *Mol Cell Biol, 15*(5), 2582-2588. doi:10.1128/mcb.15.5.2582

Kim, W., Zhang, L., Wilton, J. H., Fetterly, G., Mohler, J. L., Weinberg, V., . . . Ryan, C. J. (2014). Sequential use of the androgen synthesis inhibitors ketoconazole and abiraterone acetate in castration-resistant prostate cancer and the predictive value of circulating androgens. *Clin Cancer Res, 20*(24), 6269-6276. doi:10.1158/1078-0432.ccr-14-1595

Kitahara, C. M., Berrington de Gonzalez, A., Freedman, N. D., Huxley, R., Mok, Y., Jee, S. H., & Samet, J. M. (2011). Total cholesterol and cancer risk in a large

prospective study in Korea. *J Clin Oncol, 29*(12), 1592-1598. doi:10.1200/jco.2010.31.5200

Kitamura, T., Seki, N., & Kihara, A. (2017). Phytosphingosine degradation pathway includes fatty acid α-oxidation reactions in the endoplasmic reticulum. *Proc Natl Acad Sci U S A, 114*(13), E2616-e2623. doi:10.1073/pnas.1700138114

Kochan, G., Pilka, E. S., von Delft, F., Oppermann, U., & Yue, W. W. (2009). Structural snapshots for the conformation-dependent catalysis by human medium-chain acyl-coenzyme A synthetase ACSM2A. *Journal of Molecular Biology, 388*(5), 997-1008.

Koivisto, P., Kononen, J., Palmberg, C., Tammela, T., Hyytinen, E., Isola, J., . . . Visakorpi, T. (1997). Androgen receptor gene amplification: a possible molecular mechanism for androgen deprivation therapy failure in prostate cancer. *Cancer research, 57*(2), 314-319.

Komiya, A., Yasuda, K., Watanabe, A., Fujiuchi, Y., Tsuzuki, T., & Fuse, H. (2013). The prognostic significance of loss of the androgen receptor and neuroendocrine differentiation in prostate biopsy specimens among castration-resistant prostate cancer patients. *Mol Clin Oncol, 1*(2), 257-262. doi:10.3892/mco.2013.69

Kridel, S. J., Axelrod, F., Rozenkrantz, N., & Smith, J. W. (2004). Orlistat is a novel inhibitor of fatty acid synthase with antitumor activity. *Cancer Research, 64*(6), 2070-2075.

Krieg, M., Weisser, H., & Tunn, S. (1995). Potential activities of androgen metabolizing enzymes in human prostate. *The Journal of Steroid Biochemistry and Molecular Biology, 53*(1), 395-400. doi:https://doi.org/10.1016/0960-0760(95)00085-E

Król, S. K., Kiełbus, M., Rivero-Müller, A., & Stepulak, A. (2015). Comprehensive review on betulin as a potent anticancer agent. *Biomed Res Int, 2015*, 584189. doi:10.1155/2015/584189

Ku, S. Y., Rosario, S., Wang, Y., Mu, P., Seshadri, M., Goodrich, Z. W., . . . Wang, J. (2017). Rb1 and Trp53 cooperate to suppress prostate cancer lineage plasticity, metastasis, and antiandrogen resistance. *Science, 355*(6320), 78-83.

Kuemmerle, N. B., Rysman, E., Lombardo, P. S., Flanagan, A. J., Lipe, B. C., Wells, W. A., . . . Kinlaw, W. B. (2011). Lipoprotein lipase links dietary fat to solid tumor cell proliferation. *Mol Cancer Ther, 10*(3), 427-436. doi:10.1158/1535-7163.mct-10-0802

Kumar, V. L., & Majumder, P. K. (1995a). Prostate gland: structure, functions and regulation. *Int Urol Nephrol, 27*(3), 231-243.

Kumar, V. L., & Majumder, P. K. (1995b). Prostate gland: Structure, functions and regulation. *Int Urol Nephrol, 27*(3), 231-243. doi:10.1007/bf02564756

Kurita, T., Wang, Y. Z., Donjacour, A. A., Zhao, C., Lydon, J. P., O'Malley, B. W., . . . Cunha, G. R. (2001). Paracrine regulation of apoptosis by steroid hormones in the male and female reproductive system. *Cell Death Differ, 8*(2), 192-200. doi:10.1038/sj.cdd.4400797

Labrie, F., BÉLANGER, A., CUSAN, L., SEGUIN, C., PELLETIER, G., KELLY, P. A., . . . GOURDEAU, Y. (1980). Antifertility effects of LHRH agonists in the male. *Journal of Andrology, 1*(5), 209-228.

Labrie, F., Belanger, A., Luu-The, V., Labrie, C., Simard, J., Cusan, L., . . . Candas, B. (2005). Gonadotropin-releasing hormone agonists in the treatment of prostate cancer. *Endocrine reviews, 26*(3), 361-379.

Lallous, N., Volik, S. V., Awrey, S., Leblanc, E., Tse, R., Murillo, J., . . . Cherkasov, A. (2016). Functional analysis of androgen receptor mutations that confer anti-androgen resistance identified in circulating cell-free DNA from prostate cancer patients. *Genome biology, 17*, 10-10. doi:10.1186/s13059-015-0864-1

Laurent, V., Guerard, A., Mazerolles, C., Le Gonidec, S., Toulet, A., Nieto, L., . . . Muller, C. (2016). Periprostatic adipocytes act as a driving force for prostate cancer progression in obesity. *Nat Commun, 7*, 10230. doi:10.1038/ncomms10230

Le Magnen, C., Shen, M. M., & Abate-Shen, C. (2018). Lineage plasticity in cancer progression and treatment. *Annual review of cancer biology, 2*, 271-289.

Leach, D. A., Need, E. F., Toivanen, R., Trotta, A. P., Palethorpe, H. M., Tamblyn, D. J., . . . Buchanan, G. (2015). Stromal androgen receptor regulates the composition of the microenvironment to influence prostate cancer outcome. *Oncotarget, 6*(18), 16135-16150. doi:10.18632/oncotarget.3873

Lee, S. J., Sekimoto, T., Yamashita, E., Nagoshi, E., Nakagawa, A., Imamoto, N., . . . Yoneda, Y. (2003). The structure of importin-beta bound to SREBP-2: nuclear import of a transcription factor. *Science, 302*(5650), 1571-1575. doi:10.1126/science.1088372

Lehman, D. M., Lorenzo, C., Hernandez, J., & Wang, C. P. (2012). Statin use as a moderator of metformin effect on risk for prostate cancer among type 2 diabetic patients. *Diabetes Care, 35*(5), 1002-1007. doi:10.2337/dc11-1829

Leibowitz-Amit, R., Seah, J. A., Atenafu, E. G., Templeton, A. J., Vera-Badillo, F. E., Alimohamed, N., . . . Joshua, A. M. (2014). Abiraterone acetate in metastatic castration-resistant prostate cancer: a retrospective review of the Princess

Margaret experience of (I) low dose abiraterone and (II) prior ketoconazole. *Eur J Cancer, 50*(14), 2399-2407. doi:10.1016/j.ejca.2014.06.004

Li, C., Yang, W., Zhang, J., Zheng, X., Yao, Y., Tu, K., & Liu, Q. (2014). SREBP-1 has a prognostic role and contributes to invasion and metastasis in human hepatocellular carcinoma. *Int J Mol Sci, 15*(5), 7124-7138. doi:10.3390/ijms15057124

Li, J., Xu, C., Lee, H. J., Ren, S., Zi, X., Zhang, Z., . . . Sun, Y. (2020). A genomic and epigenomic atlas of prostate cancer in Asian populations. *Nature, 580*(7801), 93-99. doi:10.1038/s41586-020-2135-x

Li, N., Zhou, Z. S., Shen, Y., Xu, J., Miao, H. H., Xiong, Y., . . . Song, B. L. (2017). Inhibition of the sterol regulatory element-binding protein pathway suppresses hepatocellular carcinoma by repressing inflammation in mice. *Hepatology, 65*(6), 1936-1947. doi:10.1002/hep.29018

Li, W., Tai, Y., Zhou, J., Gu, W., Bai, Z., Zhou, T., . . . Wang, C. (2012). Repression of endometrial tumor growth by targeting SREBP1 and lipogenesis. *Cell Cycle, 11*(12), 2348-2358. doi:10.4161/cc.20811

Li, X., Chen, Y. T., Hu, P., & Huang, W. C. (2014). Fatostatin displays high antitumor activity in prostate cancer by blocking SREBP-regulated metabolic pathways and androgen receptor signaling. *Mol Cancer Ther, 13*(4), 855-866. doi:10.1158/1535-7163.Mct-13-0797

Li, X., Wu, J. B., Chung, L. W., & Huang, W. C. (2015). Anti-cancer efficacy of SREBP inhibitor, alone or in combination with docetaxel, in prostate cancer harboring p53 mutations. *Oncotarget, 6*(38), 41018-41032. doi:10.18632/oncotarget.5879

Li, Y., Xu, S., Mihaylova, M. M., Zheng, B., Hou, X., Jiang, B., . . . Shyy, J. Y. (2011). AMPK phosphorylates and inhibits SREBP activity to attenuate hepatic steatosis and atherosclerosis in diet-induced insulin-resistant mice. *Cell Metab, 13*, 376-388.

Linder, S., van der Poel, H., Bergman, A. M., Zwart, W., & Prekovic, S. (2018). Enzalutamide therapy for advanced prostate cancer: efficacy, resistance and beyond. *Endocrine-Related Cancer, 1*(aop).

Lines, M. A., Jobling, R., Brady, L., Marshall, C. R., Scherer, S. W., Rodriguez, A. R., . . . Tarnopolsky, M. A. (2014). Peroxisomal D-bifunctional protein deficiency. *Three adults diagnosed by whole-exome sequencing, 82*(11), 963-968. doi:10.1212/wnl.0000000000000219

Lipianskaya, J., Cohen, A., Chen, C. J., Hsia, E., Squires, J., Li, Z., . . . Huang, J. (2014). Androgen-deprivation therapy-induced aggressive prostate cancer with neuroendocrine differentiation. *Asian journal of andrology, 16*(4), 541-544. doi:10.4103/1008-682x.123669

Lissbrant, I. F., Lissbrant, E., Damber, J. E., & Bergh, A. (2001). Blood vessels are regulators of growth, diagnostic markers and therapeutic targets in prostate cancer. *Scand J Urol Nephrol, 35*(6), 437-452. doi:10.1080/003655901753367532

Liu, L., Zhang, K., Sandoval, H., Yamamoto, S., Jaiswal, M., Sanz, E., . . . Bellen, H. J. (2015). Glial lipid droplets and ROS induced by mitochondrial defects promote neurodegeneration. *Cell, 160*(1-2), 177-190. doi:10.1016/j.cell.2014.12.019

Liu, Y. (2006). Fatty acid oxidation is a dominant bioenergetic pathway in prostate cancer. *Prostate Cancer and Prostatic Diseases, 9*(3), 230-234. doi:10.1038/sj.pcan.4500879

Liu, Y., Zuckier, L., & Ghesani, N. (2010). Dominant uptake of fatty acid over glucose by prostate cells: a potential new diagnostic and therapeutic approach. *Anticancer Research, 30*, 369-374.

Lloyd, M. D., Yevglevskis, M., Lee, G. L., Wood, P. J., Threadgill, M. D., & Woodman, T. J. (2013). alpha-Methylacyl-CoA racemase (AMACR): metabolic enzyme, drug metabolizer and cancer marker P504S. *Prog Lipid Res, 52*(2), 220-230. doi:10.1016/j.plipres.2013.01.001

Llufrio, E. M., Cho, K., & Patti, G. J. (2019). Systems-level analysis of isotopic labeling in untargeted metabolomic data by X13CMS. *Nature Protocols, 14*(7), 1970-1990. doi:10.1038/s41596-019-0167-1

Locke, J. A., Guns, E. S., Lubik, A. A., Adomat, H. H., Hendy, S. C., Wood, C. A., . . . Nelson, C. C. (2008). Androgen levels increase by intratumoral de novo steroidogenesis during progression of castration-resistant prostate cancer. *Cancer Res, 68*(15), 6407-6415. doi:10.1158/0008-5472.can-07-5997

Lonergan, P. E., & Tindall, D. J. (2011). Androgen receptor signaling in prostate cancer development and progression. *J Carcinog, 10*. doi:10.4103/1477-3163.83937

Lubahn, D. B., Joseph, D. R., Sar, M., Tan, J., Higgs, H. N., Larson, R. E., . . . Wilson, E. M. (1988). The human androgen receptor: complementary deoxyribonucleic acid cloning, sequence analysis and gene expression in prostate. *Mol Endocrinol, 2*(12), 1265-1275. doi:10.1210/mend-2-12-1265

Luo, X., Cheng, C., Tan, Z., Li, N., Tang, M., Yang, L., & Cao, Y. (2017). Emerging roles of lipid metabolism in cancer metastasis. *Molecular Cancer, 16*(1), 76. doi:10.1186/s12943-017-0646-3

Lustman, A., Nakar, S., Cohen, A. D., & Vinker, S. (2014). Statin use and incident prostate cancer risk: does the statin brand matter? A population-based cohort study. *Prostate Cancer Prostatic Dis, 17*(1), 6-9. doi:10.1038/pcan.2013.34

Magaña, M. M., Koo, S. H., Towle, H. C., & Osborne, T. F. (2000). Different sterol regulatory element-binding protein-1 isoforms utilize distinct co-regulatory factors to activate the promoter for fatty acid synthase. *J Biol Chem, 275*(7), 4726-4733. doi:10.1074/jbc.275.7.4726

Mah, C. Y., Nassar, Z. D., Swinnen, J. V., & Butler, L. M. (2019). Lipogenic effects of androgen signaling in normal and malignant prostate. *Asian Journal of Urology*. doi:https://doi.org/10.1016/j.ajur.2019.12.003

Maltais, R., Luu-The, V., & Poirier, D. (2002). Synthesis and Optimization of a New Family of Type 3 17β-Hydroxysteroid Dehydrogenase Inhibitors by Parallel Liquid-Phase Chemistry. *Journal of Medicinal Chemistry, 45*(3), 640-653. doi:10.1021/jm010286y

Massie, C. E., Lynch, A., Ramos-Montoya, A., Boren, J., Stark, R., Fazli, L., . . . Mills, I. G. (2011). The androgen receptor fuels prostate cancer by regulating central metabolism and biosynthesis. *Embo j, 30*(13), 2719-2733. doi:10.1038/emboj.2011.158

Maxfield, F. R. (2002). Plasma membrane microdomains. *Curr Opin Cell Biol, 14*(4), 483-487. doi:10.1016/s0955-0674(02)00351-4

McLean, C. Y., Bristor, D., Hiller, M., Clarke, S. L., Schaar, B. T., Lowe, C. B., . . . Bejerano, G. (2010). GREAT improves functional interpretation of cis-regulatory regions. *Nature biotechnology, 28*(5), 495-501. doi:10.1038/nbt.1630

McNeal, J. E. (1988). Normal histology of the prostate. *Am J Surg Pathol, 12*(8), 619-633. doi:10.1097/00000478-198808000-00003

Medh, R. D., & Thompson, E. B. (2000). Hormonal regulation of physiological cell turnover and apoptosis. *Cell Tissue Res, 301*(1), 101-124. doi:10.1007/s004419900159

Medrano, A., Fernández-Novell, J. M., Ramió, L., Alvarez, J., Goldberg, E., Montserrat Rivera, M., . . . Rodríguez-Gil, J. E. (2006). Utilization of citrate and lactate through a lactate dehydrogenase and ATP-regulated pathway in boar spermatozoa. *Molecular Reproduction and Development, 73*(3), 369-378. doi:10.1002/mrd.20414

Menendez, J. A., & Lupu, R. (2007). Fatty acid synthase and the lipogenic phenotype in cancer pathogenesis. *Nature Reviews Cancer, 7*(10), 763-777. doi:10.1038/nrc2222

Menendez, J. A., & Lupu, R. (2007). Fatty acid synthase and the lipogenic phenotype in cancer pathogenesis. *Nat Rev Cancer, 7*(10), 763-777. doi:10.1038/nrc2222

Migita, T., Ruiz, S., Fornari, A., Fiorentino, M., Priolo, C., Zadra, G., . . . Loda, M. (2009). Fatty acid synthase: a metabolic enzyme and candidate oncogene in prostate cancer. *J Natl Cancer Inst, 101*(7), 519-532. doi:10.1093/jnci/djp030

Mirosevich, J., Bentel, J. M., Zeps, N., Redmond, S. L., D'Antuono, M. F., & Dawkins, H. J. (1999). Androgen receptor expression of proliferating basal and luminal cells in adult murine ventral prostate. *J Endocrinol, 162*(3), 341-350. doi:10.1677/joe.0.1620341

Miserez, A. R., Cao, G., Probst, L. C., & Hobbs, H. H. (1997). Structure of the Human Gene Encoding Sterol Regulatory Element Binding Protein 2 (SREBF2). *Genomics, 40*(1), 31-40. doi:https://doi.org/10.1006/geno.1996.4525

Miyata, S., Inoue, J., Shimizu, M., & Sato, R. (2015). Xanthohumol Improves Diet-induced Obesity and Fatty Liver by Suppressing Sterol Regulatory Element-binding Protein (SREBP) Activation. *J Biol Chem, 290*(33), 20565-20579. doi:10.1074/jbc.M115.656975

The Molecular Taxonomy of Primary Prostate Cancer. (2015). *Cell, 163*(4), 1011-1025. doi:10.1016/j.cell.2015.10.025

Mondul, A. M., Clipp, S. L., Helzlsouer, K. J., & Platz, E. A. (2010). Association between plasma total cholesterol concentration and incident prostate cancer in the CLUE II cohort. *Cancer Causes Control, 21*(1), 61-68. doi:10.1007/s10552-009-9434-8

Monteiro, R., Calhau, C., Silva, A. O., Pinheiro-Silva, S., Guerreiro, S., Gärtner, F., . . . Soares, R. (2008). Xanthohumol inhibits inflammatory factor production and angiogenesis in breast cancer xenografts. *J Cell Biochem, 104*(5), 1699-1707. doi:10.1002/jcb.21738

Montgomery, R. B., Mostaghel, E. A., Vessella, R., Hess, D. L., Kalhorn, T. F., Higano, C. S., . . . Nelson, P. S. (2008). Maintenance of intratumoral androgens in metastatic prostate cancer: a mechanism for castration-resistant tumor growth. *Cancer Res, 68*(11), 4447-4454. doi:10.1158/0008-5472.can-08-0249

Morash, C., Tey, R., Agbassi, C., Klotz, L., McGowan, T., Srigley, J., & Evans, A. (2015). Active surveillance for the management of localized prostate cancer:

Guideline recommendations. *Canadian Urological Association journal = Journal de l'Association des urologues du Canada, 9*(5-6), 171-178. doi:10.5489/cuaj.2806

Morova, T., McNeill, D. R., Lallous, N., Gönen, M., Dalal, K., Wilson, D. M., . . . Lack, N. A. (2020). Androgen receptor-binding sites are highly mutated in prostate cancer. *Nature Communications, 11*(1), 832. doi:10.1038/s41467-020-14644-y

Morton, J. D., & Shimomura, L. (1999). Sterol regulatory element-binding proteins: activators of cholesterol and fatty acid biosynthesis. *Current Opinion in Lipidology, 10*(2).

Mosquera, J. M., Beltran, H., Park, K., MacDonald, T. Y., Robinson, B. D., Tagawa, S. T., . . . Dhir, R. (2013). Concurrent AURKA and MYCN gene amplifications are harbingers of lethal treatment-related neuroendocrine prostate cancer. *Neoplasia (New York, NY), 15*(1), 1.

Mostaghel, E. A. (2014). Abiraterone in the treatment of metastatic castration-resistant prostate cancer. *Cancer Manag Res, 6*, 39-51. doi:10.2147/cmar.s39318

Mottet, N., Bellmunt, J., Bolla, M., Briers, E., Cumberbatch, M. G., De Santis, M., . . . Joniau, S. (2017). EAU-ESTRO-SIOG guidelines on prostate cancer. Part 1: screening, diagnosis, and local treatment with curative intent. *European urology, 71*(4), 618-629.

Mottet, N., Bellmunt, J., Bolla, M., Joniau, S., Mason, M., Matveev, V., . . . Heidenreich, A. (2011). EAU guidelines on prostate cancer. Part II: Treatment of advanced, relapsing, and castration-resistant prostate cancer. *Eur Urol, 59*(4), 572-583. doi:10.1016/j.eururo.2011.01.025

Mu, P., Zhang, Z., Benelli, M., Karthaus, W. R., Hoover, E., Chen, C.-C., . . . Cao, Z. (2017). SOX2 promotes lineage plasticity and antiandrogen resistance in TP53- and RB1-deficient prostate cancer. *Science, 355*(6320), 84-88.

Muhammad, A., Khalid, A., Nadia, T., & Muhammad, Y. (1970). Zonal Anatomy of Prostate. *Annals of King Edward Medical University, 16*(3). doi:10.21649/akemu.v16i3.212

Mukherjee, S., & Maxfield, F. R. (2004). Membrane domains. *Annu Rev Cell Dev Biol, 20*, 839-866. doi:10.1146/annurev.cellbio.20.010403.095451

Näär, A. M., Beaurang, P. A., Zhou, S., Abraham, S., Solomon, W., & Tjian, R. (1999). Composite co-activator ARC mediates chromatin-directed transcriptional activation. *Nature, 398*(6730), 828-832. doi:10.1038/19789

Nakahara, K., Ohkuni, A., Kitamura, T., Abe, K., Naganuma, T., Ohno, Y., . . . Kihara, A. (2012). The Sjögren-Larsson syndrome gene encodes a hexadecenal dehydrogenase of the sphingosine 1-phosphate degradation pathway. *Mol Cell, 46*(4), 461-471. doi:10.1016/j.molcel.2012.04.033

Nambiar, D. K., Deep, G., Singh, R. P., Agarwal, C., & Agarwal, R. (2014). Silibinin inhibits aberrant lipid metabolism, proliferation and emergence of androgen-independence in prostate cancer cells via primarily targeting the sterol response element binding protein 1. *Oncotarget, 5*(20), 10017-10033. doi:10.18632/oncotarget.2488

Nassar, Z., Centenera, M., Machiels, J., Zinonos, I., Hanson, A., Bloch, K., . . . Swinnen, J. (2019). Lipid elongation in prostate cancer: an androgen regulated process and a novel therapeutic target. *Oncology Abstracts*. doi:10.1530/oncolabs.1.P036

Nassar, Z. D., Aref, A. T., Miladinovic, D., Mah, C. Y., Raj, G. V., Hoy, A. J., & Butler, L. M. (2018). Peri-prostatic adipose tissue: the metabolic microenvironment of prostate cancer. *BJU International, 121*(S3), 9-21. doi:10.1111/bju.14173

Nelson, P. S., Clegg, N., Arnold, H., Ferguson, C., Bonham, M., White, J., . . . Lin, B. (2002). The program of androgen-responsive genes in neoplastic prostate epithelium. *Proc Natl Acad Sci U S A, 99*(18), 11890-11895. doi:10.1073/pnas.182376299

Ngan, S., Stronach, E. A., Photiou, A., Waxman, J., Ali, S., & Buluwela, L. (2009). Microarray coupled to quantitative RT-PCR analysis of androgen-regulated genes in human LNCaP prostate cancer cells. *Oncogene, 28*(19), 2051-2063. doi:10.1038/onc.2009.68

Nie, L. Y., Lu, Q. T., Li, W. H., Yang, N., Dongol, S., Zhang, X., & Jiang, J. (2013). Sterol regulatory element-binding protein 1 is required for ovarian tumor growth. *Oncol Rep, 30*(3), 1346-1354. doi:10.3892/or.2013.2575

Nieman, K., Romero, I., Van Houten, B., & Lengyel, E. (2013). Adipose tissue and adipocytes support tumorigenesis and metastasis. *Biochimica et Biophysica Acta, 1831*, 1533-1541.

Norris, J. D., Ellison, S. J., Baker, J. G., Stagg, D. B., Wardell, S. E., Park, S., . . . McDonnell, D. P. (2017). Androgen receptor antagonism drives cytochrome P450 17A1 inhibitor efficacy in prostate cancer. *J Clin Invest, 127*(6), 2326-2338. doi:10.1172/jci87328

Nugteren, D. H. (1965). The enzymic chain elongation of fatty acids by rat-liver microsomes. *Biochimica et Biophysica Acta (BBA) - Lipids and Lipid Metabolism, 106*(2), 280-290. doi:https://doi.org/10.1016/0005-2760(65)90036-6

Nyden, S. J., & Williams-Ashman, H. G. (1953). Influence of androgens on synthetic reactions in ventral prostate tissue. *Am J Physiol, 172*(3), 588-600. doi:10.1152/ajplegacy.1953.172.3.588

Nyquist, M. D., Li, Y., Hwang, T. H., Manlove, L. S., Vessella, R. L., Silverstein, K. A., . . . Dehm, S. M. (2013). TALEN-engineered AR gene rearrangements reveal endocrine uncoupling of androgen receptor in prostate cancer. *Proc Natl Acad Sci U S A, 110*(43), 17492-17497. doi:10.1073/pnas.1308587110

O'Reilly, M., House, P., & Tomlinson, J. (2014). Understanding androgen action in adipose tissue. *Journal of Steroid Biochemistry and Molecular Biology, 143*, 277-284.

Ojewola, R. W., Jeje, E. A., Tijani, K. H., Ogunjimi, M. A., & Anunobi, C. C. (2013). Clinico-pathological Correlation of Digital Rectal Examination Findings Amongst Nigerian Men with Prostatic Diseases: A Prospective Study of 236 Cases. *Niger J Surg, 19*(1), 26-31. doi:10.4103/1117-6806.111506

Oliner, J. D., Andresen, J. M., Hansen, S. K., Zhou, S., & Tjian, R. (1996). SREBP transcriptional activity is mediated through an interaction with the CREB-binding protein. *Genes Dev, 10*(22), 2903-2911. doi:10.1101/gad.10.22.2903

Padanad, M. S., Konstantinidou, G., Venkateswaran, N., Melegari, M., Rindhe, S., Mitsche, M., . . . Scaglioni, P. P. (2016). Fatty Acid Oxidation Mediated by Acyl-CoA Synthetase Long Chain 3 Is Required for Mutant KRAS Lung Tumorigenesis. *Cell Rep, 16*(6), 1614-1628. doi:10.1016/j.celrep.2016.07.009

Paltoglou, S., Das, R., Townley, S. L., Hickey, T. E., Tarulli, G. A., Coutinho, I., . . . Selth, L. A. (2017). Novel Androgen Receptor Coregulator GRHL2 Exerts Both

Oncogenic and Antimetastatic Functions in Prostate Cancer. *Cancer Res, 77*(13), 3417-3430. doi:10.1158/0008-5472.can-16-1616

Park, Jun H., Vithayathil, S., Kumar, S., Sung, P.-L., Dobrolecki, Lacey E., Putluri, V., . . . Kaipparettu, Benny A. (2016). Fatty Acid Oxidation-Driven Src Links Mitochondrial Energy Reprogramming and Oncogenic Properties in Triple-Negative Breast Cancer. *Cell Reports, 14*(9), 2154-2165. doi:https://doi.org/10.1016/j.celrep.2016.02.004

Parker, C., Nilsson, S., Heinrich, D., Helle, S. I., O'sullivan, J., Fosså, S. D., . . . Seke, M. (2013). Alpha emitter radium-223 and survival in metastatic prostate cancer. *New England Journal of Medicine, 369*(3), 213-223.

Patterson, A. D., Gonzalez, F. J., & Idle, J. R. (2010). Xenobiotic metabolism: a view through the metabolometer. *Chemical research in toxicology, 23*(5), 851-860. doi:10.1021/tx100020p

Peck, B., Schug, Z. T., Zhang, Q., Dankworth, B., Jones, D. T., Smethurst, E., . . . Schulze, A. (2016). Inhibition of fatty acid desaturation is detrimental to cancer cell survival in metabolically compromised environments. *Cancer Metab, 4*, 6. doi:10.1186/s40170-016-0146-8

Pernicová, Z., Slabáková, E., Fedr, R., Šimečková, Š., Jaroš, J., Suchánková, T., . . . Souček, K. (2014). The role of high cell density in the promotion of neuroendocrine transdifferentiation of prostate cancer cells. *Mol Cancer, 13*, 113. doi:10.1186/1476-4598-13-113

Petersen, K. F., Oral, E. A., Dufour, S., Befroy, D., Ariyan, C., Yu, C., . . . Shulman, G. I. (2002). Leptin reverses insulin resistance and hepatic steatosis in patients with severe lipodystrophy. *J Clin Invest, 109*(10), 1345-1350. doi:10.1172/jci15001

Piccinini, F., Tesei, A., Arienti, C., & Bevilacqua, A. (2015). Cancer multicellular spheroids: volume assessment from a single 2D projection. *Comput Methods Programs Biomed, 118*(2), 95-106. doi:10.1016/j.cmpb.2014.12.003

Pienta, K. J., & Bradley, D. (2006). Mechanisms underlying the development of androgen-independent prostate cancer. *Clinical Cancer Research, 12*(6), 1665-1671.

Pierorazio, P. M., Walsh, P. C., Partin, A. W., & Epstein, J. I. (2013). Prognostic Gleason grade grouping: data based on the modified Gleason scoring system. *BJU Int, 111*(5), 753-760. doi:10.1111/j.1464-410X.2012.11611.x

Pinthus, J. H., Lu, J.-P., Bidaisee, L. A., Lin, H., Bryskine, I., Gupta, R. S., & Singh, G. (2007). Androgen-dependent regulation of medium and long chain fatty acids uptake in prostate cancer. *Prostate, 67*(12), 1330-1338. doi:10.1002/pros.20609

Pisansky, T. M. (2005). External beam radiotherapy as curative treatment of prostate cancer. *Mayo Clin Proc, 80*(7), 883-898. doi:10.4065/80.7.883

Plessl, T., Bürer, C., Lutz, S., Yue, W. W., Baumgartner, M. R., & Froese, D. S. (2017). Protein destabilization and loss of protein-protein interaction are fundamental mechanisms in cblA-type methylmalonic aciduria. *Hum Mutat, 38*(8), 988-1001. doi:10.1002/humu.23251

Pomerantz, M. M., Li, F., Takeda, D. Y., Lenci, R., Chonkar, A., Chabot, M., . . . Freedman, M. L. (2015). The androgen receptor cistrome is extensively reprogrammed in human prostate tumorigenesis. *Nat Genet, 47*(11), 1346-1351. doi:10.1038/ng.3419

Pomorski, T., Hrafnsdóttir, S., Devaux, P. F., & van Meer, G. (2001). Lipid distribution and transport across cellular membranes. *Semin Cell Dev Biol, 12*(2), 139-148. doi:10.1006/scdb.2000.0231

Powers, E., Karachaliou, G. S., Kao, C., Harrison, M. R., Hoimes, C. J., George, D. J., . . . Zhang, T. (2020). Novel therapies are changing treatment paradigms in metastatic prostate cancer. *Journal of Hematology & Oncology, 13*(1), 144. doi:10.1186/s13045-020-00978-z

Prekovic, S., van Royen, M. E., Voet, A. R., Geverts, B., Houtman, R., Melchers, D., . . . Helsen, C. (2016). The Effect of F877L and T878A Mutations on Androgen Receptor Response to Enzalutamide. *Mol Cancer Ther, 15*(7), 1702-1712. doi:10.1158/1535-7163.Mct-15-0892

Prins, G. S., & Birch, L. (1993). Immunocytochemical analysis of androgen receptor along the ducts of the separate rat prostate lobes after androgen withdrawal and replacement. *Endocrinology, 132*(1), 169-178. doi:10.1210/endo.132.1.8419121

Qian, K., Franklin, R. B., & Costello, L. C. (1993). Testosterone regulates mitochondrial aspartate aminotransferase gene expression and mRNA stability in prostate. *Journal of Steroid Biochemistry and Molecular Biology, 44*(1), 13-19. doi:10.1016/0960-0760(93)90146-N

Qu, Q., Zeng, F., Liu, X., Wang, Q. J., & Deng, F. (2016). Fatty acid oxidation and carnitine palmitoyltransferase I: emerging therapeutic targets in cancer. *Cell Death & Disease, 7*(5), e2226-e2226. doi:10.1038/cddis.2016.132

Qu, Y., Dai, B., Ye, D., Kong, Y., Chang, K., Jia, Z., . . . Shi, G. (2015). Constitutively active AR-V7 plays an essential role in the development and progression of castration-resistant prostate cancer. *Sci Rep, 5*, 7654. doi:10.1038/srep07654

Raj, G., Selth, L., Day, T. K., & Tilley, W. (2015). Evolution of androgen deprivation therapy. *39*, 189-194.

Rathkopf, D. E., Antonarakis, E. S., Shore, N. D., Tutrone, R. F., Alumkal, J. J., Ryan, C. J., . . . Maneval, E. C. (2017). Safety and antitumor activity of apalutamide (ARN-509) in metastatic castration-resistant prostate cancer with and without prior abiraterone acetate and prednisone. *Clinical Cancer Research*.

Ray, U., & Roy, S. S. (2018). Aberrant lipid metabolism in cancer cells - the role of oncolipid-activated signaling. *Febs j, 285*(3), 432-443. doi:10.1111/febs.14281

Reeves, F. A., & Corcoran, N. M. (2020). Advances in prostate cancer. *Aust J Gen Pract, 49*(4), 200-205. doi:10.31128/ajgp-09-19-5055

Ribeiro, R., Monteiro, C., Cunha, V., Oliveira, M., Freitas, M., Fraga, A., . . . Morais, A. (2012). Human periprostatic adipose tissue promotes prostate cancer aggressiveness in vitro. *Journal of Experimental & Clinical Cancer Research, 31*, 32.

Risbridger, G. P., Davis, I. D., Birrell, S. N., & Tilley, W. D. (2010). Breast and prostate cancer: more similar than different. *Nat Rev Cancer, 10*(3), 205-212. doi:10.1038/nrc2795

Robinson, D., Van Allen, E. M., Wu, Y.-M., Schultz, N., Lonigro, R. J., Mosquera, J.-M., . . . Attard, G. (2015). Integrative clinical genomics of advanced prostate cancer. *Cell, 161*(5), 1215-1228.

Robinson, D., Van Allen, E. M., Wu, Y. M., Schultz, N., Lonigro, R. J., Mosquera, J. M., . . . Chinnaiyan, A. M. (2015). Integrative Clinical Genomics of Advanced Prostate Cancer. *Cell, 162*(2), 454. doi:10.1016/j.cell.2015.06.053

Robinson, D., Van Allen, E. M., Wu, Y. M., Schultz, N., Lonigro, R. J., Mosquera, J. M., . . . Chinnaiyan, A. M. (2015a). Integrative clinical genomics of advanced prostate cancer. *Cell, 161*(5), 1215-1228. doi:10.1016/j.cell.2015.05.001

Robinson, D., Van Allen, E. M., Wu, Y. M., Schultz, N., Lonigro, R. J., Mosquera, J. M., . . . Chinnaiyan, A. M. (2015b). Integrative clinical genomics of advanced prostate cancer. *Cell, 161*(5), 1215-1228. doi:10.1016/j.cell.2015.05.001

Robinson, J. T., Thorvaldsdóttir, H., Winckler, W., Guttman, M., Lander, E. S., Getz, G., & Mesirov, J. P. (2011). Integrative genomics viewer. *Nature biotechnology, 29*(1), 24-26. doi:10.1038/nbt.1754

Roderick, S. L., Chan, W. W., Agate, D. S., Olsen, L. R., Vetting, M. W., Rajashankar, K. R., & Cohen, D. E. (2002). Structure of human phosphatidylcholine transfer protein in complex with its ligand. *Nat Struct Biol, 9*(7), 507-511. doi:10.1038/nsb812

Rodrigues, G., Warde, P., Pickles, T., Crook, J., Brundage, M., Souhami, L., . . . Genitourinary Radiation Oncologists of, C. (2012). Pre-treatment risk stratification of prostate cancer patients: A critical review. *Canadian Urological Association journal = Journal de l'Association des urologues du Canada, 6*(2), 121-127. doi:10.5489/cuaj.11085

Ross-Innes, C. S., Stark, R., Teschendorff, A. E., Holmes, K. A., Ali, H. R., Dunning, M. J., . . . Carroll, J. S. (2012). Differential oestrogen receptor binding is associated with clinical outcome in breast cancer. *Nature, 481*(7381), 389-393. doi:10.1038/nature10730

Ross, R. W., Oh, W. K., Xie, W., Pomerantz, M., Nakabayashi, M., Sartor, O., . . . Freedman, M. (2008). Inherited variation in the androgen pathway is associated

with the efficacy of androgen-deprivation therapy in men with prostate cancer. *J Clin Oncol, 26*(6), 842-847. doi:10.1200/jco.2007.13.6804

Roy, A. K., Lavrovsky, Y., Song, C. S., Chen, S., Jung, M. H., Velu, N. K., . . . Chatterjee, B. (1998). Regulation of Androgen Action. In G. Litwack (Ed.), *Vitamins & Hormones* (Vol. 55, pp. 309-352): Academic Press.

Roy, A. K., Lavrovsky, Y., Song, C. S., Chen, S., Jung, M. H., Velu, N. K., . . . Chatterjee, B. (1999). Regulation of androgen action. *Vitam Horm, 55*, 309-352.

Ruizeveld de Winter, J. A., Janssen, P. J., Sleddens, H. M., Verleun-Mooijman, M. C., Trapman, J., Brinkmann, A. O., . . . van der Kwast, T. H. (1994). Androgen receptor status in localized and locally progressive hormone refractory human prostate cancer. *Am J Pathol, 144*(4), 735-746.

Rysman, E., Brusselmans, K., Scheys, K., Timmermans, L., Derua, R., Munck, S., . . . Machiels, J. (2010). De novo lipogenesis protects cancer cells from free radicals and chemotherapeutics by promoting membrane lipid saturation. *Cancer Res, 70*, 8117-8126.

Sack, J. S., Kish, K. F., Wang, C., Attar, R. M., Kiefer, S. E., An, Y., . . . Einspahr, H. M. (2001). Crystallographic structures of the ligand-binding domains of the androgen receptor and its T877A mutant complexed with the natural agonist dihydrotestosterone. *Proc Natl Acad Sci U S A, 98*(9), 4904-4909. doi:10.1073/pnas.081565498

Sadi, M. V., Walsh, P. C., & Barrack, E. R. (1991). Immunohistochemical study of androgen receptors in metastatic prostate cancer. Comparison of receptor content and response to hormonal therapy. *Cancer, 67*(12), 3057-3064. doi:10.1002/1097-0142(19910615)67:12<3057::Aid-cncr2820671221>3.0.Co;2-s

Sakai, J., Duncan, E. A., Rawson, R. B., Hua, X., Brown, M. S., & Goldstein, J. L. (1996). Sterol-Regulated Release of SREBP-2 from Cell Membranes Requires Two Sequential Cleavages, One Within a Transmembrane Segment. *Cell, 85*(7), 1037-1046. doi:https://doi.org/10.1016/S0092-8674(00)81304-5

Sakakura, Y., Shimano, H., Sone, H., Takahashi, A., Inoue, K., Toyoshima, H., . . . Yamada, N. (2001). Sterol Regulatory Element-Binding Proteins Induce an Entire Pathway of Cholesterol Synthesis. *Biochemical and Biophysical Research Communications, 286*(1), 176-183. doi:https://doi.org/10.1006/bbrc.2001.5375

Sanchez, H. B., Yieh, L., & Osborne, T. F. (1995). Cooperation by sterol regulatory element-binding protein and Sp1 in sterol regulation of low density lipoprotein receptor gene. *J Biol Chem, 270*(3), 1161-1169. doi:10.1074/jbc.270.3.1161

Santoni, M., Conti, A., Burattini, L., Berardi, R., Scarpelli, M., Cheng, L., . . . Montironi, R. (2014). Neuroendocrine differentiation in prostate cancer: novel morphological insights and future therapeutic perspectives. *Biochim Biophys Acta, 1846*(2), 630-637. doi:10.1016/j.bbcan.2014.10.008

Sathianathen, N. J., Konety, B. R., Crook, J., Saad, F., & Lawrentschuk, N. (2018). Landmarks in prostate cancer. *Nature Reviews Urology, 15*(10), 627-642. doi:10.1038/s41585-018-0060-7

Scher, H. I., Buchanan, G., Gerald, W., Butler, L. M., & Tilley, W. D. (2004). Targeting the androgen receptor: improving outcomes for castration-resistant prostate cancer. *Endocrine-Related Cancer, 11*(3), 459-476.

Schiewer, M. J., Augello, M. A., & Knudsen, K. E. (2012). The AR dependent cell cycle: mechanisms and cancer relevance. *Mol Cell Endocrinol, 352*(1-2), 34-45. doi:10.1016/j.mce.2011.06.033

Schlaepfer, I. R., Rider, L., Rodrigues, L. U., Gijón, M. A., Pac, C. T., Romero, L., . . . Cramer, S. D. (2014). Lipid catabolism via CPT1 as a therapeutic target for prostate cancer. *Mol Cancer Ther, 13*(10), 2361-2371. doi:10.1158/1535-7163.mct-14-0183

Scott, K. E., Wheeler, F. B., Davis, A. L., Thomas, M. J., Ntambi, J. M., Seals, D. F., & Kridel, S. J. (2012). Metabolic regulation of invadopodia and invasion by acetyl-CoA carboxylase 1 and de novo lipogenesis. *PLoS One, 7*(1), e29761. doi:10.1371/journal.pone.0029761

Searcy, R. L., & Simms, N. M. (1967). A practical approach for acid-base characterization of human semen. *International journal of fertility, 12*(3), 329-334.

Segawa, T., Nau, M. E., Xu, L. L., Chilukuri, R. N., Makarem, M., Zhang, W., . . . Srivastava, S. (2002). Androgen-induced expression of endoplasmic reticulum (ER) stress response genes in prostate cancer cells. *Oncogene, 21*(57), 8749-8758. doi:10.1038/sj.onc.1205992

Shah, R. B. (2009). Current perspectives on the Gleason grading of prostate cancer. *Arch Pathol Lab Med, 133*(11), 1810-1816. doi:10.1043/1543-2165-133.11.1810

Shah, U. S., Dhir, R., Gollin, S. M., Chandran, U. R., Lewis, D., Acquafondata, M., & Pflug, B. R. (2006). Fatty acid synthase gene overexpression and copy number gain in prostate adenocarcinoma. *Hum Pathol, 37*(4), 401-409. doi:https://doi.org/10.1016/j.humpath.2005.11.022

Shao, W., Machamer, C. E., & Espenshade, P. J. (2016). Fatostatin blocks ER exit of SCAP but inhibits cell growth in a SCAP-independent manner. *J Lipid Res, 57*(8), 1564-1573. doi:10.1194/jlr.M069583

Shimano, H. (2001). Sterol regulatory element-binding proteins (SREBPs): transcriptional regulators of lipid synthetic genes. *Prog Lipid Res, 40*(6), 439-452. doi:10.1016/s0163-7827(01)00010-8

Shore, N. (2014). Management of early-stage prostate cancer. *Am J Manag Care, 20*(12 Suppl), S260-272.

Singh, K. B., & Singh, S. V. (2017). Fatty Acid Synthesis Intermediates Represent Novel Noninvasive Biomarkers of Prostate Cancer Chemoprevention by Phenethyl Isothiocyanate. *Cancer prevention research (Philadelphia, Pa.), 10*(5), 279-289. doi:10.1158/1940-6207.capr-17-0001

Singh, M., Jha, R., Melamed, J., Shapiro, E., Hayward, S. W., & Lee, P. (2014). Stromal androgen receptor in prostate development and cancer. *Am J Pathol, 184*(10), 2598-2607. doi:10.1016/j.ajpath.2014.06.022

Soica, C., Dehelean, C., Danciu, C., Wang, H. M., Wenz, G., Ambrus, R., . . . Anghel, M. (2012). Betulin complex in γ-cyclodextrin derivatives: properties and antineoplasic activities in in vitro and in vivo tumor models. *Int J Mol Sci, 13*(11), 14992-15011. doi:10.3390/ijms131114992

Soupene, E., & Kuypers, F. A. (2008). Mammalian long-chain acyl-CoA synthetases. *Exp Biol Med (Maywood), 233*(5), 507-521. doi:10.3181/0710-mr-287

Sowalsky, A. G., Ye, H., Bhasin, M., Van Allen, E. M., Loda, M., Lis, R. T., . . . Balk, S. P. (2018). Neoadjuvant-Intensive Androgen Deprivation Therapy Selects for Prostate Tumor Foci with Diverse Subclonal Oncogenic Alterations. *Cancer Res, 78*(16), 4716-4730. doi:10.1158/0008-5472.Can-18-0610

Soyal, S. M., Nofziger, C., Dossena, S., Paulmichl, M., & Patsch, W. (2015). Targeting SREBPs for treatment of the metabolic syndrome. *Trends Pharmacol Sci, 36*(6), 406-416. doi:10.1016/j.tips.2015.04.010

Srodon, M., & Epstein, J. I. (2002). Central zone histology of the prostate: a mimicker of high-grade prostatic intraepithelial neoplasia. *Hum Pathol, 33*(5), 518-523. doi:10.1053/hupa.2002.124032

Stanbrough, M., Bubley, G. J., Ross, K., Golub, T. R., Rubin, M. A., Penning, T. M., . . . Balk, S. P. (2006). Increased expression of genes converting adrenal androgens to testosterone in androgen-independent prostate cancer. *Cancer Res, 66*(5), 2815-2825. doi:10.1158/0008-5472.can-05-4000

Staubach, S., & Hanisch, F. G. (2011). Lipid rafts: signaling and sorting platforms of cells and their roles in cancer. *Expert Rev Proteomics, 8*(2), 263-277. doi:10.1586/epr.11.2

Steinkamp, M. P., O'Mahony, O. A., Brogley, M., Rehman, H., LaPensee, E. W., Dhanasekaran, S., . . . Rubin, M. A. (2009). Treatment-dependent androgen receptor mutations in prostate cancer exploit multiple mechanisms to evade therapy. *Cancer research, 69*(10), 4434-4442.

Stephan, C., Rittenhouse, H., Hu, X., Cammann, H., & Jung, K. (2014). Prostate-Specific Antigen (PSA) Screening and New Biomarkers for Prostate Cancer (PCa). *Ejifcc, 25*(1), 55-78.

Suburu, J., & Chen, Y. Q. (2012). Lipids and Prostate Cancer. *Prostaglandins Other Lipid Mediat, 98*(0), 1-10. doi:10.1016/j.prostaglandins.2012.03.003

Sun, L. P., Li, L., Goldstein, J. L., & Brown, M. S. (2005). Insig required for sterol-mediated inhibition of Scap/SREBP binding to COPII proteins in vitro. *J Biol Chem, 280*(28), 26483-26490. doi:10.1074/jbc.M504041200

Sun, S., Sprenger, C. C., Vessella, R. L., Haugk, K., Soriano, K., Mostaghel, E. A., . . . Sun, H. (2010). Castration resistance in human prostate cancer is conferred by a frequently occurring androgen receptor splice variant. *J Clin Invest, 120*(8), 2715.

Sun, Y., He, W., Luo, M., Zhou, Y., Chang, G., Ren, W., . . . Hu, Y. (2015). SREBP1 regulates tumorigenesis and prognosis of pancreatic cancer through targeting lipid metabolism. *Tumour Biol, 36*(6), 4133-4141. doi:10.1007/s13277-015-3047-5

Suzuki, H., Akakura, K., Komiya, A., Aida, S., Akimoto, S., & Shimazaki, J. (1996). Codon 877 mutation in the androgen receptor gene in advanced prostate cancer: relation to antiandrogen withdrawal syndrome. *Prostate, 29*(3), 153-158.

Swinnen, J., Van Veldhoven, P. P., Esquenet, M., Heyns, W., & Verhoeven, G. (1996). Androgens markedly stimulate the accumulation of neutral lipids in the human prostatic adenocarcinoma cell line LNCaP. *Endocrinology, 137*(10), 4468-4474.

Swinnen, J. V., Esquenet, M., Goossens, K., Heyns, W., & Verhoeven, G. (1997). Androgens stimulate fatty acid synthease in the human prostate cancer cell line LNCaP. *Cancer Res, 57*(6), 1086-1090.

Swinnen, J. V., Ulrix, W., Heyns, W., & Verhoeven, G. (1997). Coordinate regulation of lipogenic gene expression by androgens: evidence for a cascade mechanism involving sterol regulatory element binding proteins. *Proc Natl Acad Sci U S A, 94*(24), 12975-12980.

Swinnen, J. V., Van Veldhoven, P. P., Esquenet, M., Heyns, W., & Verhoeven, G. (1996). Androgens markedly stimulate the accumulation of neutral lipids in the human prostatic adenocarcinoma cell line LNCaP. *Endocrinology, 137*(10), 4468-4474. doi:10.1210/endo.137.10.8828509

Swinnen, J. V., Van Veldhoven, P. P., Timmermans, L., De Schrijver, E., Brusselmans, K., Vanderhoydonc, F., . . . Verhoeven, G. (2003). Fatty acid synthase drives the synthesis of phospholipids partitioning into detergent-resistant membrane microdomains. *Biochemical and Biophysical Research Communications, 302*(4), 898-903. doi:https://doi.org/10.1016/S0006-291X(03)00265-1

Tamura, K., Makino, A., Hullin-Matsuda, F., Kobayashi, T., Furihata, M., Chung, S., . . . Nakagawa, H. (2009). Novel Lipogenic Enzyme ELOVL7 Is Involved in Prostate Cancer Growth through Saturated Long-Chain Fatty Acid Metabolism. *Cancer Res, 69*(20), 8133-8140. doi:10.1158/0008-5472.Can-09-0775

Tan, H.-L., Sood, A., Rahimi, H. A., Wang, W., Gupta, N., Hicks, J., . . . Netto, G. J. (2014). Rb loss is characteristic of prostatic small cell neuroendocrine carcinoma. *Clinical Cancer Research, 20*(4), 890-903.

Tan, P., Wei, S., Yang, L., Tang, Z., Cao, D., Liu, L., . . . Wei, Q. (2016). The effect of statins on prostate cancer recurrence and mortality after definitive therapy: a systematic review and meta-analysis. *Scientific reports, 6*, 29106. doi:10.1038/srep29106

Tang, J.-J., Li, J.-G., Qi, W., Qiu, W.-W., Li, P.-S., Li, B.-L., & Song, B.-L. (2011). Inhibition of SREBP by a Small Molecule, Betulin, Improves Hyperlipidemia and

Insulin Resistance and Reduces Atherosclerotic Plaques. *Cell Metab, 13*(1), 44-56. doi:https://doi.org/10.1016/j.cmet.2010.12.004

Taplin, M.-E., Bubley, G. J., Shuster, T. D., Frantz, M. E., Spooner, A. E., Ogata, G. K., . . . Balk, S. P. (1995). Mutation of the androgen-receptor gene in metastatic androgen-independent prostate cancer. *New England Journal of Medicine, 332*(21), 1393-1398.

Taylor, B. S., Schultz, N., Hieronymus, H., Gopalan, A., Xiao, Y., Carver, B. S., . . . Gerald, W. L. (2010). Integrative genomic profiling of human prostate cancer. *Cancer Cell, 18*(1), 11-22. doi:10.1016/j.ccr.2010.05.026

Taylor, R. A., Lo, J., Ascui, N., & Watt, M. J. (2015). Linking obesogenic dysregulation to prostate cancer progression. *Endocr Connect, 4*(4), R68-80. doi:10.1530/ec-15-0080

Tennakoon, J. B., Shi, Y., Han, J. J., Tsouko, E., White, M. A., Burns, A. R., . . . Frigo, D. E. (2014). Androgens regulate prostate cancer cell growth via an AMPK-PGC-1alpha-mediated metabolic switch. *Oncogene, 33*(45), 5251-5261. doi:10.1038/onc.2013.463

Teran-Garcia, M., Adamson, A. W., Yu, G., Rufo, C., Suchankova, G., Dreesen, T. D., . . . Gettys, T. W. (2007). Polyunsaturated fatty acid suppression of fatty acid synthase (FASN): evidence for dietary modulation of NF-Y binding to the Fasn promoter by SREBP-1c. *Biochem J, 402*(3), 591-600. doi:10.1042/BJ20061722

Thompson, I. M. (2001). Flare associated with LHRH-agonist therapy. *Reviews in urology, 3*(Suppl 3), S10.

Tilley, W. D., Marcelli, M., Wilson, J. D., & McPhaul, M. J. (1989). Characterization and expression of a cDNA encoding the human androgen receptor. *Proc Natl Acad Sci U S A, 86*(1), 327-331. doi:10.1073/pnas.86.1.327

Tomlins, A. M., Foxall, P. J. D., Lynch, M. J., Parkinson, J., Everett, J. R., & Nicholson, J. K. (1998). High resolution 1H NMR spectroscopic studies on dynamic biochemical processes in incubated human seminal fluid samples. *Biochimica et Biophysica Acta (BBA) - General Subjects, 1379*(3), 367-380. doi:https://doi.org/10.1016/S0304-4165(97)00116-5

Tousignant, K. D., Rockstroh, A., Taherian Fard, A., Lehman, M. L., Wang, C., McPherson, S. J., . . . Sadowski, M. C. (2019). Lipid Uptake Is an Androgen-Enhanced Lipid Supply Pathway Associated with Prostate Cancer Disease Progression and Bone Metastasis. *Molecular Cancer Research, 17*(5), 1166-1179. doi:10.1158/1541-7786.Mcr-18-1147

Tran, C., Ouk, S., Clegg, N. J., Chen, Y., Watson, P. A., Arora, V., . . . Kwon, A. (2009). Development of a second-generation antiandrogen for treatment of advanced prostate cancer. *Science, 324*(5928), 787-790.

Valentino, A., Calarco, A., Di Salle, A., Finicelli, M., Crispi, S., Calogero, R. A., . . . Peluso, G. (2017). Deregulation of MicroRNAs mediated control of carnitine cycle in prostate cancer: molecular basis and pathophysiological consequences. *Oncogene, 36*(43), 6030-6040. doi:10.1038/onc.2017.216

Van den Broeck, T., van den Bergh, R. C. N., Briers, E., Cornford, P., Cumberbatch, M., Tilki, D., . . . Mottet, N. (2020). Biochemical Recurrence in Prostate Cancer: The European Association of Urology Prostate Cancer Guidelines Panel Recommendations. *Eur Urol Focus, 6*(2), 231-234. doi:10.1016/j.euf.2019.06.004

van Helvoort, A., de Brouwer, A., Ottenhoff, R., Brouwers, J. F. H. M., Wijnholds, J., Beijnen, J. H., . . . Borst, P. (1999). Mice without phosphatidylcholine transfer protein have no defects in the secretion of phosphatidylcholine into bile or into lung airspaces. *Proceedings of the National Academy of Sciences, 96*(20), 11501-11506. doi:10.1073/pnas.96.20.11501

van Laar, J. H., Bolt-de Vries, J., Voorhorst-Ogink, M. M., & Brinkmann, A. O. (1989). The human androgen receptor is a 110 kDa protein. *Mol Cell Endocrinol, 63*(1-2), 39-44. doi:10.1016/0303-7207(89)90079-8

van Meer, G. (2010). Membranes in motion. *EMBO Rep, 11*(5), 331-333. doi:10.1038/embor.2010.60

van Meer, G., Voelker, D. R., & Feigenson, G. W. (2008). Membrane lipids: where they are and how they behave. *Nat Rev Mol Cell Biol, 9*(2), 112-124. doi:10.1038/nrm2330

Verze, P., Cai, T., & Lorenzetti, S. (2016). The role of the prostate in male fertility, health and disease. *Nat Rev Urol, 13*(7), 379-386. doi:10.1038/nrurol.2016.89

Vessey, D. A., Kelley, M., & Warren, R. S. (1999). Characterization of the CoA ligases of human liver mitochondria catalyzing the activation of short- and medium-chain fatty acids and xenobiotic carboxylic acids. *Biochim Biophys Acta, 1428*(2-3), 455-462. doi:10.1016/s0304-4165(99)00088-4

Visakorpi, T., Hyytinen, E., Koivisto, P., Tanner, M., Keinänen, R., Palmberg, C., . . . Kallioniemi, O.-P. (1995). In vivo amplification of the androgen receptor gene and progression of human prostate cancer. *Nature genetics, 9*(4), 401.

von Roemeling, C. A., Marlow, L. A., Wei, J. J., Cooper, S. J., Caulfield, T. R., Wu, K., . . . Copland, J. A. (2013). Stearoyl-CoA desaturase 1 is a novel molecular

therapeutic target for clear cell renal cell carcinoma. *Clin Cancer Res, 19*(9), 2368-2380. doi:10.1158/1078-0432.Ccr-12-3249

Waghray, A., Feroze, F., Schober, M. S., Yao, F., Wood, C., Puravs, E., . . . Chen, Y. Q. (2001). Identification of androgen-regulated genes in the prostate cancer cell line LNCaP by serial analysis of gene expression and proteomic analysis. *Proteomics, 1*(10), 1327-1338. doi:10.1002/1615-9861(200110)1:10<1327::aid-prot1327>3.0.co;2-b

Wang, Q., Carroll, J. S., & Brown, M. (2005). Spatial and temporal recruitment of androgen receptor and its coactivators involves chromosomal looping and polymerase tracking. *Mol Cell, 19*(5), 631-642. doi:10.1016/j.molcel.2005.07.018

Wang, W., & Epstein, J. I. (2008). Small cell carcinoma of the prostate. A morphologic and immunohistochemical study of 95 cases. *Am J Surg Pathol, 32*(1), 65-71. doi:10.1097/PAS.0b013e318058a96b

Wang, X., Sato, R., Brown, M. S., Hua, X., & Goldstein, J. L. (1994). SREBP-1, a membrane-bound transcription factor released by sterol-regulated proteolysis. *Cell, 77*(1), 53-62.

Watson, P. A., Arora, V. K., & Sawyers, C. L. (2015). Emerging mechanisms of resistance to androgen receptor inhibitors in prostate cancer. *Nat Rev Cancer, 15*(12), 701-711. doi:10.1038/nrc4016

Watt, M. J., Clark, A. K., Selth, L. A., Haynes, V. R., Lister, N., Rebello, R., . . . Taylor, R. A. (2019). Suppressing fatty acid uptake has therapeutic effects in preclinical models of prostate cancer. *Sci Transl Med, 11*(478). doi:10.1126/scitranslmed.aau5758

Weber, L.-W., Boll, M., & Stampfl, A. (2004). Maintaining cholesterol homeostasis: sterol regulatory element-binding proteins. *World journal of gastroenterology, 10*(21), 3081-3087. doi:10.3748/wjg.v10.i21.3081

Wen, P. Y., & Reardon, D. A. (2016). Neuro-oncology in 2015: Progress in glioma diagnosis, classification and treatment. *Nat Rev Neurol, 12*(2), 69-70. doi:10.1038/nrneurol.2015.242

Wikstrom, P., Lissbrant, I. F., Stattin, P., Egevad, L., & Bergh, A. (2002). Endoglin (CD105) is expressed on immature blood vessels and is a marker for survival in prostate cancer. *Prostate, 51*(4), 268-275. doi:10.1002/pros.10083

Willemarck, N., Rysman, E., Brusselmans, K., Van Imschoot, G., Vanderhoydonc, F., Moerloose, K., . . . Swinnen, J. V. (2010). Aberrant activation of fatty acid synthesis suppresses primary cilium formation and distorts tissue development. *Cancer Res, 70*(22), 9453-9462. doi:10.1158/0008-5472.can-10-2324

Williams, K. J., Argus, J. P., Zhu, Y., Wilks, M. Q., Marbois, B. N., York, A. G., . . . Bensinger, S. J. (2013). An essential requirement for the SCAP/SREBP signaling axis to protect cancer cells from lipotoxicity. *Cancer Res, 73*(9), 2850-2862. doi:10.1158/0008-5472.Can-13-0382-t

Wirtz, K. W., & Zilversmit, D. B. (1968). Exchange of phospholipids between liver mitochondria and microsomes in vitro. *J Biol Chem, 243*(13), 3596-3602.

Wirtz, K. W. A. (1991). PHOSPHOLIPID TRANSFER PROTEINS. *Annual Review of Biochemistry, 60*(1), 73-99. doi:10.1146/annurev.bi.60.070191.000445

Wright, A. S., Thomas, L. N., Douglas, R. C., Lazier, C. B., & Rittmaster, R. S. (1996). Relative potency of testosterone and dihydrotestosterone in preventing

atrophy and apoptosis in the prostate of the castrated rat. *J Clin Invest, 98*(11), 2558-2563. doi:10.1172/jci119074

Wu, D., Zhang, C., Shen, Y., Nephew, K. P., & Wang, Q. (2011). Androgen receptor-driven chromatin looping in prostate cancer. *Trends in Endocrinology & Metabolism, 22*(12), 474-480. doi:https://doi.org/10.1016/j.tem.2011.07.006

Wu, L., Runkle, C., Jin, H. J., Yu, J., Li, J., Yang, X., . . . Yu, J. (2014). CCN3/NOV gene expression in human prostate cancer is directly suppressed by the androgen receptor. *Oncogene, 33*(4), 504-513. doi:10.1038/onc.2012.602

Wu, M. K., Boylan, M. O., & Cohen, D. E. (1999). Cloning and gene structure of rat phosphatidylcholine transfer protein, Pctp. *Gene, 235*(1), 111-120. doi:https://doi.org/10.1016/S0378-1119(99)00204-8

Wu, X., Daniels, G., Lee, P., & Monaco, M. E. (2014). Lipid metabolism in prostate cancer. *American journal of clinical and experimental urology, 2*(2), 111-120.

Wu, Y. H., Ko, T. P., Guo, R. T., Hu, S. M., Chuang, L. M., & Wang, A. H. (2008). Structural basis for catalytic and inhibitory mechanisms of human prostaglandin reductase PTGR2. *Structure, 16*(11), 1714-1723. doi:10.1016/j.str.2008.09.007

Xu, L. L., Su, Y. P., Labiche, R., Segawa, T., Shanmugam, N., McLeod, D. G., . . . Srivastava, S. (2001). Quantitative expression profile of androgen-regulated genes in prostate cancer cells and identification of prostate-specific genes. *Int J Cancer, 92*(3), 322-328.

Yang, Y., Chen, R., Sun, T., Zhao, L., Liu, F., Ren, S., . . . Xu, C. (2019). Efficacy and safety of combined androgen blockade with antiandrogen for advanced prostate cancer. *Current Oncology, 26*(1), e39.

Yao, H., & Ye, J. (2008). Long chain acyl-CoA synthetase 3-mediated phosphatidylcholine synthesis is required for assembly of very low density lipoproteins in human hepatoma Huh7 cells. *J Biol Chem, 283*(2), 849-854. doi:10.1074/jbc.M706160200

Ye, J., Davé, U. P., Grishin, N. V., Goldstein, J. L., & Brown, M. S. (2000). Asparagine-proline sequence within membrane-spanning segment of SREBP triggers intramembrane cleavage by site-2 protease. *Proc Natl Acad Sci U S A, 97*(10), 5123-5128. doi:10.1073/pnas.97.10.5123

Yokoyama, C., Wang, X., Briggs, M. R., Admon, A., Wu, J., Hua, X., . . . Brown, M. S. (1993). SREBP-1, a basic-helix-loop-helix-leucine zipper protein that controls transcription of the low density lipoprotein receptor gene. *Cell, 75*(1), 187-197. doi:https://doi.org/10.1016/S0092-8674(05)80095-9

Yue, S., Li, J., Lee, S.-Y., Lee, H. J., Shao, T., Song, B., . . . Ratliff, T. L. (2014). Cholesteryl ester accumulation induced by PTEN loss and PI3K/AKT activation underlies human prostate cancer aggressiveness. *Cell Metab, 19*(3), 393-406.

Yue, S., Li, J., Lee, S.-Y., Lee, H. J., Shao, T., Song, B., . . . Cheng, J.-X. (2014). Cholesteryl ester accumulation induced by PTEN loss and PI3K/AKT activation underlies human prostate cancer aggressiveness. *Cell Metab, 19*(3), 393-406. doi:10.1016/j.cmet.2014.01.019

Zadra, G., Photopoulos, C., & Loda, M. (2013). The fat side of Prostate Cancer. *Biochim Biophys Acta, 1831*(10), 1518-1532. doi:10.1016/j.bbalip.2013.03.010

Zaytseva, Y. Y., Elliott, V. A., Rychahou, P., Mustain, W. C., Kim, J. T., Valentino, J., . . . Evers, B. M. (2014). Cancer cell-associated fatty acid synthase activates

endothelial cells and promotes angiogenesis in colorectal cancer. *Carcinogenesis, 35*(6), 1341-1351. doi:10.1093/carcin/bgu042

Zaytseva, Y. Y., Harris, J. W., Mitov, M. I., Kim, J. T., Butterfield, D. A., Lee, E. Y., . . . Evers, B. M. (2015). Increased expression of fatty acid synthase provides a survival advantage to colorectal cancer cells via upregulation of cellular respiration. *Oncotarget, 6*(22), 18891-18904. doi:10.18632/oncotarget.3783

Zhao, X. Y., Malloy, P. J., Krishnan, A. V., Swami, S., Navone, N. M., Peehl, D. M., & Feldman, D. (2000). Glucocorticoids can promote androgen-independent growth of prostate cancer cells through a mutated androgen receptor. *Nat Med, 6*(6), 703-706. doi:10.1038/76287

Zhou, Y., Bolton, E. C., & Jones, J. O. (2015). Androgens and androgen receptor signaling in prostate tumorigenesis. *J Mol Endocrinol, 54*(1), R15-29. doi:10.1530/jme-14-0203

Zhou, Z. X., Lane, M. V., Kemppainen, J. A., French, F. S., & Wilson, E. M. (1995). Specificity of ligand-dependent androgen receptor stabilization: receptor domain interactions influence ligand dissociation and receptor stability. *Mol Endocrinol, 9*(2), 208-218. doi:10.1210/mend.9.2.7776971

Zhu, Z., Zhao, X., Zhao, L., Yang, H., Liu, L., Li, J., . . . Liu, J. (2016). p54(nrb)/NONO regulates lipid metabolism and breast cancer growth through SREBP-1A. *Oncogene, 35*(11), 1399-1410. doi:10.1038/onc.2015.197

Zobniw, C. M., Causebrook, A., & Fong, M. K. (2014). Clinical use of abiraterone in the treatment of metastatic castration-resistant prostate cancer. *Res Rep Urol, 6*, 97-105. doi:10.2147/rru.s29003

Zong, Y., & Goldstein, A. S. (2013). Adaptation or selection--mechanisms of castration-resistant prostate cancer. *Nat Rev Urol, 10*(2), 90-98. doi:10.1038/nrurol.2012.237